

WCAP-7931


PWR FLECHT FINAL REPORT SUPPLEMENT

Westinghouse Atomic Power Divisions



4th

Internal Distribution for WCAP-7931

H. N. Andrews	J. J. Lescisin
K. M. Beatty	R. H. Leyse (5)
L. Berkowitz	Library (5)
J. A. Blaisdell	J. D. McAdoo
F. F. Cadek (5) 	D. L. Miller
C. L. Caso	J. S. Moore
J. O. Cermak	M. Mulligan
L. Chajson	K. L. Rieke
W. P. DiPietro	G. T. Rymer
D. P. Dominicis (5)	R. Salvatori
D. J. Engle	M. Slafka
H. J. Fix	A. P. Suda
J. G. Gallagher	G. R. Thomas
J. Greenawalt	L. S. Tong
W. B. Henderson	J. Waring
L. E. Hochreiter	N. Washington
J. S. Kalo	R. A. Wieseemann
A. S. Kitzes	H. C. Yeh (5)
J. L. Koetting	

PWR FLECHT FINAL REPORT SUPPLEMENT

F. F. Cadek
D. P. Dominicus
H. C. Yeh
R. H. Leyse

OCTOBER 1972

APPROVED: J. O. Cermak
J. O. Cermak, Manager
Safety Analysis

APPROVED: A. P. Suda
A. P. Suda
Project Engineer

Work performed under Contract AT(10-1)-1375 Subcontract S-7045
between Westinghouse Electric Corporation and Aerojet Nuclear
Company.

Westinghouse Electric Corporation
Nuclear Energy Systems
Box 355
Pittsburgh, Pennsylvania 15230

LEGAL NOTICE

This report was prepared as an account of Government sponsored work. Neither the United States, nor the Commission, nor any person acting on behalf of the Commission:

A. Makes any warranty or representation, expressed or implied, with respect to the accuracy, completeness, or usefulness of the information contained in this report, or that the use of any information, apparatus, method, or process disclosed in this report may not infringe privately owned rights; or

B. Assumes any liabilities with respect to the use of, or for damages resulting from the use of any information, apparatus, method, or process disclosed in this report.

As used in the above, "Persons acting on behalf of the Commission" includes any employee or contractor of the Commission, or employee of such contractor, to the extent that such employee or contractor of the Commission, or employee of such contractor prepares, disseminates, or provides access to, any information pursuant to his employment or contract with the Commission, or his employment with such contractor.

ABSTRACT

A series of sixteen bottom flooding tests were performed with the PWR-FLECHT test facility to extend the range of FLECHT data to various combinations of low system pressure (15-20 psia), low flooding rate (as low as 0.4 in/sec) and low subcooling ($\sim 20^{\circ}\text{F}$). Also, the effect of peak power and test section flow housing temperature were investigated at these conditions. The test results include transient heat transfer coefficients and clad temperatures at different axial and radial locations. Axial pressure drop, local coolant temperature and liquid carryover were also measured.

It was found that heat transfer coefficients increased with flooding rate and system pressure. It was also observed that lower system pressure increased the measured liquid carryover and lowered the velocity of the quench front. Low subcooling was found to increase the quench time but had no effect on heat transfer coefficient until late in the runs. Lowering the peak power increased the heat transfer coefficient for times greater than 120 seconds after flood.

The heat transfer coefficient correlation presented in WCAP-7665 was modified to more accurately predict the data at the conditions of the current tests.

TABLE OF CONTENTS

Section	Title	Page
1	INTRODUCTION	1-1
2	TEST DESCRIPTION	2-1
3	DISCUSSION OF TEST RESULTS	3-1
3.1	SUMMARY OF RUN CONDITIONS AND TEST RESULTS	3-1
3.2	DATA VERIFICATION	3-5
3.2.1	Checkout Runs and Data Repeatability	3-5
3.2.2	Rod Bundle Housing	3-15
3.2.2.1	Housing Temperature Criteria	3-15
3.2.2.2	Effect of Housing Temperature	3-16
3.2.2.3	Effect of Bundle Size and Radiation to the Housing	3-28
3.3	PARAMETER EFFECTS	3-44
3.3.1	Flooding Rate	3-44
3.3.2	Pressure	3-44
3.3.3	Inlet Coolant Subcooling	3-55
3.3.4	Peak Power Generation	3-55
3.3.5	Comments on Parameter Effects	3-62
3.4	HEAT TRANSFER BEHAVIOR AT OTHER ELEVATIONS	3-65
3.5	EXTERNAL THERMOCOUPLE DATA	3-68
3.6	HEAT TRANSFER COEFFICIENT CORRELATION	3-71
3.6.1	Modifications to Include Current Data	3-71
3.6.2	Initial Heat Transfer Coefficient	3-86
3.7	PRESSURE TRANSDUCER RESULTS	3-90
3.8	LOCAL COOLANT TEMPERATURE DATA	3-93
3.9	LIQUID CARRYOVER RESULTS	3-101

TABLE OF CONTENTS (Cont'd)

Section	Title	Page
4	SUMMARY AND CONCLUSIONS	4-1
	4.1 SYSTEM PARAMETER EFFECTS ON HEAT TRANSFER	4-1
	4.2 HEAT TRANSFER AT OTHER ELEVATIONS	4-1
	4.3 DATA VERIFICATION	4-2
	4.4 CORRELATION	4-2
	4.5 PRESSURE TRANSDUCER RESULTS	4-2
	4.6 LOCAL COOLANT DATA	
	4.7 LIQUID CARRYOVER	4-3
5	REFERENCES	5-1
APPENDIX A	FLECHT DATA SHEETS	A-1
APPENDIX B	METHOD OF CALCULATION OF ROD AND HOUSING HEAT RELEASE	B-1
APPENDIX C	INITIAL TEMPERATURE DISTRIBUTIONS	C-1
APPENDIX D	FORTRAN PROGRAM LISTING OF CORRELATION	D-1
APPENDIX E	RADIATIVE HEAT TRANSFER ANALYSIS OF A HEATER ROD	E-1

LIST OF ILLUSTRATIONS

Figure	Title	Page
2-1	Location of Instrumented Heated Rods in the 10 x 10 Array	2-2
2-2	Location of Steam Temperature Detectors and Coolant Thermocouples Relative to Midplane	2-3
2-3	Power Decay Rates Used in Current Test Series	2-4
3-1	Typical Transient Midplane Clad Temperature Behavior for Constant Flooding Rate Tests	3-2
3-2	Repeatability of Heat Transfer Coefficient for Current and Previous Test Series - 2 In/Sec Flood Rate	3-6
3-3	Repeatability of Midplane Heat Transfer Coefficient for Current and Previous Test Series - 1 In/Sec Flood Rate	3-7
3-4	Repeatability of Midplane Heat Transfer Coefficient for Current Test Series	3-8
3-5	Repeatability of Midplane Heat Transfer Coefficient for High Flooding Rate, High Pressure and High Subcooling	3-10
3-6	Repeatability of Midplane Heat Transfer Coefficient for High Flooding Rate, High Pressure and Low Subcooling	3-11
3-7	Repeatability of Heat Transfer Coefficient at High Flooding Rate, High Pressure, High Subcooling and 1800°F Initial Clad Temperature	3-12
3-8	Repeatability of Heat Transfer Coefficient at Low Flooding Rate and Low Pressure	3-13
3-9	Repeatability of Heat Transfer Coefficient at Low Flooding Rate and High Pressure	3-14
3-10	Effect of Housing Temperature on Temperature Rise, Turnaround Time and Quench Time	3-17
3-11	Effect of Housing Temperature on Heat Transfer Coefficient	3-18
3-12	Effect of Housing Temperature at 1 in/sec Flooding Rate	3-21
3-13	Effect of Low Housing Temperature at Elevation Below Midplane	3-23
3-14	Comparison of Housing and Equivalent Row of Rods Integrated Heat Release	3-24

LIST OF ILLUSTRATIONS (Continued)

Figure	Title	Page
3-15	Comparison of the Rate of Heat Release at 2 Ft Elevation of a Normal Temperature Housing, a Cold Housing and an Equivalent Row of Rods	3-25
3-16	Comparison of the Rate of Heat Release Below 6 Ft Elevation of a Normal Temperature Housing, a Cold Housing and an Equivalent Row of Rods	3-26
3-17	Comparison of Heat Release Below 6 Ft Elevation of a Normal Temperature Housing, a Cold Housing and an Equivalent Row of Rods	3-27
3-18	Heat Transfer Coefficients at Midplane of Equivalent Heater Rods in the 7 x 7 and 10 x 10 Bundles, Runs 1002 and 3541	3-30
3-19	Heat Transfer Coefficients at the Midplane of Equivalent Heater Rods in the 7 x 7 and 10 x 10 Bundles, Runs 1720 and 3920	3-31
3-20	Comparison of Equivalent Central Rods in 7 x 7 and 10 x 10 Bundles for 1 in/sec Flooding Rate	3-32
3-21	Radial Variation of Heat Transfer Coefficient for 10 x 10 and 7 x 7 Bundles at 6 in/sec.	3-33
3-22	Radial Variation in Heat Transfer Coefficient for 10 x 10 and 7 x 7 Bundles at 1.0 in/sec.	3-34
3-23	Comparison of FLECHT and PWR Radial Temperature Distribution Along Row F Rods at the Start of Reflood	3-39
3-24	Comparison of FLECHT and PWR Radial Temperature Distribution Along Column 6 Rods at the Start of Reflood	3-40
3-25	Effect of Flooding Rate on Temperature Rise, Turnaround Time, and Quench Time	3-41
3-26	Effect of Flooding Rate on Temperature Rise (Log-Log Plot)	3-42
3-27	Effect of Flooding Rate on Midplane (6') Heat Transfer Coefficient at 1600°F Initial Clad Temperature, High Pressure and High Subcooling	3-44
3-28	Effect of Flooding Rate at Low Pressure and High Subcooling	3-45
3-29	Effect of Flooding Rate at Low Pressure and Low Subcooling	3-46
3-30	Effect of Flooding Rate at High Pressure and Low Subcooling	3-47

LIST OF ILLUSTRATIONS (Continued)

Figure	Title	Page
3-31	Effect of Flooding Rate at Low Pressure, Low Subcooling and 0.69 kw/ft Peak Power	3-48
3-32	Effect of System Pressure on Temperature Rise, Turnaround Time and Quench Time	3-49
3-33	Effect of Pressure on Heat Transfer Coefficient at High Subcooling for 6 in/sec Flooding Rate	3-50
3-34	Effect of Pressure at 2 in/sec Flooding Rate and High Subcooling	3-51
3-35	Effect of Pressure at 1 in/sec Flooding Rate and High Subcooling	3-52
3-36	Effect of Pressure at 1 in/sec Flooding Rate and Low Subcooling	3-53
3-37	Effect of Inlet Coolant Subcooling on Temperature Rise, Turnaround Time, and Quench Time	3-56
3-38	Effect of Subcooling on Heat Transfer Coefficient at 2 and 6 in/sec Flooding Rate and High Pressure	3-57
3-39	Effect of Inlet Coolant Subcooling at 1 in/sec Flooding Rate and High Pressure	3-58
3-40	Effect of Inlet Coolant Subcooling at 1 in/sec Flooding Rate and Low Pressure	3-59
3-41	Effect of Peak Power on Heat Transfer Coefficient for 6 and 2 in/sec Flooding Rate	3-60
3-42	Effect of Peak Power for Current Data	3-61
3-43	Effect of Peak Power on Temperature Rise, Turnaround Time and Quench Time	3-63
3-44	Heat Transfer Coefficient at Five Elevations in High Subcooling Tests at 58 and 21 PSIA	3-66
3-45	Heat Transfer Coefficient at Five Elevations in Low Subcooling Tests at 58 and 21 PSIA	3-67
3-46	External Thermocouple Behavior, Run 8000	3-70
3-47	Comparison of Measured and Predicted Heat Transfer Coefficients, Run 9782	3-75
3-48	Comparison of Measured and Predicted Heat Transfer Coefficients, Run 8000	3-76
3-49	Comparison of Measured and Predicted Heat Transfer Coefficients, Run 0085	3-77
3-50	Comparison of Measured and Predicted Heat Transfer Coefficients, Run 0183	3-78

LIST OF ILLUSTRATIONS (Continued)

Figure	Title	Page
3-51	Comparison of Measured and Predicted Heat Transfer Coefficients , Run 0284	3-79
3-52	Comparison of Measured and Predicted Heat Transfer Coefficients , Run 0386	3-80
3-53	Comparison of Measured and Predicted Heat Transfer Coefficients , Run 0487	3-81
3-54	Comparison of Measured and Predicted Heat Transfer Coefficients , Run 0588	3-82
3-55	Comparison of Measured and Predicted Heat Transfer Coefficients , Run 0690	3-83
3-56	Comparison of Measured and Predicted Heat Transfer Coefficients , Run 0791	3-84
3-57	Comparison of Measured and Predicted Heat Transfer Coefficients , Run 0889	3-85
3-58	Heat Transfer Coefficients of a Hot Rod During Initial Heatup Period Computed from 4-Surface Gray Body Radiation Model	3-87
3-59	Comparison of Measured Initial Heat Transfer Coefficient with that Computed from 4-Surface Gray Body Radiation Model	3-89
3-60	Comparison of Measured Initial Heat Transfer Coefficient and that Predicted with Correlation	3-91
3-61	Axial Pressure Drop (0-8 ft) for Various Pressure and Subcooling	3-92
3-62	Comparison of Pressure Drop and Rod Quench Data, Run 9881	3-94
3-63	Comparison of Pressure Drop and Rod Quench Data, Run 8000	3-95
3-64	Comparison of Pressure Drop and Rod Quench Data, Run 0183	3-96
3-65	Comparison of Pressure Drop and Rod Quench Data, Run 0284	3-97
3-66	Local Coolant and Clad Temperature, Run 8000	3-98
3-67	Local Coolant and Clad Temperature, Run 0183	3-99
3-68	Local Coolant and Clad Temperature, Run 0284	3-100
3-69	Effect of Flooding Rate on Liquid Carryover Collected	3-103
3-70	Effect of Pressure on Liquid Carryover Collected	3-104

LIST OF ILLUSTRATIONS (Continued)

Figure	Title	Page
3-71	Liquid Carryover Collected for Various Pressure and Subcooling at 1 in/sec Flooding Rate	3-105
3-72	Effect of Peak Power on Liquid Carryover Collected	3-107
3-73	Total Mass Effluent Flow Rate Fraction versus Time	3-109
B-1	Housing Temperature of FLECHT Run 9077 and 9176	B-3
B-2	Rate of Heat Release of an Equivalent Row of Rods vs Elevation	B-4
B-3	Housing Quench Front Elevation versus Time	B-5
B-4	Temperature of the Housing vs Elevation. The Abrupt Change in Temperature Indicates the Quench. The Quench Front Elevation is Determined by Figure B-3	B-8
B-5	Comparison of Housing Heat Releases Computed with Two Methods	B-9
C-1	Clad Temperature Distribution at the Start of Flood, Run 9681	C-2
C-2	Clad Temperature Distribution at the Start of Flood, Run 9782	C-3
C-3	Clad Temperature Distribution at the Start of Flood, Run 9881	C-4
C-4	Clad Temperature Distribution at the Start of Flood, Run 9983	C-5
C-5	Clad Temperature Distribution at the Start of Flood, Run 8000	C-6
C-6	Clad Temperature Distribution at the Start of Flood, Run 0085	C-7
C-7	Clad Temperature Distribution at the Start of Flood, Run 0183	C-8
C-8	Clad Temperature Distribution at the Start of Flood, Run 0284	C-9
C-9	Clad Temperature Distribution at the Start of Flood, Run 0386	C-10
C-10	Clad Temperature Distribution at the Start of Flood, Run 0487	C-11
C-11	Clad Temperature Distribution at the Start of Flood, Run 0588	C-12
C-12	Clad Temperature Distribution at the Start of Flood, Run 0690	C-13

LIST OF ILLUSTRATIONS (Continued)

Figure	Title	Page
C-13	Clad Temperature Distribution at the Start of Flood, Run 0791	C-14
C-14	Clad Temperature Distribution at the Start of Flood, Run 0889	C-15
C-15	Clad Temperature Distribution at the Start of Flood, Run 0984	C-16
C-16	Clad Temperature Distribution at the Start of Flood, Run 1084	C-17
E-1	Configuration of Heater Rods and Thimbles Surrounding a Hot Rod	E-3
E-2	Equivalent Model of Configuration (E1)	E-3

LIST OF TABLES

TABLE	TITLE	PAGE
3-1	FLECHT Data Summary, Stainless Steel Clad Constant Flow Tests, Hot Rod Midplane Elevation (6-Foot)	3-3
3-2	Repeatability Checks	3-9
3-3	Effect of Housing Temperature on Clad Temperature Response	3-20
3-4	Comparison of 7 x 7 and 10 x 10 Central Hot Rod Temperature Response	3-29
3-5	Radiation from a Central Rod (Midplane Elevation) to Housing in 10 x 10 Bundle for a FLECHT Run	3-36
3-6	Radiation from a Central Rod (Midplane Elevation) in 10 x 10 Bundle for a Checkout Run	3-37
3-7	Observed Trends for Various Parameter Effects	3-64

SECTION 1

INTRODUCTION

1.1 OBJECTIVE

The objective of the PWR FLECHT (Full Length Emergency Cooling Heat Transfer) test program was to obtain experimental reflooding heat transfer data under simulated loss-of-coolant accident conditions for use in evaluating the heat transfer capabilities of PWR emergency core cooling systems.

To achieve this objective, the test program was planned to investigate the effects of the following parameters on transient heat transfer coefficients:

- Initial Clad Temperature
- Flooding Rate
- Power
- Inlet Coolant Subcooling
- Pressure

In addition, various special tests were included for validation purposes and to investigate the effects of such things as soluble poison, cladding damage, power decay rate, variable flooding rate, entrained liquid "fallback" and metal-water reaction.

The data resulting from these tests was analyzed, and correlations which can be used to evaluate PWR emergency core cooling system capabilities were developed and were reported in WCAP-7665.

The objective of this additional test series was to extend the range of the earlier data to various combinations of low pressure, low coolant subcooling, and low flood rates not previously tested and to modify the heat transfer correlation presented in WCAP-7665 to more accurately predict the data at these conditions, if necessary.

SECTION 2

TEST DESCRIPTION

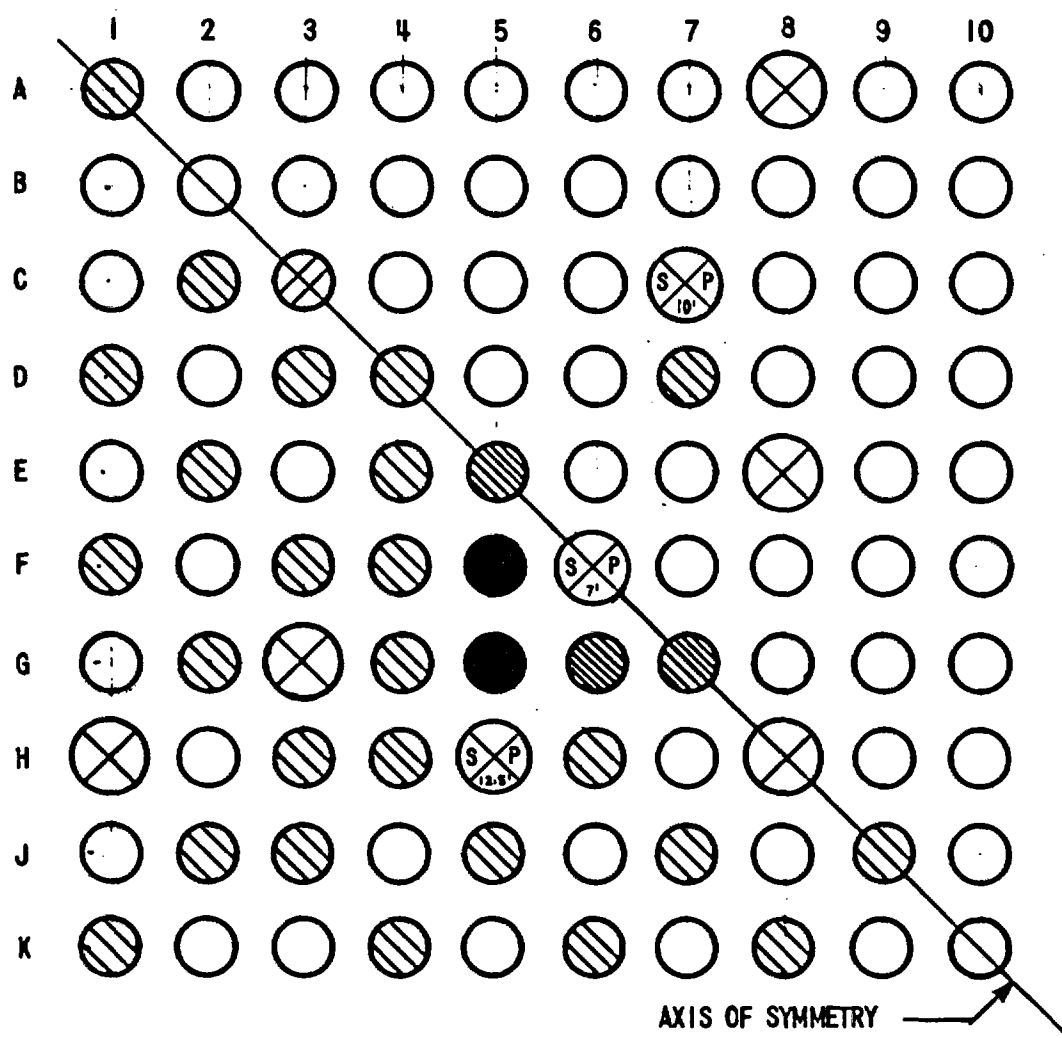
The test section used in the current test series was the 10 x 10 bundle previously used for Group II flow blockage testing with the blockage plate removed. Test section instrumentation was identical to that of the 10 x 10 flow blockage bundle as shown in Figure 2-1. A complete test description is given in Reference 1. The procedures and hardware described therein are identical to those used in this test series.

Modifications for these tests included the following:

1. External thermocouples were located at 6, 12, 18, 24 and 36 inches from the bottom of the heated length on rod 5G. The purpose was to determine the location of the quench front at early times and the initial temperature distribution.
2. An additional steam probe, SP-3, was installed at 12.5 ft from the bottom of the heated length in guide tube 5H.
3. To prevent a pressure surge at early times in the atmospheric tests, the valved exit line in the upper plenum was removed and replaced by a 3-inch pipe.
4. In the atmospheric tests, a vacuum line was connected to the steam probes to maintain flow in the tube. Normally, the probes went from inside the higher pressure housing to atmosphere.
5. The 3-inch carryover collection pipe was replaced by a 4-inch schedule 40 pipe to increase the collection capacity.

Figure 2-2 shows the location of the coolant temperature instrumentation and the carryover collector pipe.

The power decay used in most of the runs was decay curve B shown in Figure 2-3.



- UNINSTRUMENTED HEATER ROD-DIAMETER 0.422-INCH
- ▨ INSTRUMENTED HEATER ROD (3 THERMOCOUPLES)
DIAMETER 0.422-INCH
- ▩ INSTRUMENTED HEATER ROD (5 THERMOCOUPLES)
DIAMETER 0.422-INCH
- INSTRUMENTED HEATER ROD (6 THERMOCOUPLES)
DIAMETER 0.422-INCH
- ▧ INSTRUMENT TUBE - DIAMETER 0.463-INCH
- ⊗ CONTROL ROD THIMBLE-DIAMETER-0.545 INCH
- ⊗(S-P) CONTROL ROD THIMBLE CONTAINING STEAM PROBE

Figure 2-1. Location of Instrumented Heated Rods in the 10 X 10 Array

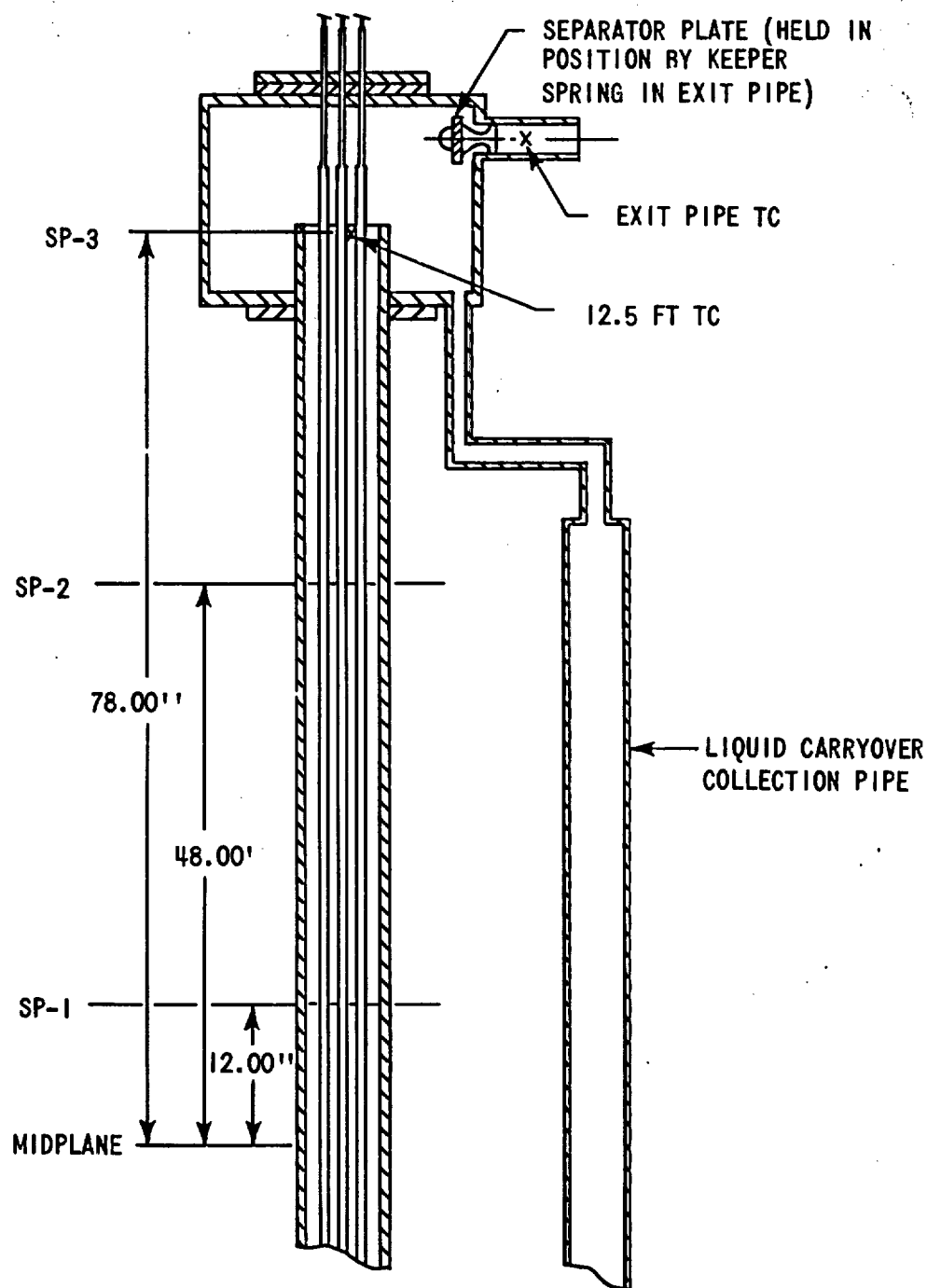


Figure 2-2. Location of Steam Temperature Detectors and Coolant Thermocouples Relative to Midplane.

2-4

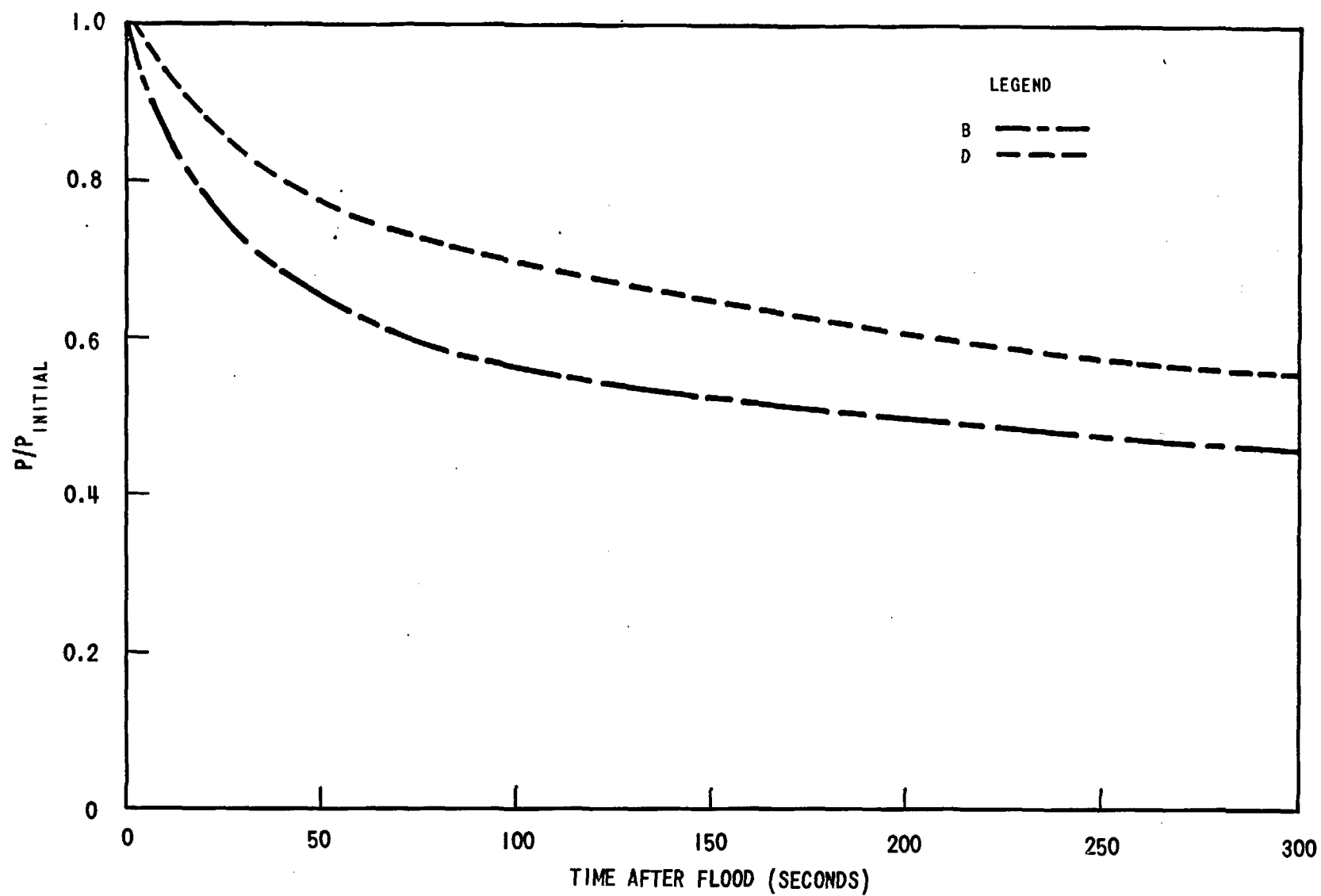


Figure 2-3. Power Decay Rates Used in Current Test Series.

For low flooding rate runs (0588-0889) power decay curve D based on the current ANS + 20% decay heat curve was used. The decay power relative to the initial power is higher in this curve, however the initial power level in these tests was lowered to 1.0 and 0.69 kw/ft to represent start of core reflood at a later time after the start of the accident.

SECTION 3

DISCUSSION OF TEST RESULTS

3.1 SUMMARY OF RUN CONDITIONS AND TEST RESULTS

In this report as in previous FLECHT reports, a particular run is characterized by the transient temperature behavior of the midplane (six-foot elevation) of the hottest rod. For each run, the hot rod was designated as the one which reached the highest midplane temperature during the test and was reasonably close to the nominal initial clad temperature for the run.

Typical transient midplane clad temperature behavior for constant flooding rate tests is illustrated in Figure 3-1. In constant flooding rate tests, midplane temperatures continued to increase after flooding was initiated until the heat transfer coefficient became large enough to turn the temperature around. The temperature then continued to decrease until the quench front (onset of clad wetting) reached the bundle midplane, at which time the clad temperature dropped rapidly to saturation.

The parameters used to characterize test behavior are:

1. Temperature Rise, ΔT_{rise} . Defined as the difference between the clad temperature at the start of flooding (initial clad temperature) and the peak temperature.
2. Turnaround Time, t_{turn} . Defined as the time after flooding at which the clad temperature reaches a maximum.
3. Quench Time, t_{quench} . Defined as the time after flooding at which clad temperatures start to drop very rapidly (i.e., almost vertically) to saturation.
4. Quench Temperature, T_{quench} . Defined as the clad temperature at t_{quench} .

Table 3-1 summarizes the exact run conditions and measured temperature behavior for the midplane elevation of the hottest rod of each run, in the latest test series. Data for previous runs was contained in Tables 3-1 - 3-3 in the FLECHT

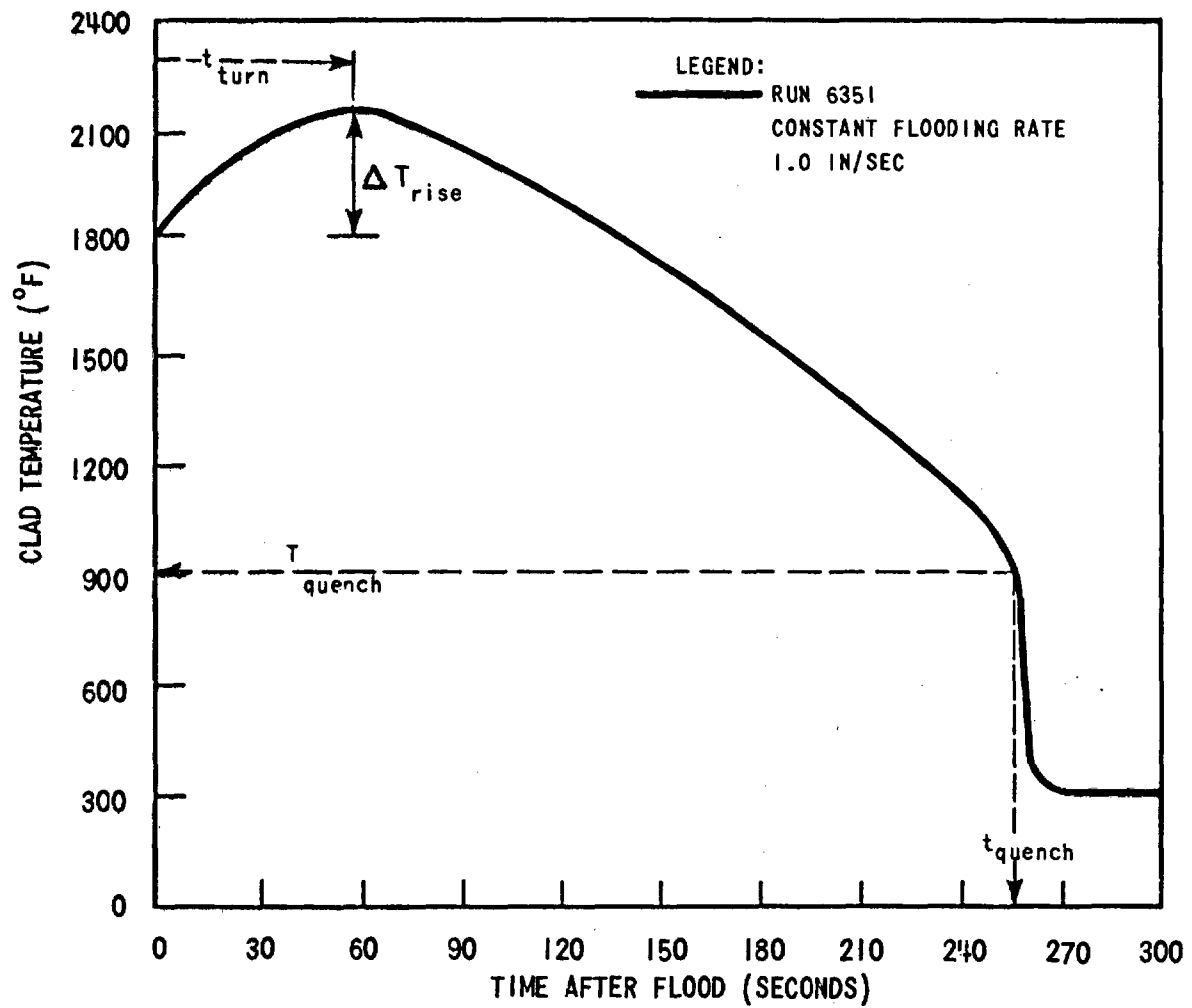


Figure 3-1. Typical Transient Midplane Clad Temperature Behavior for Constant Flooding Rate Tests.

Run No.	Pressure (psia)	Peak Power (kw/ft)	Decay Power ^a	Flooding Rate (in./sec)	Inlet Subcooling (°F)	Initial Temperature (°F)	Temperature Rise (°F)	Turnaround Time (sec)	Quench Temperature (°F)	Quench Time (sec)	Bundle Size	Remarks
CURRENT TEST SERIES												
9681	61	1.24	B	2.0	144	1586	234	40	877	147	10 x 10	
9782	56	1.24	B	1.0	28	1590	493	91	916	323	10 x 10	
9881	60	1.24	B	2.0	137	1576	293	43	857	164	10 x 10	
9983	19	1.24	B	1.0	137	1586	668	146	1049	424	10 x 10	
8000	58	1.24	B	1.0	156	1689	422	74	949	262	10 x 10	
0085	25	1.24	B	2.0	138	1586	302	57	858	231	10 x 10	
0183	21	1.24	B	1.0	147	1598	636	142	1020	420	10 x 10	
0284	21	1.24	B	1.0	48	1590	634	144	774	614	10 x 10	
0386	20	0.69	B	1.0	39	1591	219	77	850	323	10 x 10	
0487	18	1.24	B	0.8	35	1582	792	153	893	819	10 x 10	
0588	15	1.00	D	0.6	24	1574	-	-	-	-	10 x 10	Power scram at 134 sec.
0690	15	0.69	D	0.6	22	1531	629	200	698	713	10 x 10	
0791	15	0.69	D	0.4	24	1593	775	234	827	931	10 x 10	Rod 7E failed
0889	15	1.00	D	0.4	18	1592	-	-	-	-	10 x 10	Power scram at 91 sec. 7D, 6E Failed.
0984	21	1.24	B	1.0	36	1530	602	126	900	576	10 x 10	Effect of Burned Out Rods
1084	21	1.24	B	1.0	38	1558	562	119	864	678	10 x 10	Hot Housing

a. Defined in Figure 2-3.

TABLE 3-1
FLECHT DATA SUMMARY, STAINLESS STEEL CLAD CONSTANT FLOW TESTS,
HOT ROD MIDPLANE ELEVATION (6-Foot)

Final Report and in Appendix A of References 2 and 3 and Appendix C of Reference 1. Appendix A of this report contains additional data for the current runs. It should be noted that the quench temperature data presented in Table 3-1 and in Appendix A is approximate. More accurate quench temperature data and a discussion of parameter effects on quench temperatures are contained in Appendix E of the FLECHT Final Report.

Although the preceding parameters are useful for characterizing test results and for parameter sensitivity studies, an understanding of heat transfer coefficient behavior is necessary to apply FLECHT test results to the prediction of reactor fuel rod behavior. Heat transfer coefficients were therefore calculated for each run, using the DATAR computer code. This code performs a transient conduction calculation based on a known temperature (heater rod thermocouple) on the inside surface of the rod cladding, and a known power generation rate. The code calculated the rod surface temperature, surface heat flux and heat transfer coefficient as a function of time. The reference heat sink temperature is the system saturation temperature for heat transfer coefficients.

Inputs to the program were the transient heater rod thermocouple temperature history, heat generation rate as a function of time, and the temperature-dependent material properties. In determining the heat generation rate, the following empirical factors were applied to the nominal axial power distribution:

<u>Elevation (ft)</u>	<u>Factor</u>
2	1.030
4	1.016
6	0.977
8	1.016
10	1.030

These factors were due to a change in heater resistance which occurred as a result of swaging the heater rods during manufacture. It should be noted that the peak powers reported in Table 3-1 and elsewhere in this report do not include the 0.977 midplane power distribution factor.

The transient clad temperature and heat transfer coefficient outputs were obtained from the DATAR code, both as printout and plots. The graphs presented in Appendix A of this report were obtained directly from the computer plotting routine.

A detailed discussion of the assumptions and numerical techniques employed in the analysis is included in Reference 2.

3.2 DATA VERIFICATION

3.2.1 Checkout Runs and Data Repeatability

Several checkout runs were performed in this test series to determine that the system was performing properly and that the heat transfer data was consistent and repeatable with respect to the previous data reported in WCAP-7665. Figure 3-2 compares heat transfer coefficients from repeat runs at a 2 in./sec flooding rate for different test series at the 4, 6, and 8 ft elevations. Figure 3-3 compares the midplane heat transfer coefficients for two repeat runs at 1 in./sec. Good repeatability between the previous and current results is shown. In addition, Figure 3-3 shows excellent agreement between runs with the same run conditions for two different bundle sizes, 7 x 7 and 10 x 10. Figure 3-4 demonstrates a repeatability check for two runs within this additional test series.

Table 3-2 shows all the repeat runs done in the FLECHT program, listing the temperature rise, turnaround time and quench time at the 6-foot elevation. Absolute difference between the runs is shown in parentheses.

In general, the values agree to within a few degrees or seconds. The turnaround time is rather difficult to measure in low flooding rate tests because the slope of the temperature-time curve becomes quite small at times near turnaround, whereas, at a high flooding rate, turnaround occurs quickly.

Temperature rise between runs 1002 and 3541 differs by about 20°F, but this may be due to a hotter housing temperature at low elevations. A hotter housing tends to give a smaller temperature rise and a longer quench time.

Another comparison may be made with heat transfer coefficients for some of these runs. Figures 3-5 through 3-9 are examples of this, with a ± 5 percent band

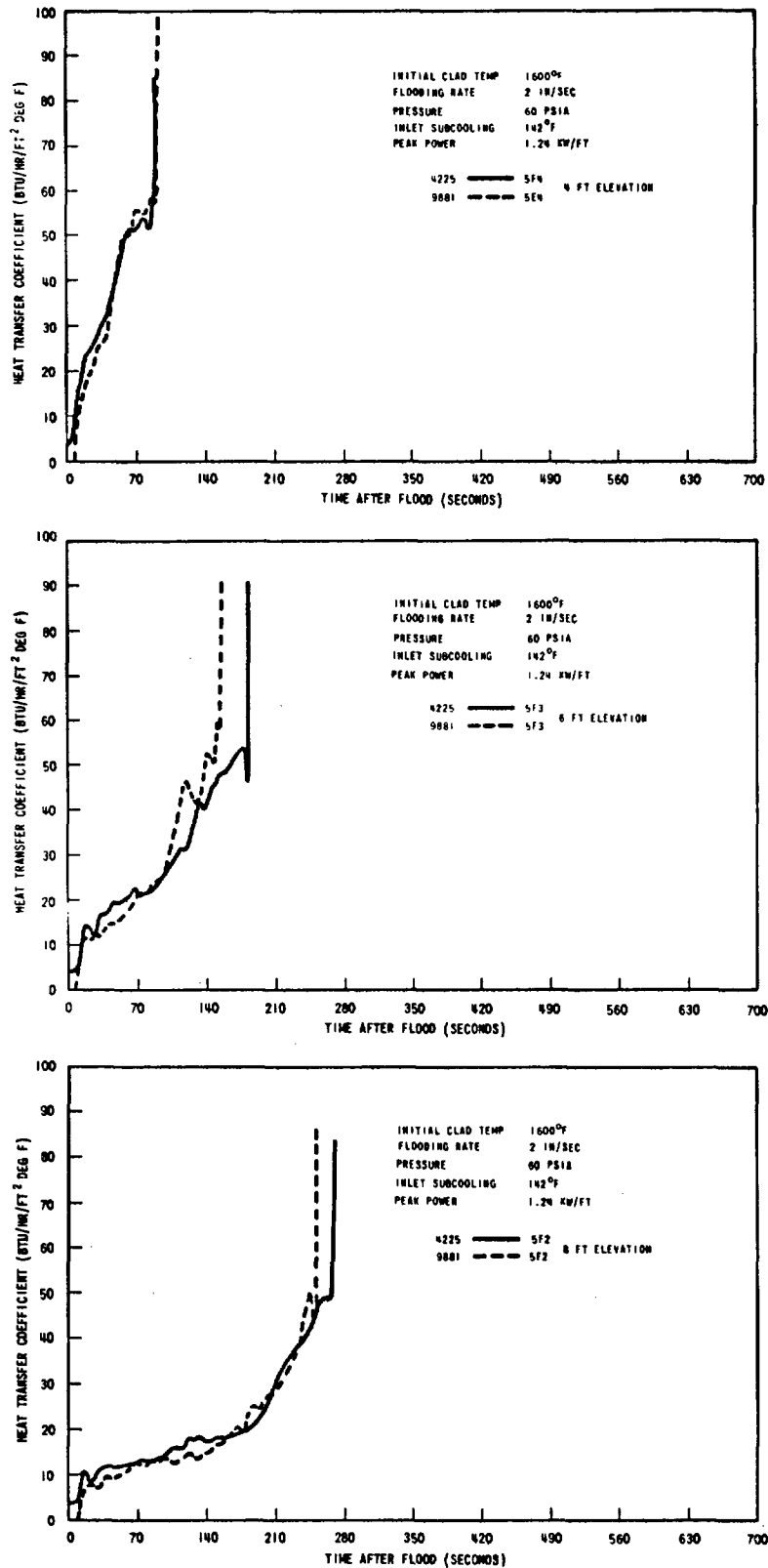


Figure 3-2. Repeatability of Heat Transfer Coefficient for Current and Previous Test Series - 2 In/Sec Flood Rate

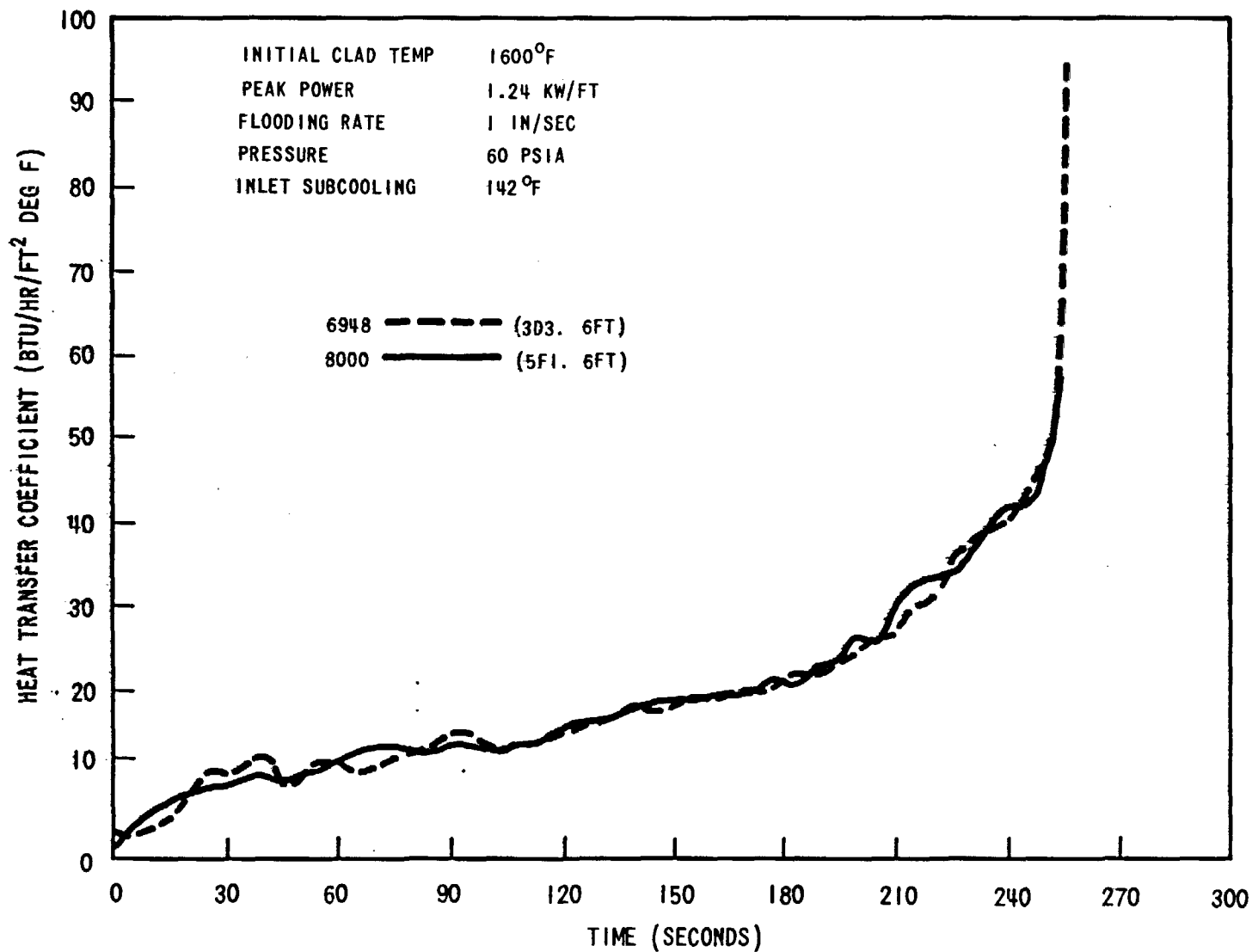


Figure 3-3. Repeatability of Midplane Heat Transfer Coefficient for Current and Previous Test Series - 1 In. Sec Flood Rate.

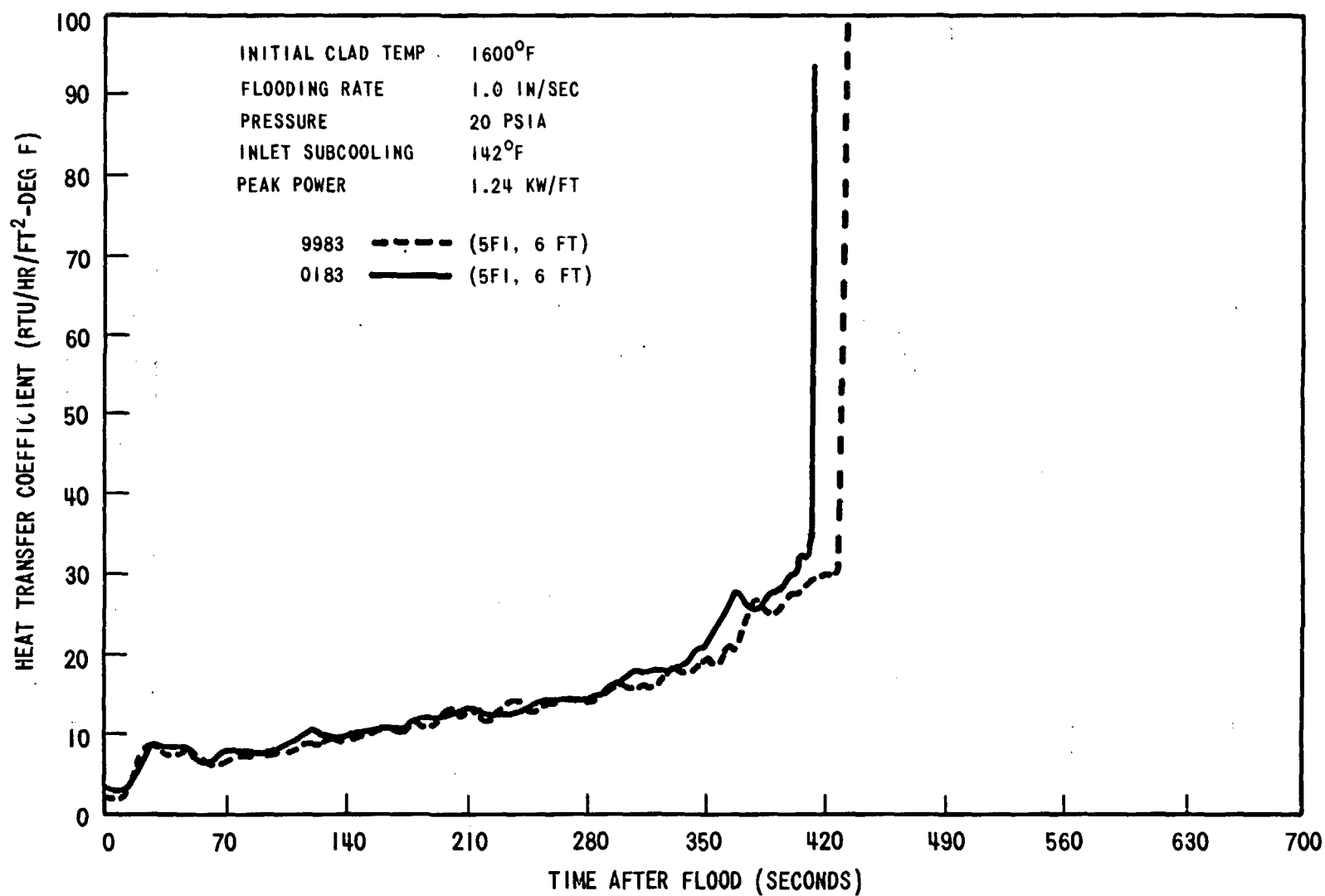


Figure 3-4. Repeatability of Midplane Heat Transfer Coefficient for Current Test Series.

TABLE 3-2

REPEATABILITY CHECKS

Run No.	Test Conditions*			Temp. Rise °F	Turnaround Time sec	Quench Time sec
	Flooding Rate in/sec	Clad Temp. °F	Sub- Cooling °F			
6948-8000	1	1600	142	465-422(43)	95-74 (21)	266-262 (4)
1002-3541	6	1600	142	70-90 (20)	6-8 (2)	76-71 (5)
1720-3920	6	1600	22	53-54 (1)	7-5 (2)	165-162 (3)
4225-9881	2	1600	142	247-293(46)	35-43 (8)	192-164 (28)
3642-4442	6	1800	142	62-69 (7)	5-5 (0)	87-74 (13)
3642-5642	6	1800	142	62-67 (5)	5-6 (1)	87-75 (12)
4442-5642	6	1800	142	69-67 (2)	5-6 (1)	74-75 (1)
9983-0183	1	1600	140	668-636(32)	146-142(4)	424-420 (4)

* Additional common test conditions:

Pressure - All runs 60 psia, except 9983-0183 20 psia

Peak power - 1.24 kw/ft

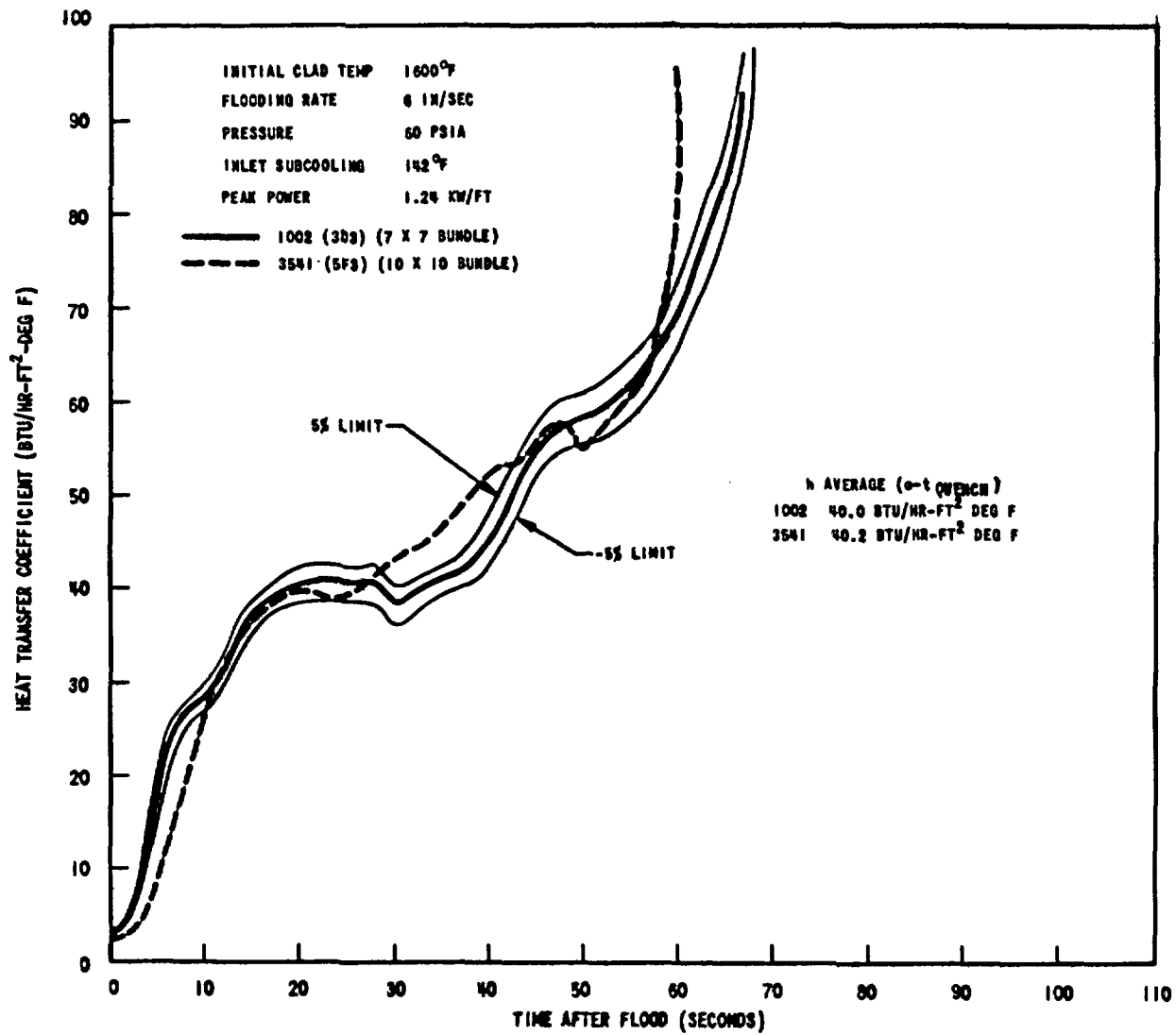


Figure 3-5. Repeatability of Midplane Heat Transfer Coefficient for High Flooding Rate, High Pressure and High Subcooling

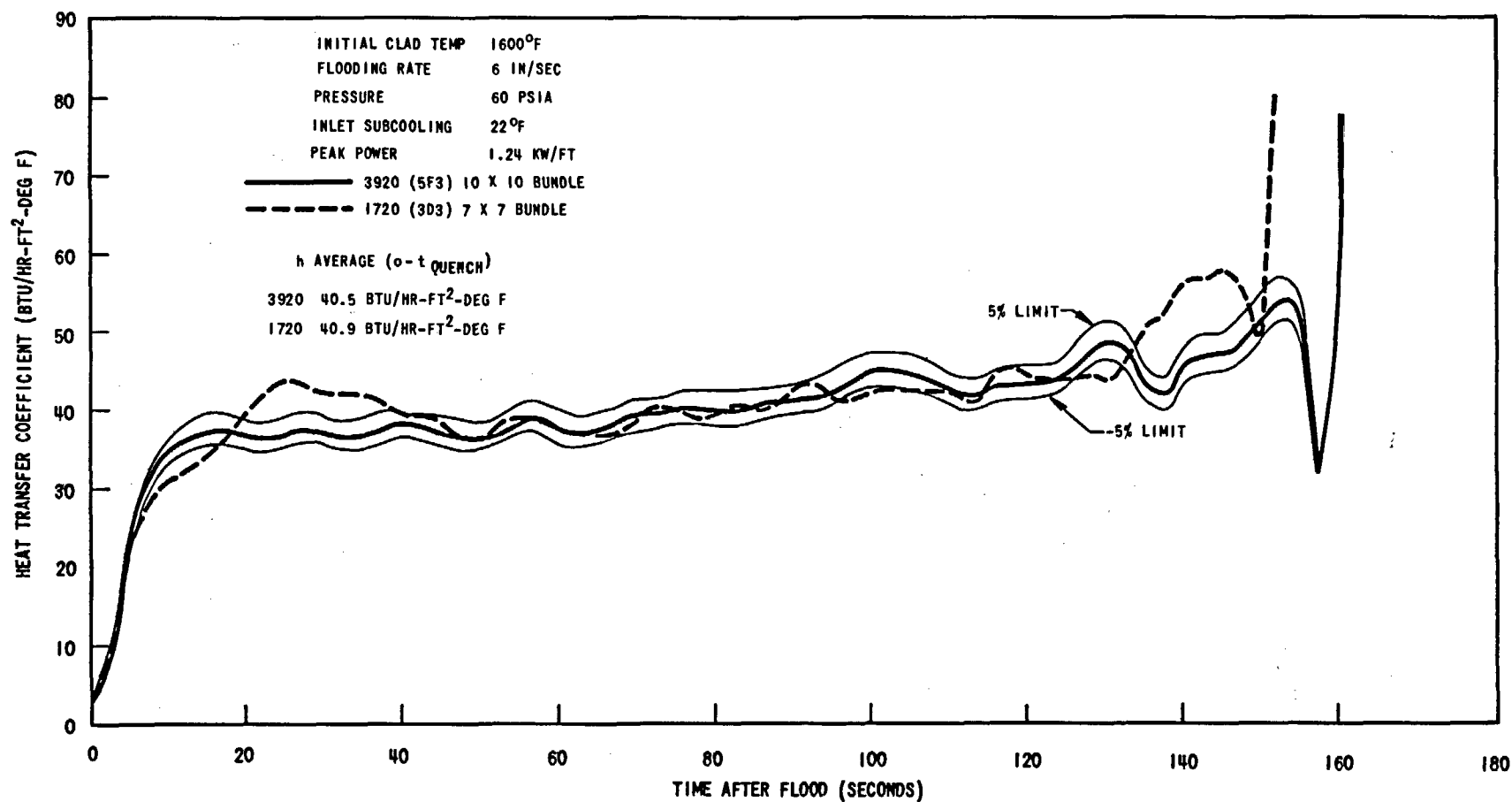


Figure 3-6. Repeatability of Midplane Heat Transfer Coefficient for High Flooding Rate, High Pressure and Low Subcooling

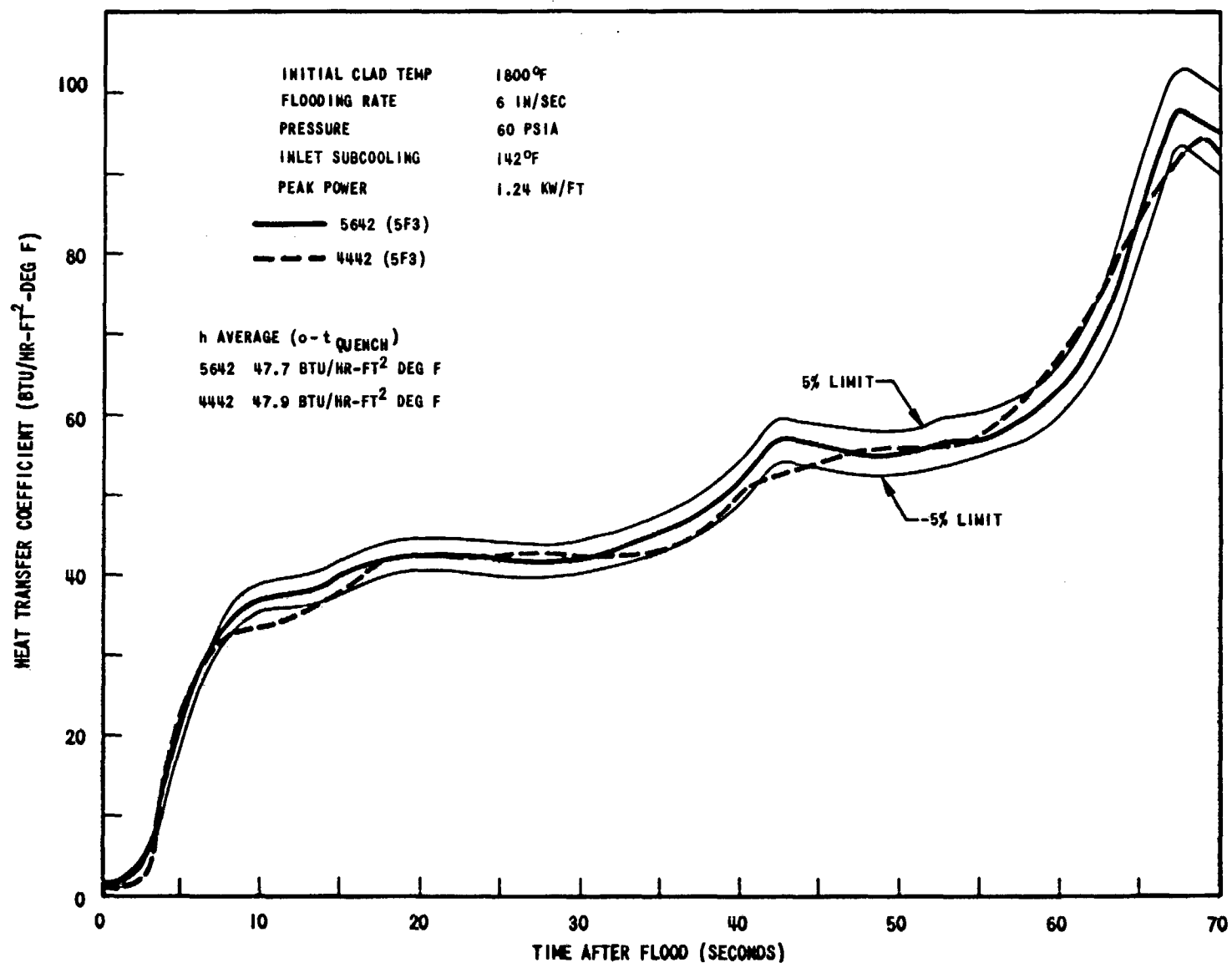


Figure 3-7. Repeatability of Heat Transfer Coefficient at High Flooding Rate, High Pressure, High Subcooling and 1800°F Initial Clad Temperature

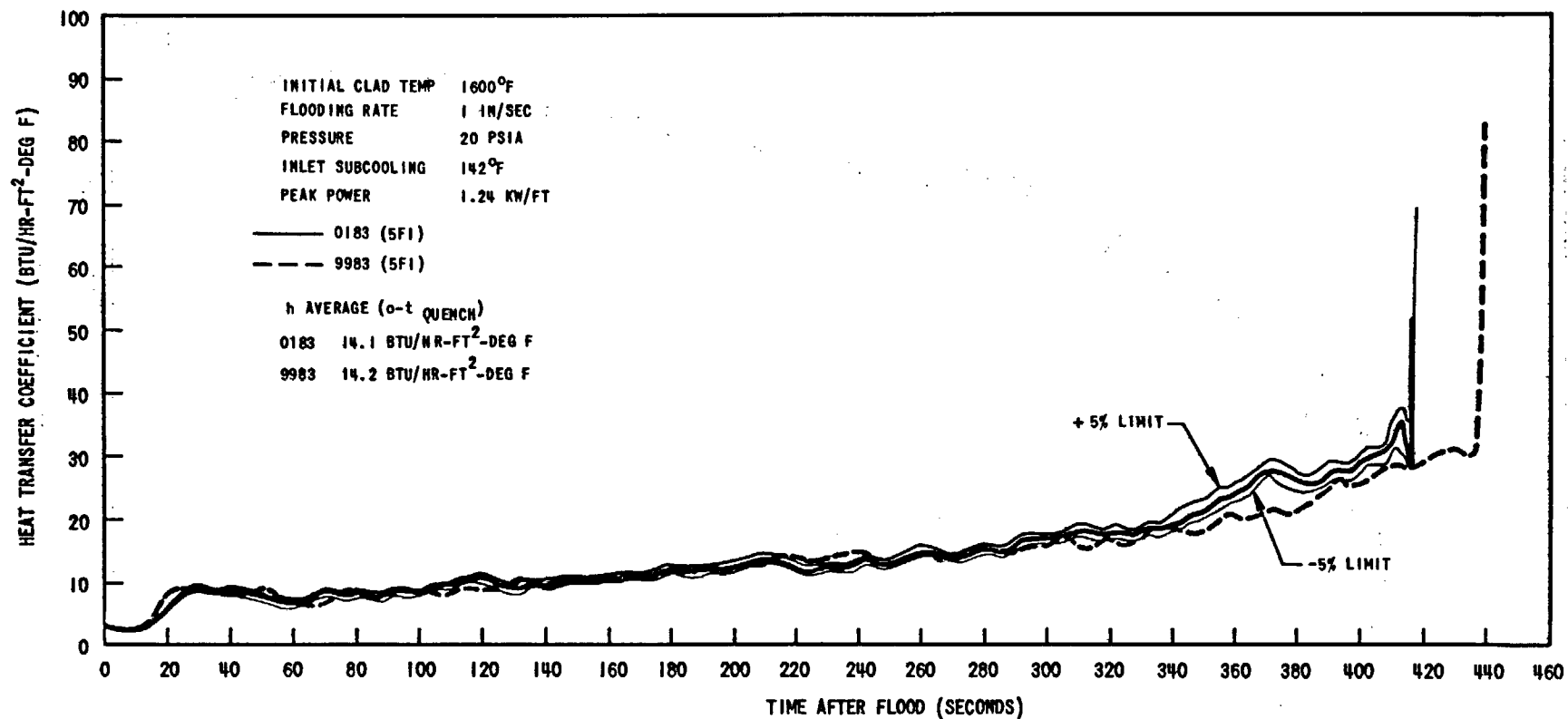


Figure 3-8. Repeatability of Heat Transfer Coefficient at Low Flooding Rate and Low Pressure

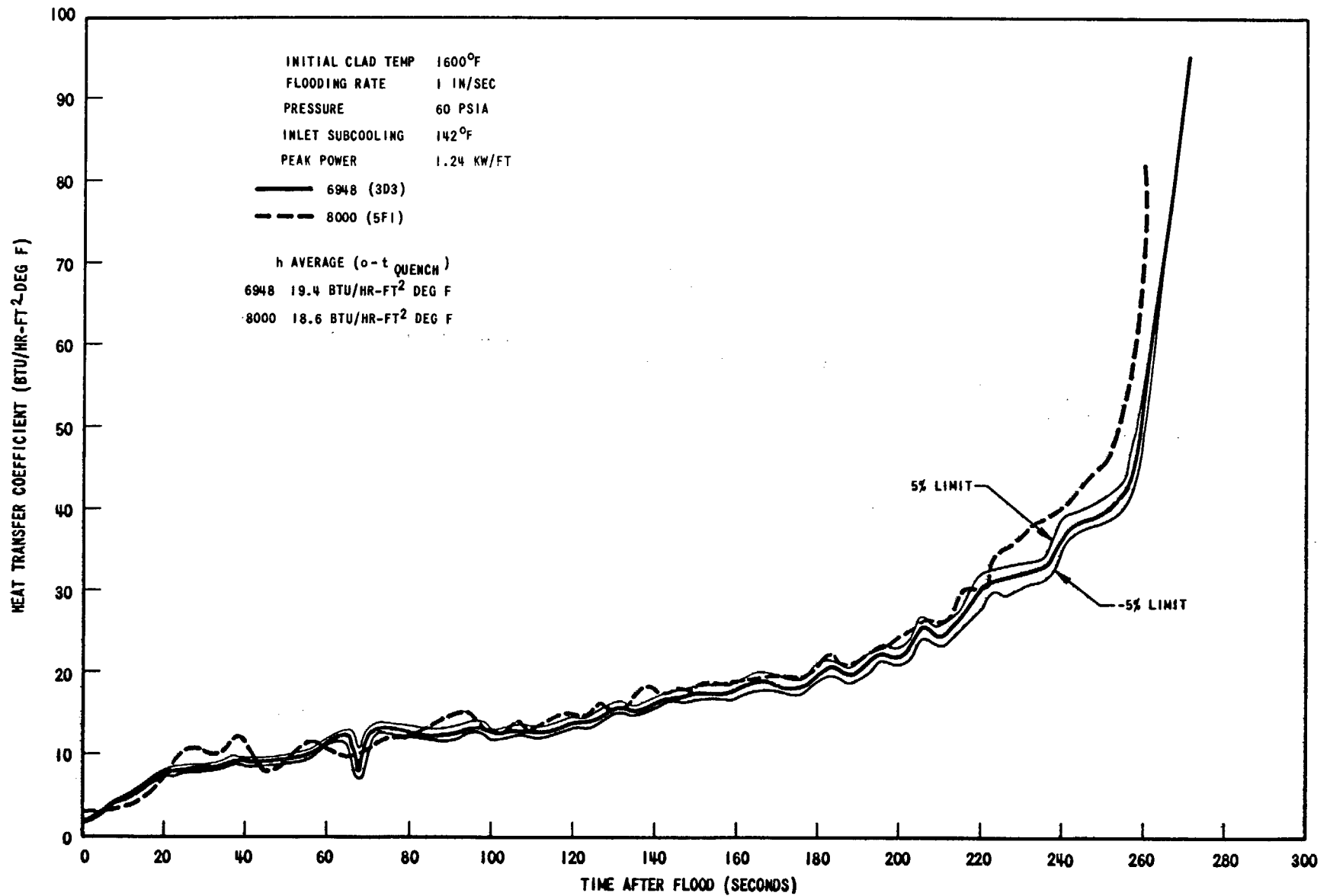


Figure 3-9. Repeatability of Heat Transfer Coefficient at Low Flooding Rate and High Pressure

drawn on one of the curves. The average heat transfer coefficients from zero to the quench time are also shown on the plots. In general, the heat transfer coefficients of the repeat runs fall within the ± 5 percent band. Small oscillations of the heat transfer coefficients cause the curve to fall above and below the band fairly equally. The average heat transfer coefficients (determined by integrating the curves out to the quench time) are within 3 percent of each other for each pair of runs. Based on these curves, reproducibility of the FLECHT data should be described as within 3 percent on a time-integrated basis, with some random deviations on the order of 5 - 10 percent for short periods of time.

3.2.2 Rod Bundle Housing

The test section consisted of a full-length rod bundle with either a seven-by-seven or a ten-by-ten rod array enclosed by a heated housing. Since the housing represents a boundary not present in an actual reactor, its effect on the observed hot rod heat transfer needs to be well understood. In particular, the effectiveness of the housing heating and possible radiation heat transfer effects must be evaluated. The following discussion treats these points in more detail than does WCAP-7665, and describes experimental data quantifying the radiation heat transfer effects.

3.2.2.1 Housing Temperature Criteria

The rod bundle housing is heated to simulate the local energy input of an equivalent row of heater rods to the peripheral flow channels. If the housing acts as an equivalent row of rods, then the bundle will behave as though it were a part of a larger array. Thus, simulation of the local energy input from an equivalent row of heater rods by controlling the housing wall temperature should result in no significant difference between the behavior of seven-by-seven and ten-by-ten bundles, except for possible radiation effects. The required simulated energy input is determined by integrating the rod heat flux along the length from inlet to midplane during the time interval from the start of flooding until quenching occurs at the heater rod midplane.

The time of the midplane quench was selected for use in the criteria since the test data, as shown in Figure 3-10 in the following section, indicates that temperature rise and turnaround time are relatively insensitive to the housing temperature. Therefore, the test results during the period up to the time of temperature turnaround will not be affected significantly by the behavior of the flow housing. Conversely, quench time is sensitive to the initial flow housing temperature, as can also be seen in Figure 3-10. Thus, the housing temperature was chosen such that the housing acts as an equivalent row of rods from the inlet elevation to the midplane elevation over the time from start of flooding to quench of the midplane thermocouples.

For a given set of run conditions, the required housing temperature was calculated based on estimates of the quench time. The quench time was obtained from the previous experimental data and by extrapolation of this data to other run conditions. These extrapolations were continuously updated to include all previous quench time data. Therefore, the proper initial housing temperature could be calculated as a function of flooding rate, power density, inlet coolant temperature, pressure, and initial heater rod temperature, assuming the housing and heater rod temperature were at saturation upon completion of quench. The test data showed that the lower half of the housing quenched to the saturation temperature at the time the local peripheral rods quenched at the midplane elevation, thereby justifying the use of saturation temperature.

3.2.2.2 Effect of Housing Temperature

Identical FLECHT tests were run with different housing temperatures in an attempt to determine the housing temperature effect. Tests were performed at six in./sec, one in./sec, and at variable flooding rates. Figure 3-10 shows the effect of housing temperature on temperature rise, turnaround time and quench time at six and one in./sec flooding rates. Figure 3-11 shows the six-foot elevation heat transfer coefficients for the three runs at different average housing temperatures. The housing temperature did not strongly affect the temperature rise and turnaround time at six in./sec, although there was a slight trend toward decreasing temperature rise and turnaround time with increasing housing temperature. This

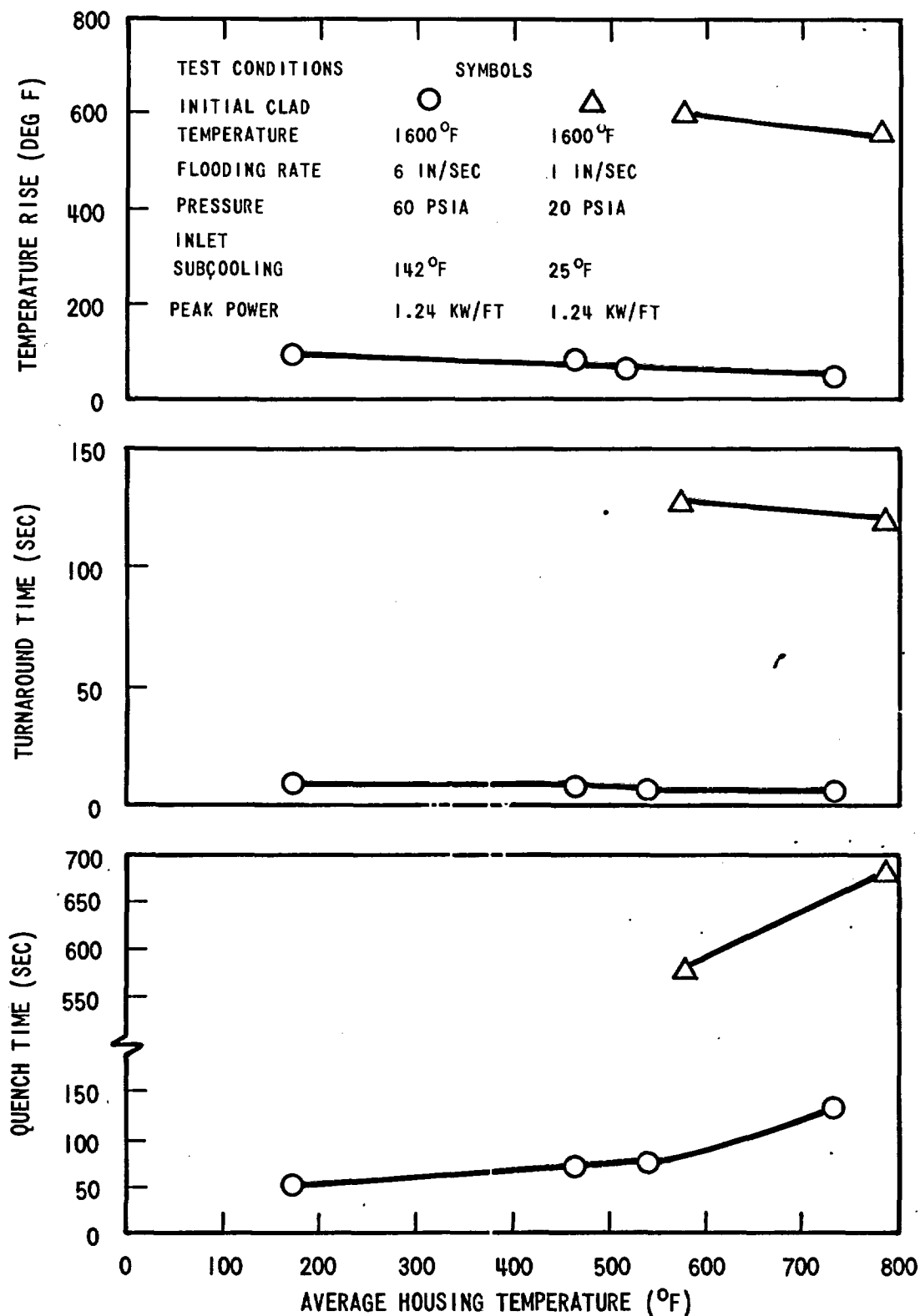


Figure 3-10. Effect of Housing Temperature on Temperature Rise, Turnaround Time and Quench Time.

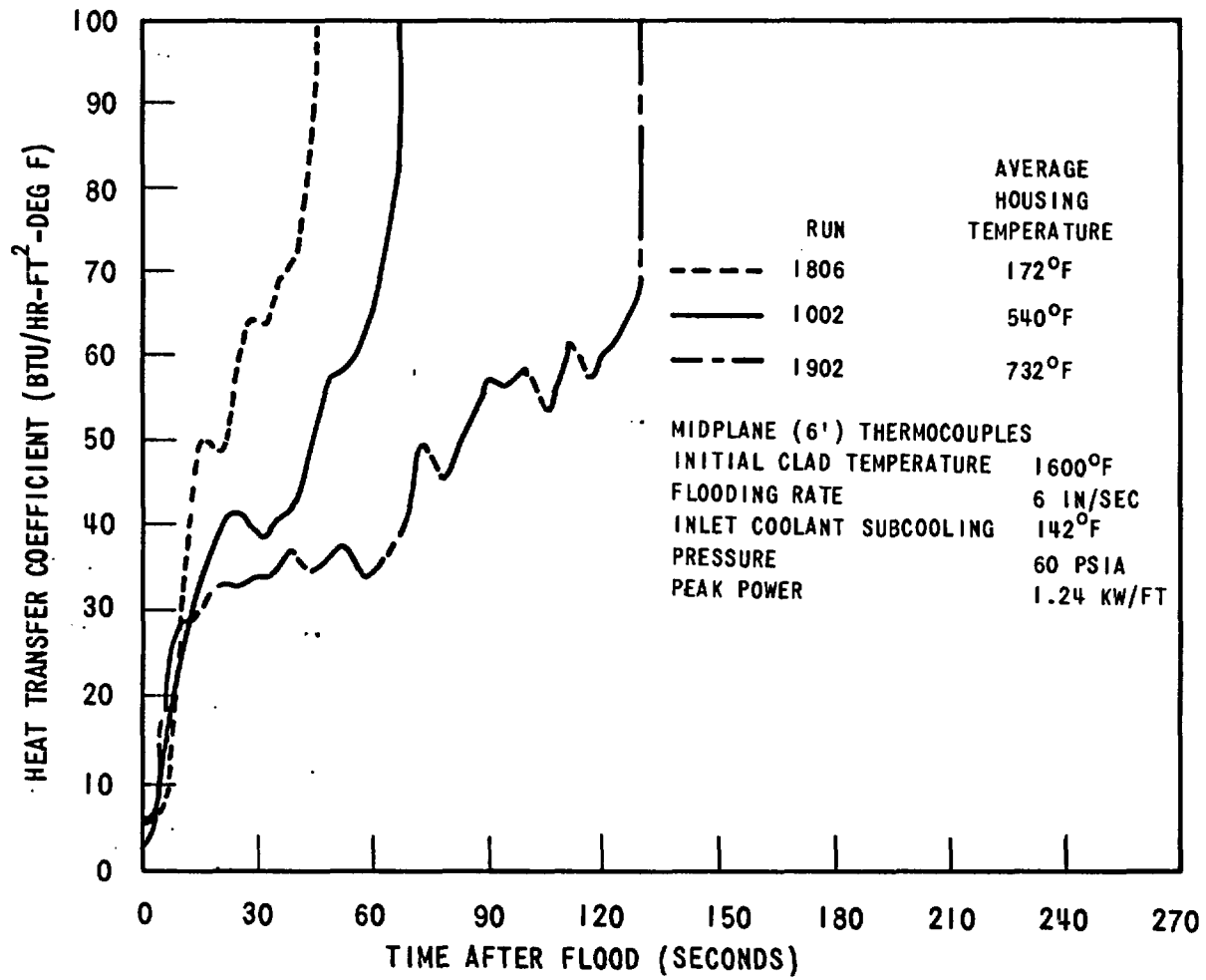


Figure 3-11. Effect of Housing Temperature on Heat Transfer Coefficient

trend would tend to exist because the heat released by the hot housing caused additional steam generation and entrainment early in the run. This same effect can be seen in the heat transfer coefficients, which were improved at early times for the hotter housing tests. Quench time increased with increasing housing temperature. Comparing the runs with a 540°F and 732°F average housing temperature, the quench time increased by 75 percent. The heat release from the hotter housing increased entrainment and therefore the quench front advanced more slowly. The high housing temperature run had the lowest heat transfer coefficient after the first ten seconds, which was due to the slower moving quench front.

A similar study was done at one in./sec flooding rate for a low pressure, low subcooling run. Run 0984 had a "normal" housing temperature and run 1084 had a higher housing temperature. The temperature behavior of the center hot rod and initial housing temperature distribution is given in Table 3-3. Again the same trend occurred. The temperature rise and turnaround time were lower for run 1084, which had a higher temperature housing. The quench time was about 15 percent longer for run 1084. Figure 3-12 shows a very small housing temperature effect on the midplane heat transfer coefficients for those two runs. The overall effect of housing temperature thus is smaller at low flooding rates, compared to that at high flooding rates.

The effect of the lower housing elevation heat release early in the transient causing entrainment and higher heat transfer was also investigated in variable flow runs 9077 and 9176. These tests determined if the reduction in housing temperature would decrease the steam generation rate early in the transient, resulting in decreased heat transfer coefficients and higher peak temperatures. The temperature behavior and initial housing temperatures are also given in Table 3-3. Run 9077 was performed with a "normal" housing temperature distribution. Run 9176 was performed with the same set of test conditions, but with reduced housing temperatures below the midplane. This was equivalent to matching the energy input from the housing and an outer row of rods over a shorter period of time than the 6 foot quench time. Also, the midplane housing temperatures were the same, thus midplane heat transfer would not be influenced by radiation to a lower temperature housing if this were a significant effect.

TABLE 3-3

EFFECT OF HOUSING TEMPERATURE ON CLAD TEMPERATURE RESPONSE

Run	Press psia	Flooding Rate (In/sec)	ΔT_{Sub} (°F)	Peak Power (Kw/ft)	T_{Initial} (°F)	ΔT_{Rise} (°F)	t_{turn} (sec)	t_{quench} (sec)	T_{Housing} (°F)		
									6' Elev	Avg to 6'	Avg to 4'
0984	21	1.0	36	1.24	1530	602	126	576	736	576	512
1084	21	1.0	38	1.24	1558	562	119	678	1013	785	707
9077	55	6.2-1.0 ⁽¹⁾	142	1.24	2138	42 ⁽²⁾	4	276	783	634	585
9176	58	5.9-1.0	140	1.24	2197	34 ⁽²⁾	4	239	794	490	396

(1) 6.2 in/sec for 4 sec and 1 in/sec rest of run

(2) First peak

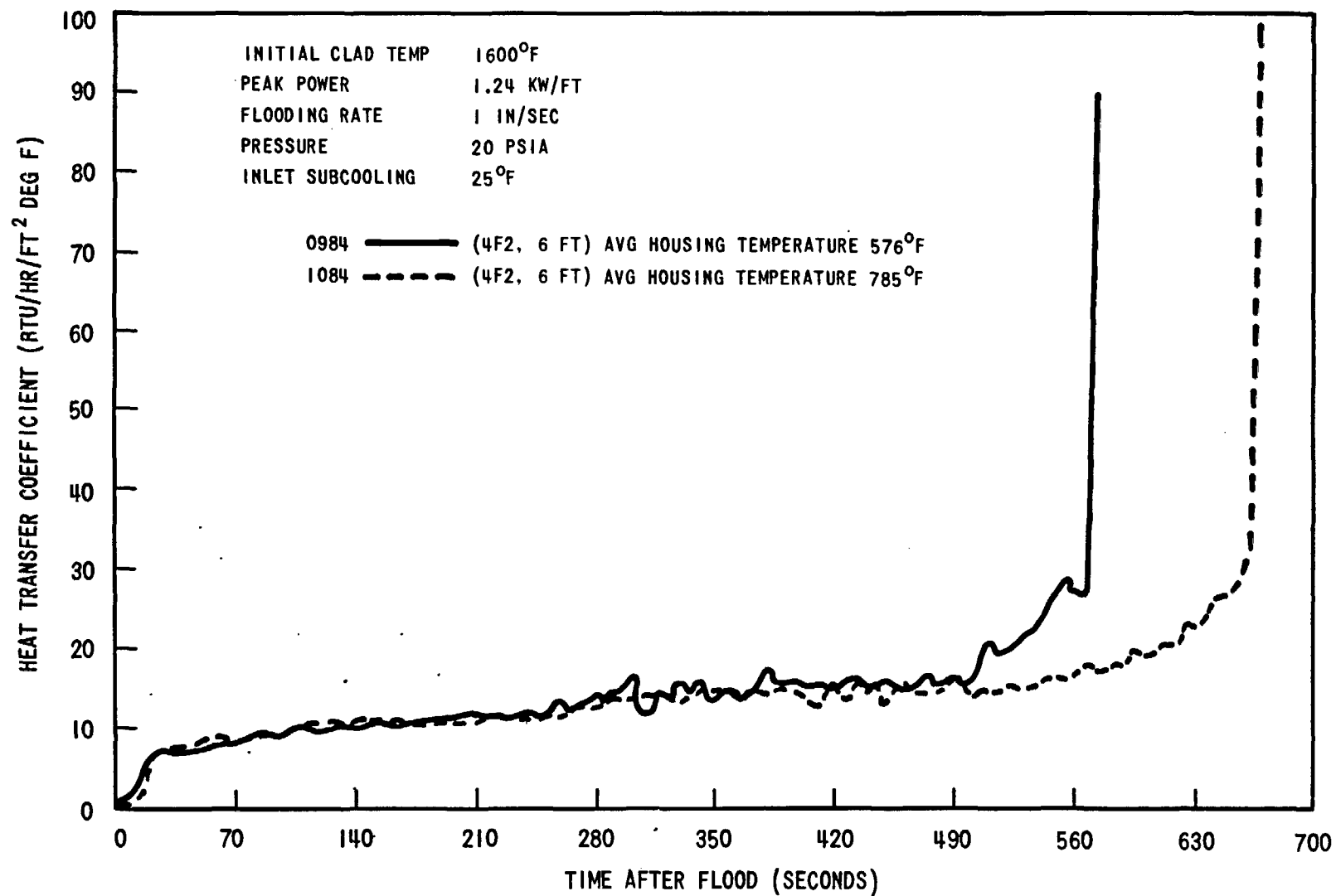


Figure 3-12. Effect of Housing Temperature at 1 in./sec Flooding Rate.

As can be seen in Table 3-3 and Figure 3-13, the reduction in housing temperatures did not have any significant effect on the temperature rise occurring during the two runs. As anticipated, however, the reduction in housing temperatures did cause a slight decrease in the value of the first peak of the heat transfer coefficient, and reduced the quench time by about thirty seconds.

The FLECHT housing temperatures were specified to simulate the heat release of an equivalent row of rods from the zero to midplane elevation over the time interval from the start of flooding to the time of the midplane heater rod quench. While this criteria was specified for the integral heat release, the rate of heat release also was examined. Figure 3-14 shows a comparison of the integrated heat release for the housing and an equivalent row of rods for a one in./sec flooding rate over the lower half of the housing. The agreement is excellent early in the transient for this low reflooding rate run. Further insight into housing behavior can be shown by analysis of the rate of heat release at the lower elevation (2 ft) for runs 9077 and 9176 to infer the effect of housing heat release on vapor generation, hence the midplane heat transfer coefficient.

The results of a calculation of the rate of heat release from the housing and an equivalent row of rods are shown in Figures 3-15 through 3-17. (See Appendix B for the method of calculation.) Figure 3-15 shows that the rate of heat release from the normal temperature housing at the 2-foot elevation is high in comparison with the rate of heat release of an equivalent row of rods, while the rate of heat release from the cold housing matches the rate of heat release of an equivalent row of rods. Figure 3-16 is a plot of the rate of heat release from the 0 to 6-foot elevation. It reveals that the rate of heat release below the 6-foot elevation of the normal temperature housing and an equivalent row of rods are about the same, and are in the same trend, whereas that of the cold housing is too low at early time and too high at later time.

Figure 3-17 shows the total heat release from 0 to 6-foot elevations from the beginning of flood to time t . The total heat release of the normal temperature housing and the equivalent row of rods match at the 6-foot quench time, as is expected from housing temperature criteria, whereas the total heat release of a cold housing is too low.

Despite the differences in housing heat release as noted above, the heat transfer coefficient and temperature at the 6-foot elevation of runs 9077 and 9176

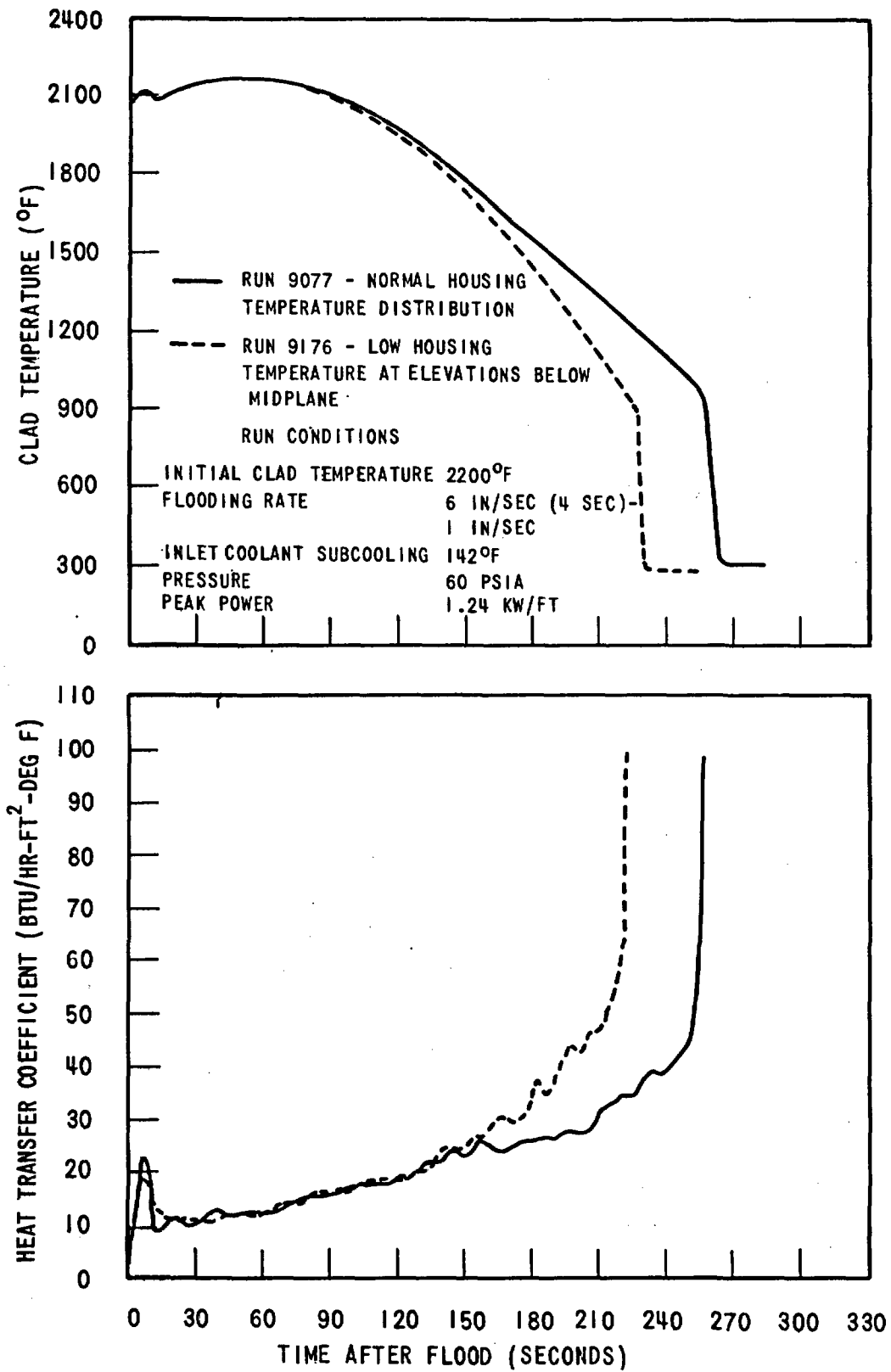


Figure 3-13. Effect of Low Housing Temperature at Elevations Below Midplane

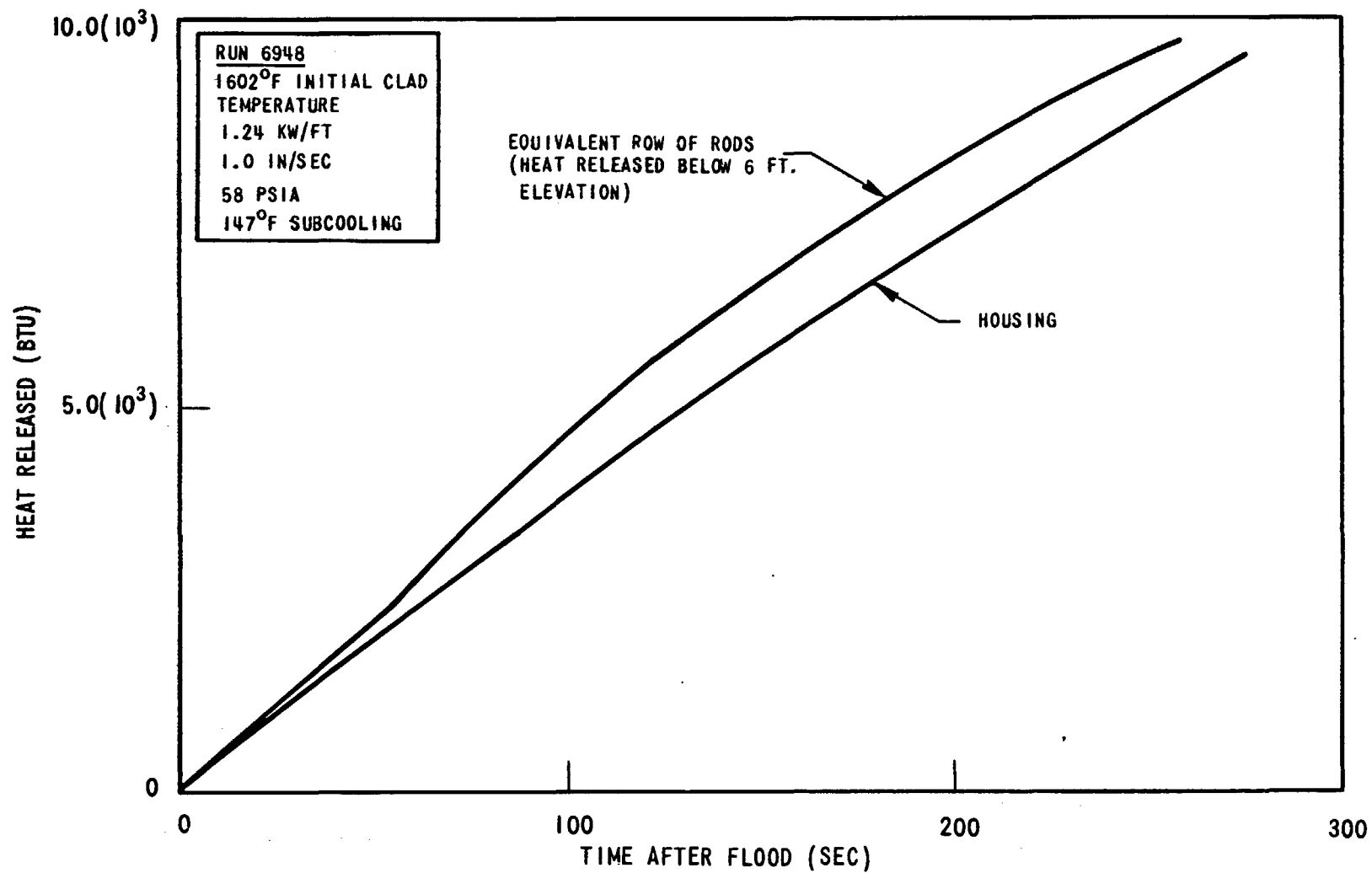


Figure 3-14. Comparison of Housing and Equivalent Row of Rods Integrated Heat Release

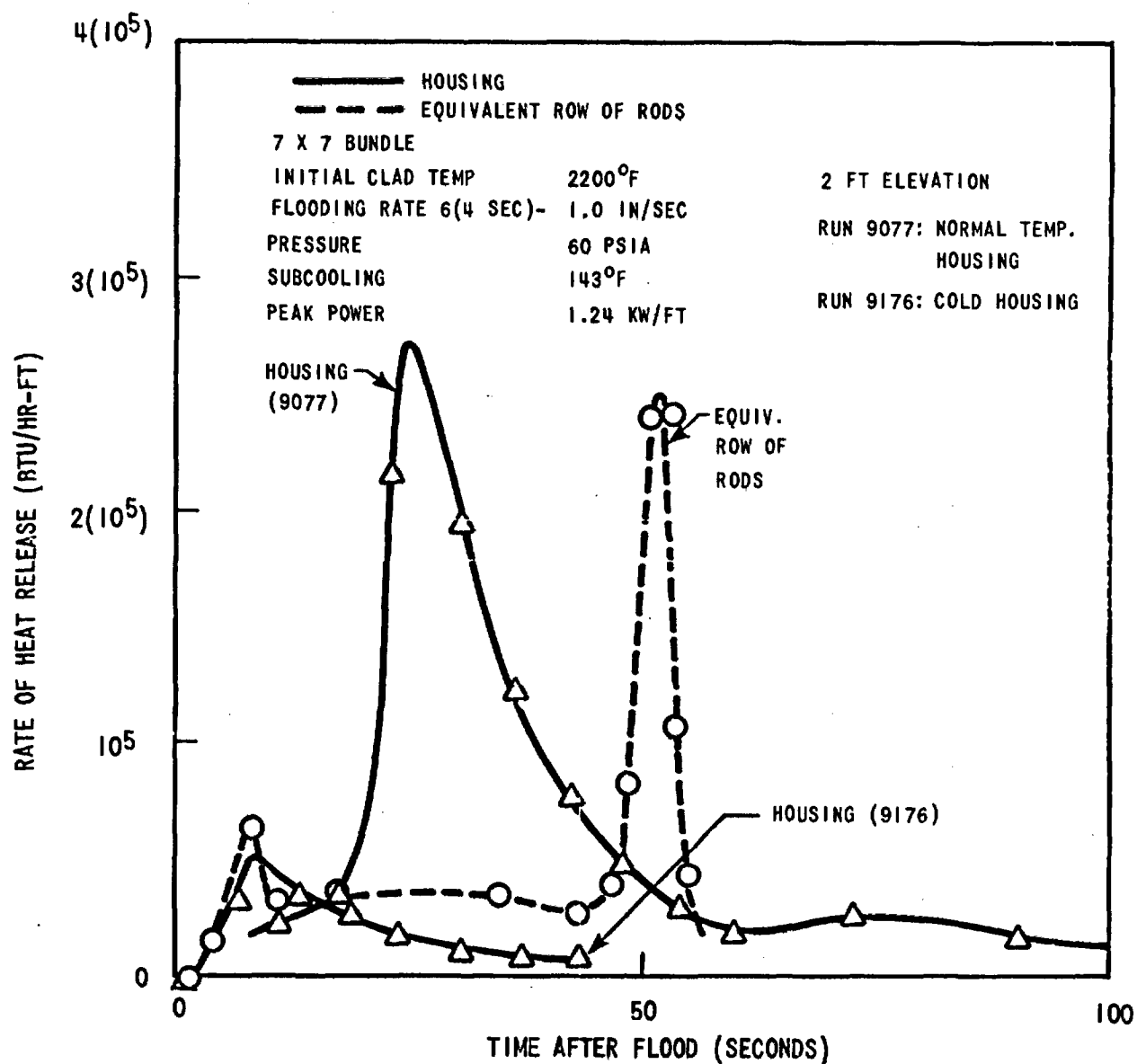


Figure 3-15. Comparison of the Rate of Heat Release at 2 Ft Elevation of a Normal Temperature Housing, a Cold Housing and an Equivalent Row of Rods.

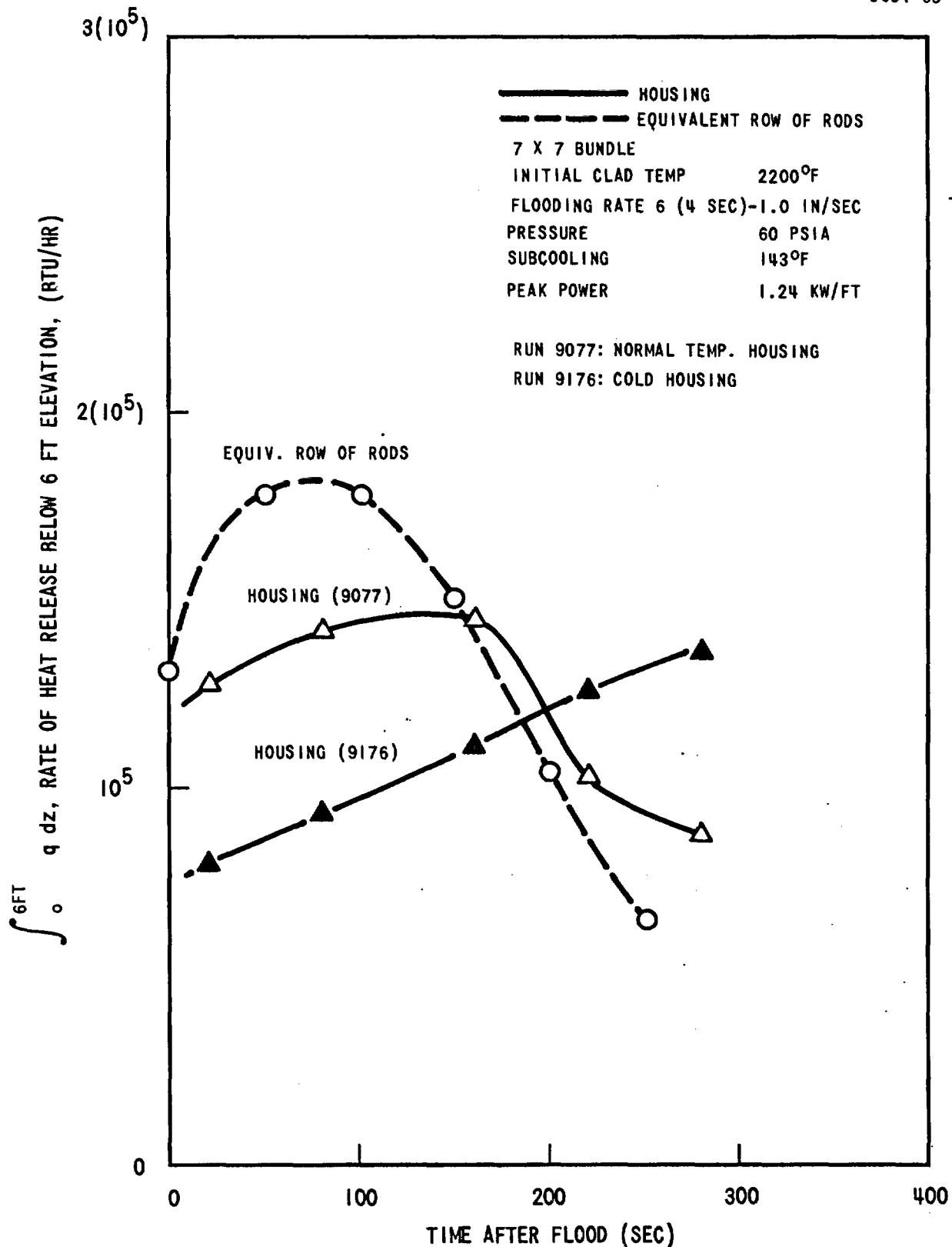


Figure 3-16. Comparison of the Rate of Heat Release Below 6 Ft Elevation of a Normal Temperature Housing, a Cold Housing and an Equivalent Row of Rods.

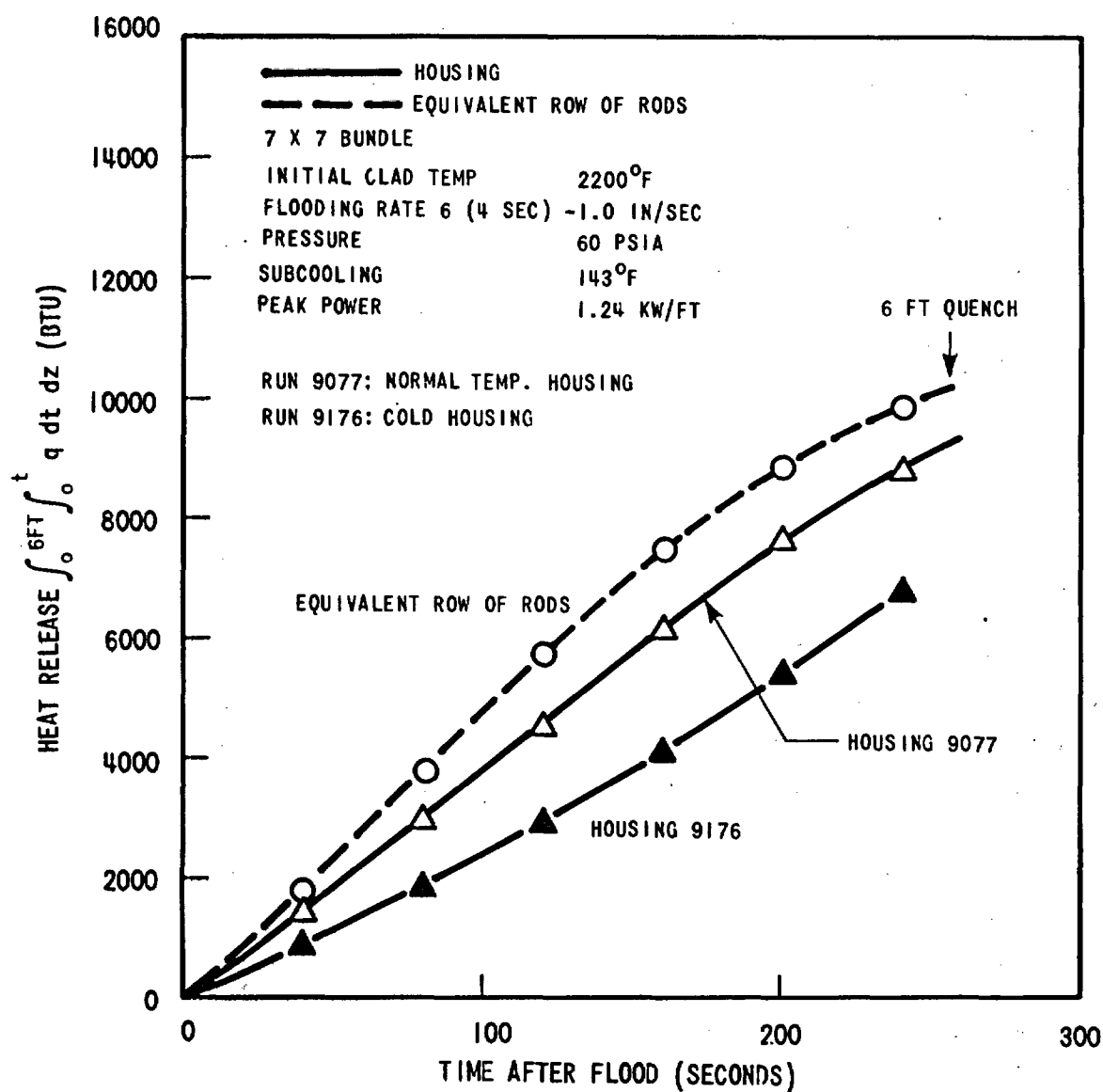


Figure 3-17. Comparison of Heat Release Below 6 Ft Elevation on a Normal Temperature Housing, a Cold Housing and an Equivalent Row of Rods.

are only slightly different, as shown in Figure 3-13, except at later time due to the difference in quench time.

3.2.2.3 Effect of Bundle Size and Radiation to the Housing

As noted in Section 3.2.2.1, simulation of the local energy input from an equivalent row of heater rods by controlling the housing wall temperature should result in no significant difference in behavior between the seven-by-seven and ten-by-ten rod bundles, except for possible radiation effects. In the ten-by-ten bundle, there is an extra row of rods between the central rods and the housing, thus radiation heat transfer to the housing, if significant, should give different heat transfer coefficients.

Several identical tests were performed in both seven-by-seven and ten-by-ten bundles, as shown in Table 3-4. Data in the table show that temperature rise, turnaround time and quench time are not affected by bundle size at high and low flooding rates. Figures 3-18, 3-19, and 3-20 show very good agreement of the heat transfer coefficients for equivalent rods in each pair of runs.

Figures 3-21 and 3-22 show the radial variation of the midplane heat transfer coefficients for runs with the seven-by-seven and ten-by-ten rod bundles at six in./sec and one in./sec flooding rates, respectively. There was good agreement between the heat transfer coefficients for all rods which were at least one row removed from the housing. In the seven-by-seven bundle, the rod in the outer row adjacent to the housing had a higher heat transfer coefficient for both high and low flooding rates. In the ten-by-ten bundle, the heat transfer coefficient for the rod in the outer row was higher only at a low flooding rate.

In all radial heat transfer coefficient distributions, except for the outer rod which showed a higher heat transfer coefficient due to radiation to the housing, there was no trend of an increasing heat transfer coefficient as the rod location moved toward the housing. The absence of this trend along with good agreement of midplane heat transfer coefficients of central rods in the 7 x 7 and 10 x 10 bundles indicates that radiation from the inner rods to the housing is not significant.

Calculations were performed to estimate the magnitude of the radiation from central rods in a ten-by-ten bundle due to the presence of the housing, using

TABLE 3-4

COMPARISON OF 7x7 AND 10x10 CENTRAL HOT ROD TEMPERATURE RESPONSE

Run No.	Pressure (psia)	Peak Power (kw/ft)	Flooding Rate (in/sec)	Inlet Subcooling (°F)	Initial Temperature (°F)
1002	56	1.24	6.0	137	1605
3541	57	1.24	5.9	141	1598
1720	61	1.24	5.9	25	1617
3920	55	1.24	5.8	16	1608
6948	58	1.24	1.0	147	1689
8000	58	1.24	1.0	156	1606

Run No.	Temperature Rise (°F)	Turnaround Time (sec)	Quench Time (sec)	Bundle Size
1002	70	6	76	7x7
3541	90	8	71	10x10
1720	53	7	165	7x7
3920	54	5	162	10x10
6948	465	95	266	7x7
8000	422	74	262	10x10

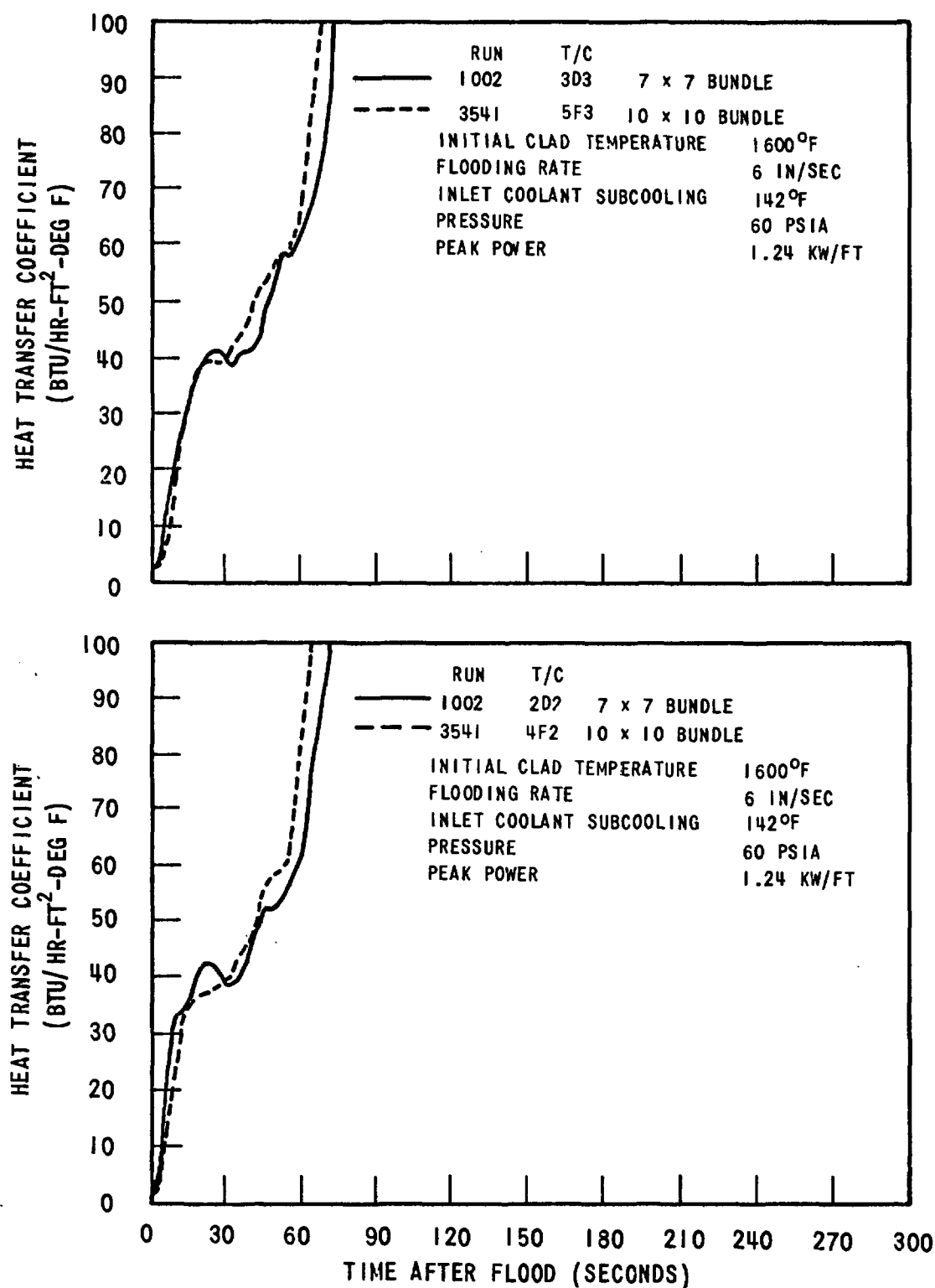


Figure 3-18. Heat Transfer Coefficients at Midplane of Equivalent Heater Rods in the 7 x 7 and 10 x 10 Bundles, Runs 1002 and 3541

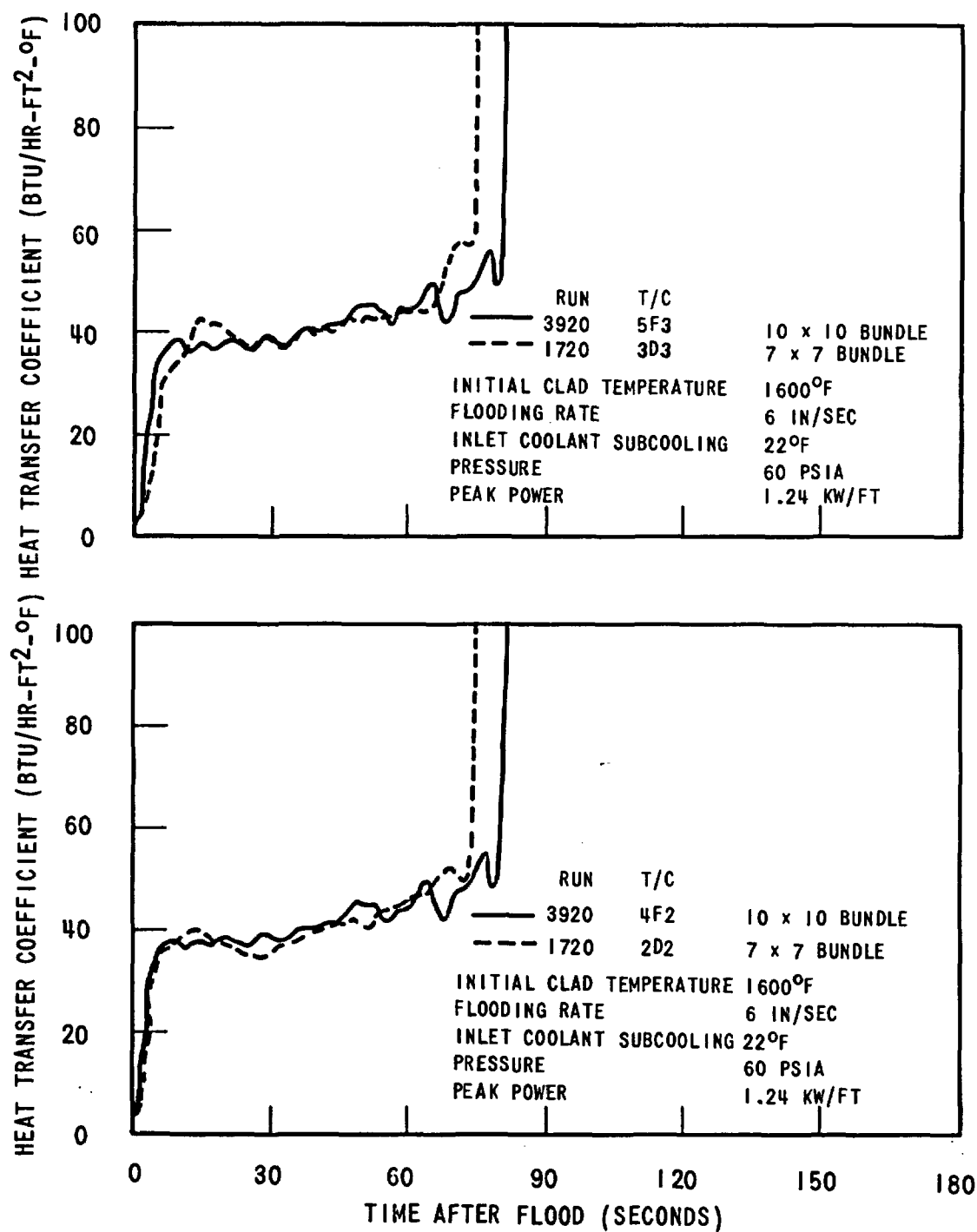


Figure 3-19. Heat Transfer Coefficients at the Midplane of Equivalent Heater Rods in the 7 x 7 and 10 x 10 Bundles, Runs 1720 and 3920

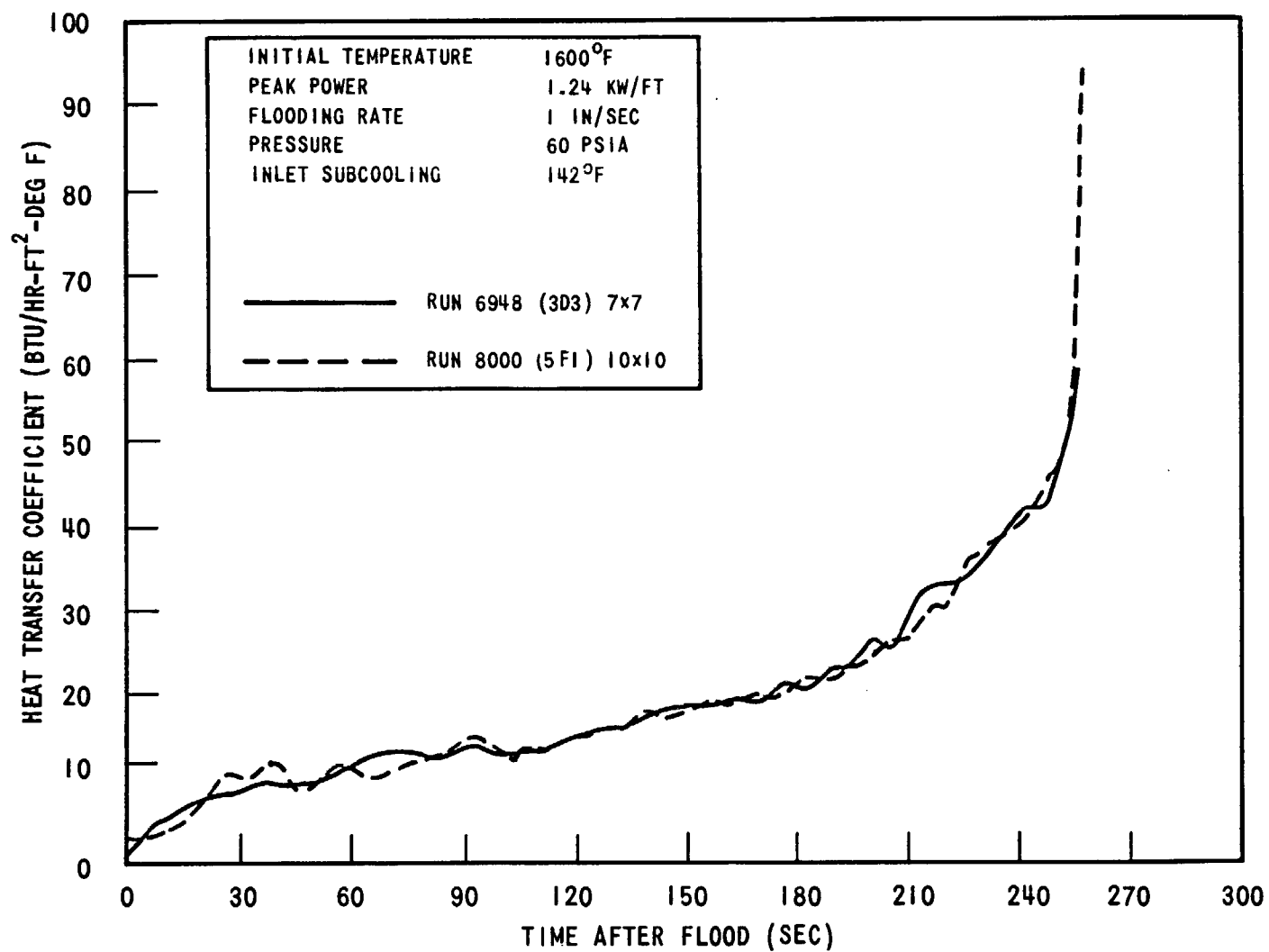


Figure 3-20. Comparison of Equivalent Central Rods in 7 x 7 and 10 x 10 Bundles for 1 in/sec Flooding Rate

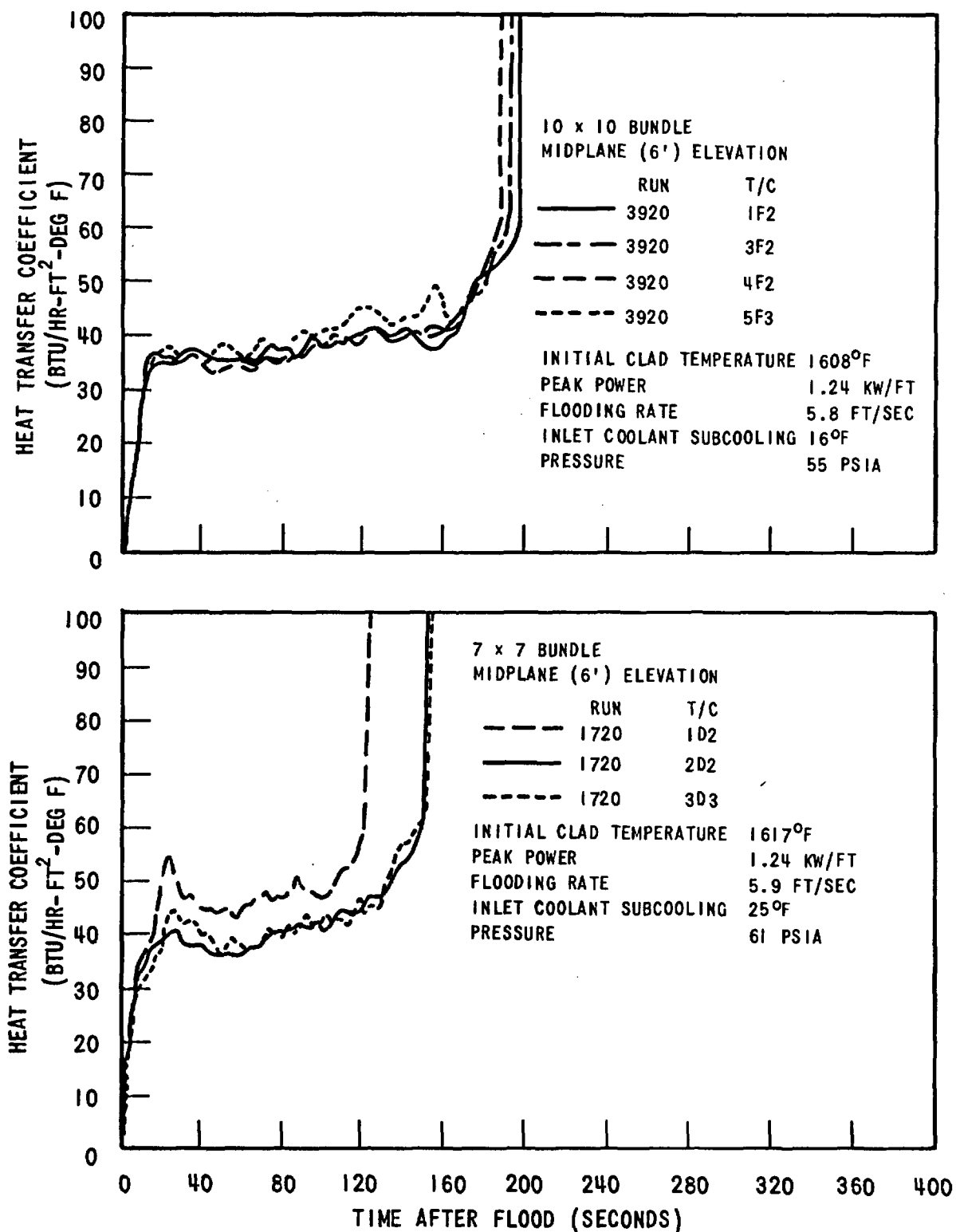


Figure 3-21. Radial Variation of Heat Transfer Coefficient for 10 X 10 and 7 X 7 Bundles at 6 in/sec.

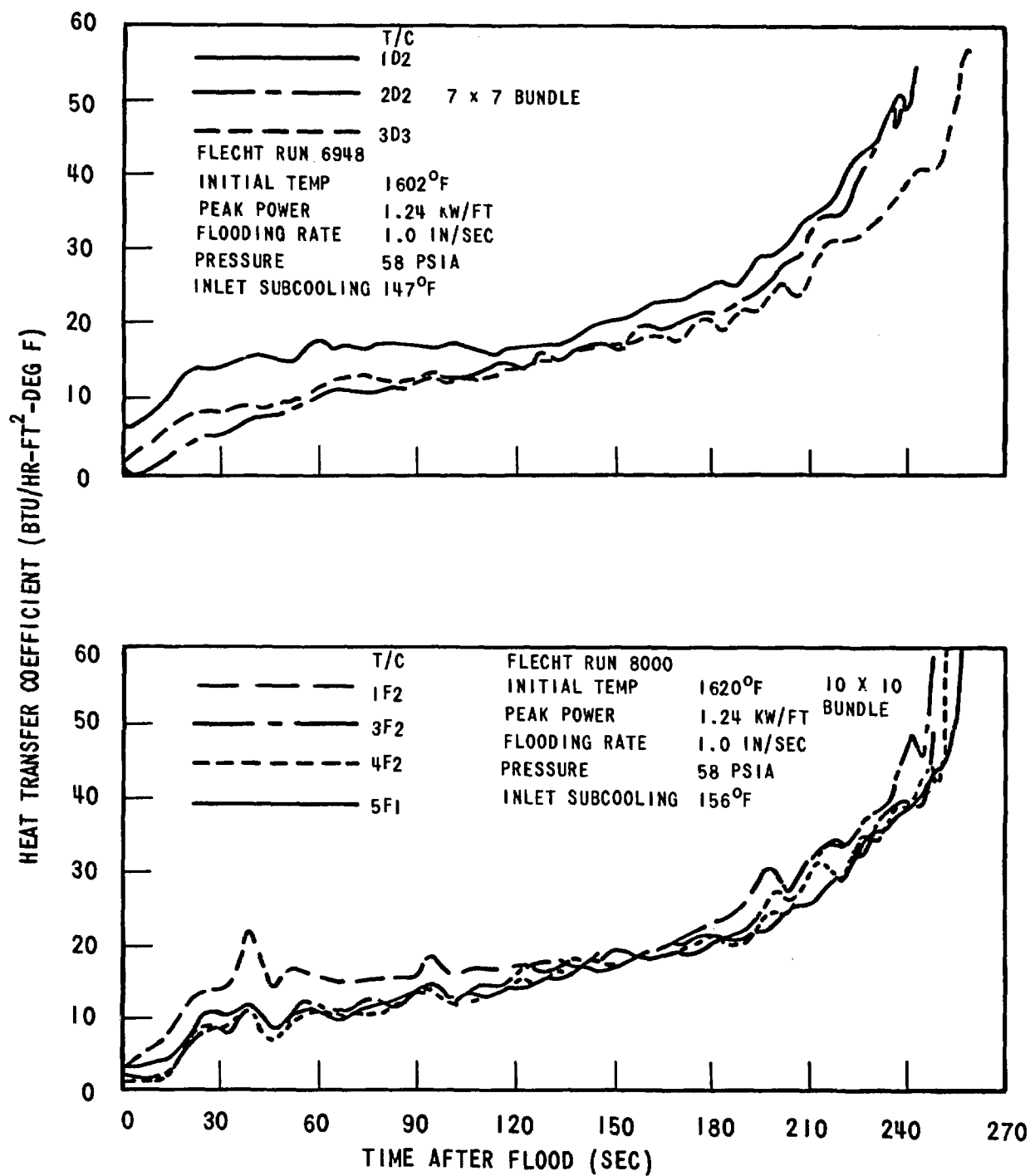


Figure 3-22. Radial Variation in Heat Transfer Coefficient for 10 X 10 and 7 X 7 Bundles at 1.0 in/sec.

typical rod and housing midplane temperatures. The results of the calculation for a FLECHT run are given in Table 3-5. The fifth column of Table 3-5 sets forth the radiation from a central rod to the outer rods due to the lower temperature of outer rods because of the housing, i.e., the differences between the heat transfer coefficient to the outer rods computed with the actual outer rod temperatures and that computed with the estimated outer rod temperatures if the housing were absent. The estimated outer rod temperatures were arrived at by multiplying the hot rod temperature increase from the start of heatup by the ratio of the outer rod power to the hot rod power, and then adding this quantity to the outer rod temperature at the start of heatup. That portion of radiation heat transfer that occurs in a FLECHT test, which is non-typical of a pressurized water reactor, is the sum of the fourth and fifth columns, and is shown in the last column of Table 3-5. Rod to rod radiation is not included in the table since this is considered typical of a reactor with radial temperature gradients as discussed below. Table 3-5 shows that the total non-typical radiation heat transfer coefficient due to the presence of the housing is only of the order of 0.2 to $0.3 \text{ Btu/hr-ft}^2\text{-}^\circ\text{F}$.

A check on these calculations was obtained from the test data of a checkout run. During an instrument checkout run, the heater rods were heated up by applying power, after which power was turned off. In this checkout run, the housing was filled with air at four psia. Table 3-6 shows the calculated equivalent radiation heat transfer coefficients from rod 5G to the adjacent rods, to the other rods, and to the housing. The sum of these heat transfer coefficients agrees with, or is greater than, the measured heat transfer coefficient which is evaluated from the temperature decrease of rod 5G.

In all of the above calculations, the emissivity of the rods and the housing was assumed to be 0.6. Actually, the emissivity and hence absorptivity of the rods and the housing is about 0.9. Thus, more radiation from the central rod will be absorbed by the adjacent rods and less will reach the housing. The above calculations also did not account for the effects of steam and water droplets. The steam and the water droplets (the absorptivity of water is 0.96) will reduce the above calculated radiation heat transfer.

TABLE 3-5

RADIATION FROM A CENTRAL ROD (MIDPLANE ELEVATION)
TO HOUSING IN 10x10 BUNDLE FOR A FLECHT RUN

Run No.	$T_{5F \text{ rod}}$ (°F)	T_{housing} (°F)	Calculated Equivalent Radiation Heat Transfer Coefficient* (Btu/hr-ft ² -°F)		
			$h_{5F \text{ directly to housing}}$	$h_{5F \text{ to outer rods due to their lower temp. because of housing}}$	$h_{\text{Tot non-typical of PWR}}$
8000	1583	830	.18	.004	.18
8000	1805	837	.25	.009	.26
8000	2002	864	.31	.02	.33

* $h = q''_{\text{radiation}} / (T_{\text{clad}} - T_{\text{sat}})$ per FLECHT h definition

TABLE 3-6

RADIATION FROM A CENTRAL ROD (MIDPLANE ELEVATION)
IN 10x10 BUNDLE FOR A CHECKOUT RUN

Equivalent Radiation Heat Transfer Coefficient*
(Btu/hr-ft² °F)

<u>T_{5G}</u> <u>°F</u>	<u>T_{housing}</u> <u>°F</u>	<u>Calculated</u>				<u>Measured</u>
		<u>h_{5G rod to}</u> <u>housing</u>	<u>h_{5G rod to}</u> <u>adjacent rods</u>	<u>h_{5G rod to}</u> <u>other rods</u>	<u>h_{5G rod}</u> <u>total</u>	<u>h_{5G rod}</u> <u>total</u>
1223	707	.158	.243	.43	.831	.7
1376	986	.154	.387	.267	.808	.705
1627	1142	.221	.326	.540	1.087	.953
1778	1319	.242	.442	.548	1.232	1.04
1907	1412	.282	.430	.587	1.299	1.05

* $h = q''_{\text{radiation}} / (T_{\text{clad}} - T_{\text{sat}})$ per FLECHT h definition

As a final check on the effect of the housing on radiation, consideration was given to the radial temperature gradient due to the housing, which causes radial radiation heat transfer from the central rods. Figures 3-23 and 3-24 show the radial temperature distribution at the start of reflood along row F and column 6 rods, respectively, for a typical pressurized water reactor hot assembly and a comparable FLECHT test. These plots show that there is a steeper or equal radial temperature gradient in a pressurized water reactor compared to the FLECHT test except for the row next to the housing. As discussed above, in the FLECHT bundle the high emissivity of the rods and absorption of steam and water droplets will attenuate the outward radiation of the central rods. Therefore, the temperature gradient near the housing has little effect on the central rod radiation heat transfer.

The temperatures for the typical PWR hot assembly were calculated using the power distribution shown in Figure D-34 of reference 4 in a single rod heatup code which included no rod to rod radiation and assumed all rods go through DNB at the same time, both assumptions per the Interim Acceptance Criteria.

This study thus confirms that the radiation from central rods to the housing is, in fact, quite small, being of the order of 0.2 to $0.3 \text{ Btu/hr-ft}^2\text{-}^\circ\text{F}$.

3.3 PARAMETER EFFECTS

The tests reported in this supplement extended the range of FLECHT data to various combinations of low pressure, low coolant subcooling and low flooding rates not investigated previously. In addition, the effect of peak power at these conditions was investigated.

3.3.1 Flooding Rate

The effect of flooding rate on temperature rise, turnaround time and quench time is shown in Figures 3-25 and 3-26. The current low pressure, low subcooling data follows the same trend with flooding rate as in the previous FLECHT results, namely the temperature rise, turnaround time and quench time increase with lower flooding rate. The effect of decreasing flooding rate on increasing quench time appears to be greater at low pressure. Figure 3-26

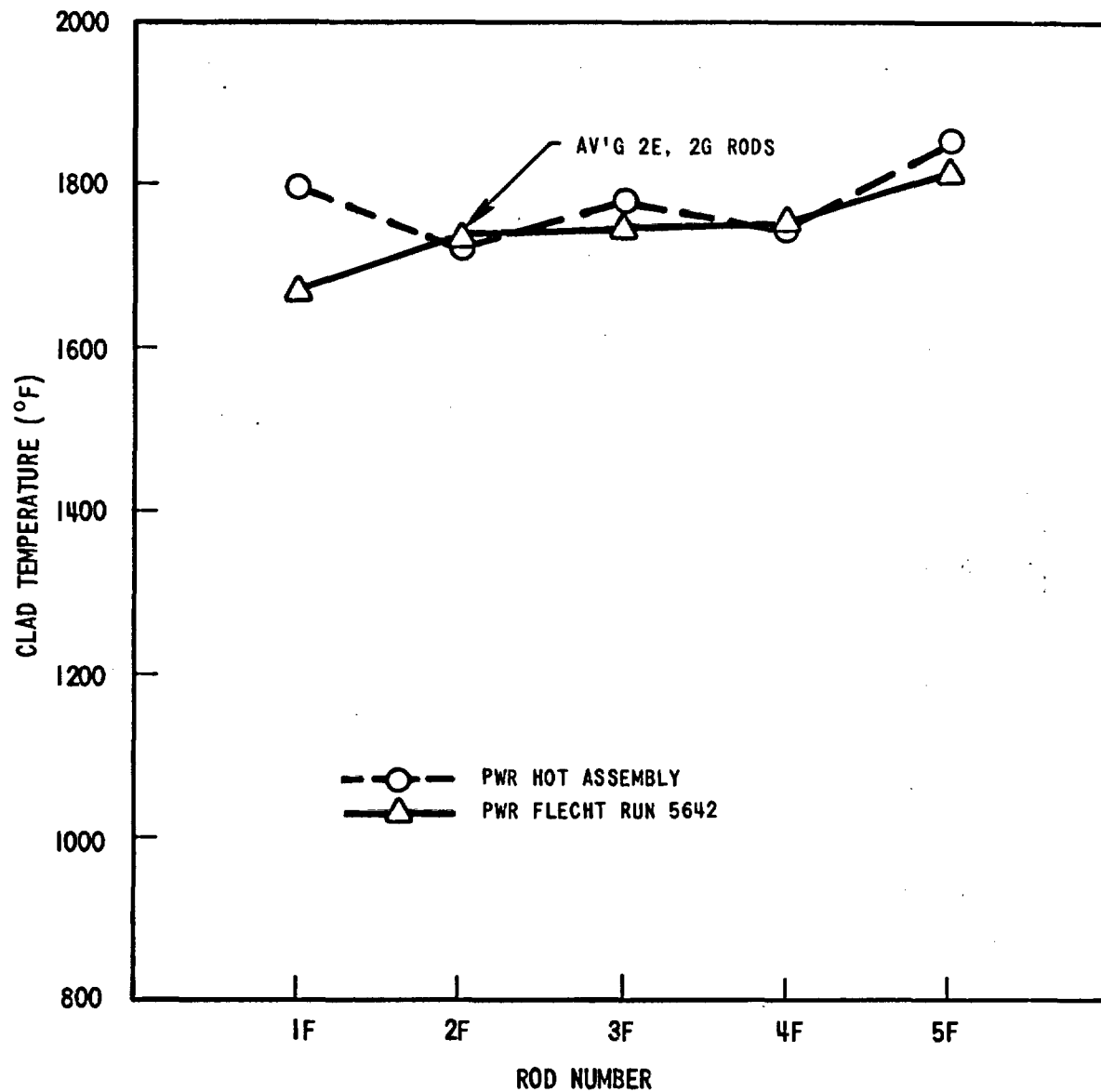


Figure 3-23. Comparison of FLECHT and PWR Radial Temperature Distribution Along Row F Rods at the Start of Reflood.

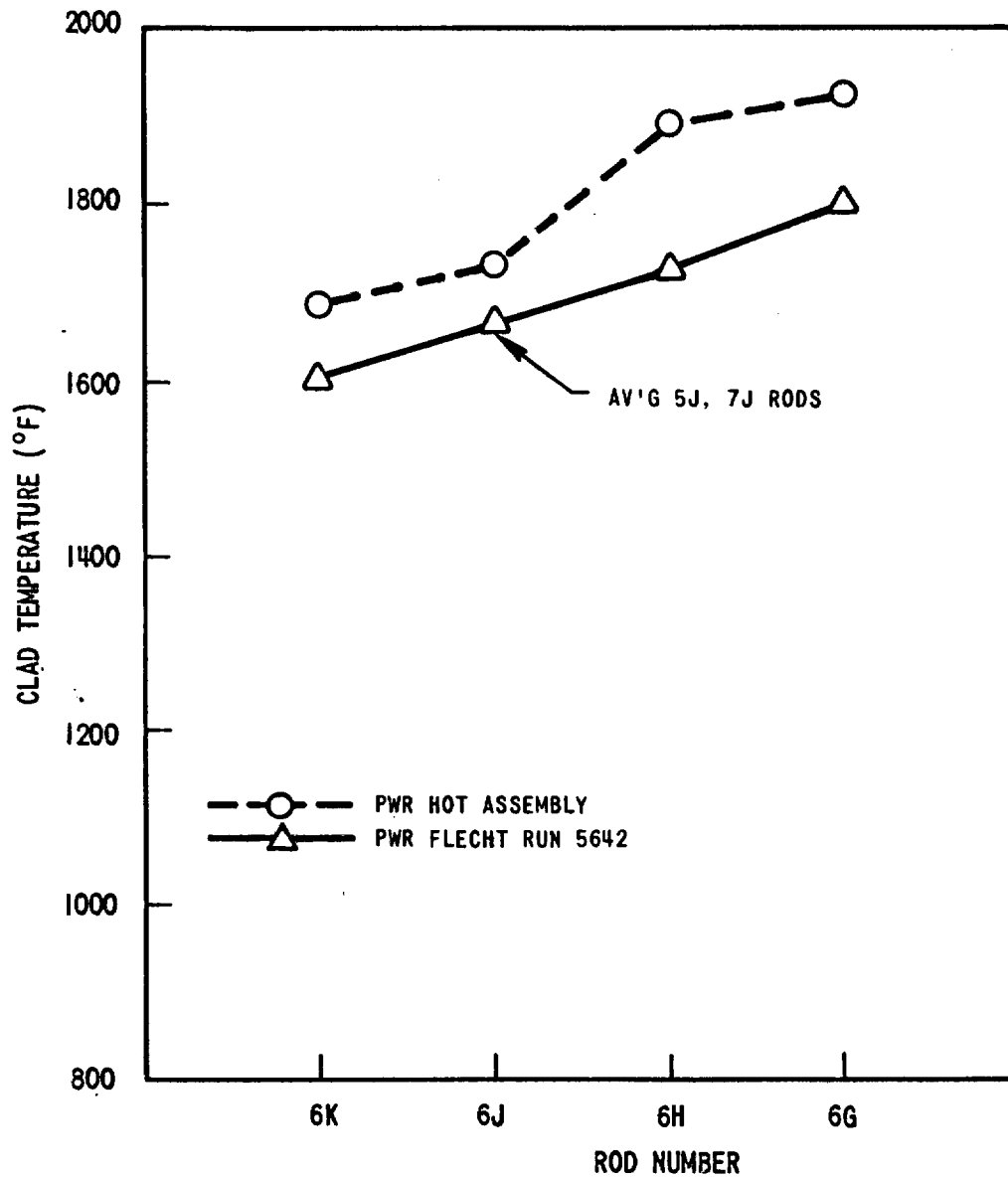


Figure 3-24. Comparison of FLECHT and PWR Radial Temperature Distribution Along Column 6 Rods. at the Start of Reflood.

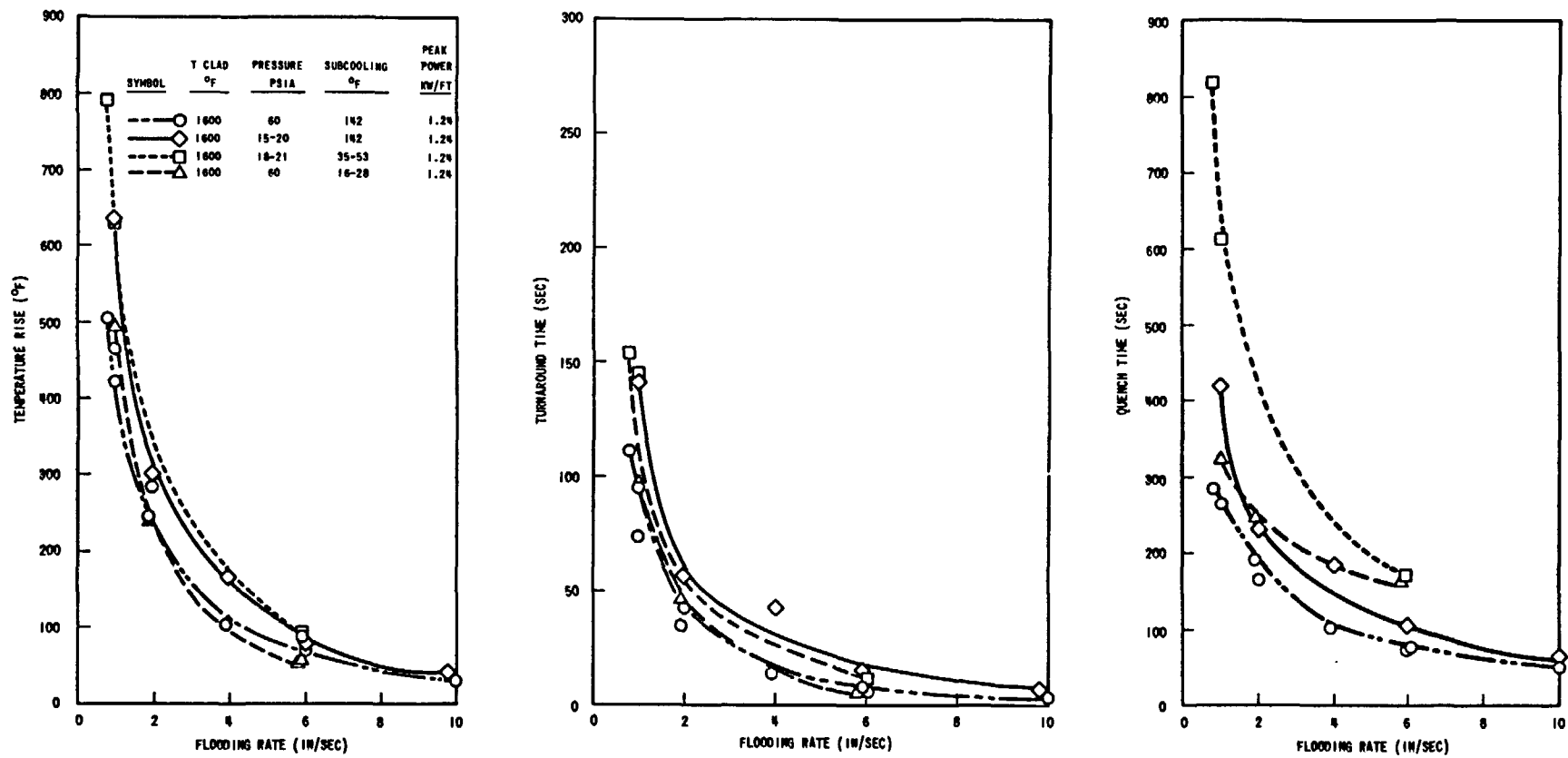


Figure 3-25. Effect of Flooding Rate on Temperature Rise, Turnaround Time, and Quench Time

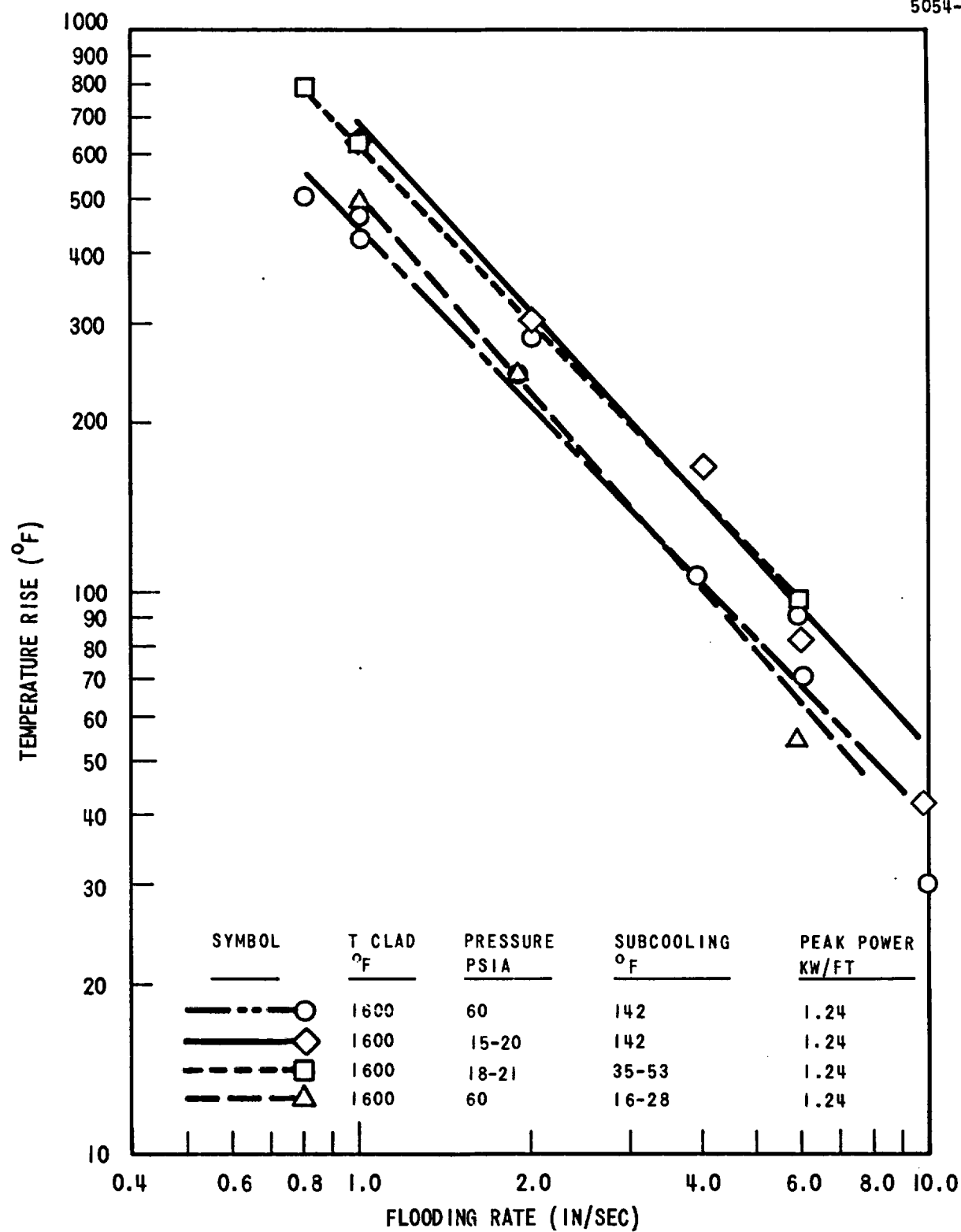


Figure 3-26. Effect of Flooding Rate on Temperature Rise (Log-Log Plot).

shows approximately the same slope in temperature rise versus flooding rate for all conditions.

Heat transfer coefficient versus time plots, showing the effect of flooding rate, are shown in Figures 3-27 through 3-31 for various levels of pressure and subcooling. As noted in Reference 1, the flooding rate has a strong influence on the heat transfer coefficient, due to its effect on steam generation and liquid entrainment, and the heat transfer coefficient always increases with increasing flooding rate.

3.3.2 Pressure

Figure 3-32 shows the effect of system pressure on temperature rise, turnaround time, and quench time at various flooding rates and for high and low subcooling. The effect of lowering system pressure is to increase the temperature rise, turnaround time and quench time for all flooding rates. The magnitude of the increase due to lower pressure (e.g., the increase in temperature rise in °F between high and low pressure runs) is larger at low flooding rates. However, on a percentage basis, the increase is of the same order for all flooding rates.

A comparison of midplane heat transfer coefficients at different pressures is shown in Figures 3-33 through 3-36 for high and low subcooling and 6, 2 and 1 in/sec flooding rates, respectively. In all cases, the heat transfer coefficient increases with increasing pressure. At 2 and 1 in/sec flooding rates, however, the heat transfer coefficients were nearly independent of pressure for about the first 30 - 40 seconds after flood. Generally, one might attribute the increase in heat transfer coefficient with increasing pressure to an expected increase in entrainment or liquid carryover with increased pressure. This is believed to be a result of smaller vapor bubbles being more efficient in ejecting liquid and a decrease in steam velocity necessary for entrainment with increasing pressure (Reference 5). However, liquid carryover measurements shown in Section 3.9 indicate higher liquid carryover at lower pressure. Also longer quench times indicate higher total mass flow out of the bundle for lower pressure. An examination of the flow patterns and mechanism of droplet entrainment gives a possible explanation of the pressure effect. Entrainment has been studied

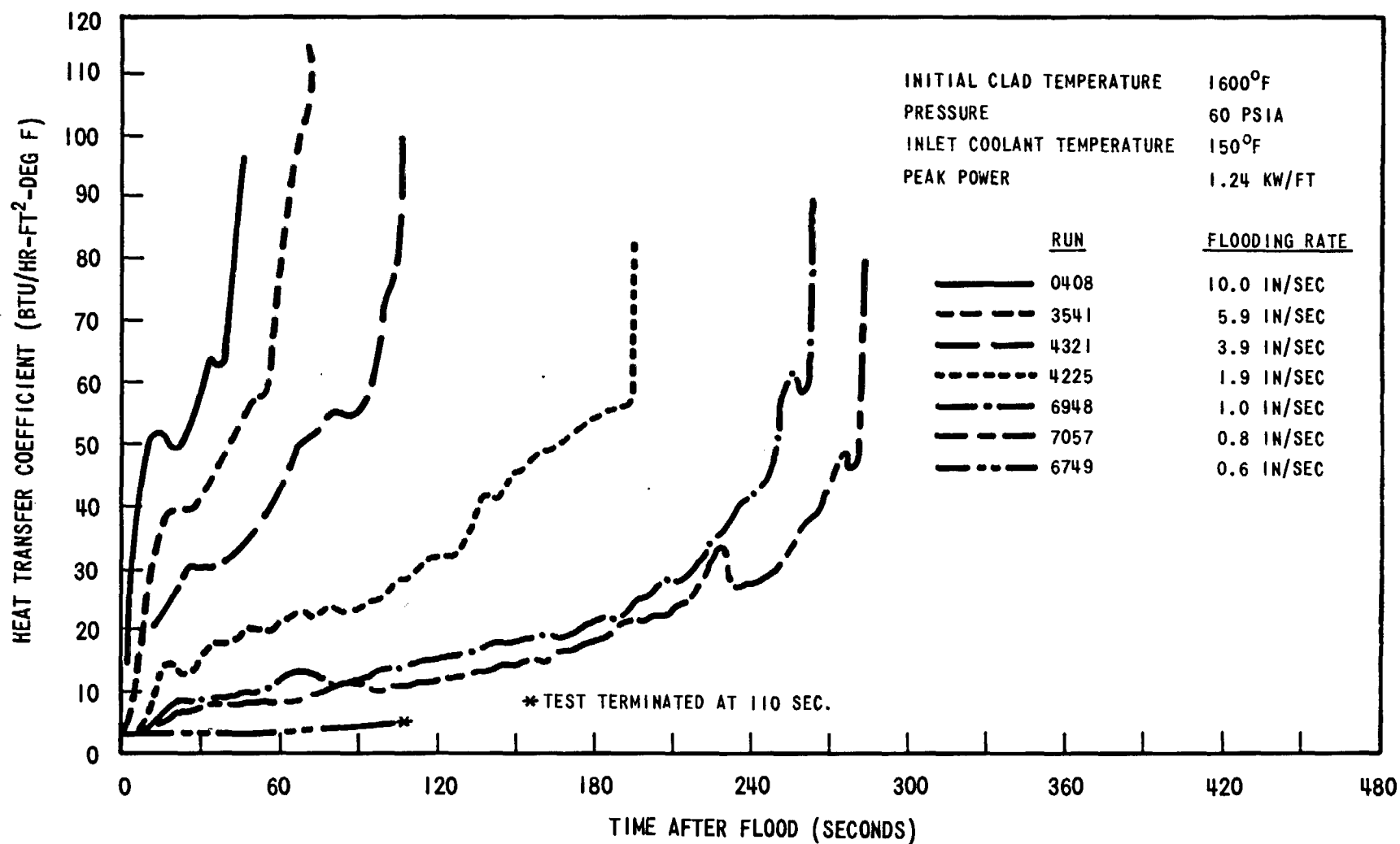


Figure 3-27. Effect of Flooding Rate on Midplane (ϕ') Heat Transfer Coefficient at 1600 °F Initial Clad Temperature, High Pressure and High Subcooling.

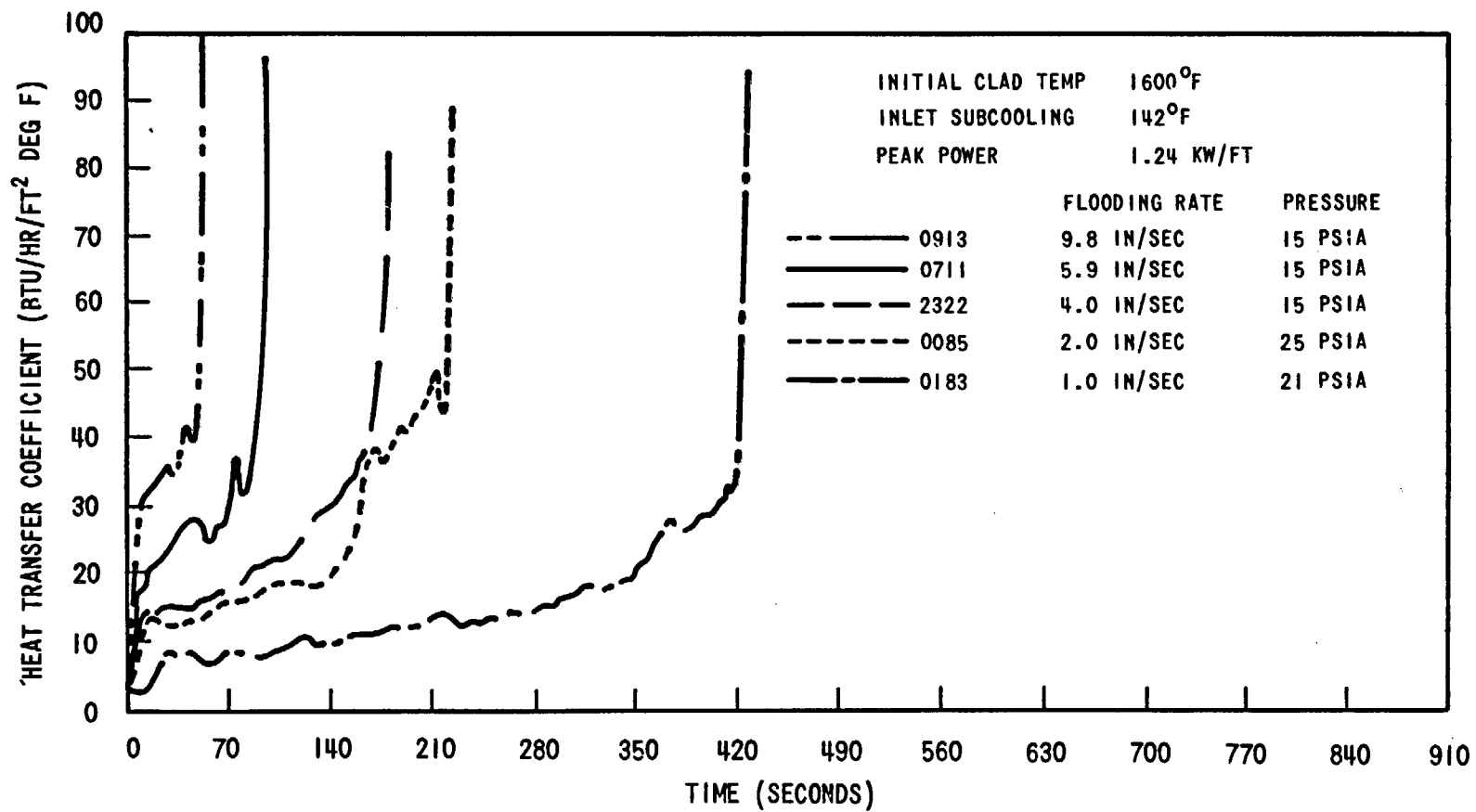


Figure 3-28. Effect of Flooding Rate at Low Pressure and High Subcooling.

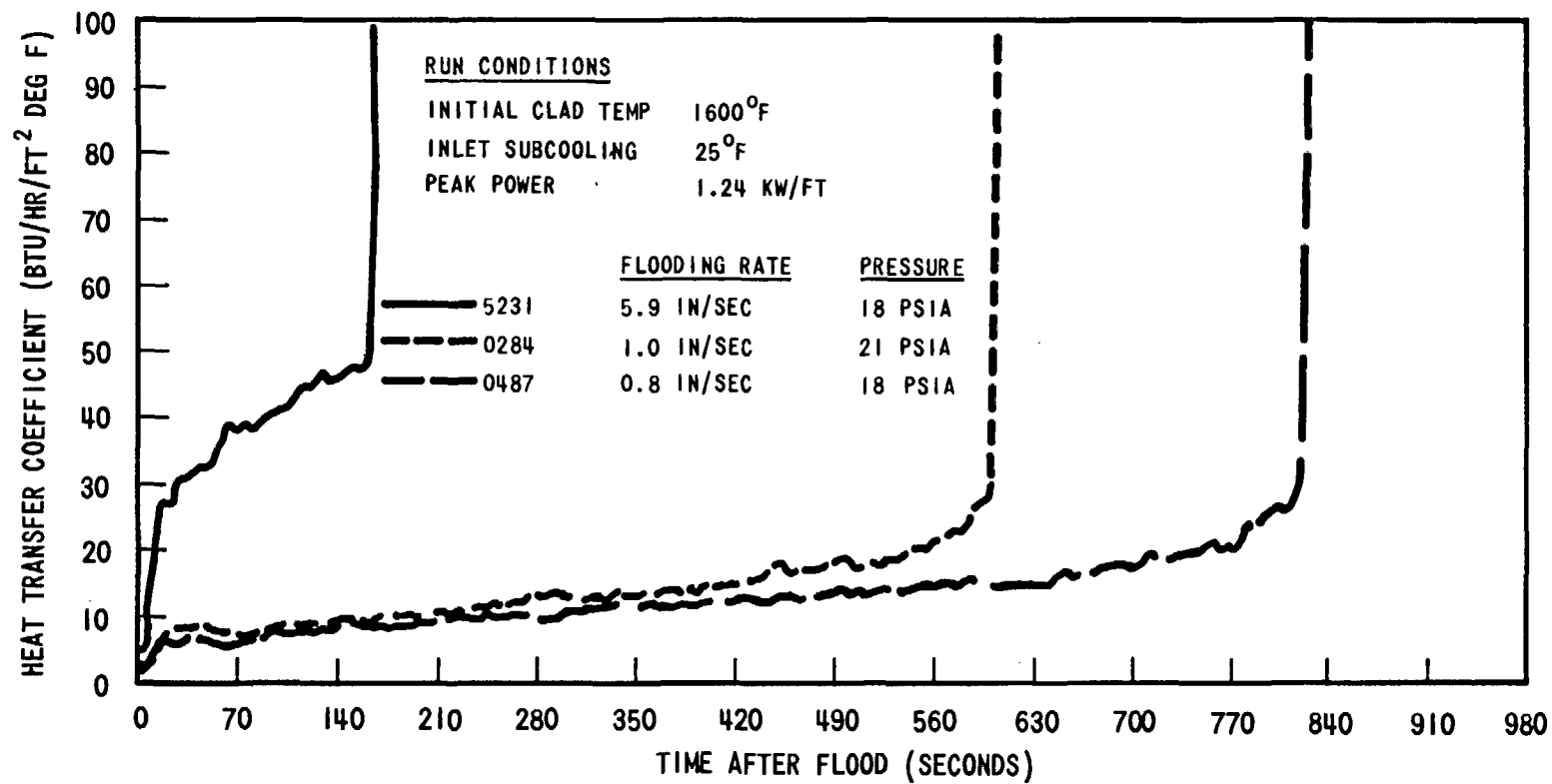


Figure 3-29. Effect of Flooding Rate at Low Pressure and Low Subcooling.

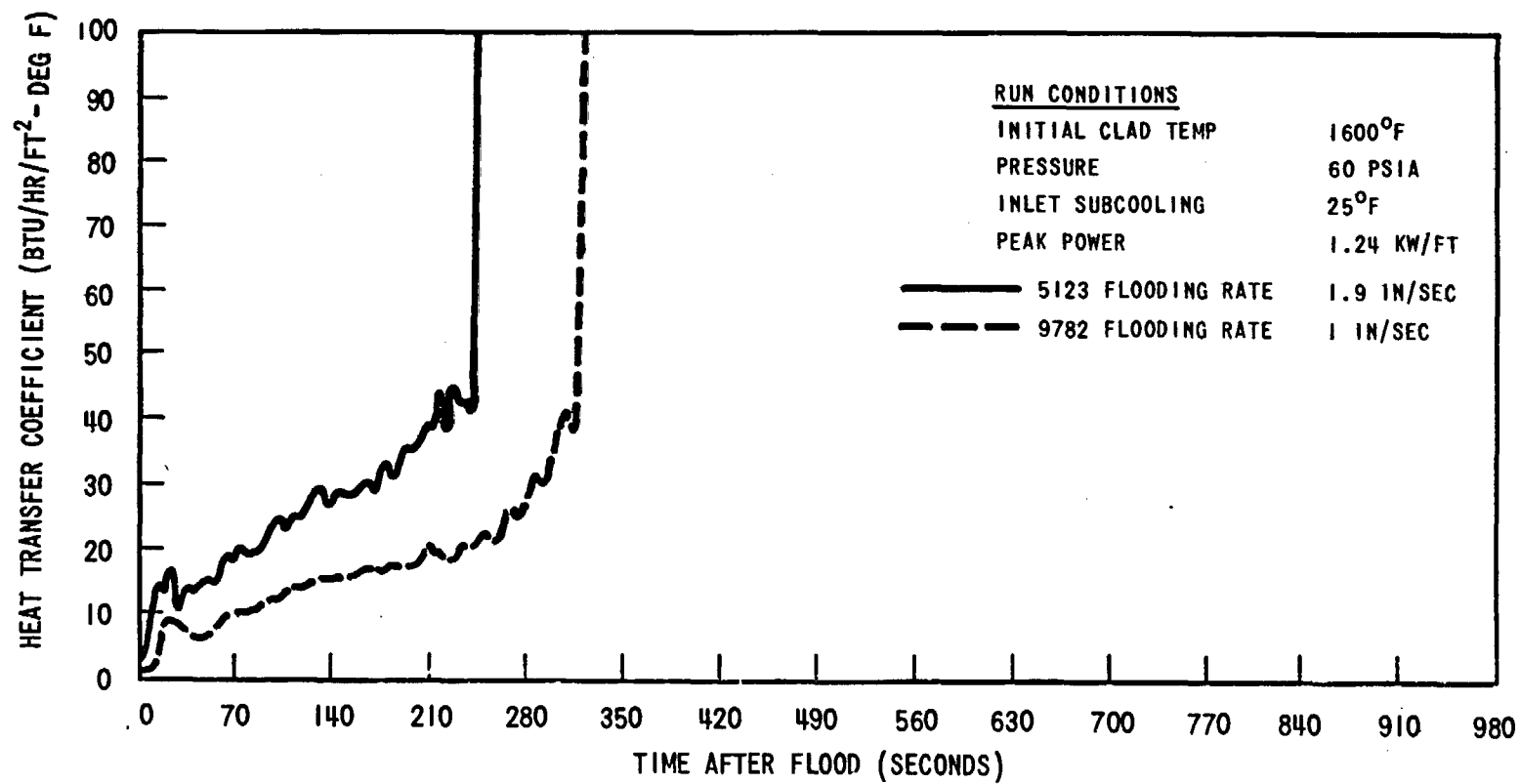


Figure 3-30. Effect of Flooding Rate at High Pressure and Low Subcooling.

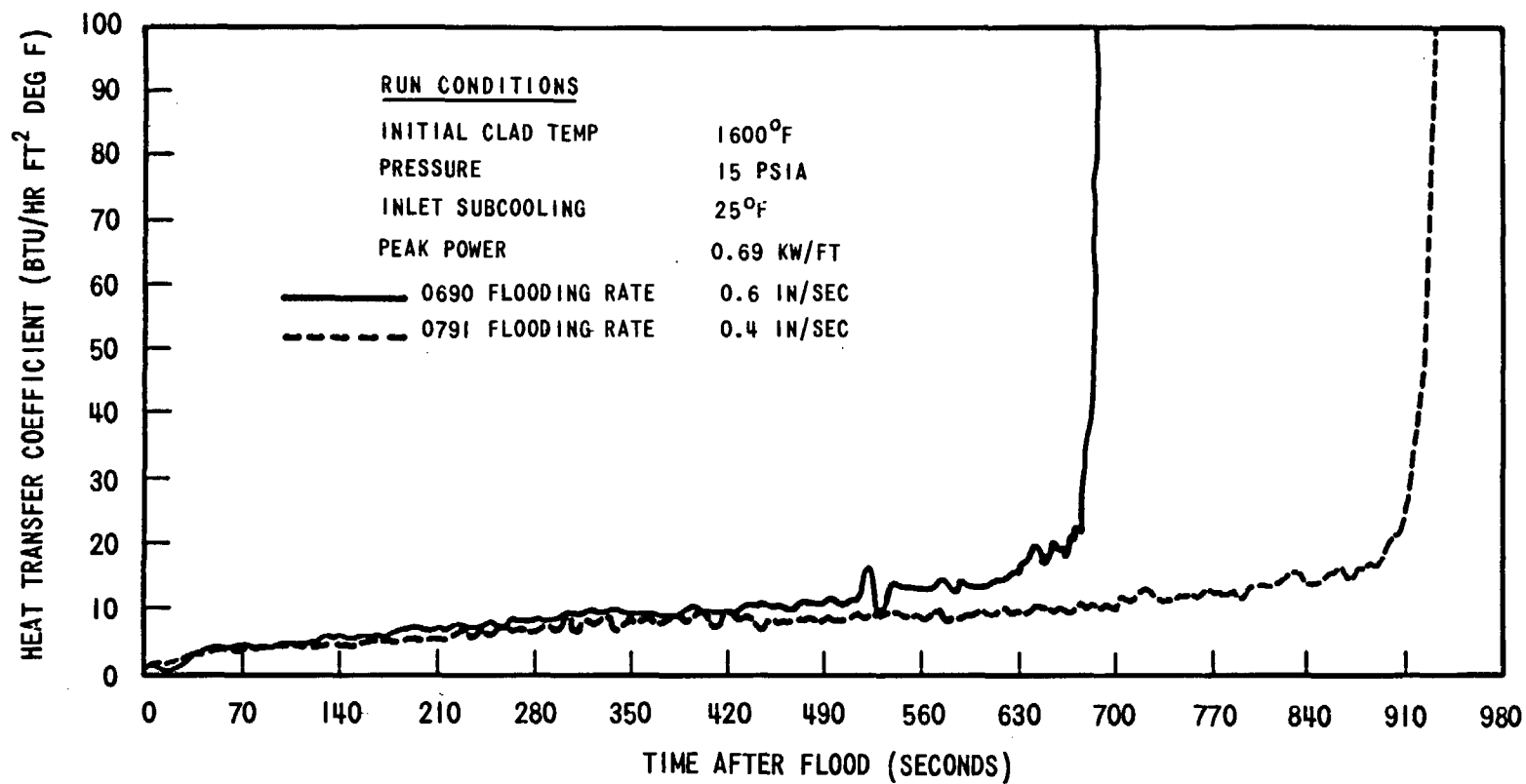


Figure 3-31. Effect of Flooding Rate at Low Pressure, Low Subcooling and 0.69 kw/ft Peak Power.

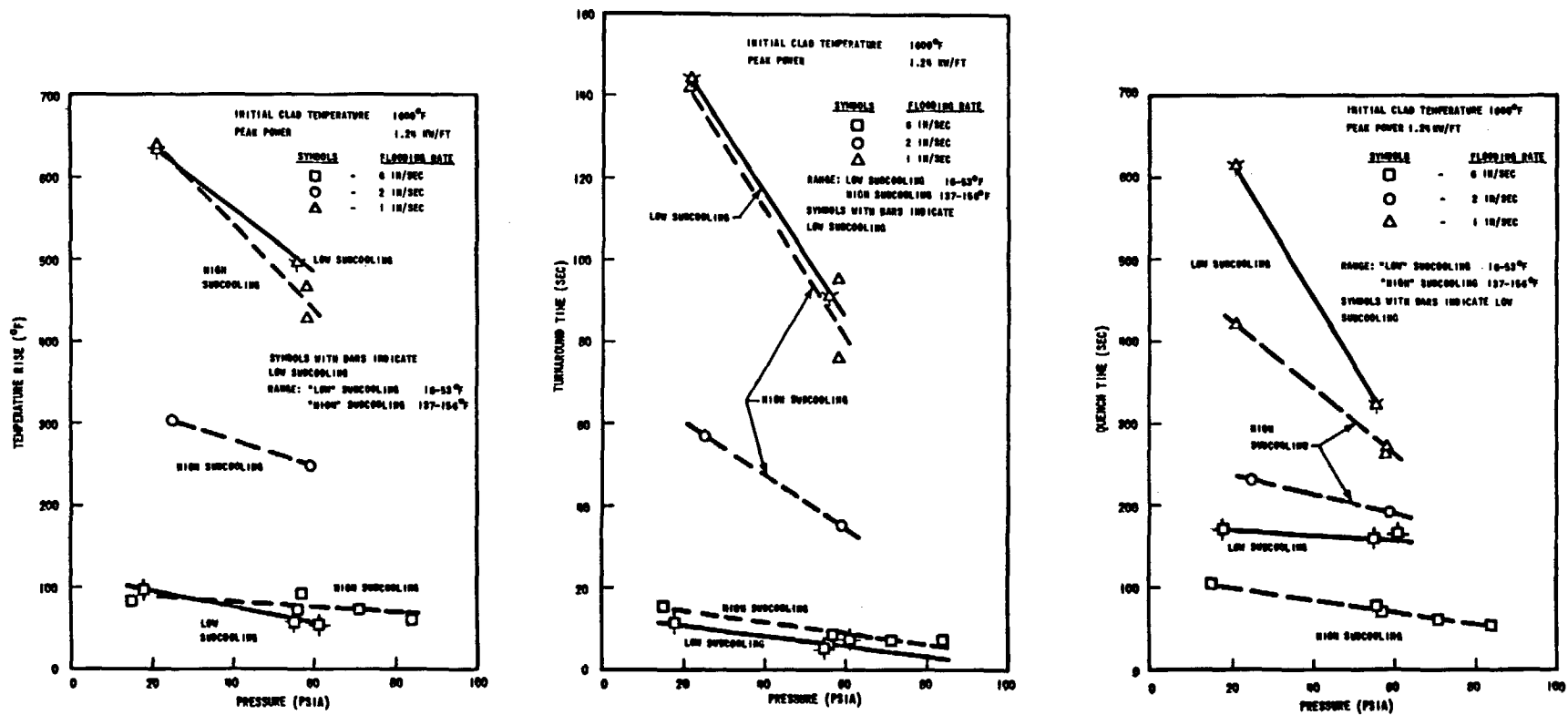


Figure 3-32. Effect of System Pressure on Temperature Rise, Turnaround Time and Quench Time

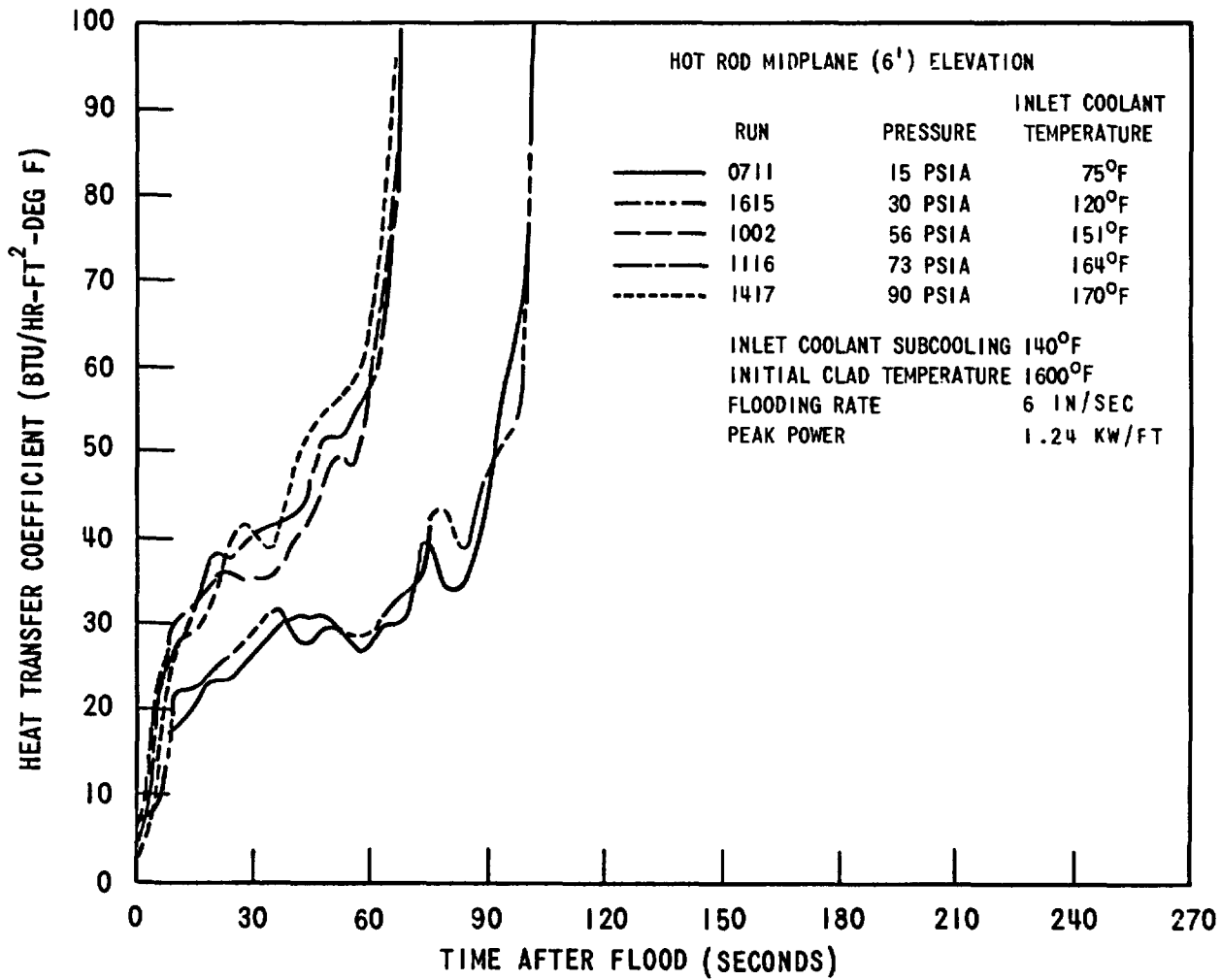


Figure 3-33. Effect of Pressure on Heat Transfer Coefficient at High Subcooling for 6 in/sec Flooding Rate.

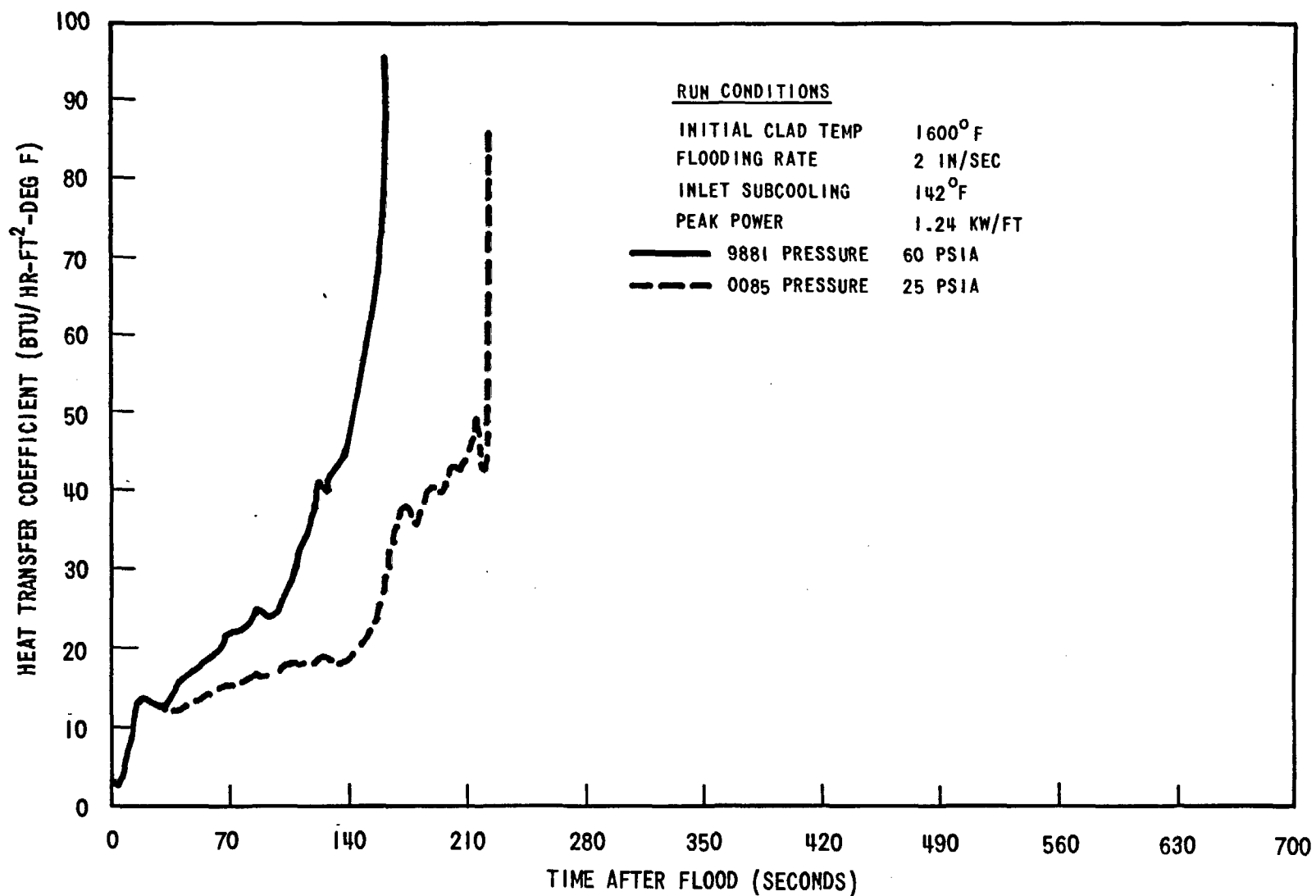


Figure 3-34. Effect of Pressure at 2 in/sec Flooding Rate and High Subcooling.

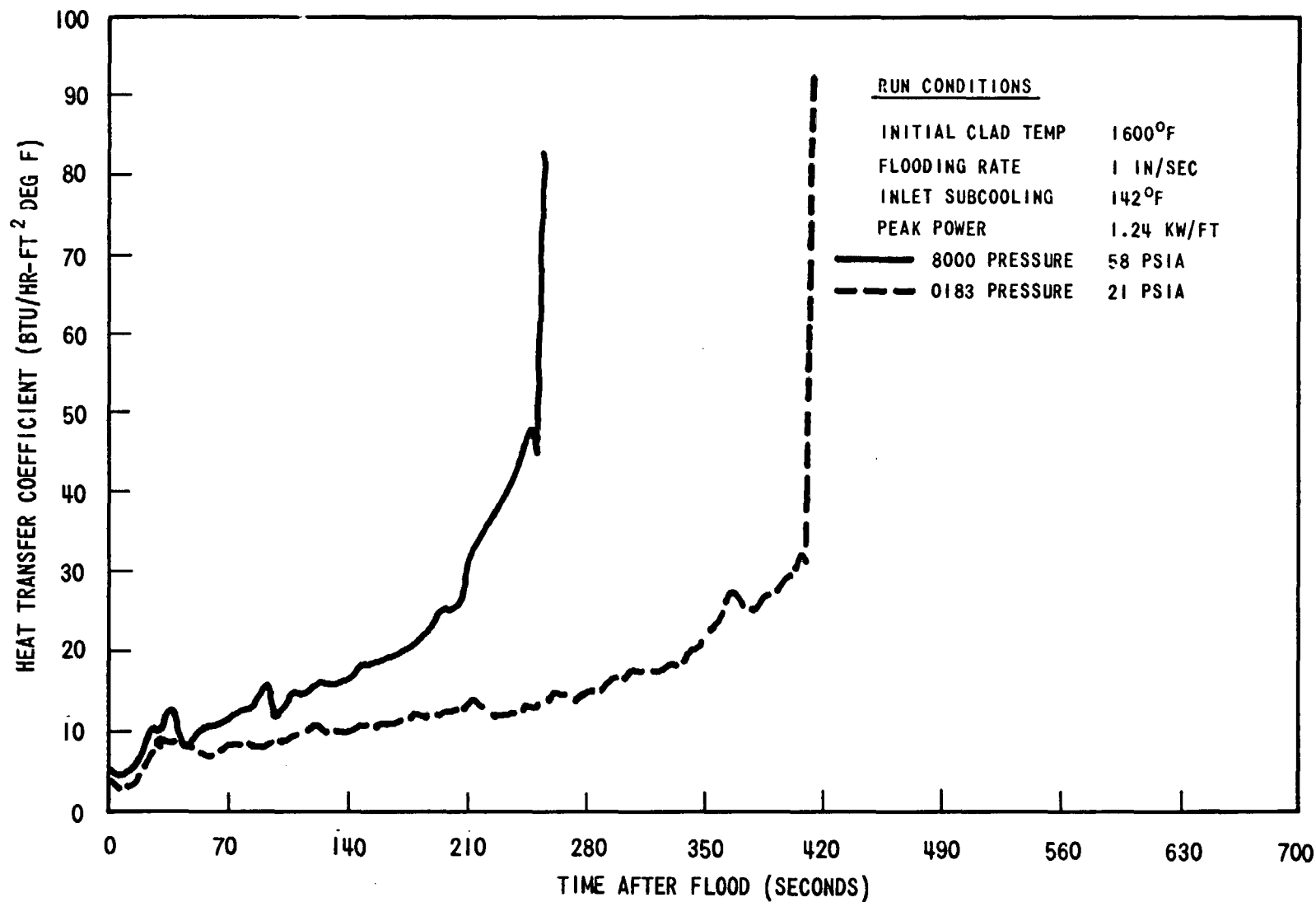


Figure 3-35. Effect of Pressure at 1 in/sec Flooding Rate and High Subcooling.

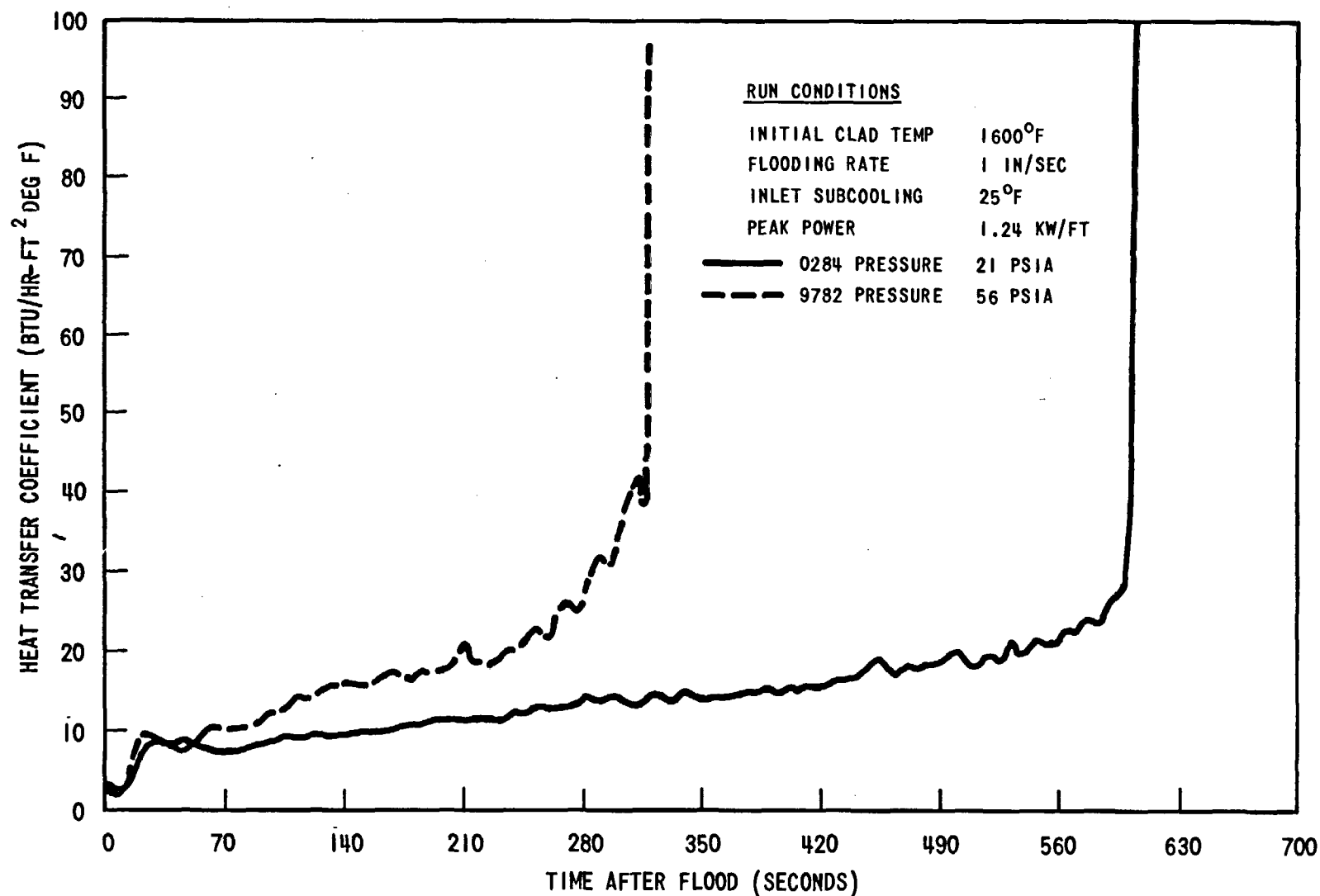


Figure 3-36. Effect of Pressure at 1 in/sec Flooding Rate and Low Subcooling.

in terms of the rise of a bubble in a quiescent pool and its collapse at the free liquid surface. The size of entrained droplets has been shown to be dependent on the bubble size in this situation. (Reference 6) However, the mechanism of vapor formation and liquid entrainment is considerably different in the FLECHT bottom flooding experiments, and it is felt that the above model is not applicable. Observations of FLECHT movies indicate several flow regimes exist above the quench front, namely steam flow, dispersed flow, "transition flow", film boiling, transition boiling and nucleate boiling. (Reference 1) (The flow regimes are listed above beginning at the farthest distance from the quench front.)

In the FLECHT tests, the rod midplane elevation is in the dispersed flow or "transition flow" regimes for most of the run. Therefore, in order to understand the effect of pressure on heat transfer coefficient, it is necessary to examine the behavior of the transition flow and dispersed flow regimes.

Steam generation begins at the quench front (nucleate boiling and transition boiling regimes) and forms a thin stable vapor film around the heater rods. As it moves up the bundle more steam is generated and the vapor film grows thicker. Finally, the vapor film becomes unstable and some of the steam departs from the rod surface as bubbles. The motion of the bubbles disturbs the flow of liquid such that the flow becomes turbulent. This is the transition flow regime. In this region, the liquid phase is continuous and the vapor displaces some of the liquid. More steam is generated as the mixture moves up the bundle, resulting in a highly turbulent mixture of steam and chunks of liquid. This is the start of the dispersed flow regime. In this region high velocity steam breaks up the liquid phase into drops which are entrained and carried out of the bundle. Examining the effect of system pressure in the transition flow regime, the specific volume of the steam formed at 60 psia is approximately 1/3 the specific volume of steam formed at 20 psia. Thus, for the same mass of steam formed the high pressure case will have a lower void fraction in the transition flow region, and thus better heat transfer.

In dispersed flow, lower vapor velocity at high pressure (due to lower specific volume) permits the entrainment of only small diameter droplets. (reference 6) At low pressure, larger droplets can be entrained because the steam velocity

is higher. Smaller droplets, however, may allow more effective heat transfer due to a larger ratio of droplet surface area to droplet volume. Thus, although less water is entrained at high pressure, it may be possible to obtain better heat transfer due to the smaller droplet size.

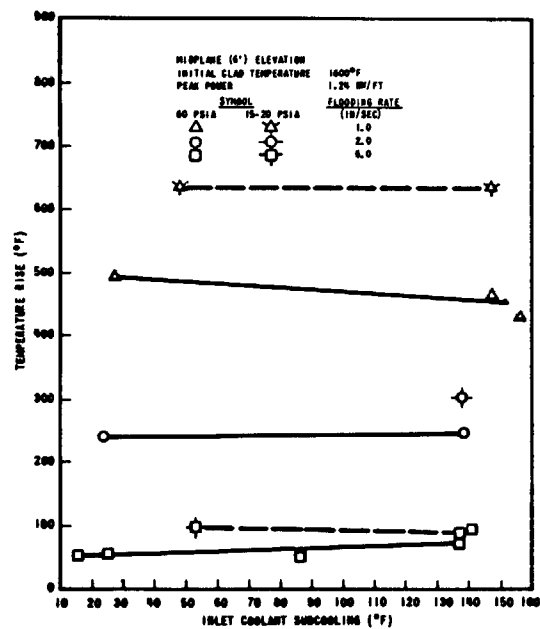
3.3.3 Inlet Coolant Subcooling

Figure 3-37 shows that the effect of inlet subcooling on temperature rise and turnaround time is not significant. Quench time increases with decreasing subcooling. The magnitude of the observed increase was about the same for all flooding rates, except at the combined condition of low pressure and low flooding rate where the subcooling effect was greater.

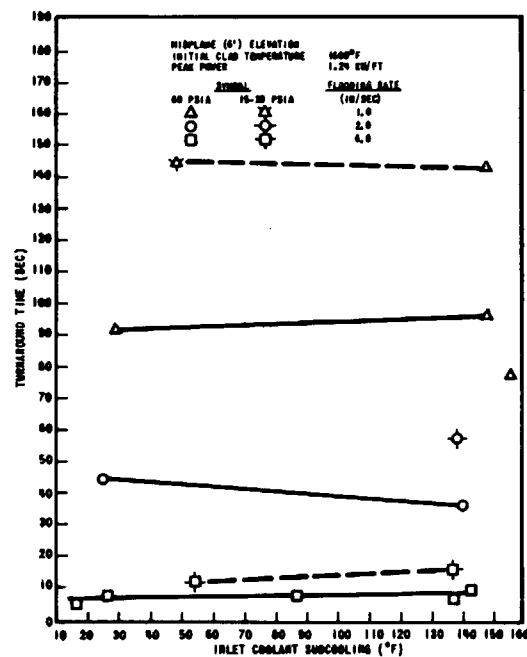
The effect of subcooling on the midplane heat transfer coefficient is shown in Figures 3-38 through 3-40, indicating that subcooling does not influence the heat transfer coefficient until late in the run at flooding rates of 2 in./sec and lower. Thus, subcooling has little effect on temperature rise and turnaround time. The main influence of low subcooling is to increase the quench time. The reverse trend of higher heat transfer coefficient at early times with low subcooling at 6 in./sec and 2 in./sec did not show up at 1 in./sec. The effect of coolant subcooling on the heat transfer coefficient is considerably less significant than that of flooding rate and pressure.

3.3.4 Peak Power Generation

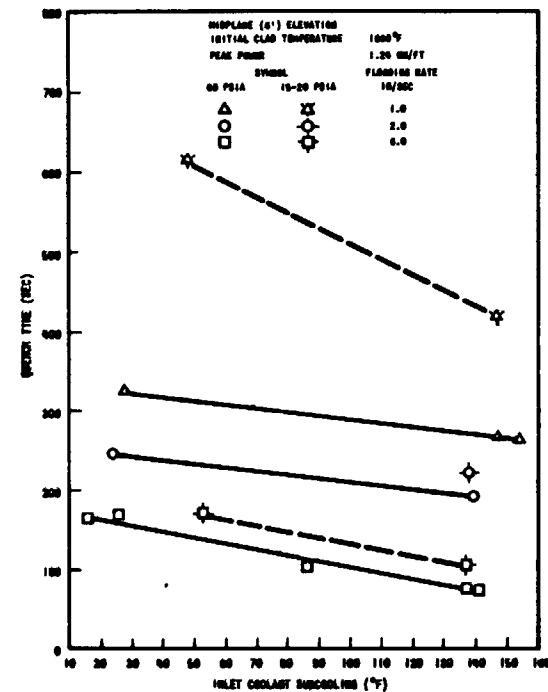
Figure 3-41 shows the heat transfer coefficients for three peak-power generation rates at 6 in./sec and 2 in./sec flooding rates. Figure 3-42 shows heat transfer coefficient comparisons using the current data. The heat transfer coefficient is independent of power at early times. The current low pressure low flooding rate data are less sensitive to peak power than the 6 and 2 in./sec data, as they show little effect of power out to about 120 seconds after flood, as shown in Figure 3-42. This is because the heat transfer coefficient at the midplane for early times is a function of the steam generation and entrainment at the low elevations. Although the midplane power differed significantly in these cases, the difference in power generation at the lower elevations was considerably less, due to the axial cosine power distribution. At later times,



A



B



C

Figure 3-37. Effect of Inlet Coolant Subcooling on Temperature Rise, Turnaround Time, Quench Time

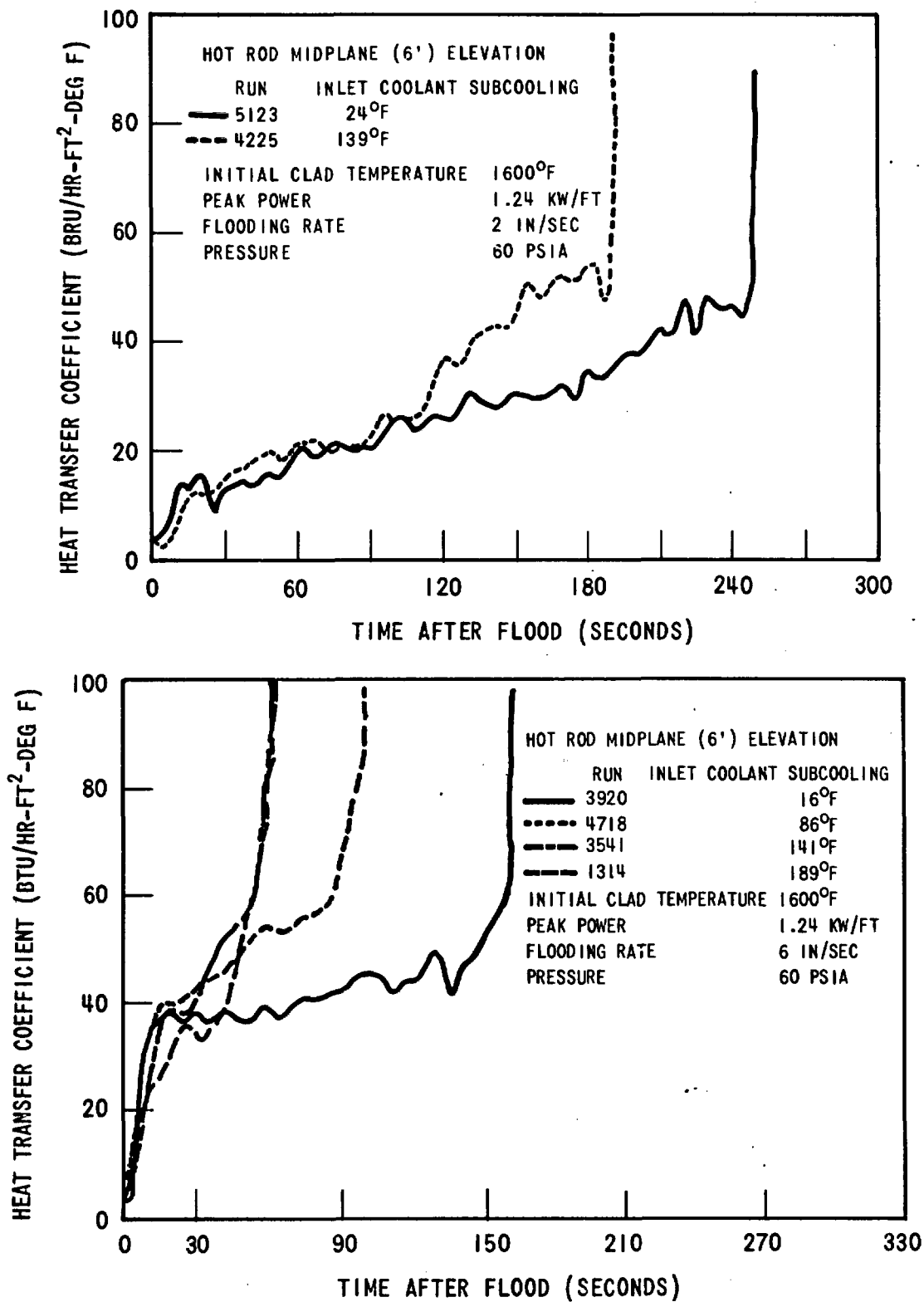


Figure 3-38. Effect of Subcooling on Heat Transfer Coefficient at 2 and 6 In/Sec Flooding Rate and High Pressure.

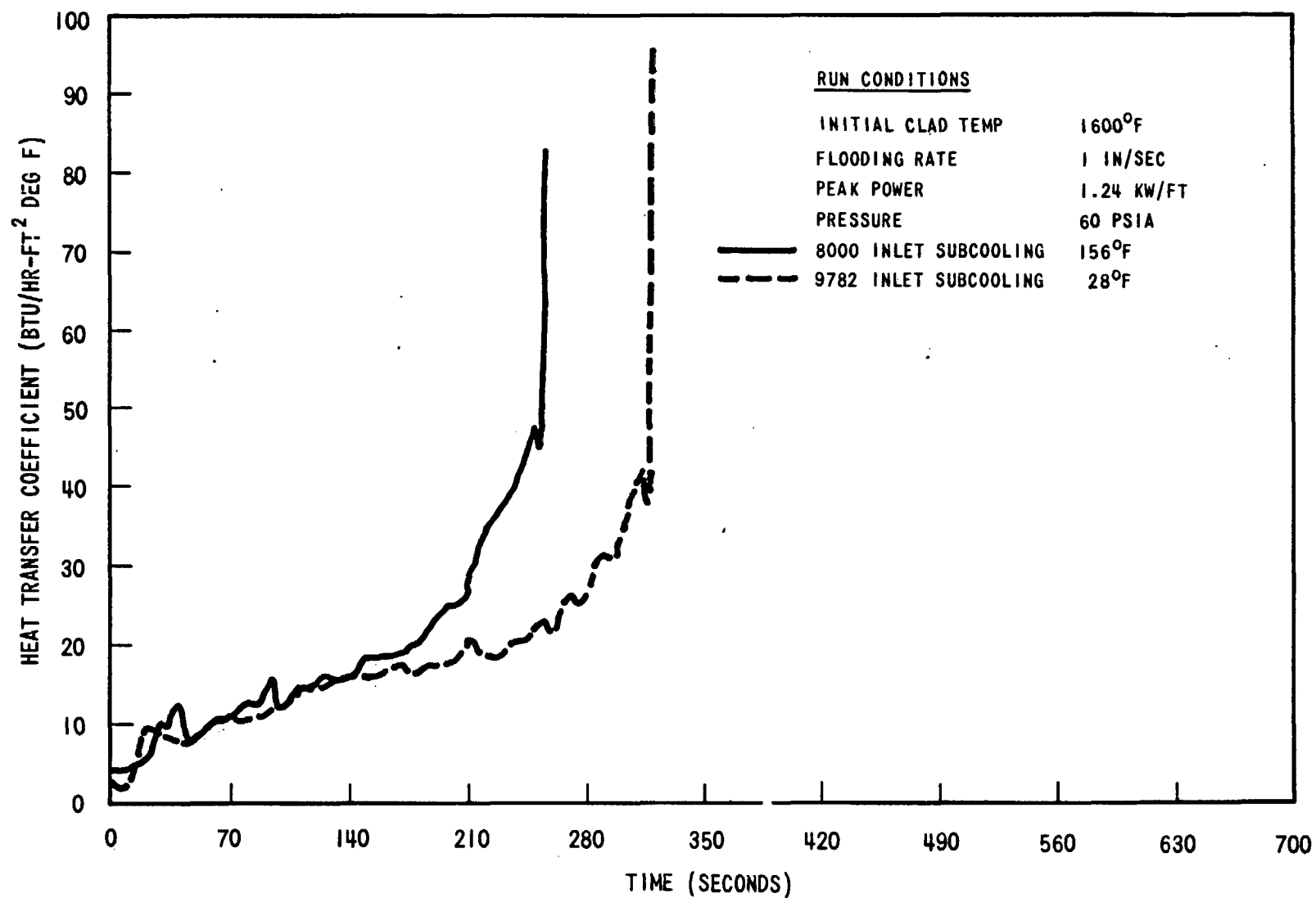


Figure 3-39. Effect of Inlet Coolant Subcooling at 1 in./sec Flooding Rate and High Pressure.

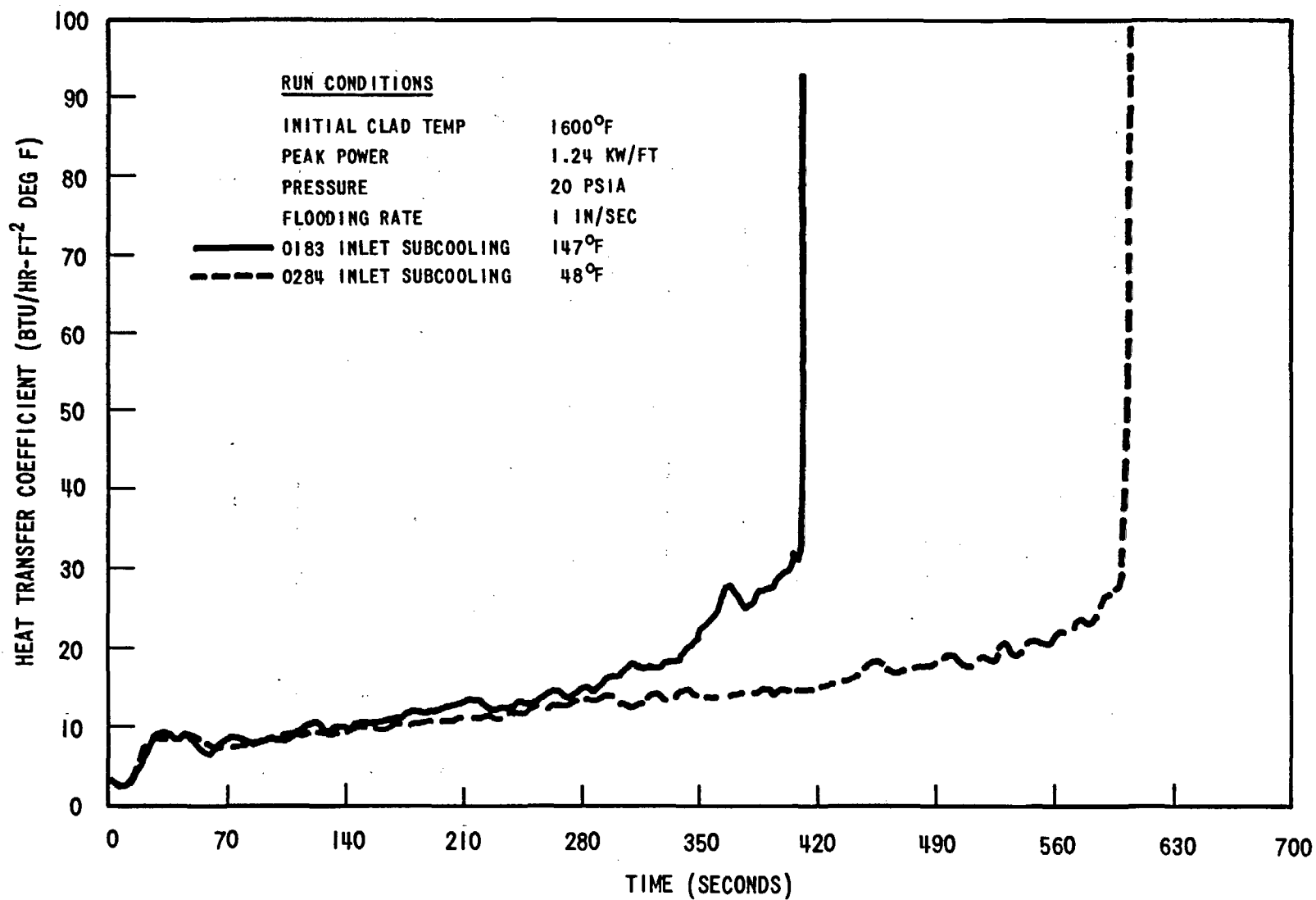


Figure 3-40. Effect of Inlet Coolant Subcooling at 1 in/sec Flooding Rate and Low Pressure.

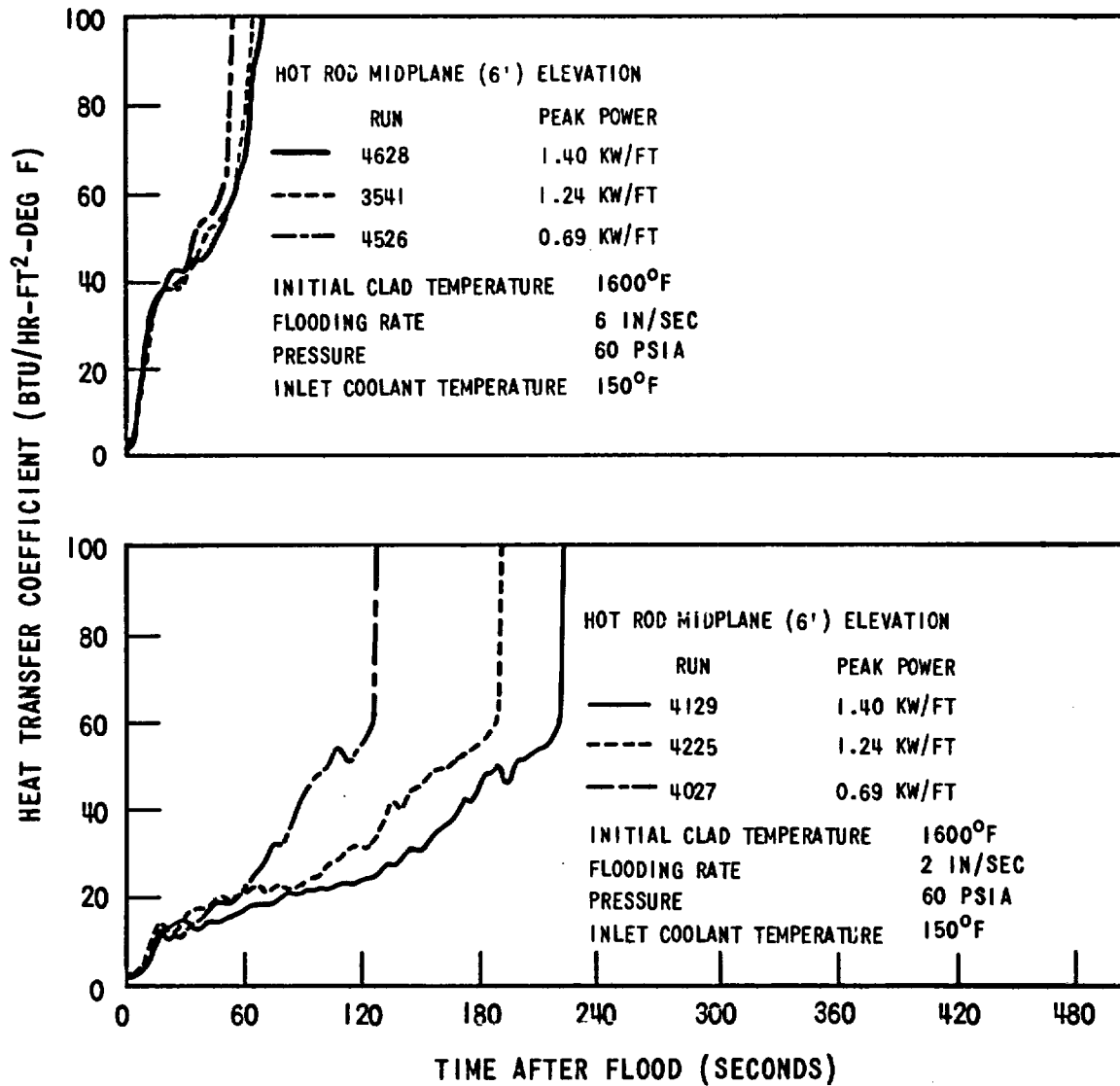


Figure 3-41. Effect of Peak Power on Heat Transfer Coefficient for 6 and 2 In/Sec Flooding Rate.

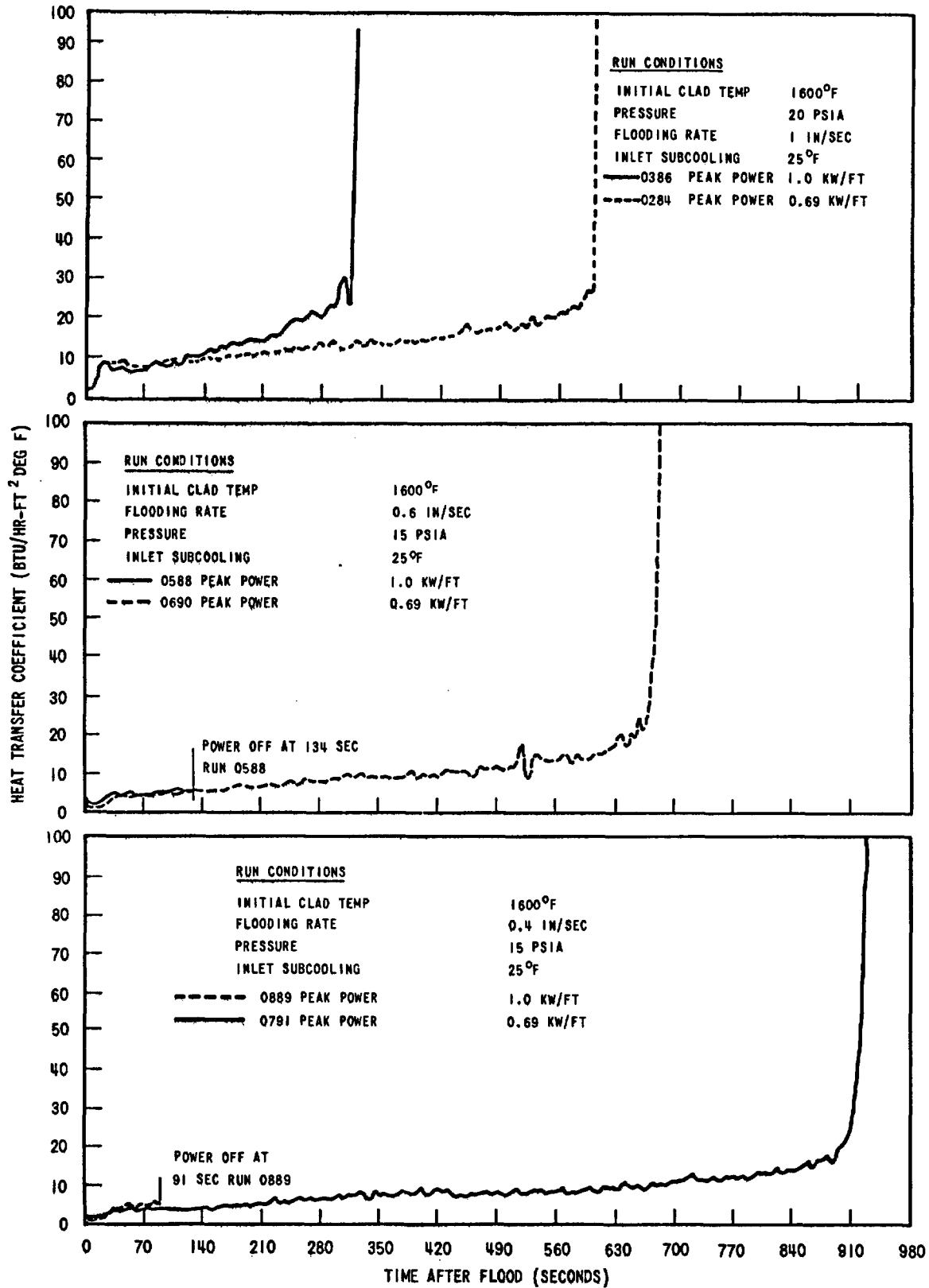


Figure 3-42. Effect of Peak Power for Current Data

the higher power generation resulted in a higher rod surface temperature and a higher steam generation rate, causing the quench front to move more slowly up the bundle. Thus, the midplane heat transfer coefficient was lower at later times as the power generation rate increased.

Temperature rise and turnaround time increased as peak power generation increased, as shown in Figure 3-43 for 6, 2 and 1 in./sec flooding rates. This is reasonable since the heat transfer coefficient necessary to cause turnaround of the clad temperature is greater with higher power generation. The effect was stronger in the low flooding rate cases because the turnaround heat transfer coefficient was reached at a later time compared to the high flooding rate runs. The quench time increased for higher power generation since the quench front advanced more slowly due to a higher steam generation rate.

3.3.5 Comments on Parameter Effects

Examination of the data has led to qualitatively similar trends which tend to explain the various parameter effects. A correspondence between quench front elevation versus time and heat transfer coefficient has been observed and is illustrated in Table 3-7 and its accompanying sketch. The curves marked Case A and Case B can be data at low and high values of some parameter such as peak power. This sketch shows that for time up to some t_1 the quench elevation and midplane heat transfer coefficient curves are fairly close for the parameter effects listed. After t_1 , the curves begin to diverge more rapidly. The value of t_1 , of course, varies for each parameter effect. Typically, the parameter effects of pressure, subcooling, peak power generation, flooding rate and initial clad temperature follow the trend above as shown in Table 3-7. With flooding rate, the curves diverge immediately, i.e., $t_1 \approx 0$. Generally, lower elevations are not too different at early time for high and low values of the parameter under study and hence the quench front velocities are quite close. It follows that the midplane heat transfer coefficients are also not far different for peak power, flooding rate and initial clad temperature effects. Pressure, flooding rate and sometimes coolant subcooling will influence the midplane heat transfer coefficient, and hence the midplane clad temperature. Peak power, of course, will affect the midplane temperature also.

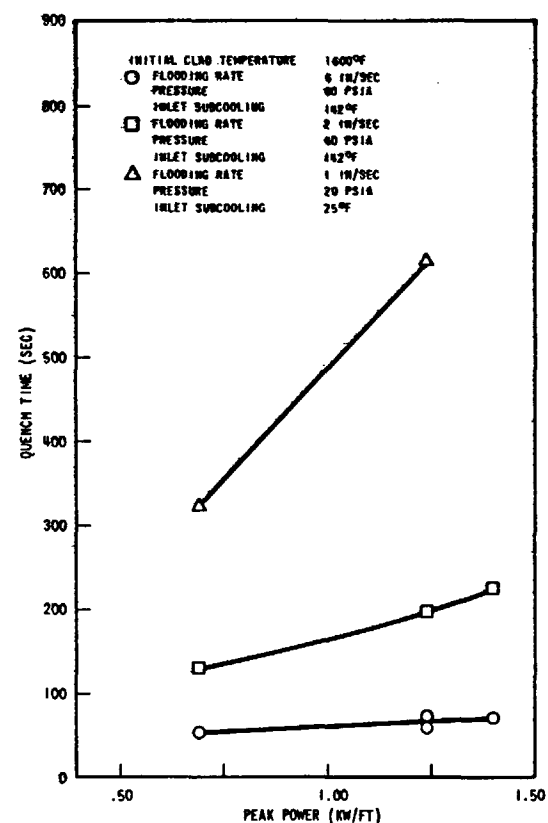
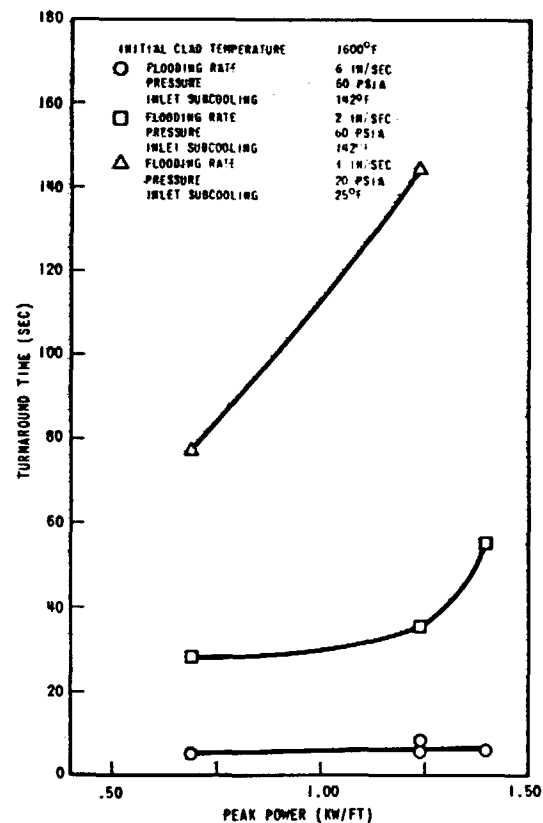
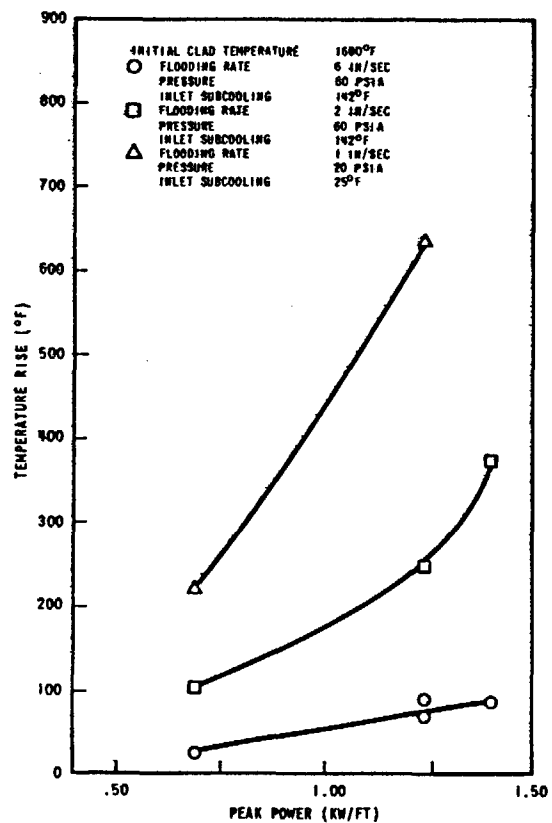
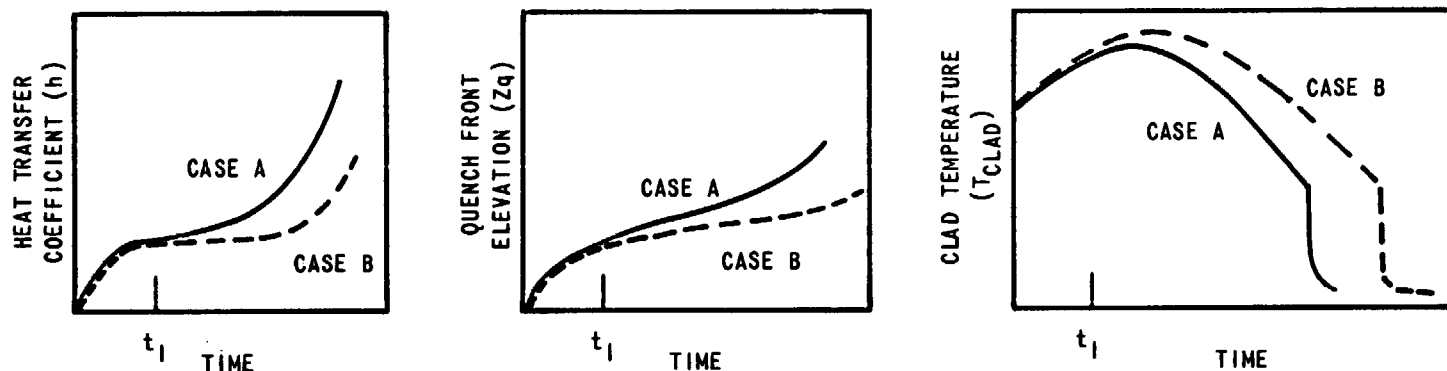


Figure 3-43. Effect of Peak Power on Temperature Rise, Turnaround Time and Quench Time

Table 3-7. Observed Trends for Various Parameter Effects



PARAMETER	CURVE REFERENCE		$t \leq t_1$			$t > t_1$		
	CASE A	CASE B	QUENCH FRONT					
			MIDPLANE h	ELEVATION Zq	MIDPLANE T _{CLAD}	MIDPLANE h	Zq	MIDPLANE T _{CLAD}
INITIAL CLAD TEMPERATURE	LOW T _{CLAD}	HIGH T _{CLAD}	$A \approx B$	$A \approx B$	$A < B$	$A \geq B$	$A \geq B$	$A < B$
PEAK POWER	LOW PEAK POWER	HIGH PEAK POWER	$A \approx B$	$A \approx B$	$A < B$	$A > B$	$A > B$	$A < B$
PRESSURE	HIGH PRESSURE	LOW PRESSURE	$A \approx B$	$A \approx B$	$A \approx B$	$A > B$	$A > B$	$A < B$
INLET COOLANT SUBCOOLING	HIGH SUBCOOLING	LOW SUBCOOLING	$A \approx B$	$A \approx B$	$A \approx B$	$A > B$	$A > B$	$A < B$
FLOODING RATE*	HIGH FLOODING RATE	LOW FLOODING RATE	$A > B$	$A > B$	$A < B$	$A > B$	$A > B$	$A < B$

* NOTE: FLOODING RATE EFFECT h AND Zq ALWAYS HIGHER FOR CASE A

At times after t_1 , the quench fronts start to diverge more rapidly due to differences in clad temperatures at higher elevations caused by differences in power generation or initial clad temperature, or by the effect of flooding rate, pressure and subcooling on heat transfer coefficients above the quench front. Hence, the movement of the quench front is controlled by clad temperature. That is, the clad at a given elevation must drop to a certain temperature range (wetting or quenching temperature) before it can quench. Once the quench fronts diverge, the effect of elevation above the quench front is the dominant influence on heat transfer coefficient. Void fraction and quality increase as may the actual coolant sink temperature with increasing distance above the quench front. Hence, the heat transfer coefficients decrease with increasing distance between a given elevation and the quench front.

3.4 HEAT TRANSFER BEHAVIOR AT OTHER ELEVATIONS

Figures 3-44 and 3-45 show the heat transfer coefficients at 2, 4, 6, 8, and 10 ft at 1 in./sec flooding rate and various pressure and subcooling. The elevation trend is consistent with previous FLECHT low flooding rate data, namely the heat transfer coefficient decreases with increased elevation.

Fluid property effects influencing the heat flux at higher elevations are as follows:

1. Increased void fraction at the upper elevations, which would lower heat transfer.
2. Increased mixture velocity with elevation, tending to increase heat transfer.
3. High coolant temperatures and a lower temperature difference between the cladding and the coolant. This is due to the axial cosine power shape, and tends to lower the heat flux. Since the heat transfer coefficients shown in the figures are referenced to the saturation temperature, a lowering of the heat flux due to high coolant temperatures results in a decrease in the heat transfer coefficient.

At low flooding rates, Effects 1 and 3 are dominant, thus decreasing the heat transfer at upper elevations.

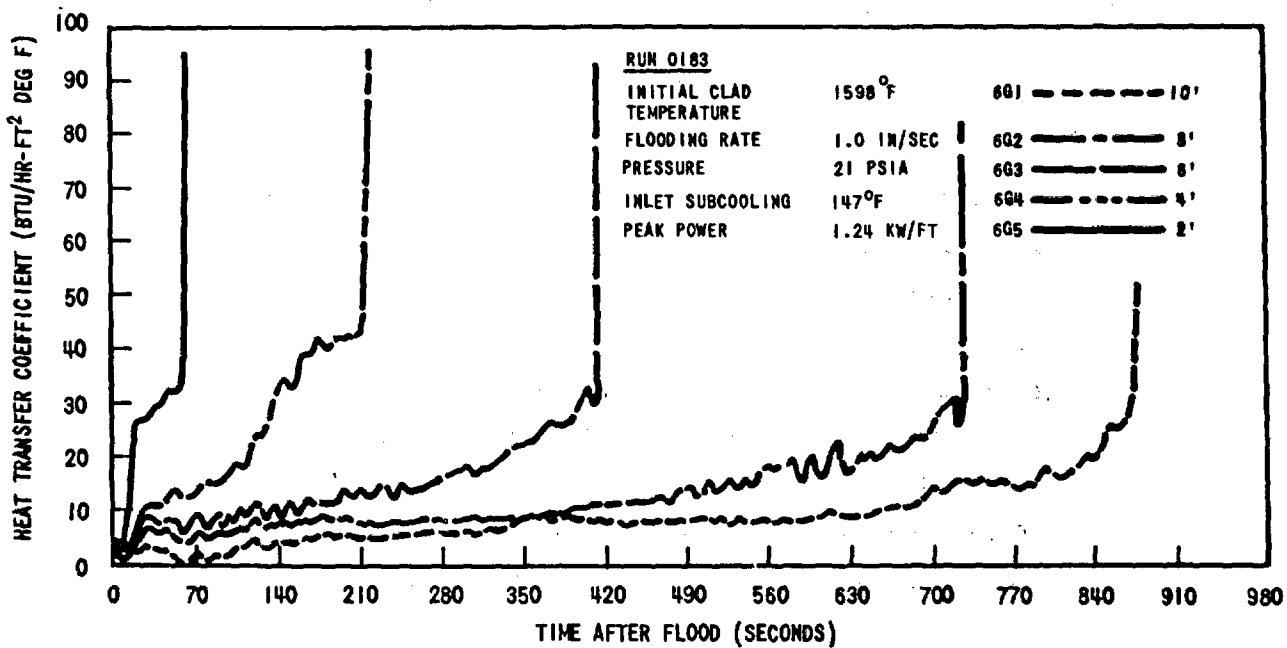
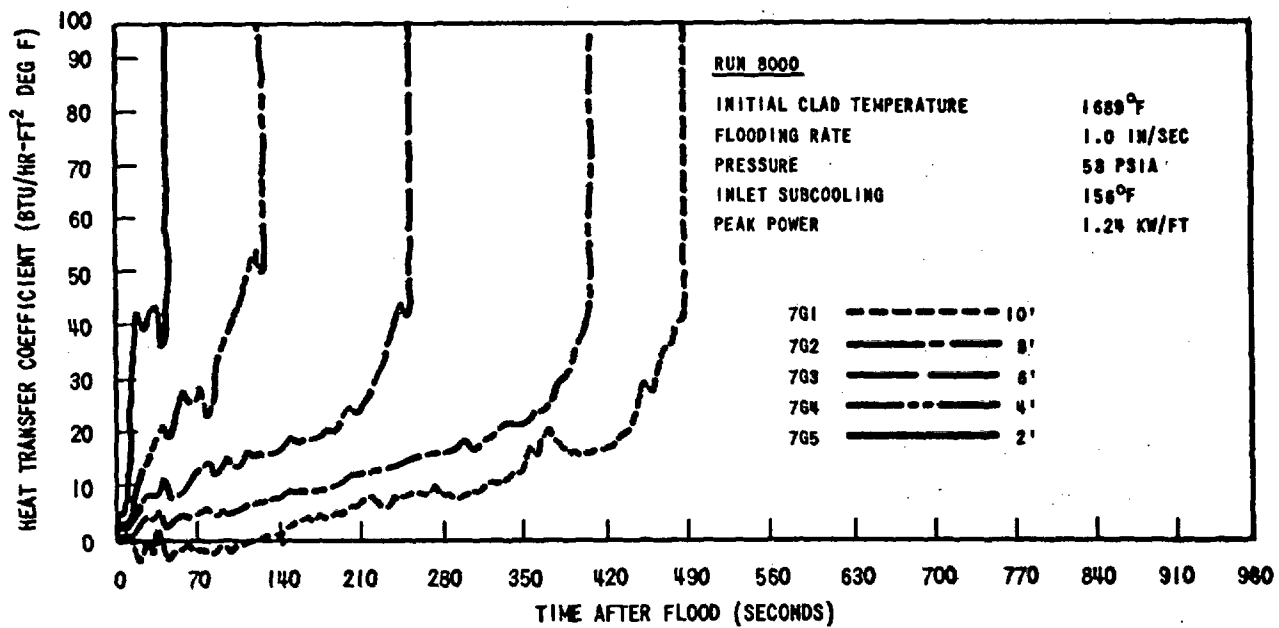


Figure 3-44. Heat Transfer Coefficient at Five Elevations in High Subcooling Tests at 58 and 21 PSIA

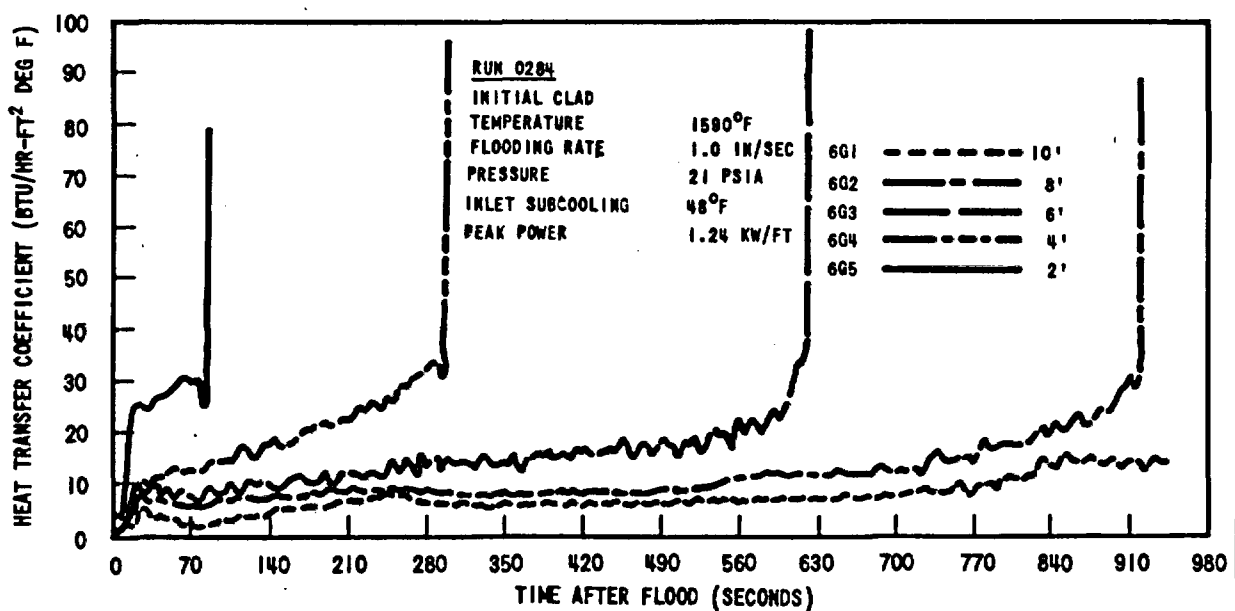
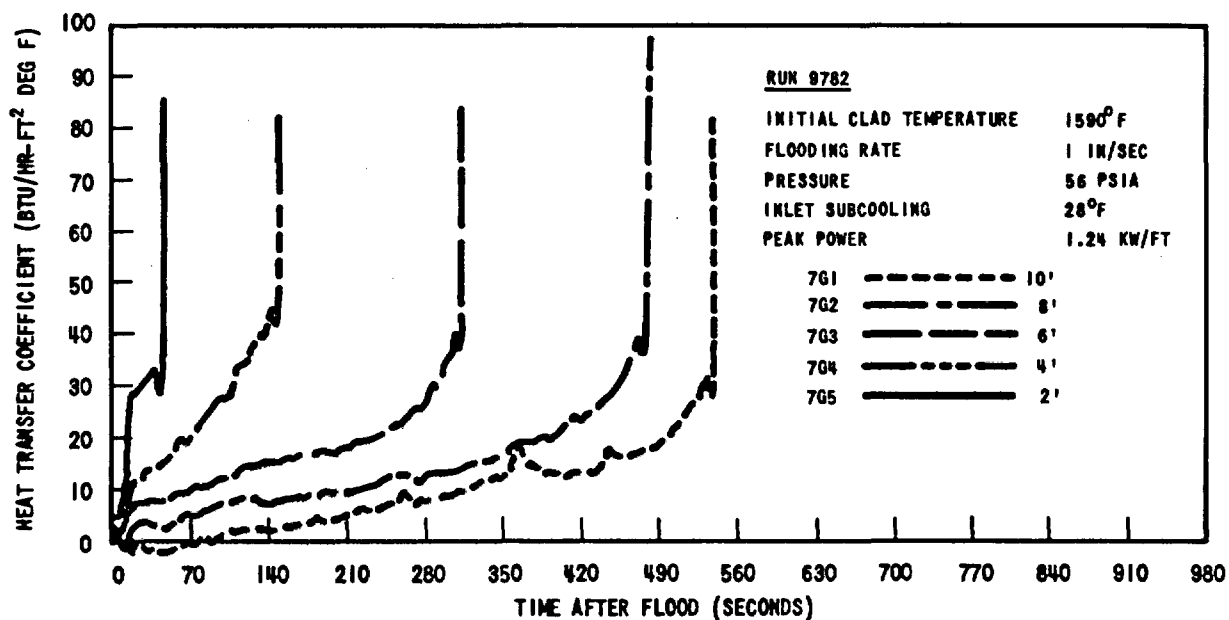


Figure 3-45. Heat Transfer Coefficient at Five Elevations in Low Subcooling Tests at 58 and 21 PSIA

Comparing the high and low pressure tests, it is important to note that while the 2, 4, and 6 ft heat transfer coefficients are lower with low pressure, the 8-foot and 10-foot heat transfer coefficients are higher for lower pressure for a considerably long time after flood. Comparison of run 8000 (56 psia) and run 0183 (21 psia) shows that the 8- and 10-foot heat transfer coefficients are greater for the lower pressure run 0183 for the first 70 and 200 seconds after flood, respectively. Comparison of runs 9782 (56 psia) and 0284 (21 psia), as presented in Figure 3-45, shows that the 8- and 10-foot heat transfer coefficients are greater for run 0284 for 70 and 260 seconds, respectively. After these times, the heat transfer coefficients cross over, and the trend is consistent with the 2, 4, and 6-foot elevations. This upper elevation pressure effect is probably due to a lower coolant temperature at the upper elevations in the low pressure tests, resulting from poorer heat transfer at lower elevations (less heat addition to the coolant) and/or increased carry-over. The steam probe data at the 10 ft elevation indicates a peak temperature of 1750°F for run 8000, but 1520°F and 1425°F peaks for runs 0183 and 0284, respectively. Additionally, reverse heat transfer coefficients at 10 feet (net heat transfer into the rod) occur only in the 60 psia cases, further indicating higher coolant temperatures resulting from greater heat transfer at lower elevations and/or lower carryover for higher pressure.

Comparison of 2 in./sec heat transfer coefficients at 60 and 20 psia showed the same trends as for the 1 in./sec data. Heat transfer coefficients at 4 and 6-ft were higher for the high pressure case. At 8 ft and 10 ft, however, the heat transfer coefficients at low pressure were equal to or higher than the higher pressure case for about 140 seconds after flood. At this time, the heat transfer coefficient for the higher pressure test increased above the low pressure test.

It was observed that the peak temperature occurred at the 8 ft elevation in runs 8000 and 9782 (see Appendix A). However, the peak temperature at the 8 ft elevation for run 9782 was only 9°F higher than the peak midplane temperature. These tests were both run at 60 psia pressure and 1 in./sec flooding rate.

In run 6948 of the Group II test series (which is a duplicate run of test 8000 but performed with the 7 x 7 test section), the peak temperature in the bundle occurred at the 6 ft elevation. Examination of the data reveals that the 8 ft clad temperature at the start of flood for run 8000 was approximately 100°F higher than for 6948. Also, the initial housing temperature for 8000 was 180°F higher at the 8 ft elevation. However, FLECHT temperature criteria for the 0 to 6 ft elevation were met as the average housing temperature from 0 to 6 ft elevation were within 150°F of each other. Also, the housing temperature distribution from 0 to 6 ft was fairly close for both runs. The difference in rod and housing temperatures could account for the difference in the 8 ft peak clad temperatures between the two runs. This should not be interpreted as a difference between the 7 x 7 and 10 x 10 bundles.

The effect of subcooling at other elevations for these low and high pressure 1 in./sec runs was similar to that discussed in Section 3.3.3 for the midplane elevation.

The current test series had a special 6-thermocouple rod, with thermocouples at the 6'4" and 6'8" elevations. This rod was reused from the Group II flow blockage test series. These results are not reported, however, because the 6'8" thermocouple was inoperative and the 6'4" thermocouple shorted out during the current series and was considered unreliable. It is intended to study these thermocouple locations more extensively in the FLECHT Systems Effects Tests.

3.5 EXTERNAL THERMOCOUPLE DATA

External thermocouples were installed on rod 5G at 6, 12, 18, 24, and 36 inches from the bottom of the bundle. A typical plot of this data as well as a 2 foot internal thermocouple from rod 6G (since rod 5G had no 2 foot thermocouple) is shown in Figure 3-46. This figure indicates consistency of the internal and external thermocouples during heatup. After flooding was started the external thermocouples were wetted and quenched soon after flood. The data shows that at the start of flood the rods reach a temperature of over 600°F as low as 6 inches above the bottom of the bundle. Appendix C shows temperature distributions at the start of flood for all runs in the current series utilizing the external thermocouple data.

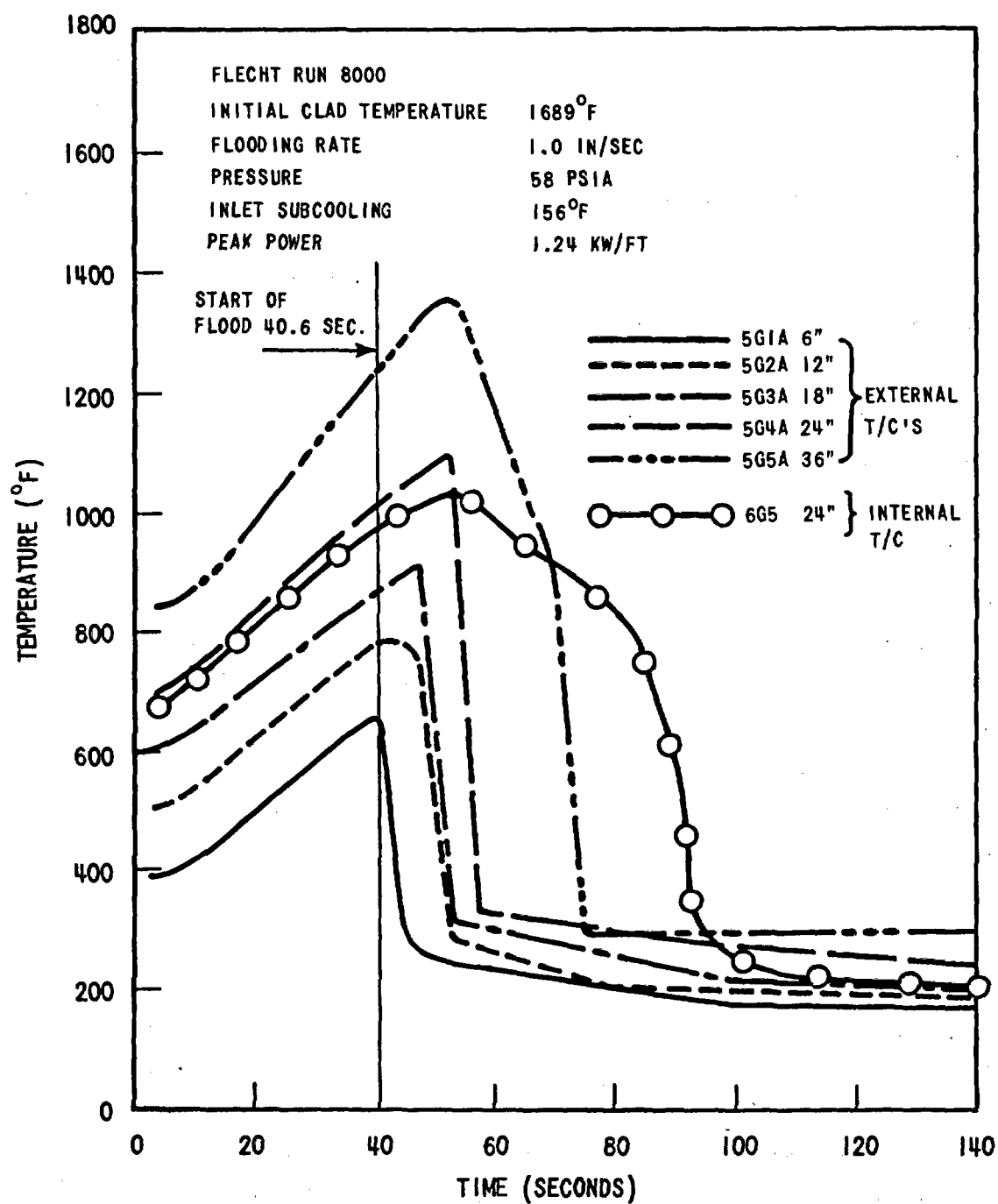


Figure 3-46. External Thermocouple Behavior, Run 8000.

3.6 HEAT TRANSFER COEFFICIENT CORRELATION

3.6.1 Modifications to Include Current Data

Comparison of the measured heat transfer coefficient of the latest FLECHT runs with that computed from the heat transfer coefficient correlation given in the FLECHT Final Report (WCAP-7665) shows that the predicted heat transfer coefficient for the combination of low flooding rate, low subcooling, and low pressure does not precisely match the measured heat transfer coefficient, because the predicted 6 ft quench time is too short. Therefore, it was necessary to modify the 6 ft quench time correlation.

The 6-foot quench time correlation is modified as follows:

$$\begin{aligned}
 t_{q6ft} = & 98.39 [e^{-.0107\Delta T_{sub}} (1 - e^{-.667 V_{in}})(1 + 0.5 e^{-.000037p^3} \\
 & + 1.3 e^{-.111 V_{in}^2} + 17.3 e^{-.000037p^3} e^{-.49 V_{in}^2})(1.207 Q_{max}^{1.5} - .667) \\
 & + (3.28/V_{in}^{1.1} - 2.8 e^{-V_{in}})(1 + 0.5 e^{-.000037p^3})] (1 + .0000588 T_{init})
 \end{aligned}$$

There are also minor changes in the heat transfer coefficient correlations. In the following equations, the changes are indicated by enclosing within rectangles.

Period I. $0 < t/t_{q6ft} < (t/t_{q6ft})_2$

$$h = h_1 [1 - e^{-10(x_2 - x)/x_2}] + [h_{12} - h_1 \{1 - e^{-10(x_2 - x)/x_2}\}]$$

$$[1 - e^{-x} - 0.9xe^{-x^2}][1 - 2.21e^{-.4 v_{in} u} \exp\{-(0.5882 - 3.824)^2\}]$$

where

t = time after flood in seconds

h_1 = initial heat transfer coefficient (See Section 3.6.2 for further discussion)

$$= 3.67 Q'_{\max} [1 - \exp\{-(T_{\text{init}} - 700)/435\}]$$

$$(t/t_{q6ft})_2 = 0.62 [(1 - e^{-0.192Z}) - 0.115Ze^{-0.0368Z^2}]$$

$$x_2 = 17.6 [1 + 4.37e^{-0.0166\Delta T_{\text{sub}}}] [1 - \exp\{-(0.00075$$

$$+ 0.0000272 (v_{\text{in}} - 8)^2 (T_{\text{init}} - 650)\}] (t/t_{q6ft})_2$$

$$h_{12} = 4 + [35.7 + (22 - 0.00303Z^{4.1})(1 - e^{-0.0333P - 0.034Pe^{-0.0011P^2}})]$$

$$[1 - e^{-0.2 V_{in}}] + 8 [1 - e^{-2 V_{in}}] [1 - e^{-B/25}]$$

$$x = 17.6 [1 + 4.37e^{-.0166\Delta T_{sub}}] [1 - \exp\{-(.00075$$

$$+ .0000272 (V_{in} - 8)^2) (T_{init} - 650)\}] (t/t_{q6ft})$$

$$u = 9 (t/t_{q6ft})^2 / (t/t_{q6ft})_2^2$$

Period II. $(t/t_{q6ft})_2 < t/t_{q6ft} < (t/t_{q6ft})_3$

$$h = h_2 + b_1 [y^2 + b_2 (y^2 - b_3 y^3) + b_4 y^2 e^{-6.38y}]$$

where:

$$(t/t_{q6ft})_3 = 1.55 [(1 - e^{-0.205Z}) - 0.154Z e^{-0.0421Z^2}]$$

$$h_2 = h_{12} [(1 - e^{-x_2}) - 0.9 x_2 e^{-x_2^2}]$$

$$b_1 = [682 - 650 (1 - e^{4-Z})] [1 - \exp\{-0.95(1 - 0.0488Z) V_{in}\}]$$

$$[1 - \exp\{-0.0238\Delta T_{sub}\}] [0.696 + 0.304e^{-B/25}]$$

$$y = (t/t_{q6ft}) - (t/t_{q6ft})_2$$

$$b_2 = 0.4Z [1 - e^{-2(Z-3.5)}] [1.33 (1 - e^{-0.0227P}) - 1]$$

$$-2.9 [1 - e^{-V_{in}/2.5}] [1 - e^{-B/25}]$$

$$b_3 = 2.55 [Z - 3.7]^2 e^{3.7-Z}$$

$$b_4 = 8.75 V_{in} e^{(-V_{in}^2)} \exp(-0.036\Delta T_{sub})$$

Period III. $t/t_{q6ft} > (t/t_{q6ft})_3$

$$h = h_3 + C [t/t_{q6ft} - (t/t_{q6ft})_3]$$

where:

$$h_3 = h_2 + b_1 [y_3^2 + b_2 (y_3^2 - b_3 y_3^3) + b_4 y_3^2 e^{-6.38 y_3}]$$

$$C = 420 [1 - e^{-0.00625 b_1}]$$

$$y_3 = (t/t_{q6ft})_3 - (t/t_{q6ft})_2$$

The above correlations are valid over the following ranges of parameters:

Flooding rate (V_{in})	0.4 - 10 in./sec
System pressure (P)	15 - 90 psia
Inlet coolant subcooling (ΔT_{sub})	16 - 189°F
Initial clad temperature (T_{init})	1200-2200°F
Peak power density (Q'_{max})	0.69-1.40 kw/ft
Elevation (Z)	4-8 ft
Percent Blockage (B)	0-75%

The comparison of the new correlation with present data is shown in Figures 3-47 to 3-57.

FORTTRAN program listing is given in Appendix D.

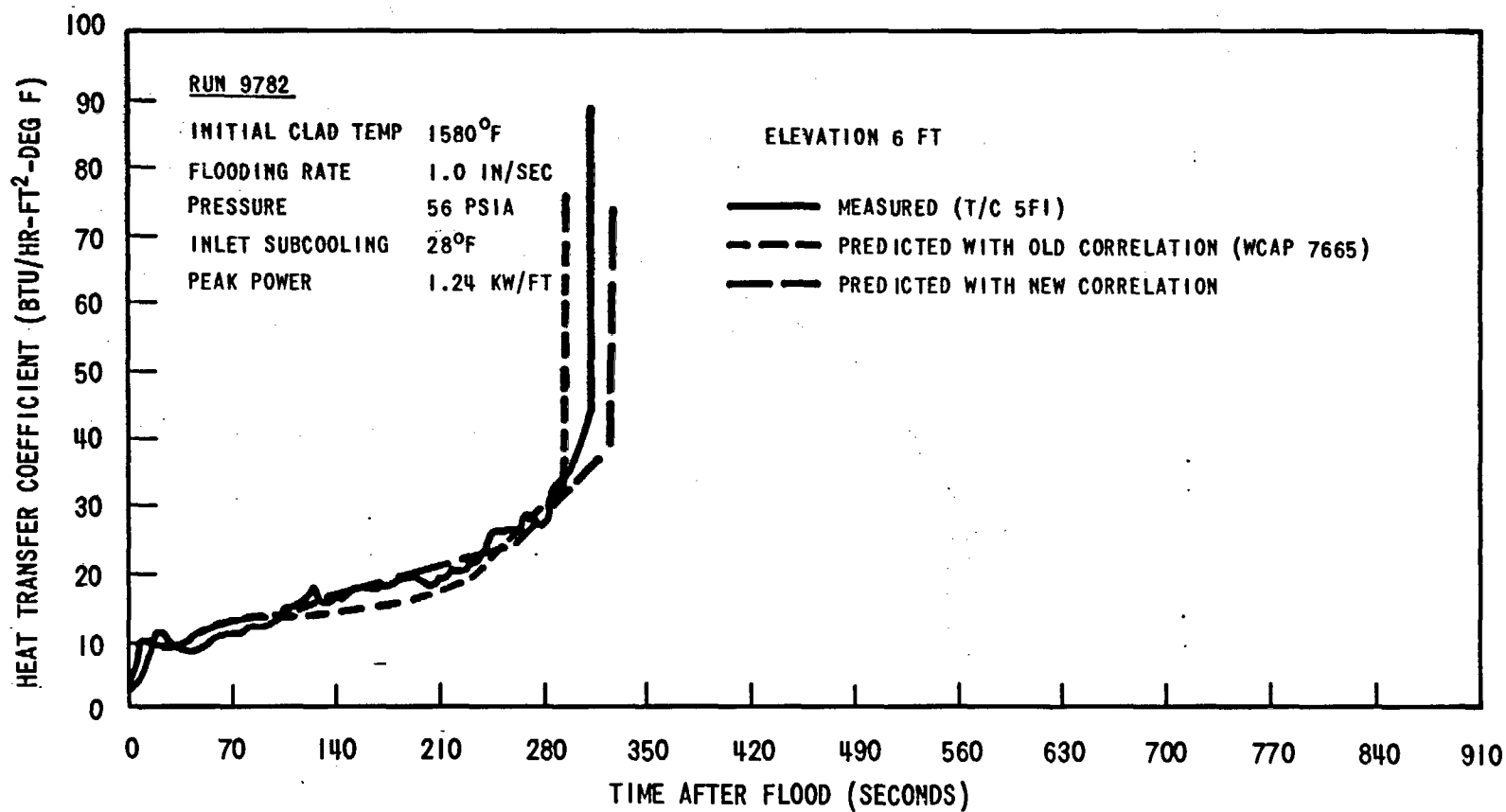


Figure 3-47. Comparison of Measured and Predicted Heat Transfer Coefficients.

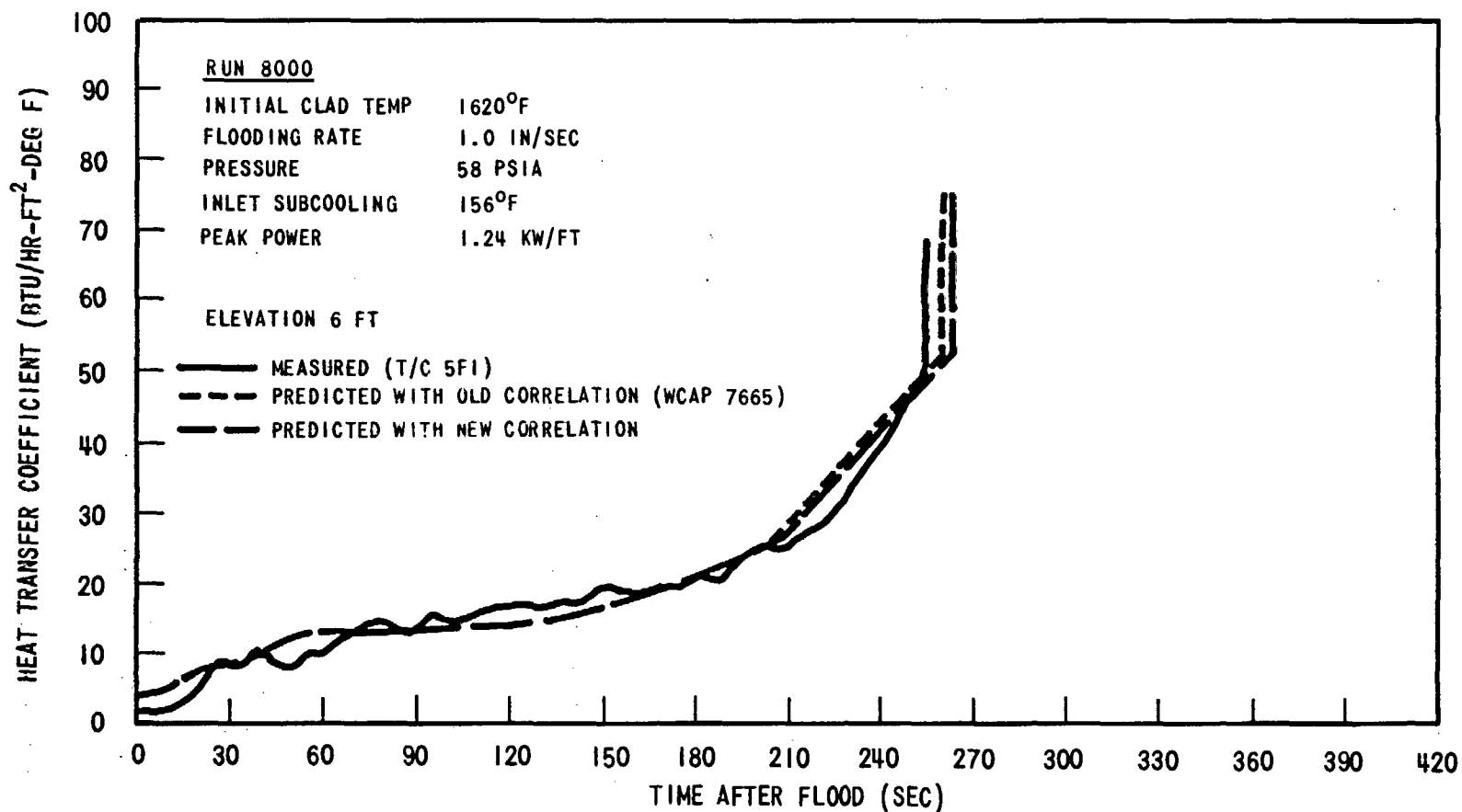


Figure 3-48. Comparison of Measured and Predicted Heat Transfer Coefficients.

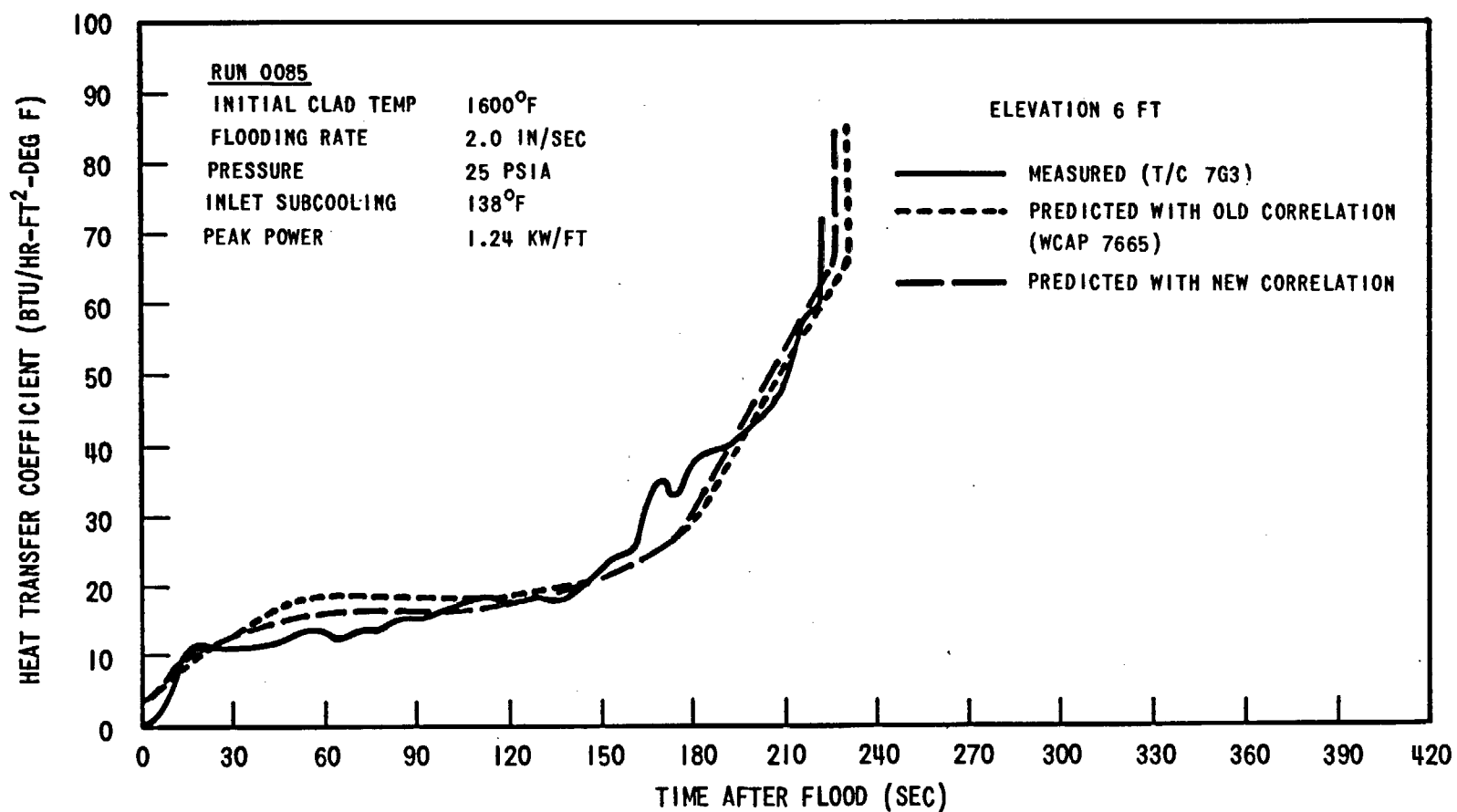


Figure 3-49. Comparison of Measured and Predicted Heat Transfer Coefficients.

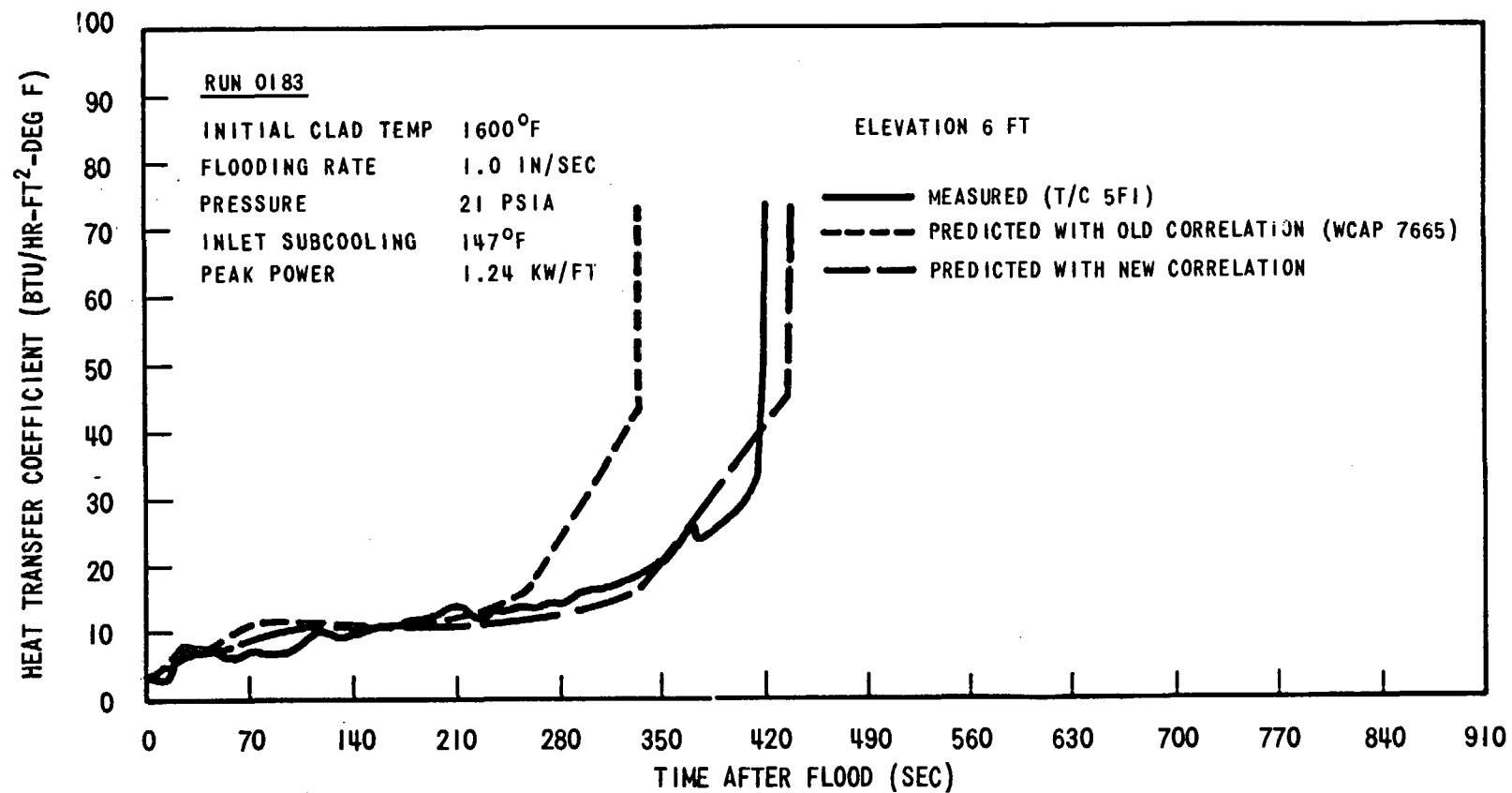


Figure 3-50. Comparison of Measured and Predicted Heat Transfer Coefficients.

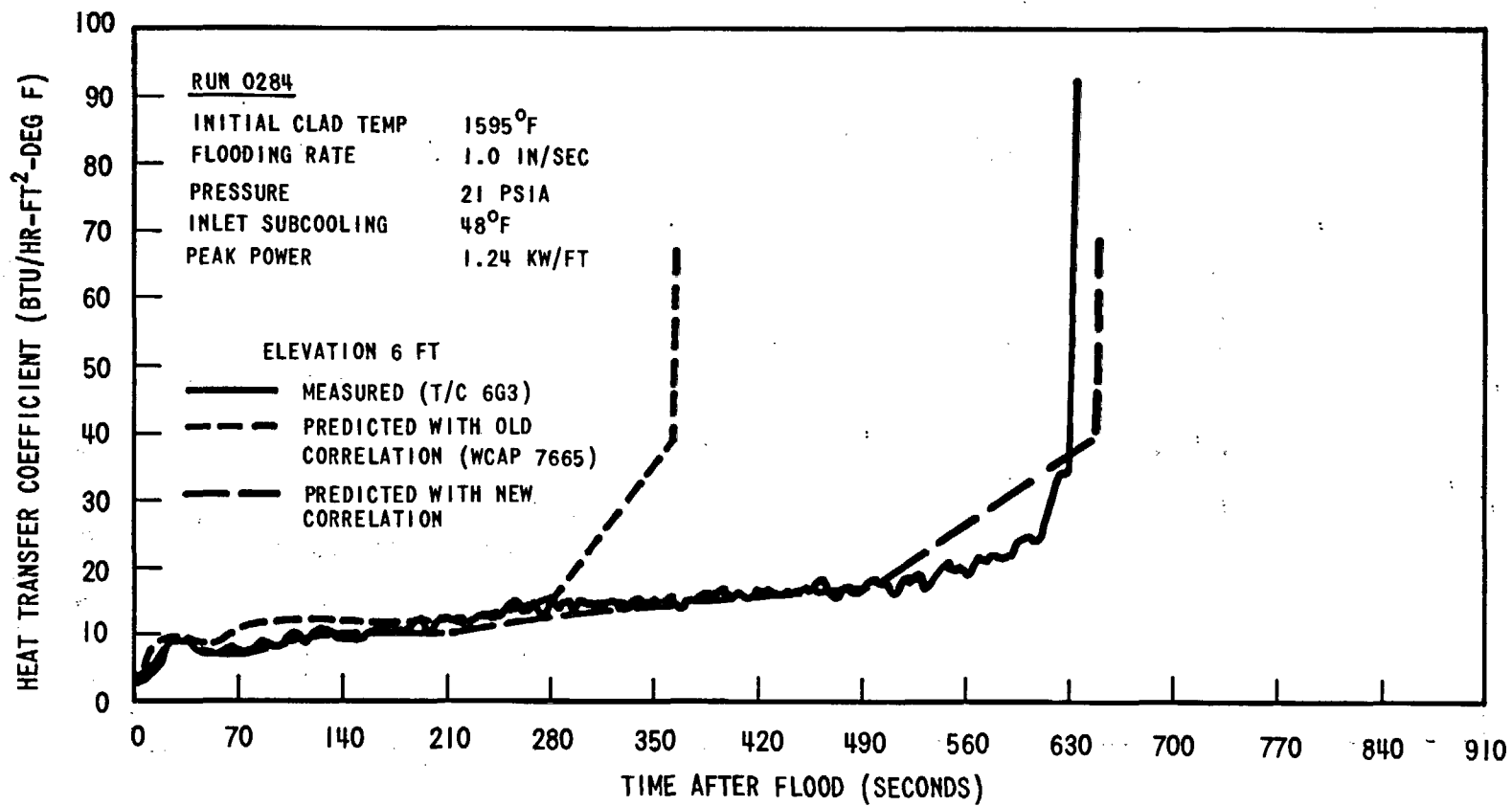


Figure 3-51. Comparison of Measured and Predicted Heat Transfer Coefficients.

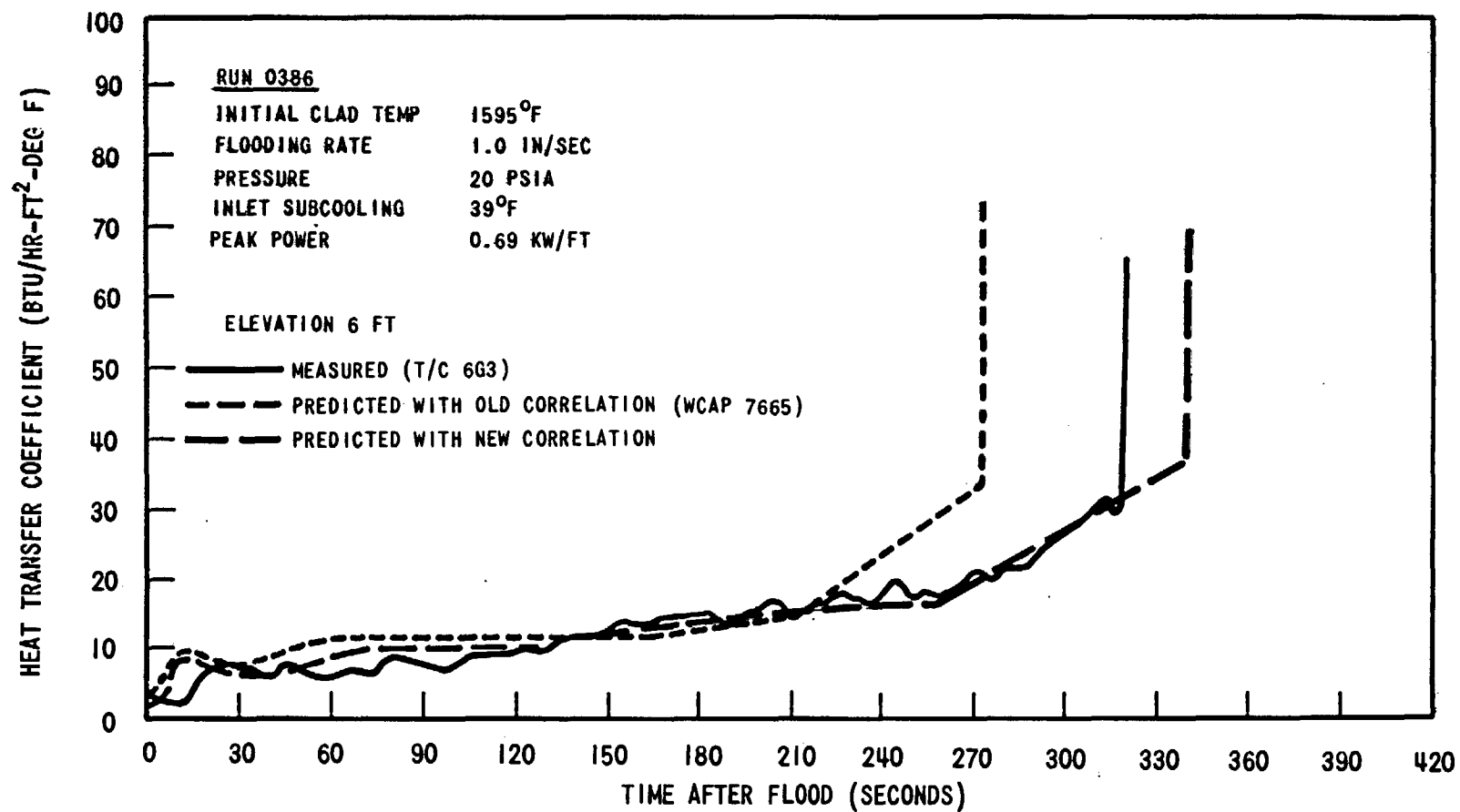


Figure 3-52. Comparison of Measured and Predicted Heat Transfer Coefficients.

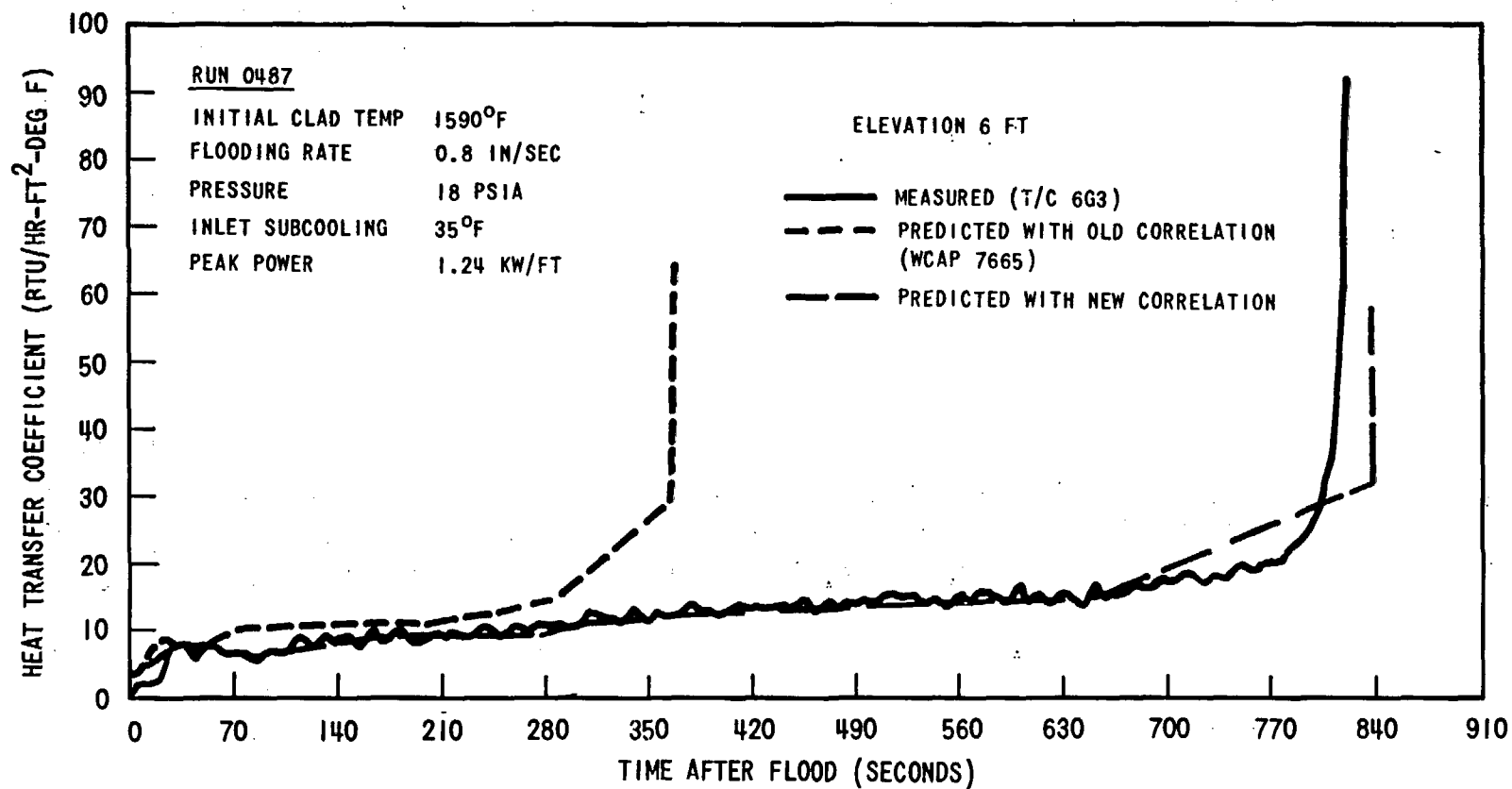


Figure 3-53. Comparison of Measured and Predicted Heat Transfer Coefficients.

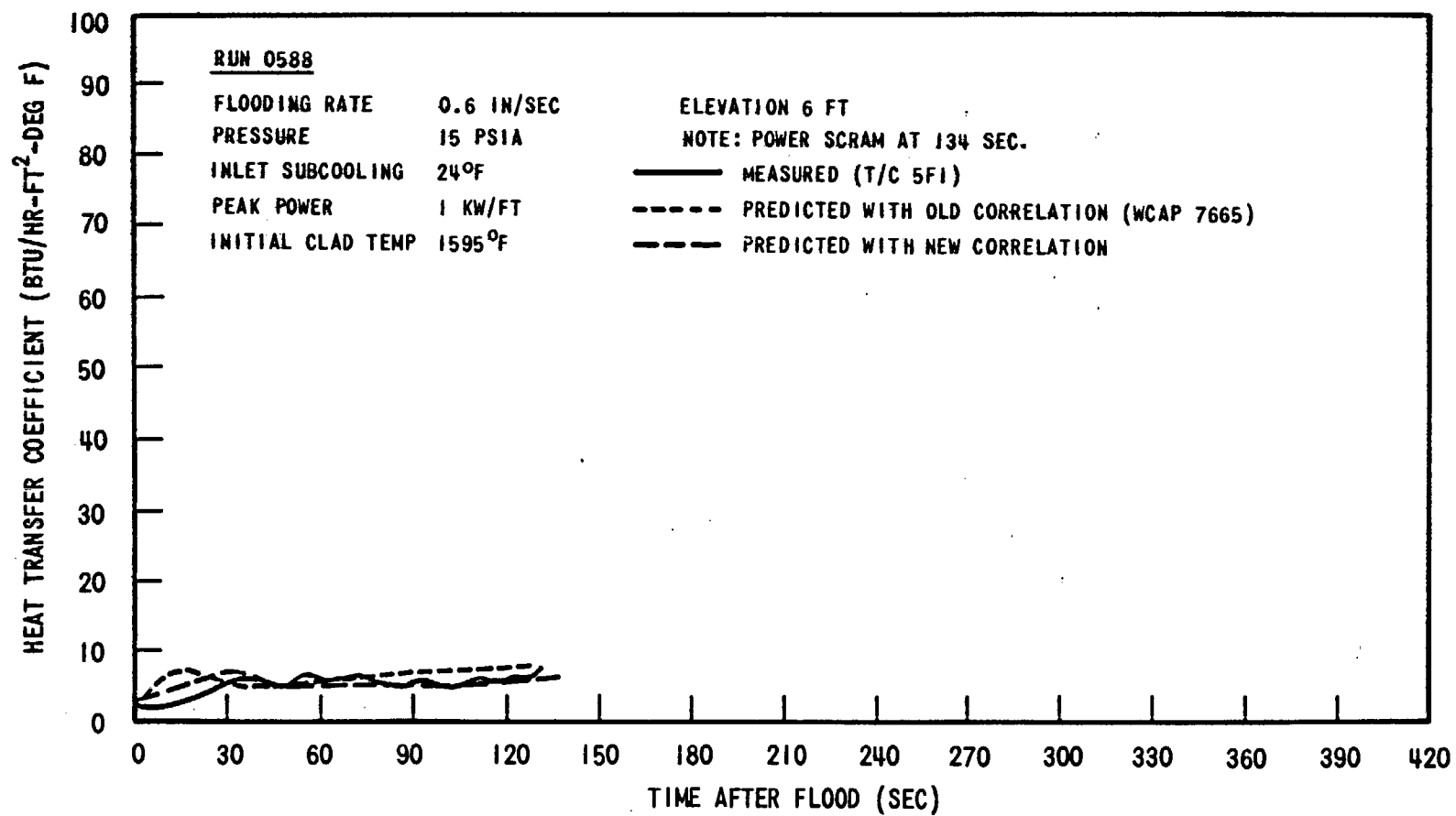


Figure 3-54. Comparison of Measured and Predicted Heat Transfer Coefficients.

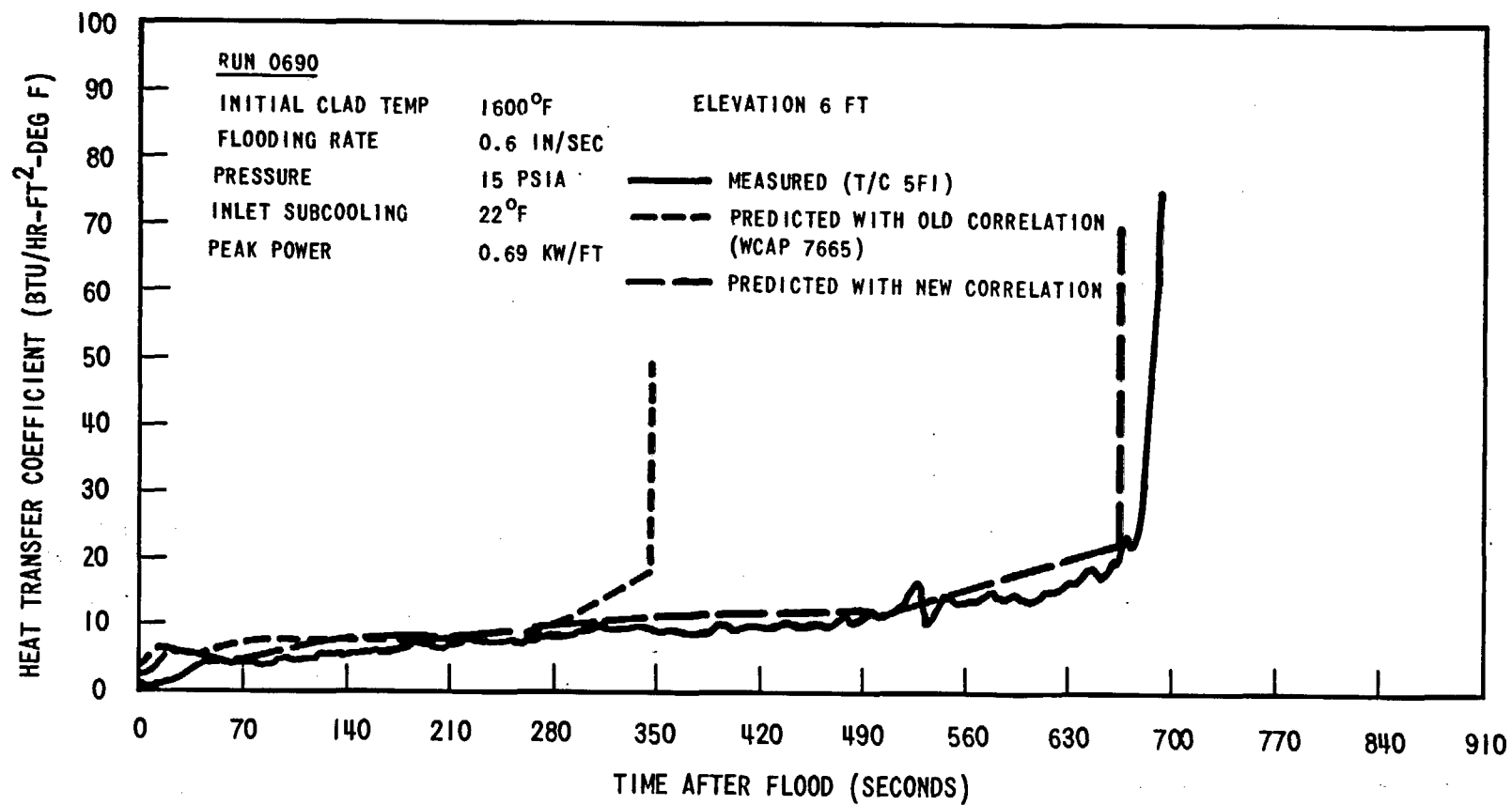


Figure 3-55. Comparison of Measured and Predicted Heat-Transfer Coefficients.

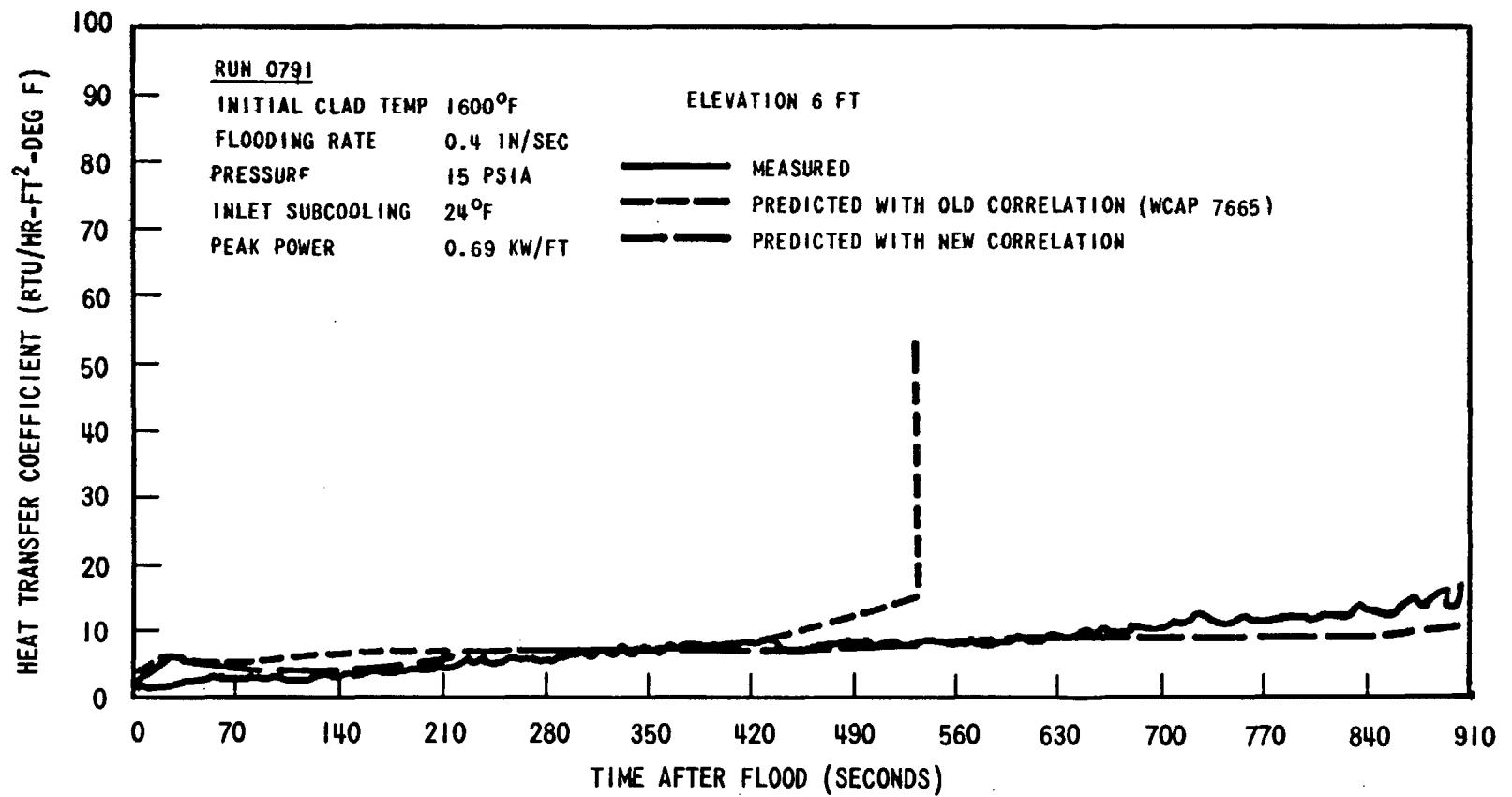


Figure 3-56. Comparison of Measured and Predicted Heat Transfer Coefficients.

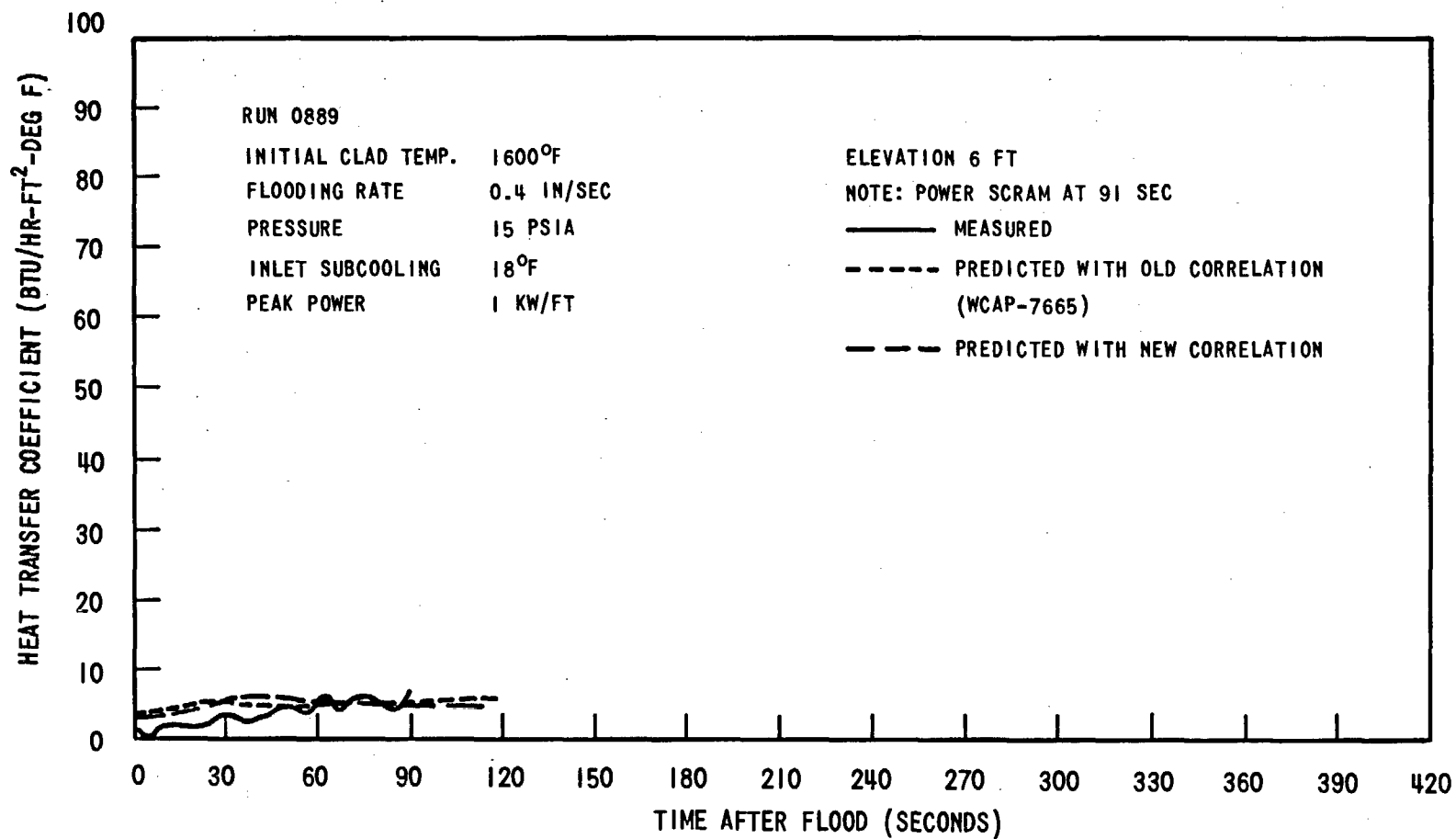


Figure 3-57. Comparison of Measured and Predicted Heat Transfer Coefficients.

3.6.2 Initial Heat Transfer Coefficient

The initial* heat transfer coefficient, h_1 , is primarily due to radiation from the hot rod to the adjacent rods and control rod thimbles. This radiation is dependent upon the temperature difference between the hot rod and the adjacent rods and control rod thimbles, and also upon the absolute temperature level (initial clad temperature).

In FLECHT tests the temperature difference between the hot rod and the adjacent rods and control rod thimbles, and hence h_1 , also depended on the initial power level. This is explained as follows: the FLECHT test procedure was to heat up the rod bundle at a prescribed initial power level from a starting temperature of approximately 700°F until the required peak initial clad temperature was reached, at which time flooding and power decay commenced. During this heatup period, the thimbles were heated by radiation from the rods. Thus the thimble temperature at the start of flood depended on the time duration of this initial heatup period. For a given initial clad temperature, the time duration of the heatup period depended on the initial power level (the power applied during heatup). The higher the initial power level, the shorter the heatup period, which resulted in a larger difference between heater rod and control rod thimble temperatures, and hence a higher h_1 . This dependence of h_1 on heatup power level and initial clad temperature is shown in Figure 3-58 for three typical FLECHT runs with peak power of 0.69, 1 and 1.24 kw/ft.

The h_1 values in Figure 3-58 are computed with a gray body radiation model which consists of a hot rod enclosed by three surfaces, two of which are the adjacent thimbles and the other one is equivalent to the surrounding heater rods. For detailed analysis the reader may refer to Appendix E. The surface temperatures needed for this calculation are obtained as follows; (1) the temperature of the surface which is equivalent to the surrounding heater rods is the actual average of the measured surrounding rod temperatures, (2) the thimble temperatures are computed by performing the following heat balance

*The word "initial" will be used as a synonym of "at the beginning of flood".

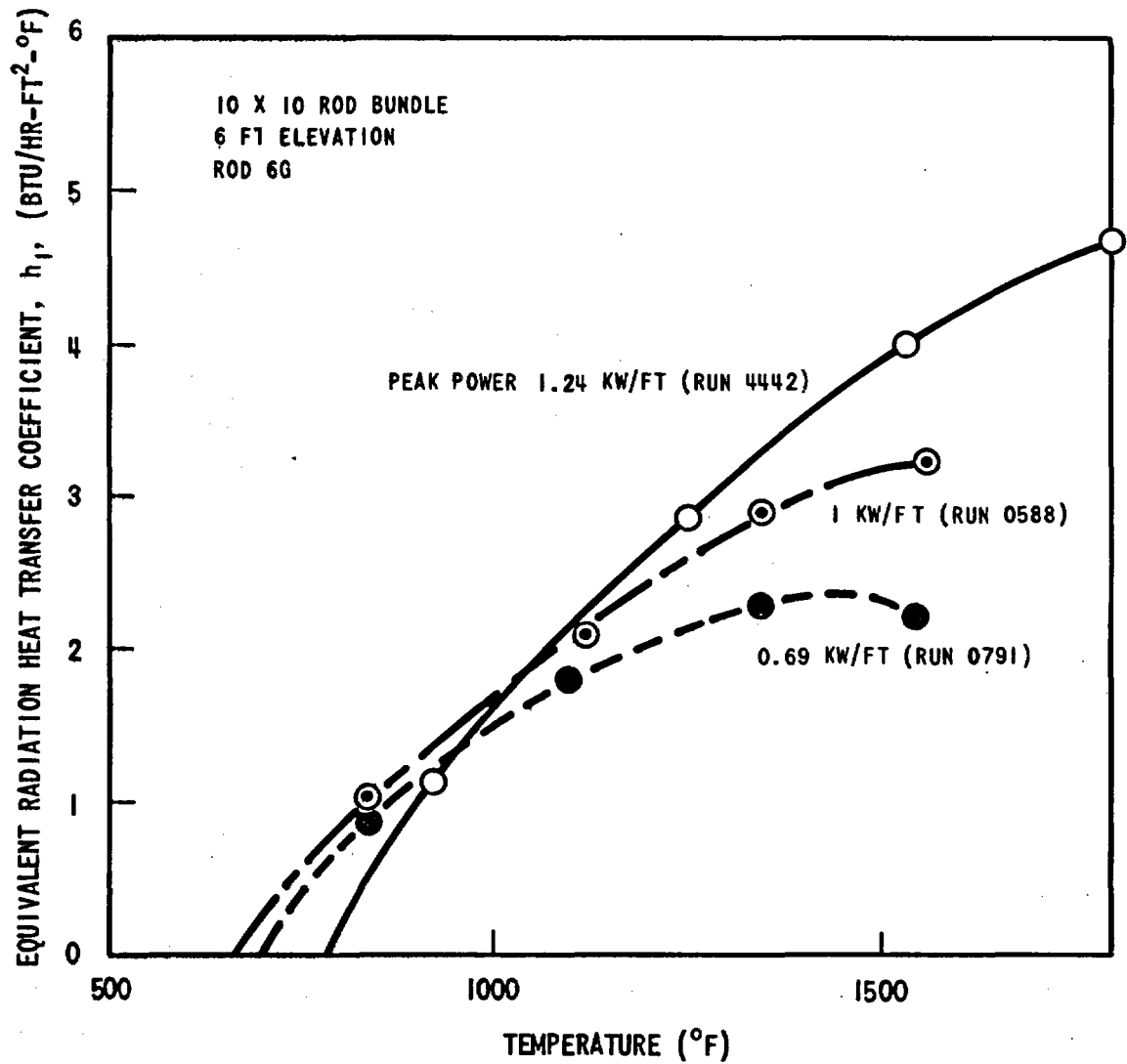


Figure 3-58. Heat Transfer Coefficient of a Hot Rod During Initial Heatup Period Computed from 4-Surface Gray Body Radiation Model.

on each thimble

$$(\rho A C_p \frac{dT}{dt})_{\text{thimble}} = \pi d \sigma F (T_{\text{rods}}^4 - T_{\text{thimble}}^4)$$

where

- ρ = thimble density
- A = thimble cross-sectional area
- C_p = thimble specific heat
- d = thimble diameter
- σ = Stefan-Boltzmann constant
- T_{rods} = average temperature of the rods surrounding the thimble
- F = interchange factor between thimble and rods
 $= 1/[1 + \frac{1-\epsilon}{\epsilon} (1 + \pi d/A_{\text{rods}})]$; A_{rods} is the equivalent area of the surrounding rods, evaluated by the method described in and corresponding to πD of Appendix E.
- ϵ = emissivity, taken to be 0.9 for the stainless steel heater rods and thimbles

The equivalent radiative heat transfer coefficient is defined as

$$h = \frac{q''_{\text{net radiation from the hot rod}}}{T_{\text{hot rod}} - T_{\text{sat}}}$$

Note that in Figure 3-58 the curve for run 4442 crosses the other curves. This is because for run 4442 heatup started at a higher temperature. Also note that the heat transfer coefficient for run 0791 drops at 1450°F. This is because the difference between the temperature of rod 6G and the average temperature of the surrounding rods decreases, and hence the heat flux q'' increases more slowly than the increase of $T_{\text{hot rod}} - T_{\text{sat}}$. This results in decreasing h because of the definition of h which used T_{sat} as the sink temperature.

Figure 3-59 plots the measured initial heat transfer coefficient, h_1 , against the computed initial heat transfer coefficient for various power levels and

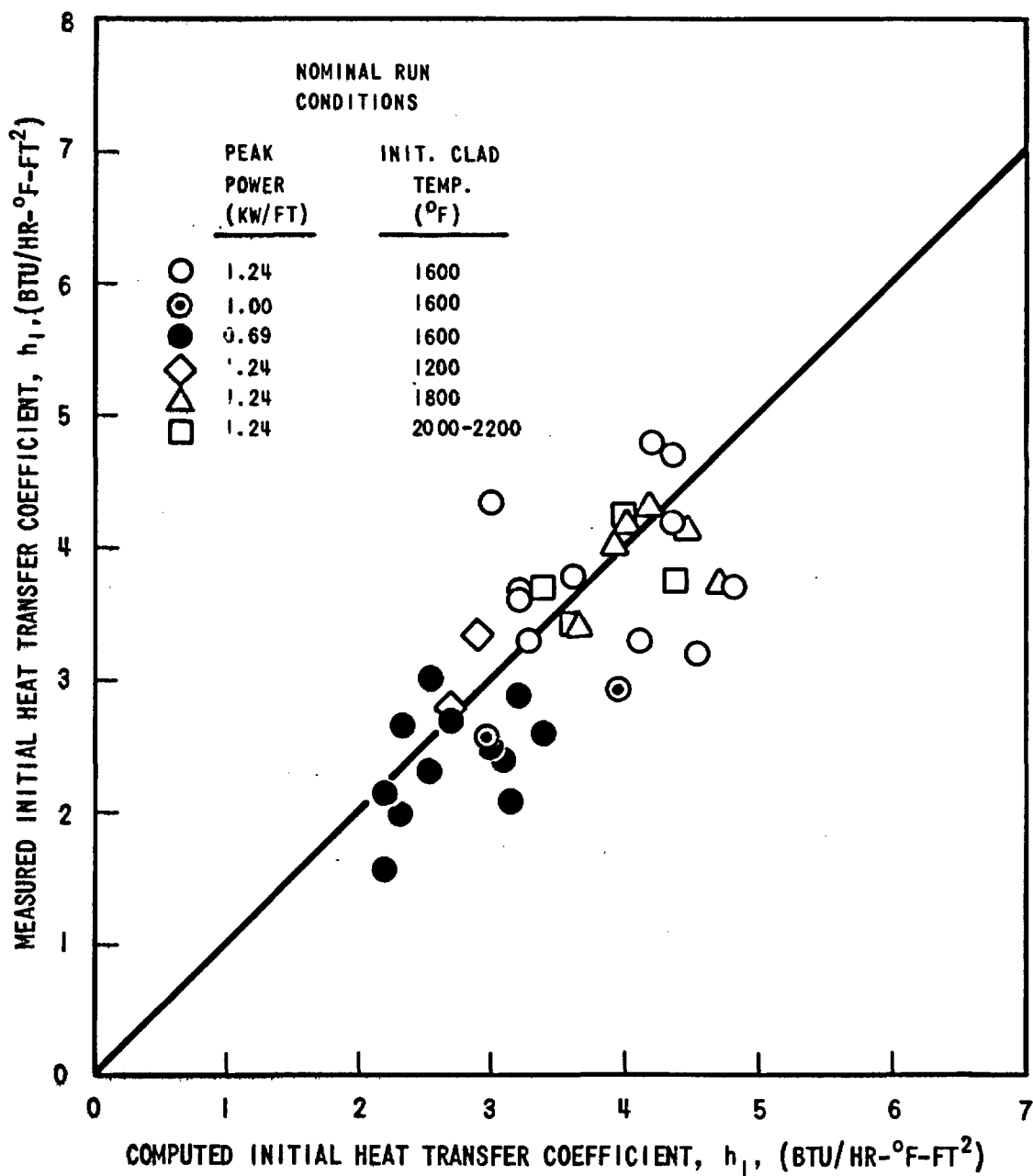


Figure 3-59. Comparison of Measured Initial Heat Transfer Coefficient with that Computed from 4-Surface Gray Body Radiation Model.

initial clad temperatures.* Figure 3-59 also exhibits the general trend of Figure 3-58, that is, the initial heat transfer coefficient, h_1 , increases with the increase of peak power. Similar calculations would have to be performed for the PWR case where different thimble configurations are utilized. Based on the data shown in Figure 3-59, the following correlation for initial heat transfer coefficient, h_1 , was derived

$$h_1 = 3.67 Q'_{\max} [1 - \exp \{-(T_{\text{init}} - 700)/435\}],$$

where Q'_{\max} is the peak power (Kw/ft) and T_{init} is the initial clad temperature ($^{\circ}\text{F}$). Figure 3-60 compares the measured initial heat transfer coefficient with that predicted by the correlation.

3.7 PRESSURE TRANSDUCER RESULTS

Axial pressure drop measurements were made at 0, 2, 4, 6, and 8 ft elevations on the flow housing. Figure 3-61 shows the effect of pressure and subcooling on axial pressure drop from 0 - 8 ft. The figure indicates that lowering the subcooling lowers the pressure drop. Lowering the system pressure also caused a slight decrease of the pressure drop.

It has been stated in Reference 2 that the axial pressure drop measured in FLECHT is due primarily to the elevation head of the mixture in the bundle. Since the quench front rises more rapidly at high pressure it is reasonable to expect the pressure drop to be higher relative to a low pressure case.

*In Ref. 1 it is stated that "Examination of data showed a scatter in h_1 (initial heat transfer coefficient) from 1 to 8 Btu/hr-ft²- $^{\circ}\text{F}$ with no consistent parameter trends. Therefore a mean value of h_1 (4 Btu-hr-ft²- $^{\circ}\text{F}$) was specified." The reason for the scatter in the initial heat transfer coefficient was found to be due to the interference of the pen recorder on the VIDAR reading, which caused h_1 for some rods to oscillate for about 30 early runs, and to oscillate with smaller amplitude for later runs after the pen recorder had been repaired. Examination of the data from other thermocouples which were not connected to the pen recorder revealed that the corrected values should be those shown in Figure 3-59 and that the mean values of the ones which oscillated agreed with the steady ones not connected to the pen recorder.

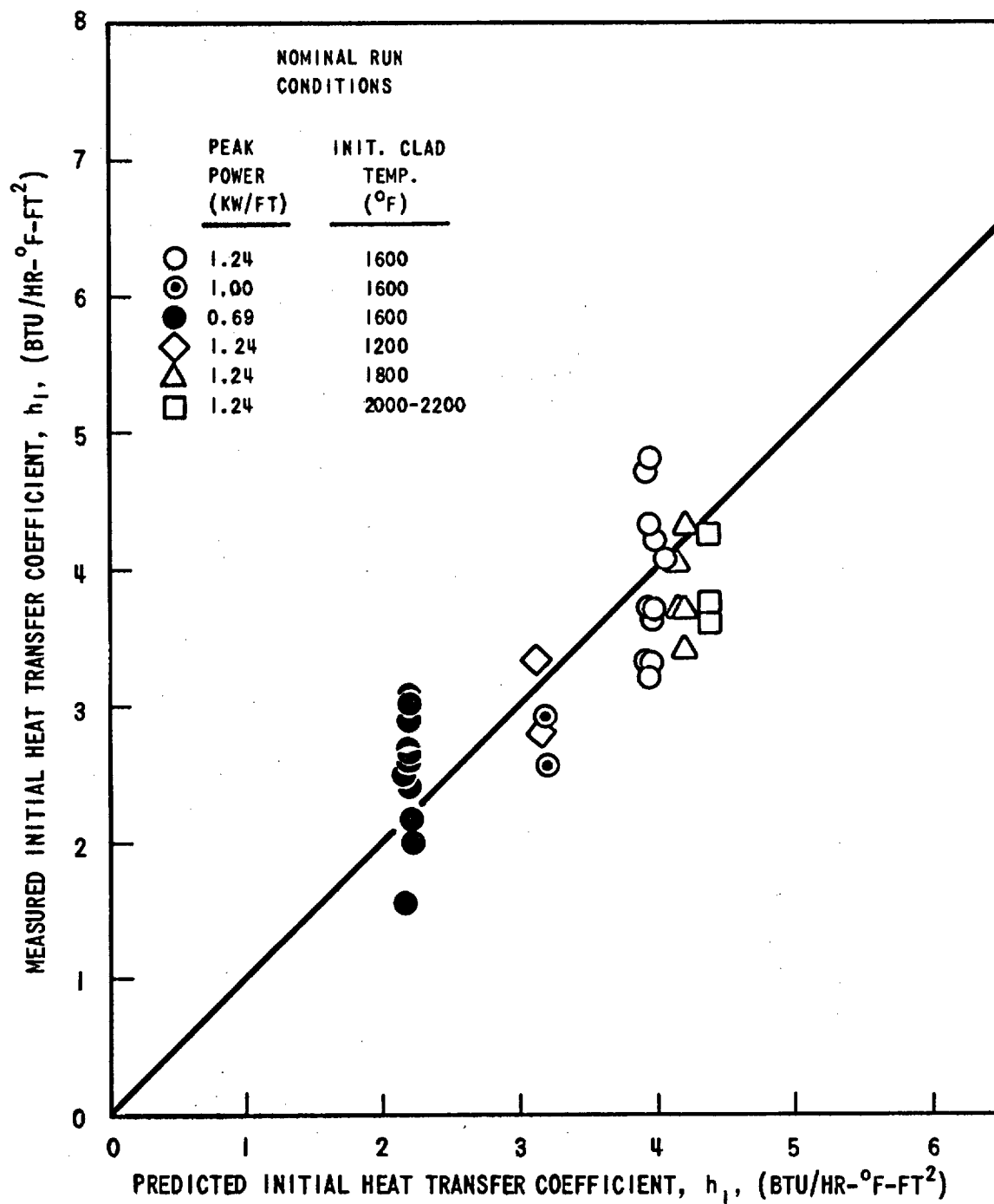


Figure 3-60. Comparison of Measured Initial Heat Transfer Coefficient and that Predicted with Correlation.

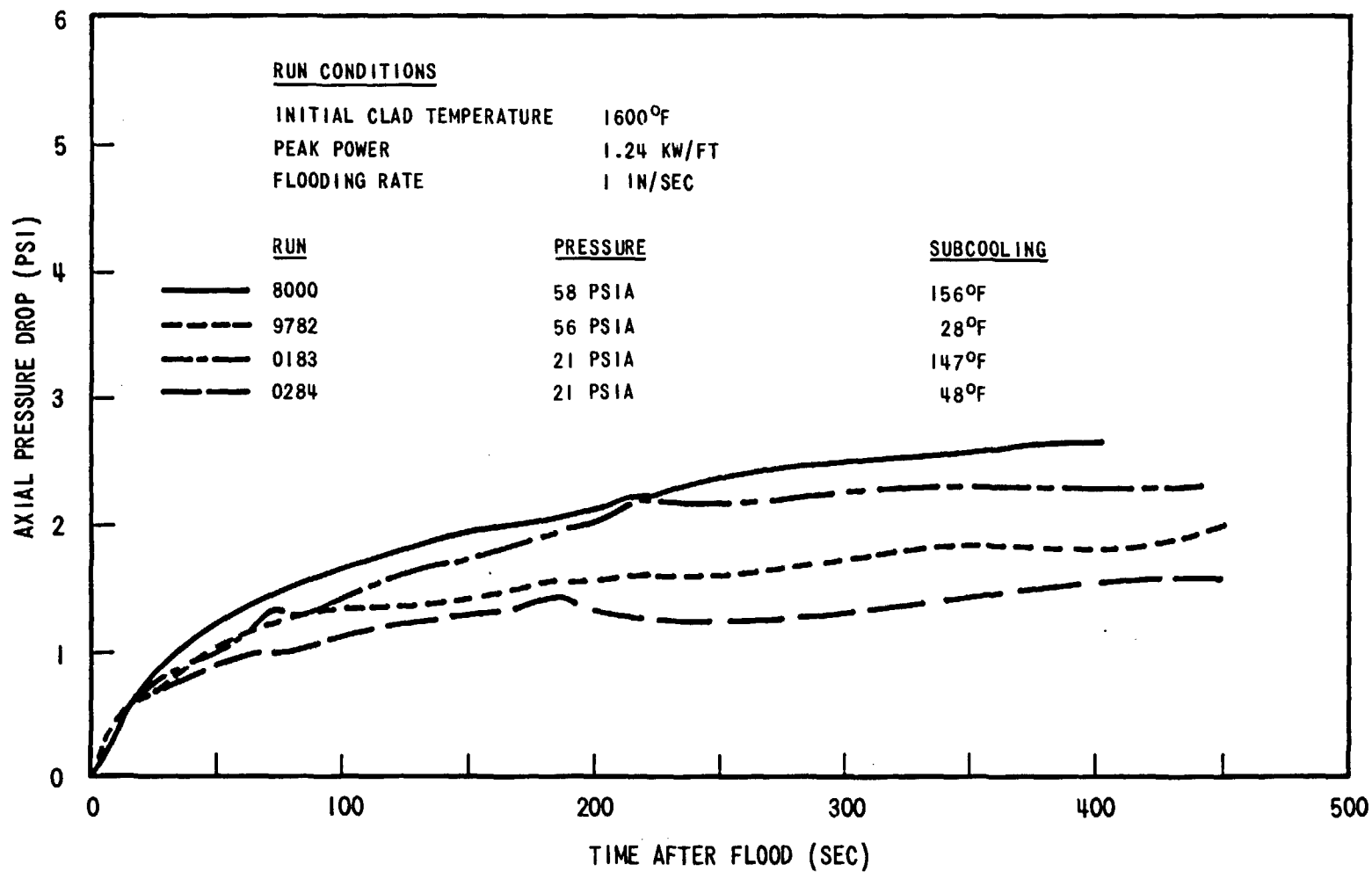


Figure 3-61. Axial Pressure Drop (0-8 Ft) for Various Pressure and Subcooling

The pressure drop in the low pressure runs (0284, 0138) is fairly close to the corresponding high pressure cases even though the quench front is lower in the bundle at any given time. This may be due to more liquid in the bundle above the quench front in the low pressure case, which gives additional elevation and momentum pressure drop. In the high pressure runs, liquid carryover is lower and thus water above the quench front does not contribute as much to the elevation pressure drop.

Low subcooling causes a lowering of the pressure drop because boiling below the quench front occurs lower in the bundle. Thus, there is only a small height of solid water contributing to the pressure drop.

Calculations of total carryover mass involve using the quench front elevation data to determine the bundle water inventory. Figures 3-62 through 3-65 show axial pressure drop data compared to quench front elevation data. The quench front elevation data was converted to elevation pressure drop assuming saturated liquid up to the quench front.

At times out to 200 to 300 seconds the use of quench elevation data to indicate bundle water inventory, yields lower bundle inventory and more carryover compared to the axial pressure drop data. At later times, the trend is reversed. The effect of these differences on total carryover mass is small since the total carryover is large compared to the stored mass in the bundle. For example, at 400 seconds in run 0284 the amount of water injected into the test section is equivalent to 400 inches in the test section. The amount stored in the bundle, using the pressure drop data, is 37.5 in. and, using the clad quench time data, is 47.5 inches. Total mass carried out of the bundle is the difference between the mass in and mass accumulated. The difference in the total carryover mass due to the choice of quench or pressure drop method is less than 3 percent. Thus, the total mass carryover calculation is not sensitive to the choice of the two methods used to determine the mass inventory in the bundle.

3.8 LOCAL COOLANT TEMPERATURE DATA

Local coolant temperature measurements were made at 7 ft, 10 ft, and 12.5 ft using steam probes, and at 12.5 ft and in the exit pipe using bare thermocouples. Figures 3-66 through 3-68 show the coolant temperature measurements for runs

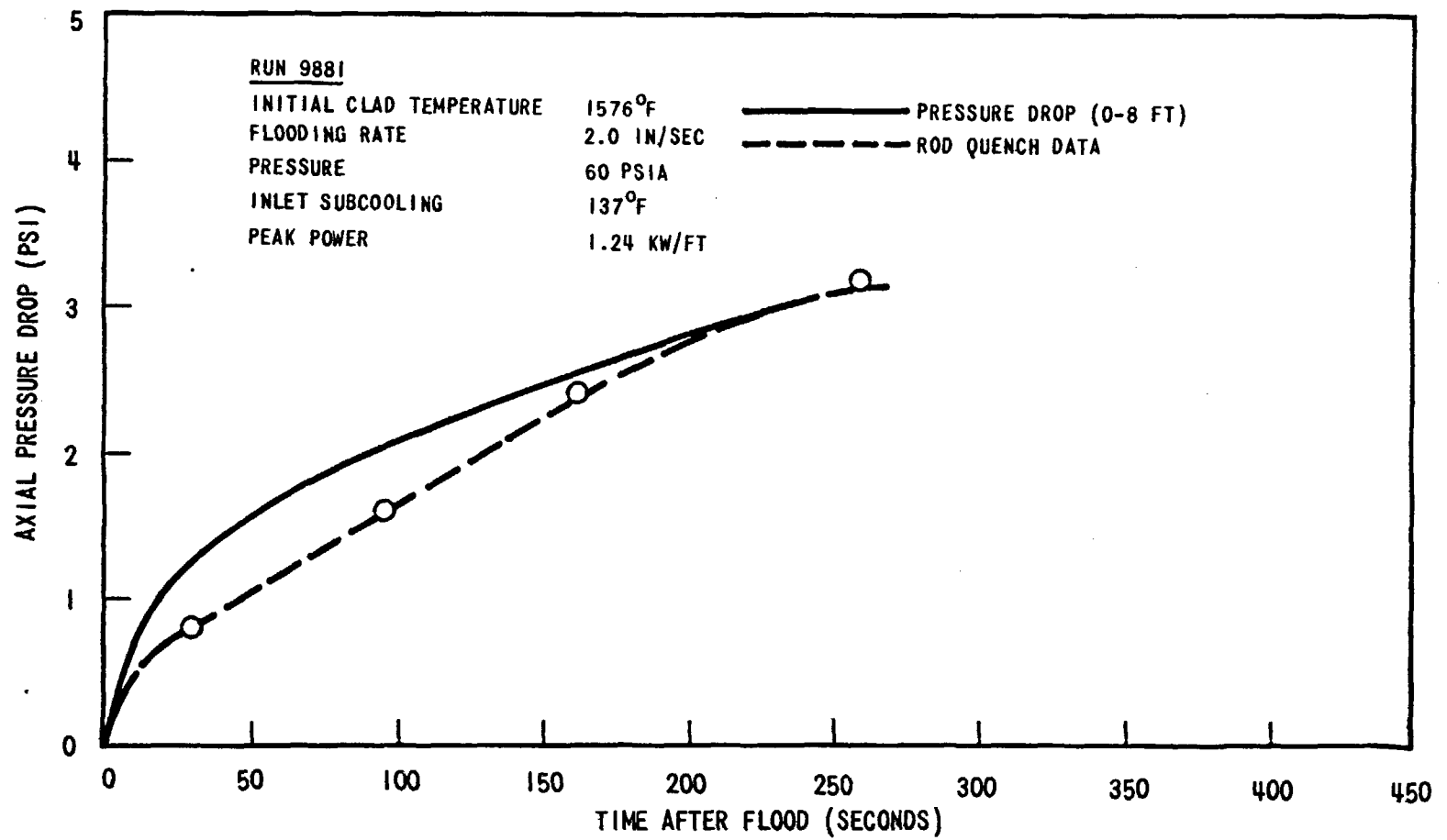


Figure 3-62. Comparison of Pressure Drop and Rod Quench Data, Run 9881.

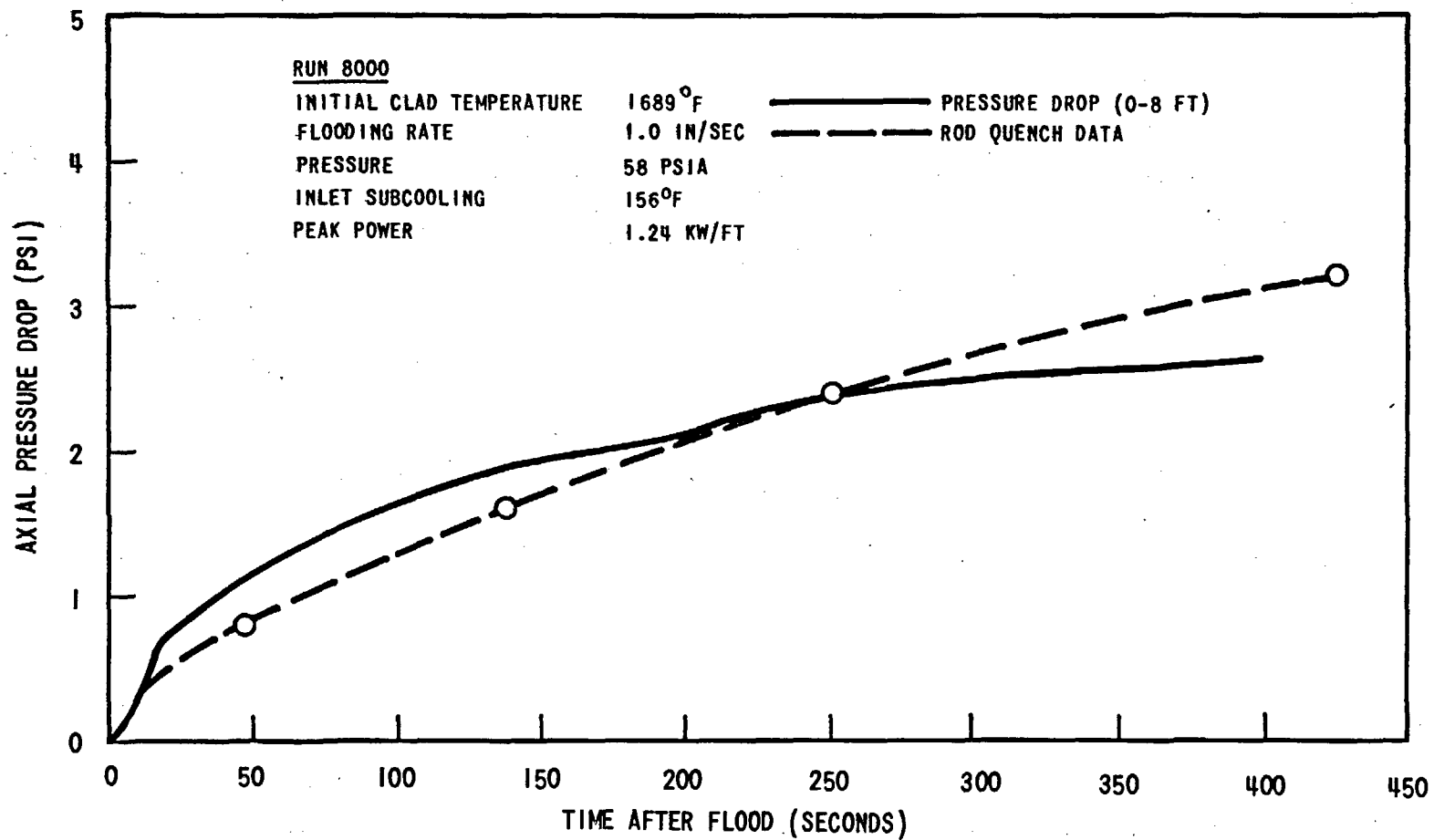


Figure 3-63. Comparison of Pressure Drop and Rod Quench Data, Run 8000.

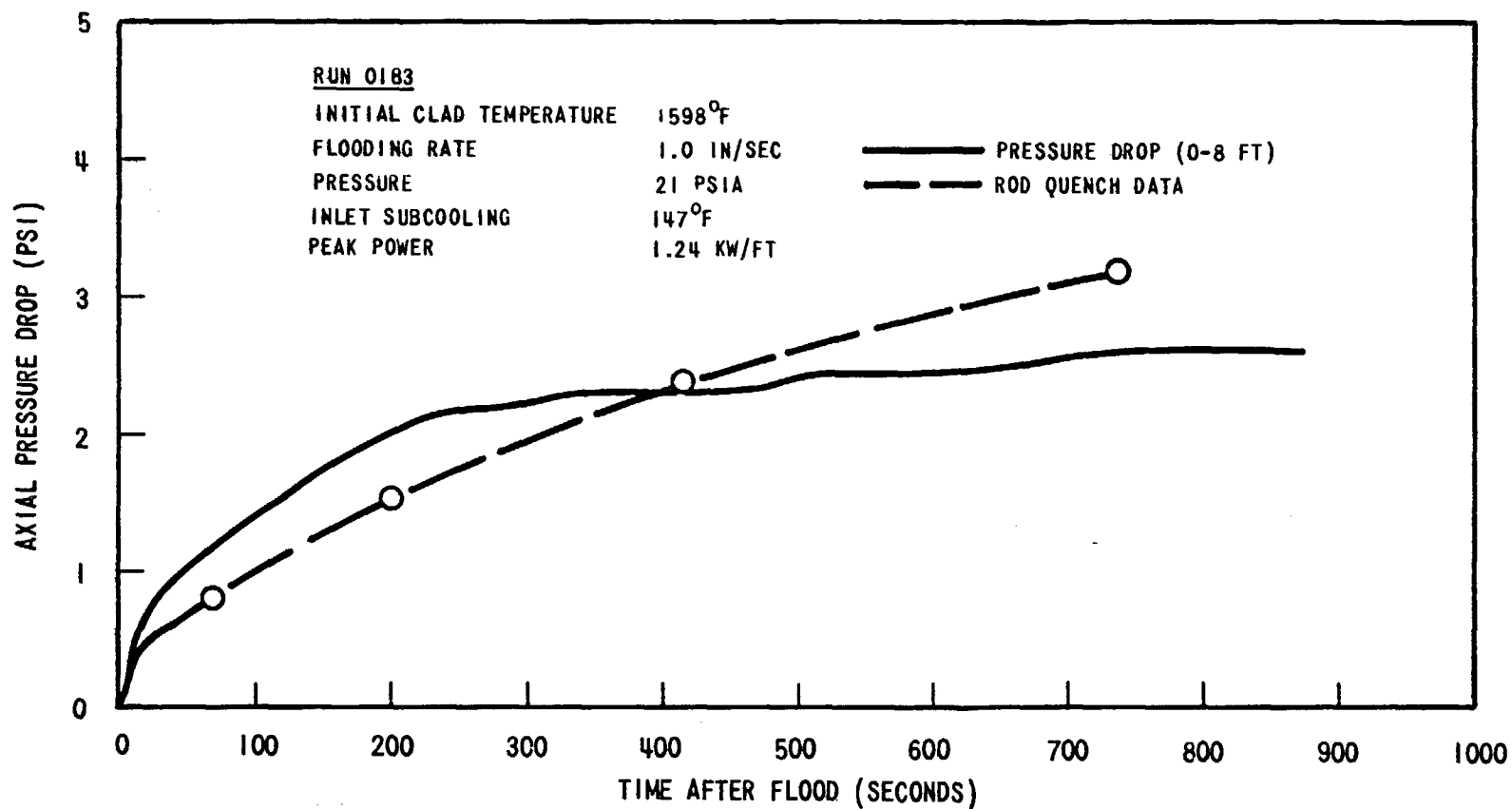


Figure 3-64. Comparison of Pressure Drop and Rod Quench Data, Run 0183.

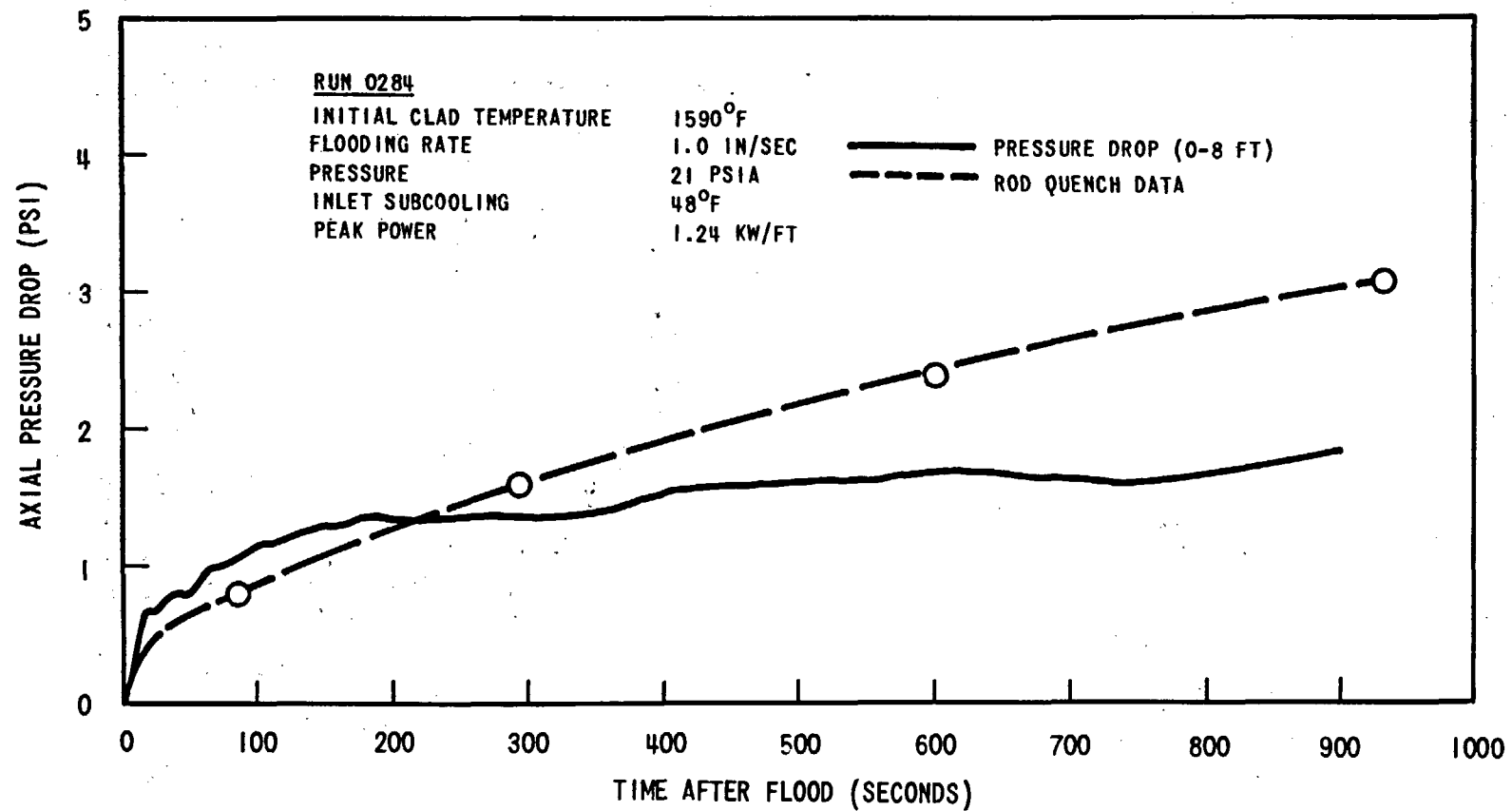


Figure 3-65. Comparison of Pressure Drop and Rod Quench Data, Run 0284.

Temperature (°F)

Time After Flood (Seconds)

FLOOD

7' SP
10' SP
12.5' SP
12.5' TC
EXIT PIPE TC
10' CLAD
8' CLAD
6' CLAD

RUN 8000
INITIAL CLAD TEMP 1689°F
FLOODING RATE 1.0 IN/SEC
PRESSURE 58 PSIA
INLET SUBCOOLING 156°F
PEAK POWER 1.24 KW/FT

Figure 3-66. Local Coolant and Clad Temperature Run 8000

5054-56

66-E

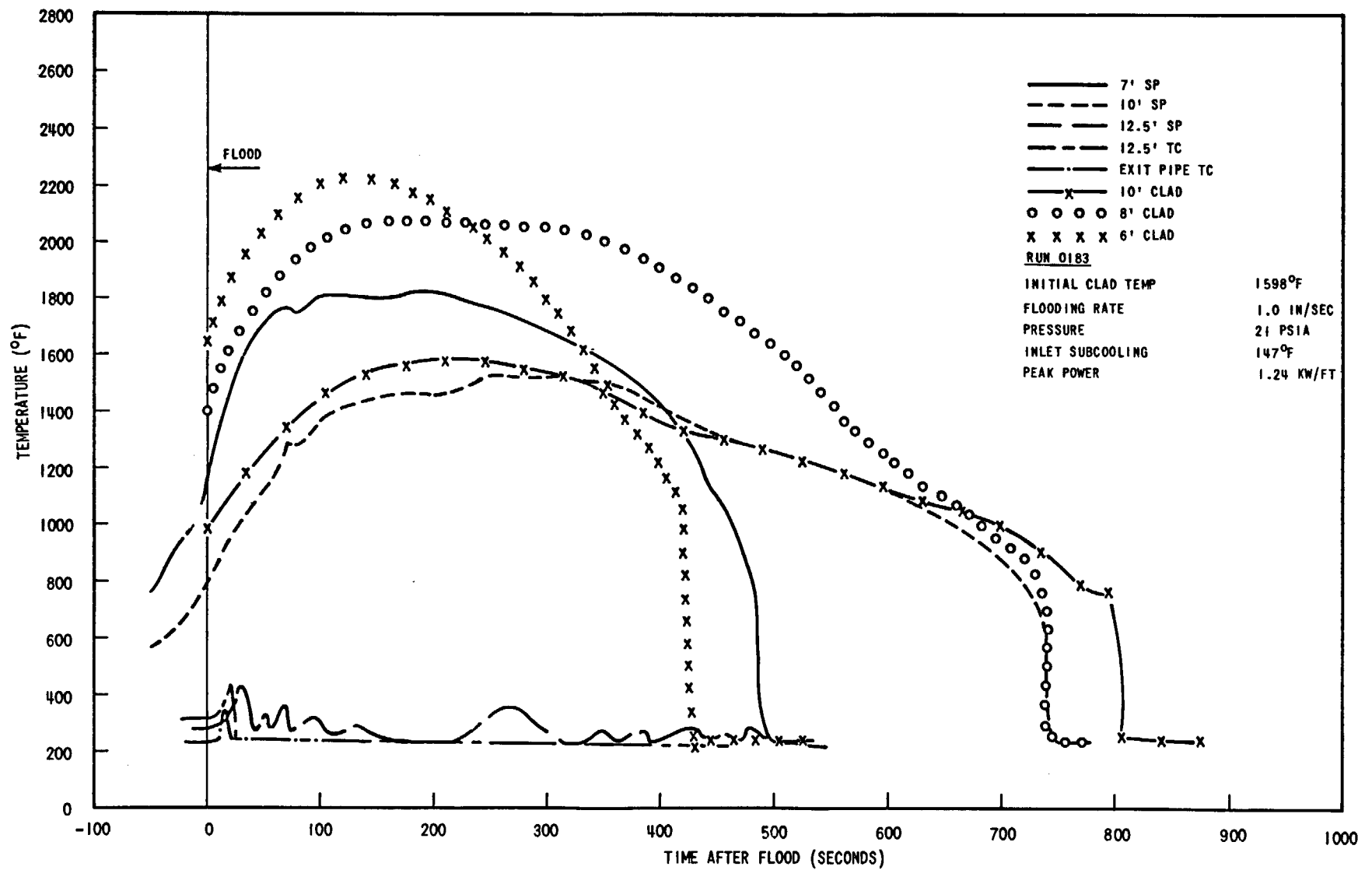


Figure 3-67. Local Coolant and Clad Temperatures, Run 0183

3-100

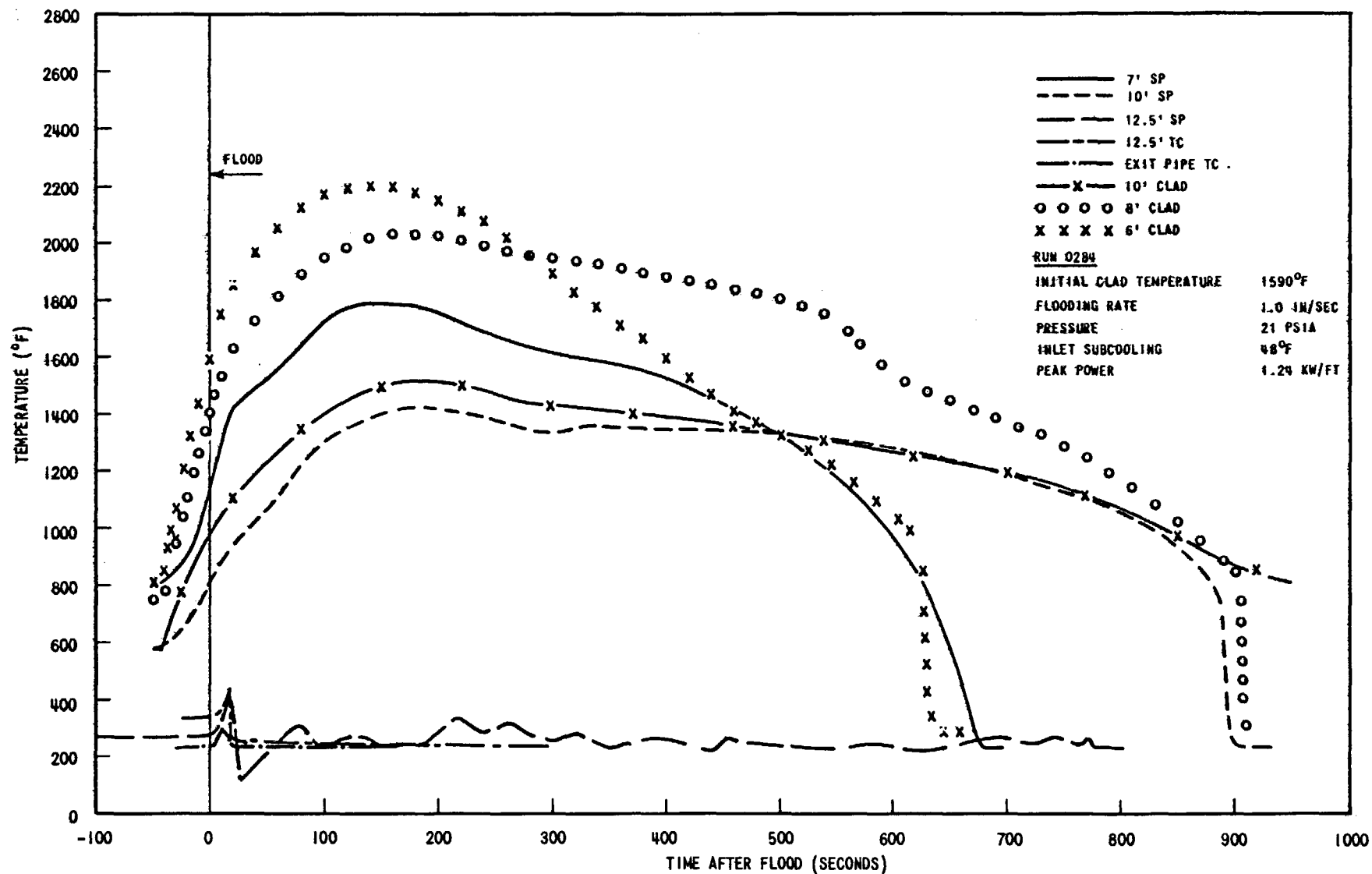


Figure 3-68. Local Coolant and Clad Temperatures, Run 0284

8000 (58 psia, 156°F subcooling), 0183 (21 psia, 147°F subcooling) and 0284 (21 psia, 48°F subcooling). Also, the curves show typical 6, 8, and 10 ft clad temperatures. These figures indicate the presence of superheated steam in the bundle at the start of flooding. Note that in all cases, the 7 ft steam probe measures approximately the same peak temperature (~1800°F). The 10 ft steam probe peaks at approximately 1750°F in run 8000 but reaches only 1525°F and 1420°F in runs 0183 and 0284, respectively. This information is consistent with the absence of reverse heat transfer coefficients at the 10 ft elevation in the low pressure tests discussed in Section 3.4.

The steam probe and thermocouples above the heated length normally had a small temperature surge shortly after the start of flood, then dropped into the temperature range of 300 - 500°F. It is believed that this instrumentation is being wetted by the coolant mixture and is thus not reading the actual steam temperature. In previous flow blockage tests, using thermocouples above the heated length, higher steam temperatures were observed at these points, however, the flow pattern in the blockage tests consisted of fine droplets due to the atomization of entrained liquid by the blockage plate. These finer droplets may not have been able to wet the thermocouples. In contrast, the larger droplets occurring in these tests could more easily wet the thermocouple sensing elements. This can be seen in the behavior of the exit pipe thermocouple in run 8000, which reached about 500°F while the 12.5 ft steam probe and thermocouple were reading saturation. Evidently, the 12.5 thermocouple was being wetted but sufficient water was separated out in the upper plenum and baffle plate at the exit pipe to not wet the exit pipe thermocouple. The 12.5 ft steam probe data sometimes oscillated, as is shown in Figures 3-67 and 3-68, and the data from this instrument was believed to be anomalous.

3.9 LIQUID CARRYOVER RESULTS

Measurements of entrained liquid expelled from the bundle were made by continuously draining this liquid into a vertical pipe as it collected in the upper plenum annulus. A pressure transducer at the lower end of the pipe recorded the liquid elevation in the pipe as a function of time. (See Figure 2-2.) A simple baffle at the entrance to the upper plenum exhaust pipe deflected

the liquid which was expelled from the bundle and which then fell down into the annulus, but was thus prevented from leaving the upper plenum via the exhaust pipe. It must be noted that the measured water collected may not be all the entrained water. Some of the water may be blown out the exit pipe, as there is no assurance that the baffle was perfectly effective as a separator. Evidence of imperfect separation is indicated by the coolant temperature data in Section 3.7. The exit pipe thermocouple (downstream of the baffle) reads saturation temperature in many cases, whereas other coolant temperatures indicate superheated steam conditions existing simultaneously at locations in the test bundle.

The following parameter effects on liquid carryover were observed:

a) Effect of Flooding Rate

Figure 3-69 shows the effect of flooding rate on liquid carryover. The liquid carryover increases with increased flooding rate. Comparison of flooding rate effect at other conditions showed the same trend.

b) Effect of Pressure

Figures 3-70 and 3-71 show the effect of pressure on liquid carryover. For both flooding rates, there was more liquid carryover collected for 20 psia than for 60 psia. This is consistent with the observation that in all cases the quench front velocity was less for the lower pressure, indicating a greater total carryover for lower pressure. Also, higher heat transfer for higher pressure would tend to increase the amount of entrained liquid at the quench front that is evaporated before leaving the bundle.

c) Effect of Inlet Subcooling

Figure 3-71 shows the effect of subcooling on liquid carryover collected at 1 in./sec flooding rate. At 60 psia, the carryover is about the same in the high and low subcooling cases for the first 120 seconds after flood, after which the low subcooling data shows more liquid carryover. At 20 psia the carryover curves are similar for ~360 sec (collector pipe full), thus there is no apparent effect of subcooling on liquid carryover out to 360 sec for these conditions.

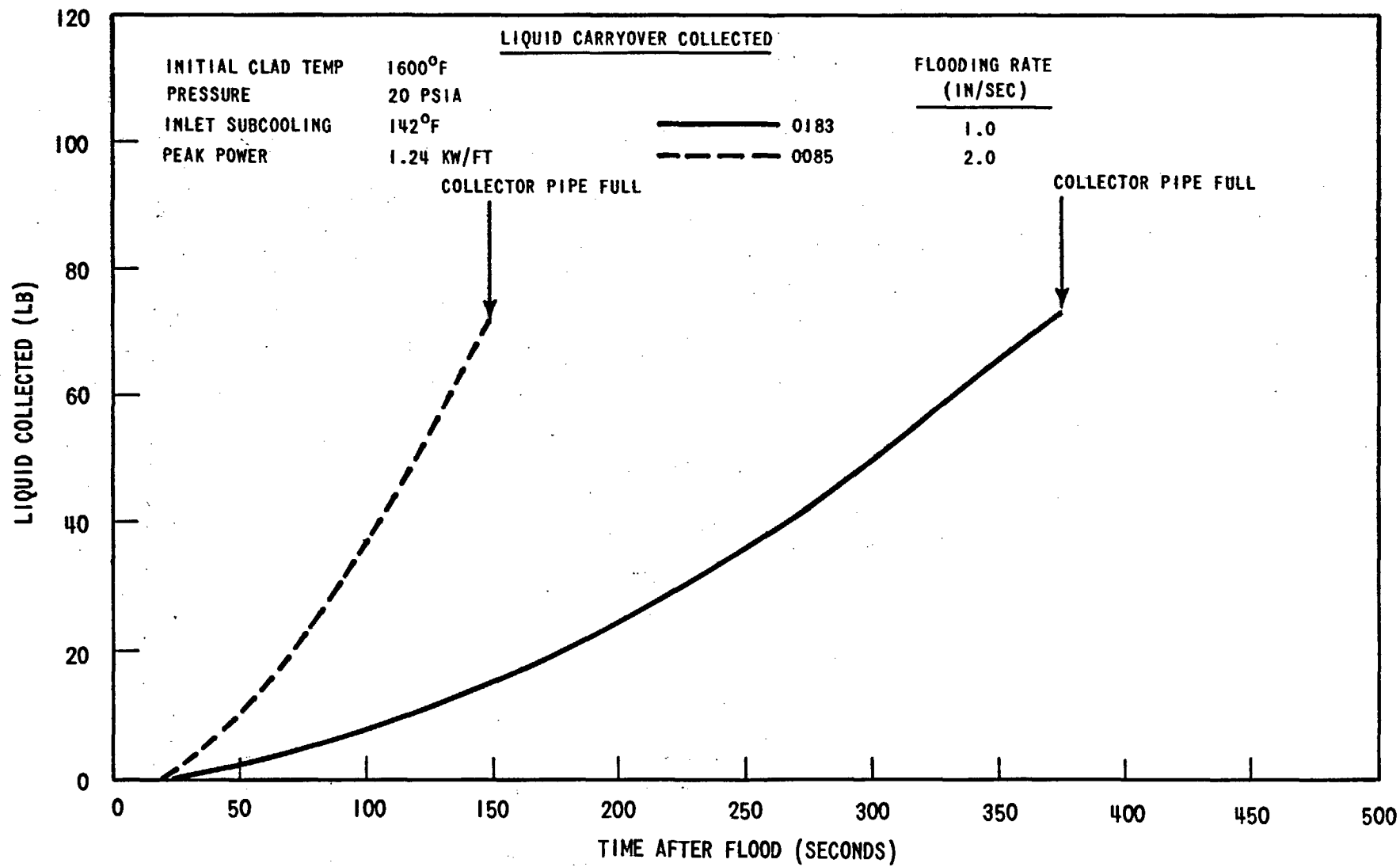


Figure 3-69. Effect of Flooding Rate on Liquid Carryover Collected.

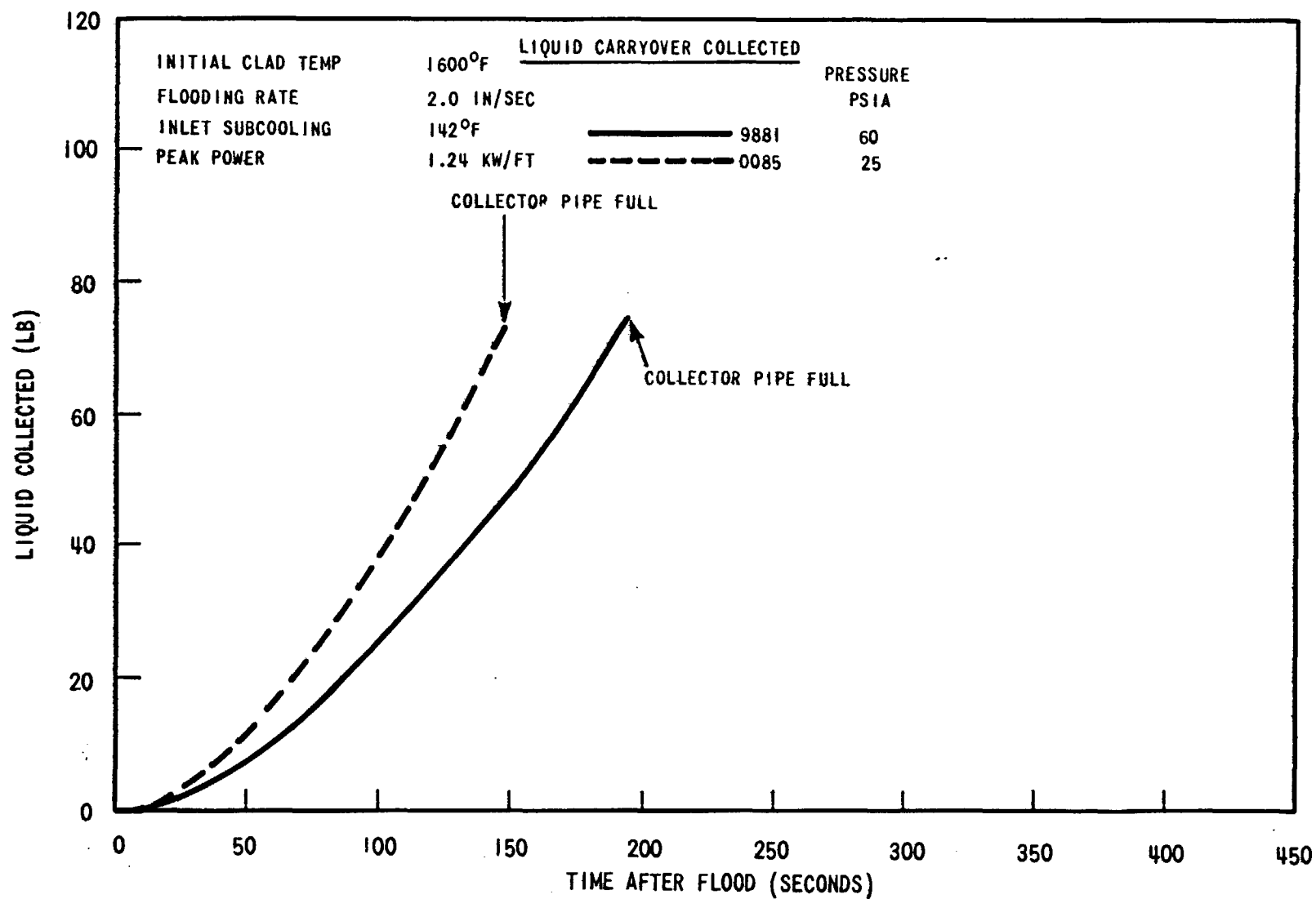


Figure 3-70. Effect of Pressure on Liquid Carryover Collected.

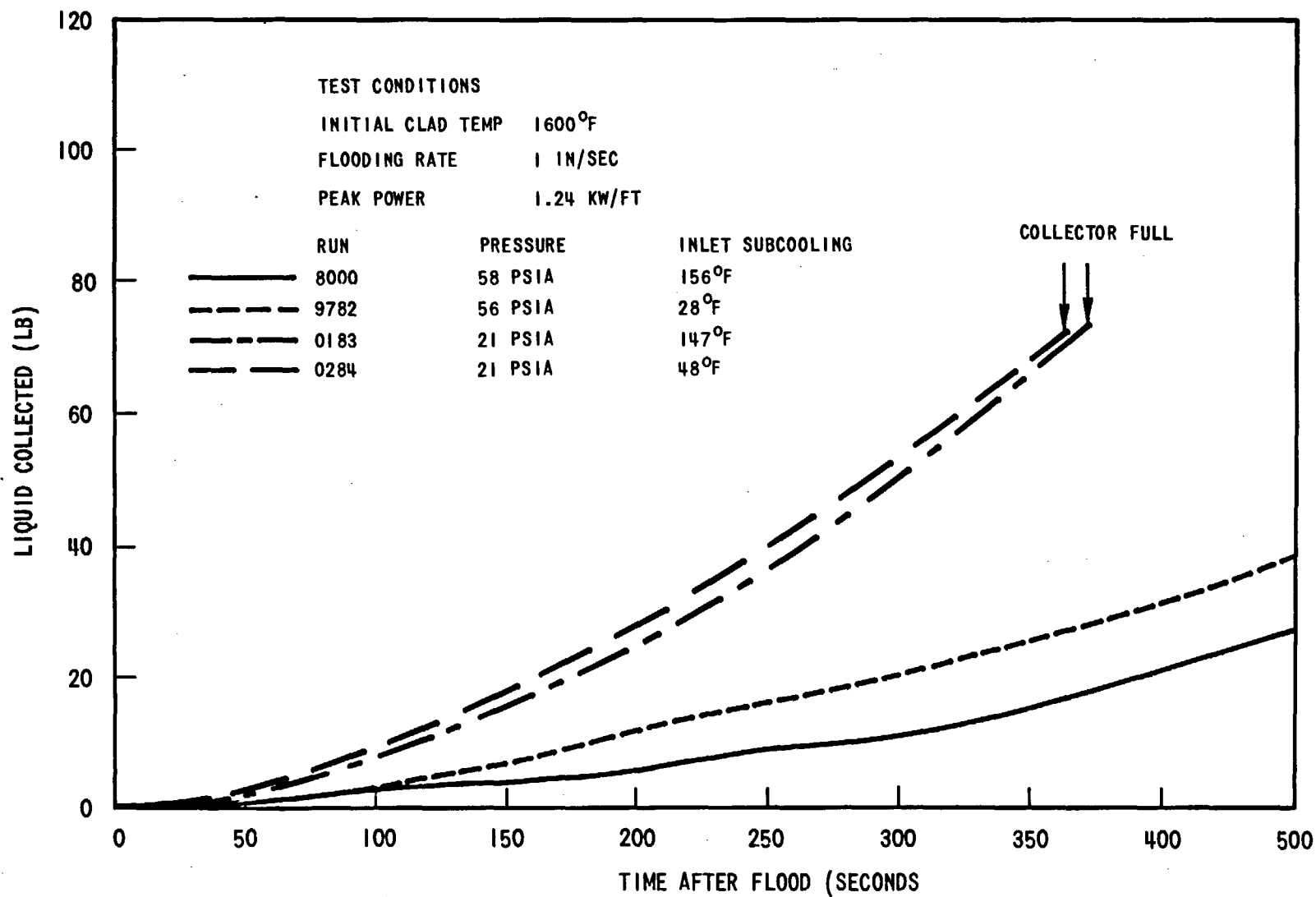


Figure 3-71. Liquid Carryover Collected for Various Pressure and Subcooling at 1 in/sec Flooding Rate.

The effect of subcooling on liquid carryover is similar to the subcooling effect on heat transfer coefficient. Heat transfer coefficients were compared in Figures 3-39 and 3-40 for the same runs shown in Figure 3-71. For runs 8000 and 9782 (60 psia) the heat transfer coefficients were also similar for 120 seconds after flood. Runs 0183 and 0284 (20 psia) had similar heat transfer coefficients for about 300 seconds after flood. These times correspond approximately to the times when the liquid carryover collected were similar for these runs.

d) Effect of Peak Power

The effect of peak power on liquid carryover is shown in Figure 3-72. Decreasing the peak power density resulted in increased liquid carryover at times greater than about 120 seconds. For the first 120 seconds after flood, liquid carryover collected is approximately independent of power. The heat transfer coefficient comparison showed the same trend with the higher heat transfer as later times associated with the combined effect of larger liquid carryover and a faster moving quench front for the lower peak power case.

Total Mass Effluent

So far, the discussion deals only with the liquid that was collected in the collection pipe. The liquid collected in the pipe does not represent the total mass of fluid that was expelled from the bundle, since some of the fluid that ejected from the quench front was in the form of steam and some of the liquid that was ejected from the quench front evaporated as it traveled upward.

The ratio of the rate of total mass of fluid that was expelled above the quench front to the rate of mass flow into the bundle, or the total mass effluent flow rate fraction above the quench front, C , can be computed from the equation

$$C = \frac{V_{in} - V_q}{V_{in}} \quad (1)$$

with the assumption that the water front moved with the same velocity as the

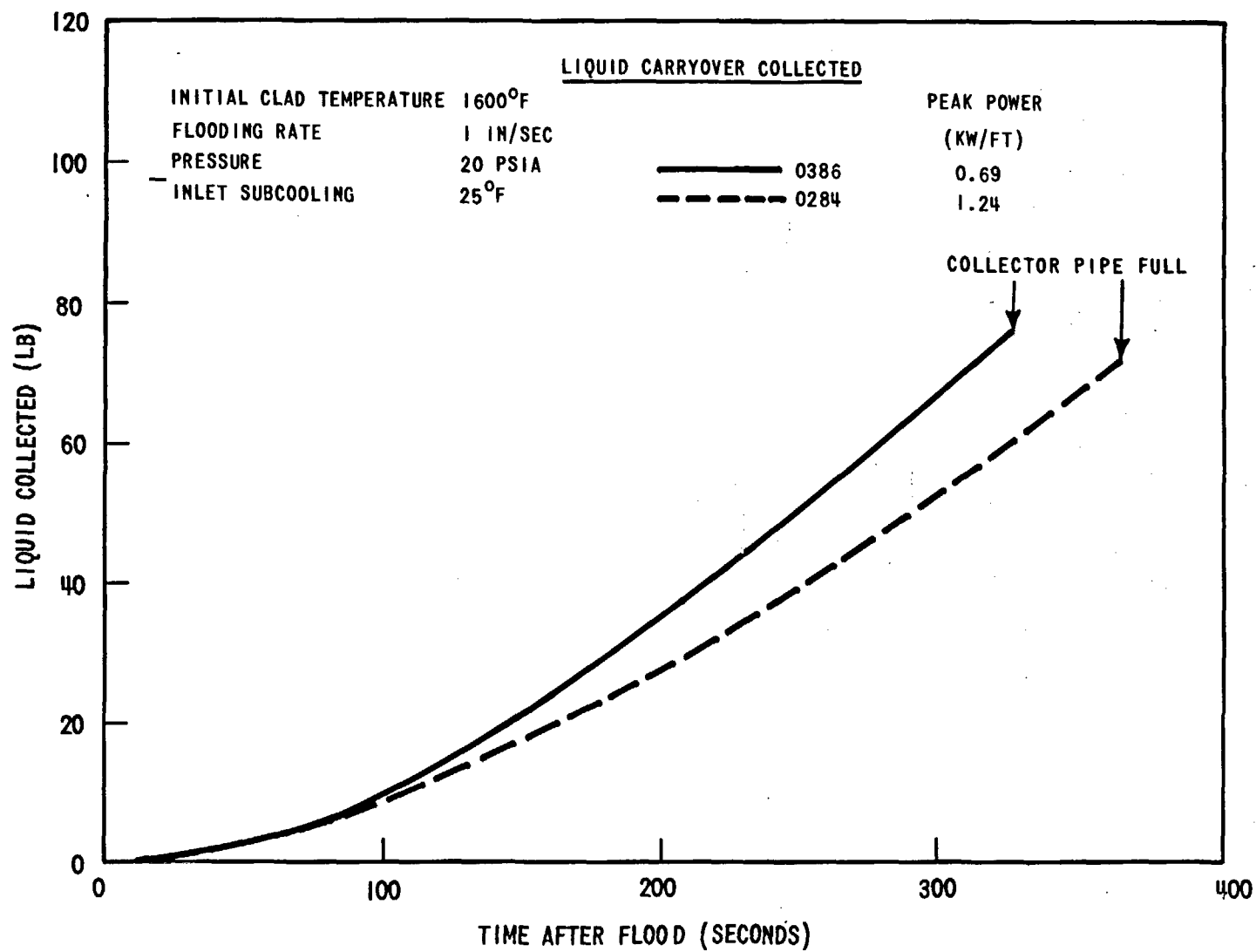


Figure 3-72. Effect of Peak Power on Liquid Carryover Collected.

quench front, where V_{in} (in/sec) and V_q (in/sec) are the flooding rate and the quench front velocity, respectively.

Figure 3-73 shows the total mass effluent flow rate fraction above the quench front for various flooding rates. In general, the total mass effluent flow rate fraction above the quench front is higher for higher flooding rate. It reaches a maximum at about the time of 6 ft quench. The maximum total mass effluent flow rate fraction above the quench front can be computed by

$$C_{max} \approx \frac{40.8}{t_{q6ft} V_{in}} \quad (2)$$

which is derived from the fact that the quench front elevation versus dimensionless time, t/t_{q6ft} , curves are similar for all runs, where t_{q6ft} (sec) is the 6 ft quench time which can be computed from Equation (1).

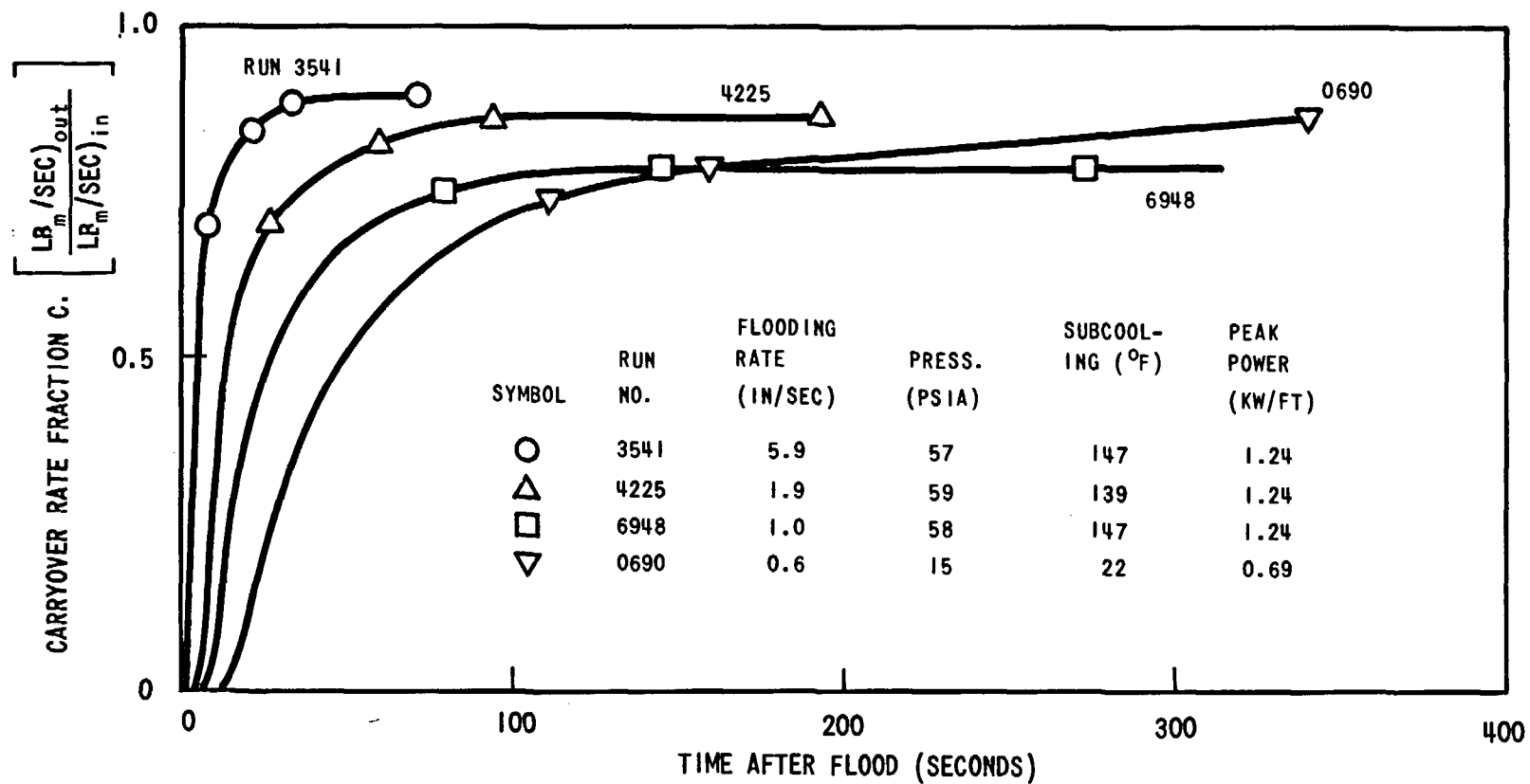


Figure 3-73. Total Mass Effluent Flow Rate Fraction versus Time

SECTION 4

SUMMARY AND CONCLUSIONS

4.1 SYSTEM PARAMETER EFFECTS ON HEAT TRANSFER

Flooding Rate

Increased flooding rate resulted in an increase in the heat transfer coefficient. Temperature rise, turnaround time and quench time increased with lower flooding rate. The flooding rate effect on quench time appears to be greater at low pressure.

Pressure

Heat transfer coefficients increased with system pressure. At 2 and 1 in/sec flooding rates, the heat transfer coefficients were nearly independent of pressure for 30 to 40 seconds after flood before the pressure effect was observed.

Inlet Coolant Subcooling

Inlet subcooling did not affect the heat transfer coefficients until late in the runs. The main influence of low subcooling was to increase the quench time. The subcooling effect on quench time was greatest at low pressure and low flooding rate.

Peak Power

The current low pressure, low flooding rate heat transfer data showed little effect of peak power out to 120 seconds after flood. At later times, lower peak power caused an increase in the heat transfer coefficient.

4.2 HEAT TRANSFER AT OTHER ELEVATIONS

For the flooding rates investigated in this report, heat transfer coefficients decreased with increased elevation. Lowering the system pressure at the 2 and 1 in/sec flooding rate caused an increase in the heat transfer coefficient at upper elevations over the first part of the run (from 70 up to 260 seconds).

At later times the high pressure heat transfer coefficient at 8 ft and 10 ft was higher than the low pressure case. Also, reverse heat transfer (net heat transfer into the rods) was observed at 10 ft only in the 60 psia tests.

4.3 DATA VERIFICATION

Reproducibility of the results was very good, and the effect of bundle size on heat transfer coefficient was found to be negligible. The effect on the central rod midplane heat transfer coefficient as a result of nontypical radiation to the flow housing was of the order of only 0.2 to 0.3 Btu/hr-ft²-°F. At the 1 in./sec flooding rate, the effect of housing temperature was found to be small. In particular, the effect of rate of housing heat release at the 2 ft elevation was shown from the test data to be small.

4.4 CORRELATION

The heat transfer coefficient correlation presented in WCAP-7665 was modified to more accurately predict the data at combined conditions of low pressure, low subcooling and low flooding rate. Modification was necessary mainly because the predicted quench time was too short. The correlation was revised and now gives good agreement for all the FLECHT data.

4.5 PRESSURE TRANSDUCER RESULTS

Increasing the system pressure or subcooling at 1 in/sec flooding rate increases the axial pressure drop because the quench front rises more rapidly, causing higher elevation pressure drop. Comparison of mass inventory in the bundle using the quench front elevation and pressure drop elevation head for current data, show that total mass carryover calculations are not sensitive to use of either of the above methods of determining mass inventory in the bundle.

4.6 LOCAL COOLANT DATA

Local coolant data indicated the presence of superheated steam in the bundle prior to and after the start of flooding. Peak coolant temperatures were generally lower in the low pressure tests compared to higher pressure cases. This

is consistent with the observation of reverse heat transfer at the 10 ft elevation, generally in 60 psia tests only, which indicates net heat transfer from the coolant to the rod.

4.7 LIQUID CARRYOVER

Liquid carryover collected increased with increasing flooding rate and decreased with increasing pressure and peak power. The subcooling effect was small compared to the above effects. A simple relationship is suggested to calculate total mass effluent flow rate fraction.

SECTION 5

REFERENCES

1. F. F. Cadek, D. P. Dominicis and R. H. Leyse, "PWR FLECHT (Full Length Emergency Cooling Heat Transfer) Final Report," WCAP-7665, April 1971.
2. J. O. Cermak, et al, "PWR Full Length Emergency Cooling Heat Transfer (FLECHT) Group I Test Report," WCAP-7435, January 1970.
3. F. F. Cadek, D. P. Dominicis and R. H. Leyse, "PWR FLECHT (Full Length Emergency Cooling Heat Transfer) Group II Test Report," WCAP-7544, September 1970.
4. Testimony of Westinghouse Electric Corporation for the ECCS Rulemaking Hearing, Docket No. RM-50-1, March 1972.
5. R. F. Davis, "The Physical Aspect of Steam Generation at High Pressure and the Problem of Steam Contamination," Inst. Mech. Engrs., 1940.
6. G. C. K. Yeh and N. Zuber, "On the Problem of Liquid Entrainment," ANL-6244, Oct. 1960.

APPENDIX A
FLECHT DATA SHEETS

FLECHT RUN SUMMARY SHEET

RUN NO. 9681

DATE 12/3/71

A. RUN CONDITIONS

Bundle Size	10 x 10 - SS
Initial Clad Temperature	1586 °F
Flooding Rate	2 in/sec
Peak Power	1.24 kw/ft
Decay Power	Curve B Figure 2-3
Inlet Coolant Temperature	149 °F
Pressure	61 psia

B. HOUSING TEMPERATURES

Elevation (ft)	Initial Temperature (°F)	Temperature at Quench Time of Hot Rod Midplane (147 Sec)
2	505	212
4	694	266
6	747	388
8	675	729
10	519	300

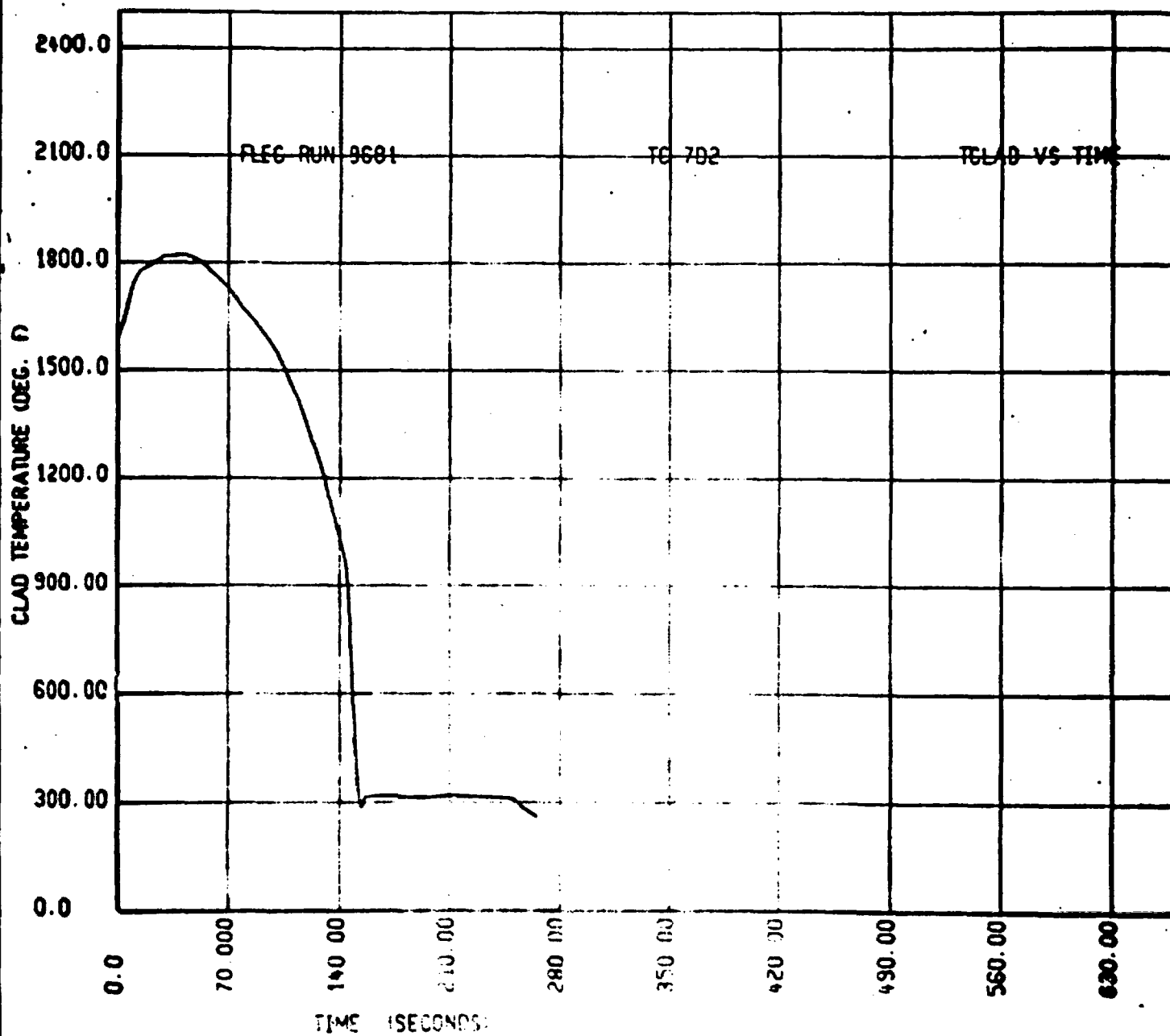
Initial T_{avg} Actual 608 °F

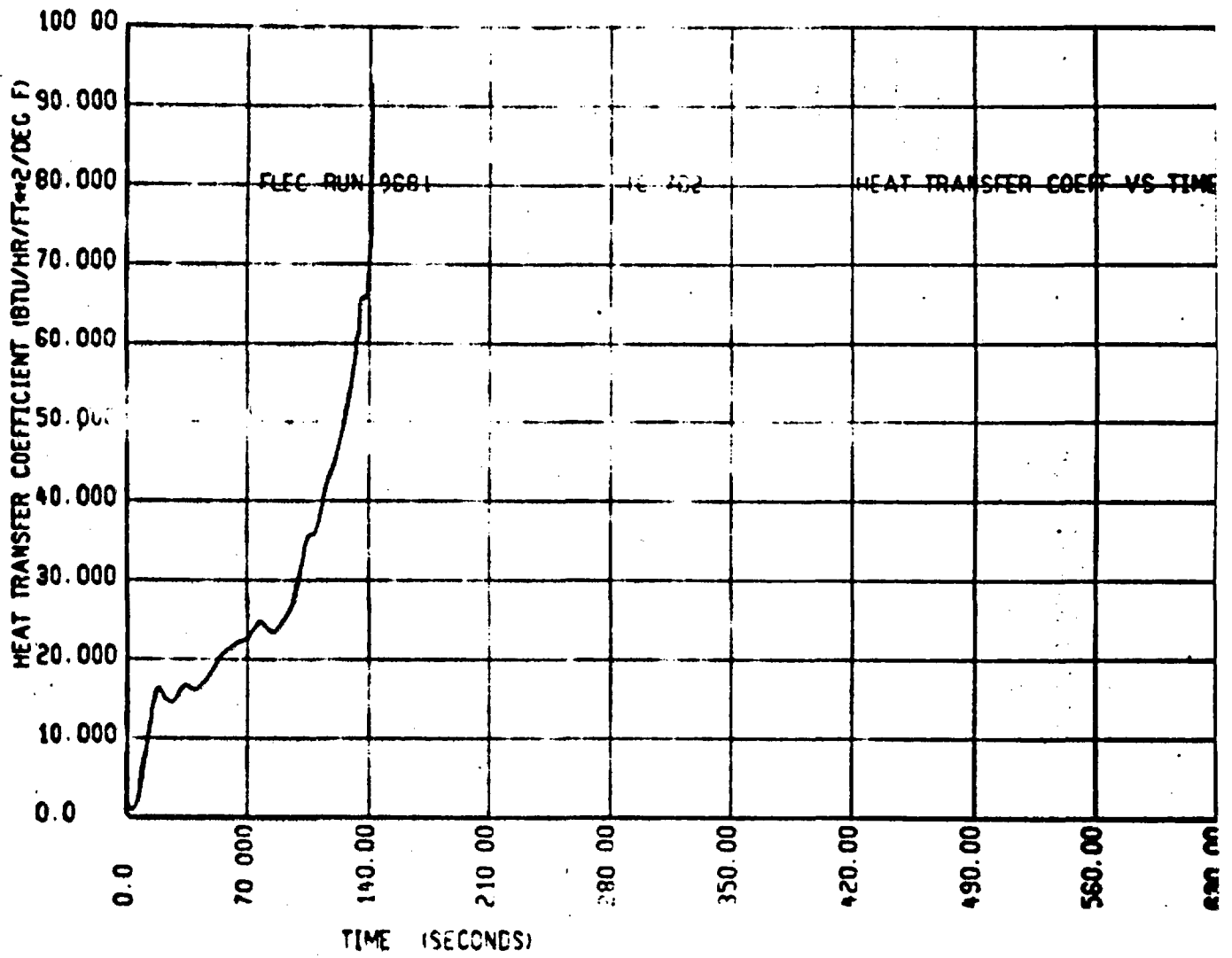
FLECHT RUN SUMMARY SHEET

RUN NO. 9681

C. HEATER THERMOCOUPLE DATA

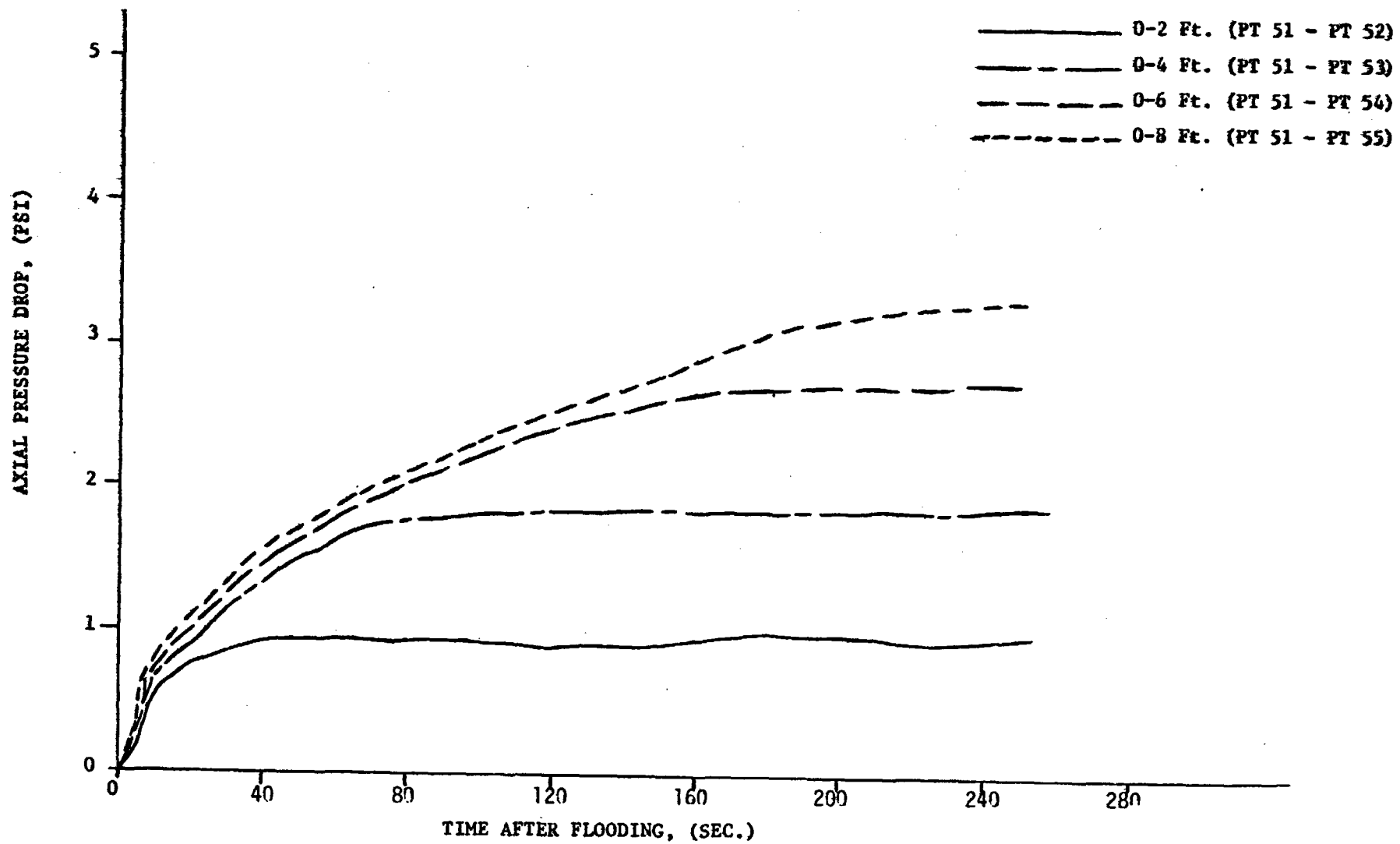
T/C No.	Elevation	Initial Temp. (°F)	Max. Temp. (°F)	Temp. Rise (°F)	Turnaround Time (Sec.)	Quench Temp. (°F)	Quench Time (sec)
5G1	6'	1599	1815	216	38	855	147
5G3	4'	1443	1583	140	15	871	87
5G5	10'	980	1204	224	61	627	255
5G6	8'	Bad TC Signal Due To Pen Recorder Hookup					
5F1	6'	1581	1802	221	38	922	148
5F6	8'	Bad TC Signal Due To Pen Recorder Hookup					
7G3	6'	1506	1750	244	40	897	143
6G3	6'	Bad TC Signal Due to Pen Recorder Hookup					
5F3	6'	1519	1768	249	40	837	147
4F2	6'	1533	1792	259	42	891	147
3F2	6'	1471	1731	260	40	892	142
1F2	6'	1470	1631	161	19	828	158
7O2	6'	1586	1820	234	40	877	147
5E2	8'	1342	1657	315	65	900	217
5E4	4'	1349	1485	139	16	1052	65
5E5	2'	951	1001	50	8	809	32
5E1	10'	942	1230	288	88	630	261
6G5	2'	961	1114	153	9	767	28





Run 9681
PRESSURE DROP VS. TIME.

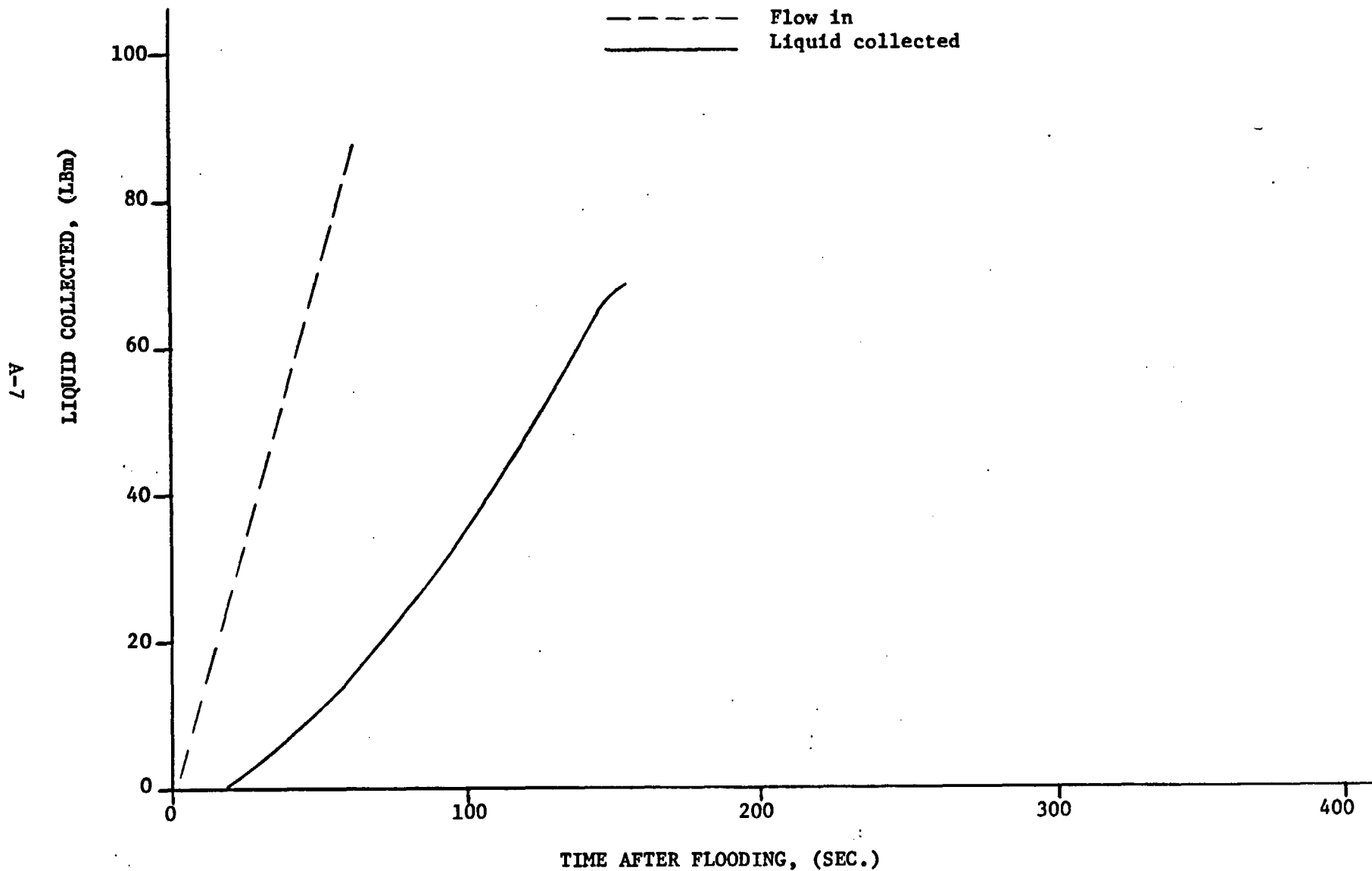
A-6



Run 9681

ENTRAINED LIQUID COLLECTED

NOTE: Liquid Collected Not Necessarily Total Liquid Carryover



FLECHT RUN SUMMARY SHEET

RUN NO. 9782

DATE 12/7/71

A. RUN CONDITIONS

Bundle Size	10 x 10 - SS
Initial Clad Temperature	1590 °F
Flooding Rate	1 in/sec
Peak Power	1.24 kw/ft
Decay Power	Curve B Figure 2-3
Inlet Coolant Temperature	260 °F
Pressure	56 psia

B. HOUSING TEMPERATURES

Elevation (ft)	Initial Temperature (°F)	Temperature at Quench Time of Hot Rod Midplane (<u>323</u> Sec)
2	520	293
4	710	289
6	759	825
8	689	844
10	496	349

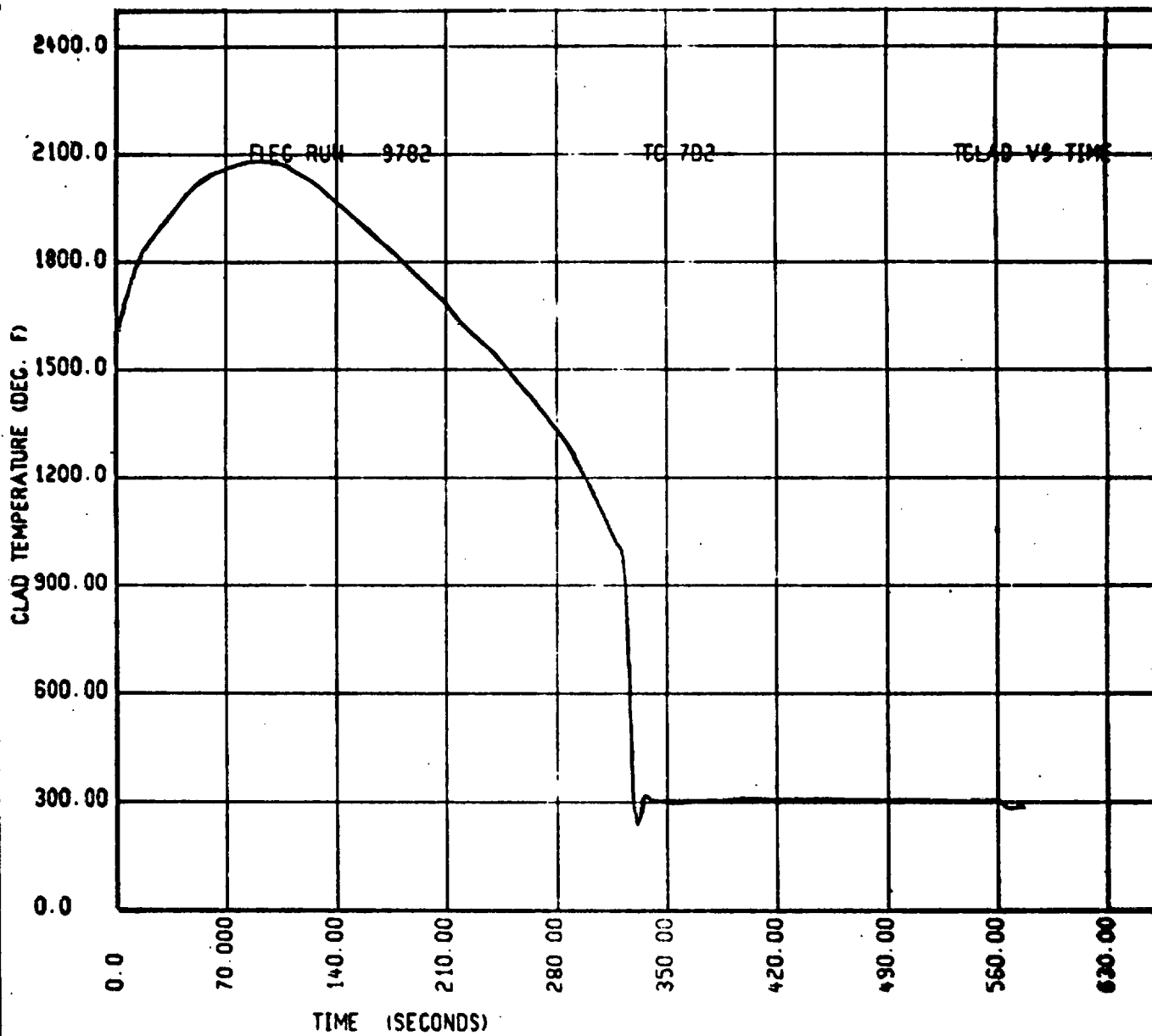
Initial T_{avg} Actual 625 °F

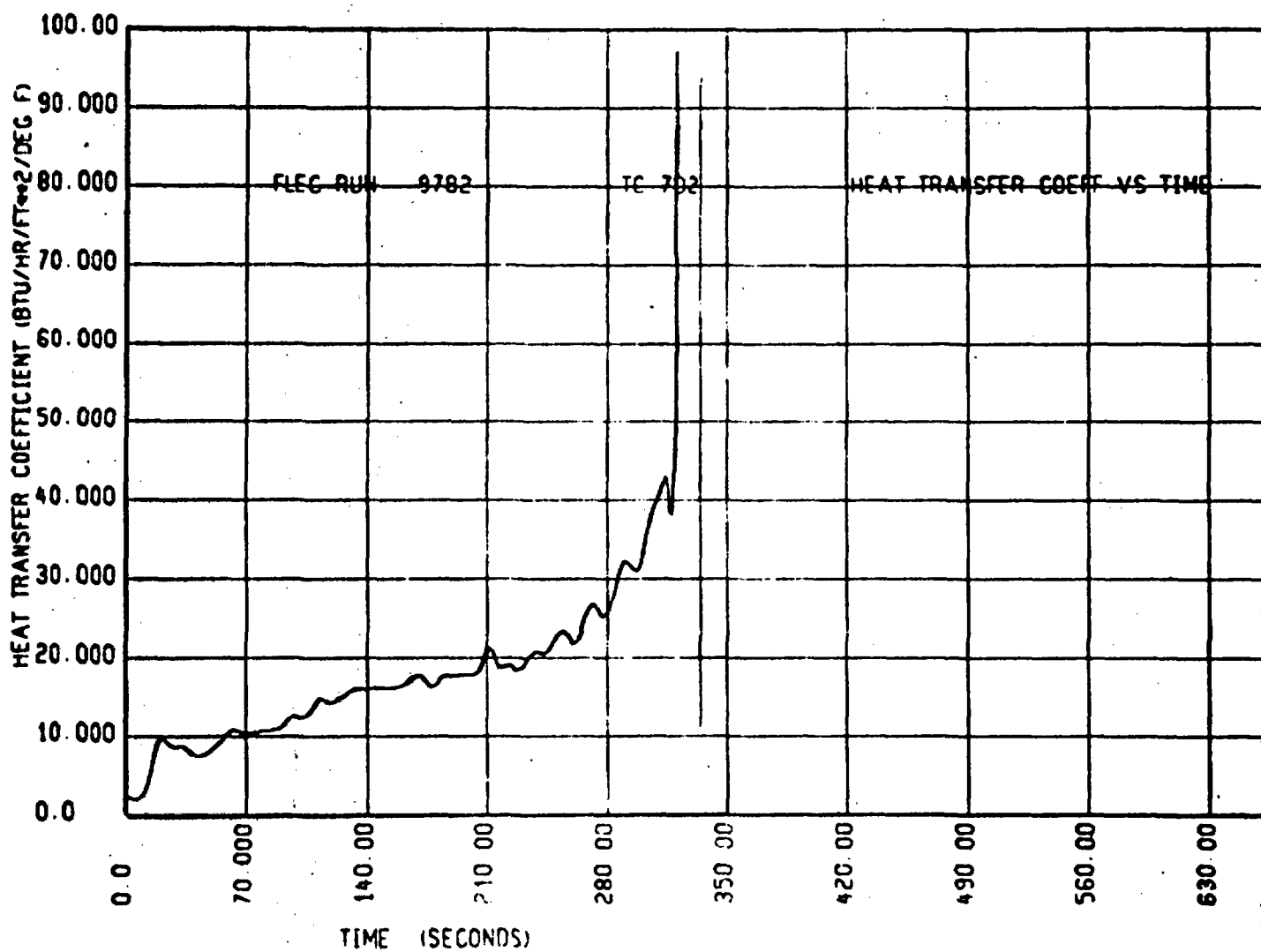
FLECHT RUN SUMMARY SHEET

RUN NO. 9782

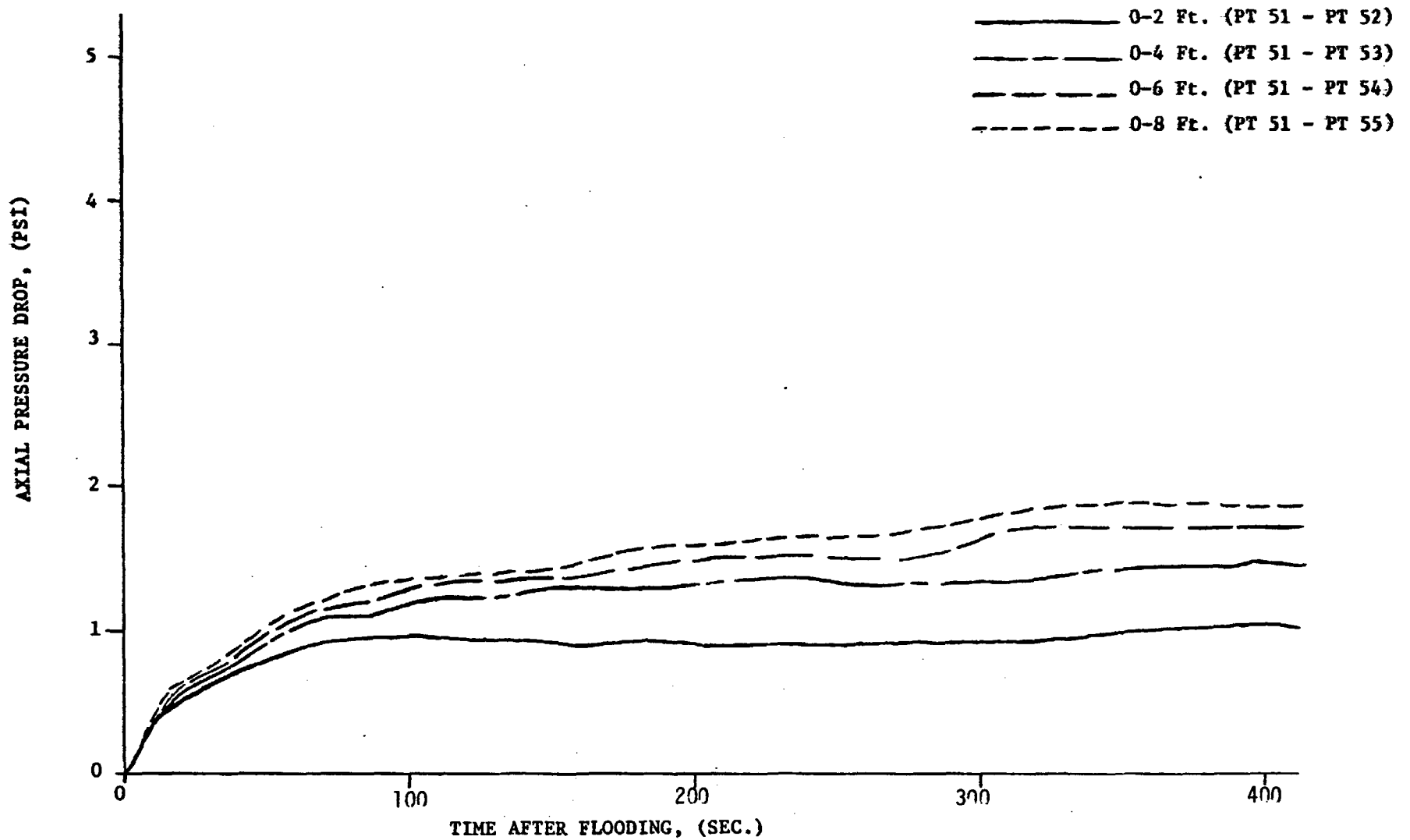
C. HEATER THERMOCOUPLE DATA

T/C No.	Elevation	Initial Temp. (°F)	Max. Temp. (°F)	Temp. Rise (°F)	Turnaround Time (Sec.)	Quench Temp. (°F)	Quench Time (sec)
5G1	6'	1600	2066	466	89	916	317
5G3	4'	1458	1682	224	49	845	159
5G5	10'	908	1737	829	220	634	559
5G6	8'	Bad TC Signal Due To Pen Recorder Hookup					
5F1	6'	1580	2082	503	97	1025	307
5F6	8'	Bad TC Signal Due To Pen Recorder Hookup					
7G3	6'	1507	2006	499	92	920	318
6G3	6'	Bad TC Signal Due To Pen Recorder Hookup					
5E3	6'	1521	2055	534	91	968	305
4F2	6'	1535	2058	523	91	917	317
3F2	6'	1475	1991	516	84	919	312
1F2	6'	1500	1753	253	46	846	317
7D2	6'	1590	2083	493	91	916	323
5E2	8'	1315	2092	777	167	780	487
5E4	4'	1360	1599	239	43	791	158
5E5	2'	959	1023	64	12	732	53
5E1	10'	887	1763	876	236	602	545
665	2'	969	1035	66	11	782	49





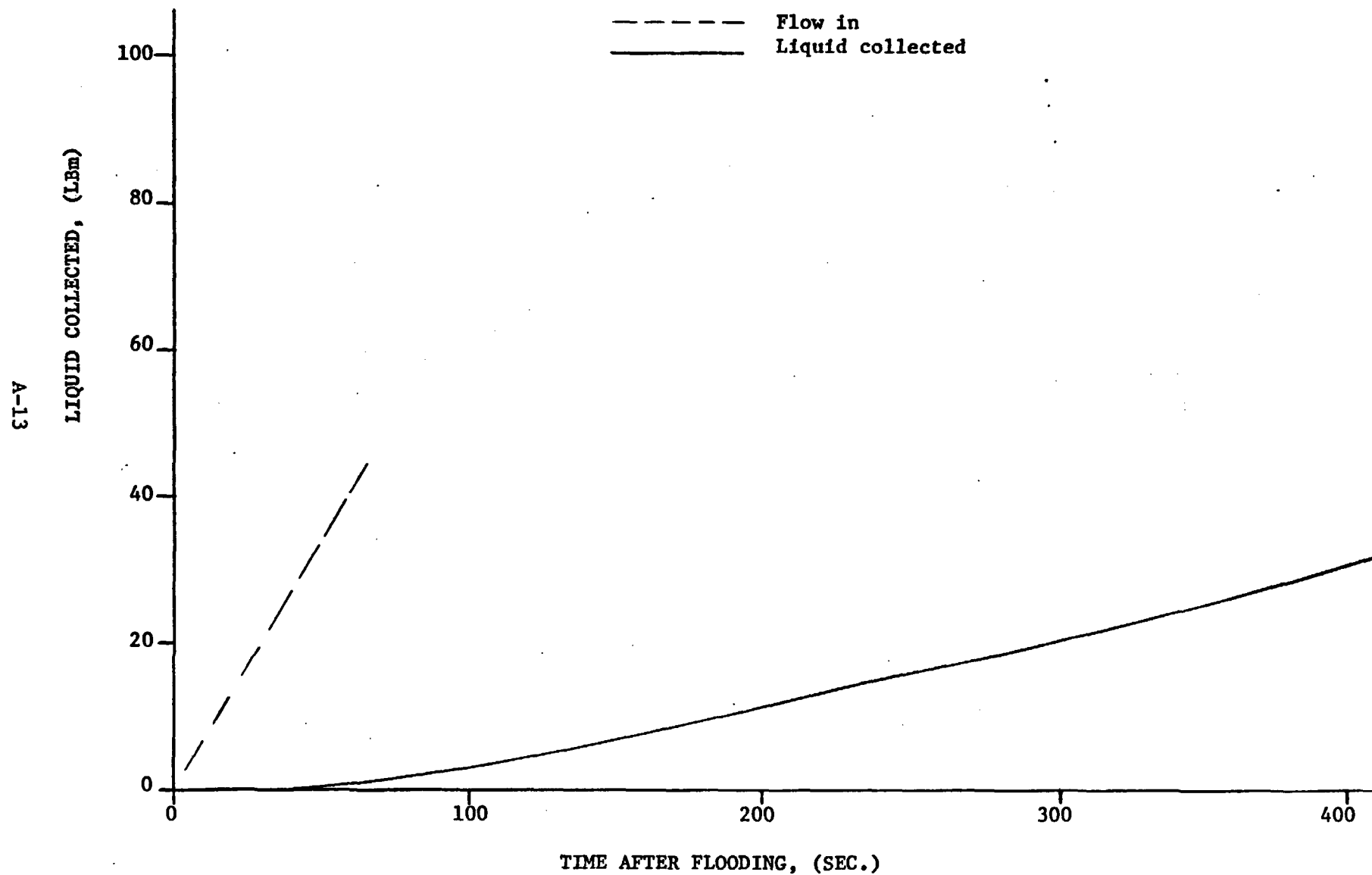
Run 9782
PRESSURE DROP VS. TIME.



Run 9782

ENTRAINED LIQUID COLLECTED

NOTE: Liquid Collected Not Necessarily Total Liquid Carryover



FLECHT RUN SUMMARY SHEET

RUN NO. 9881

DATE 12/8/71

A. RUN CONDITIONS

Bundle Size	10 x 10 - SS
Initial Clad Temperature	1576 °F
Flooding Rate	2 in/sec
Peak Power	1.24 kw/ft
Decay Power	Curve B Figure 2-3
Inlet Coolant Temperature	155 °F
Pressure	60 psia

B. HOUSING TEMPERATURES

Elevation (ft)	Initial Temperature (°F)	Temperature at Quench Time of Hot Rod Midplane (<u>164</u> Sec)
2	499	217
4	652	267
6	739	319
8	698	774
10	493	297

Initial T_{avg} Actual 590 °F

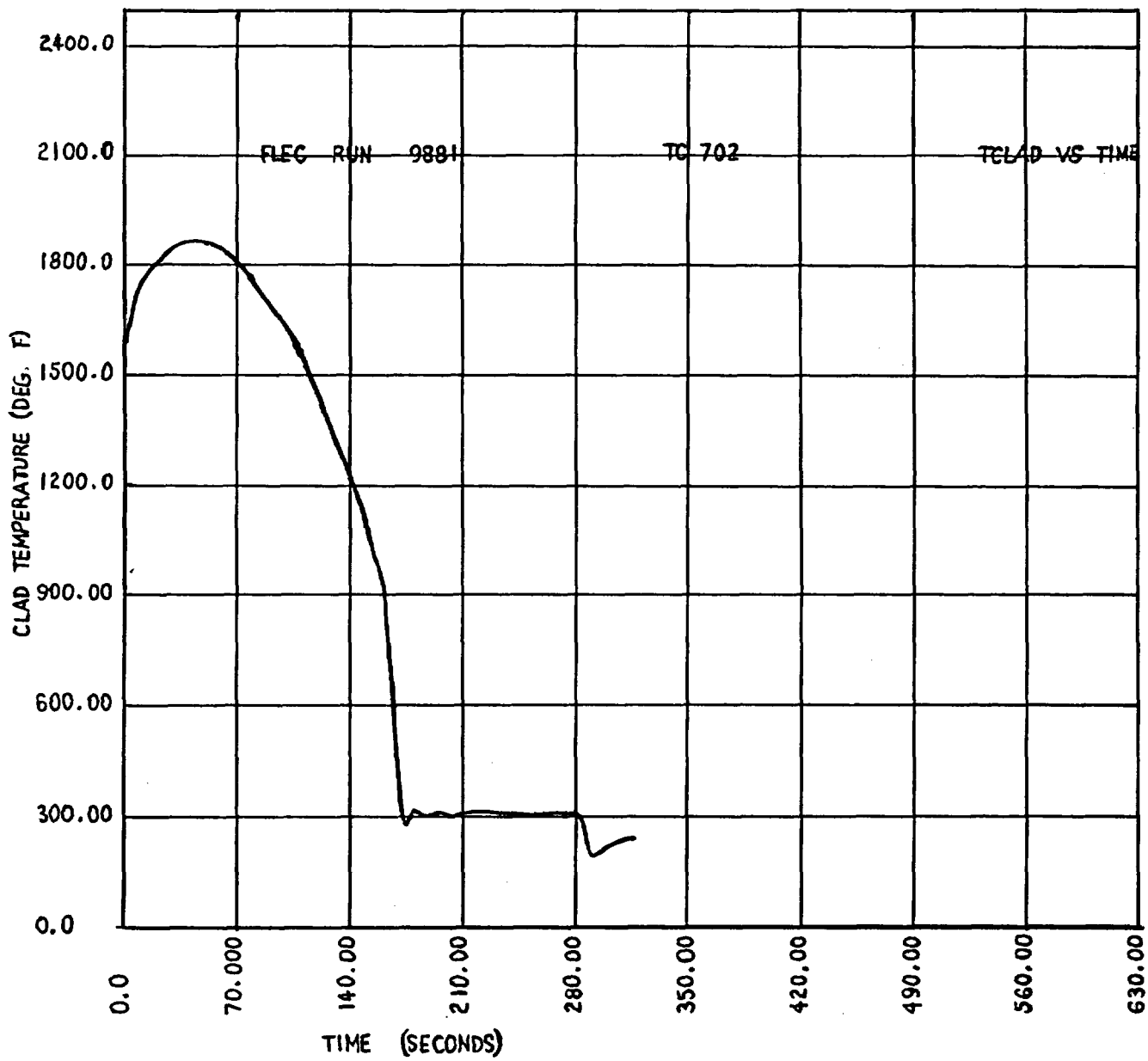
FLECHT RUN SUMMARY SHEET

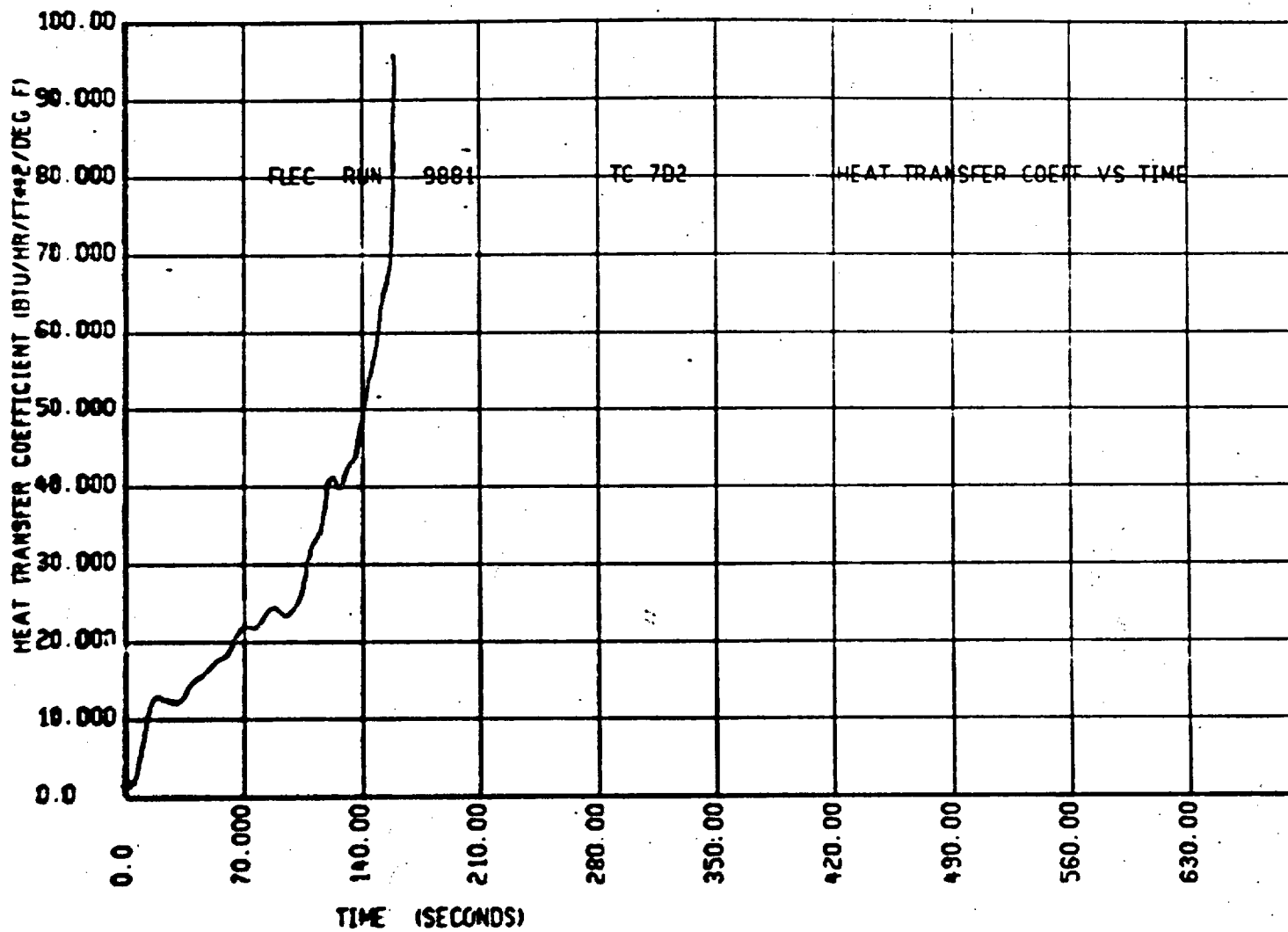
RUN NO. 9881

C. HEATER THERMOCOUPLE DATA

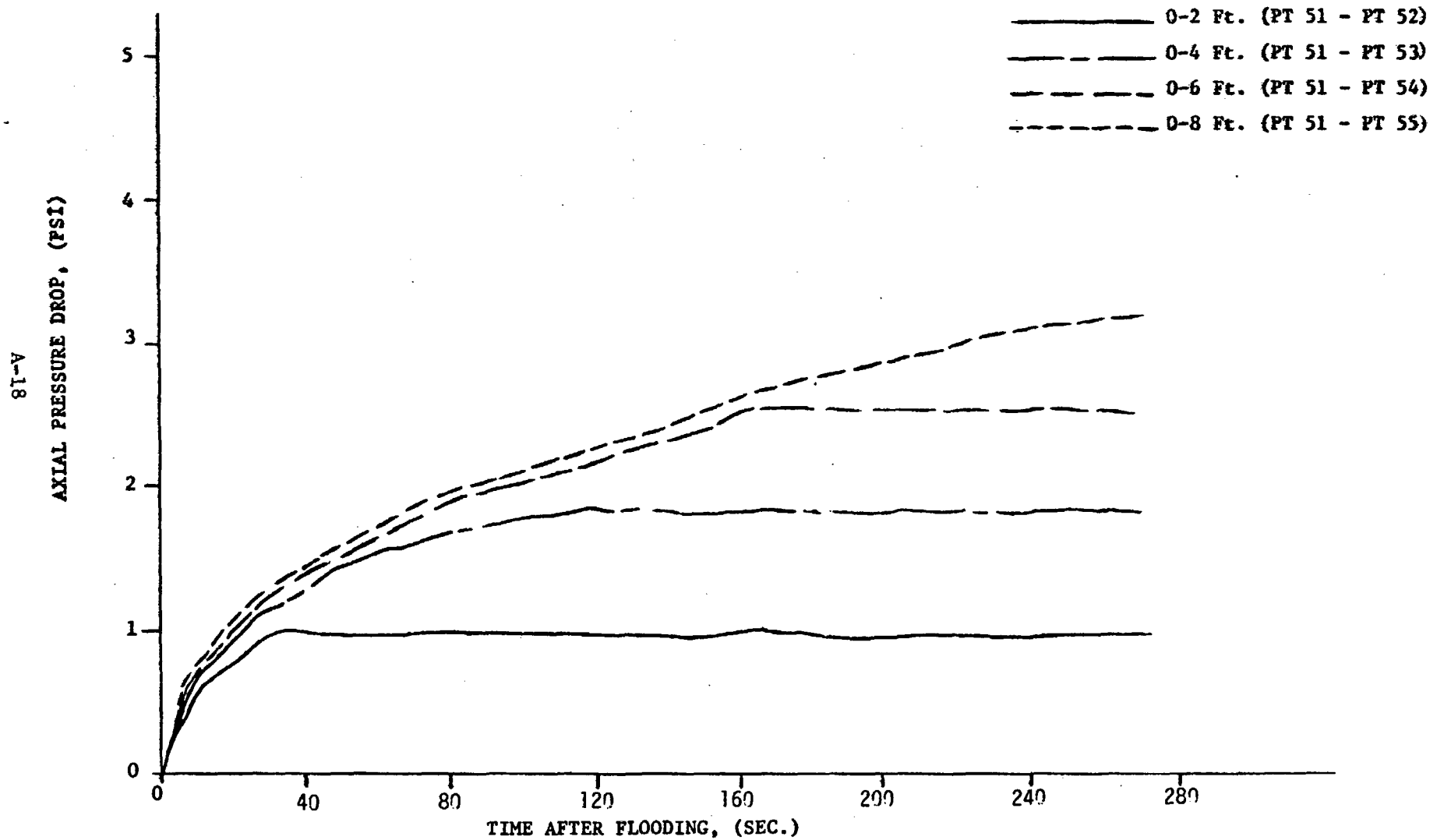
T/C No.	Elevation	Initial Temp. (°F)	Max. Temp. (°F)	Temp. Rise (°F)	Turnaround Time (Sec.)	Quench Temp. (°F)	Quench Time (sec)
5G1	6'	1597	1850	253	46	832	160
5G3	4'	1427	1529	152	23	833	95
5G5	10'	967	1279	312	93	623	286
5G6	8'	Bad TC Signal Due To Pen Recorder Hookup					
5F1	6'	1591	1842	251	47	895	162
5F6	8'	Bad TC Signal Due To Pen Recorder Hookup					
7G3	6'	1499	1788	289	49	696	162
6G3	6'	Bad TC Signal Due To Pen Recorder Hookup					
5F3	6'	1526	1812	286	47	820	161
4F2	6'	1540	1822	282	50	851	161
3F2	6'	1478	1766	288	44	859	156
1F2	6'	1477	1641	164	23	811	172
7D2	6'	1576	1869	293	43	857	164
5E2	8'	1354	1716	262	81	817	258
5E4	4'	1332	1481	149	20	726	96
5E5	2'	933	982	49	8	826	29
5F1	10'	920	1309	389	143	677	286
6G5	2'	944	998	54	9	829	31

A-15





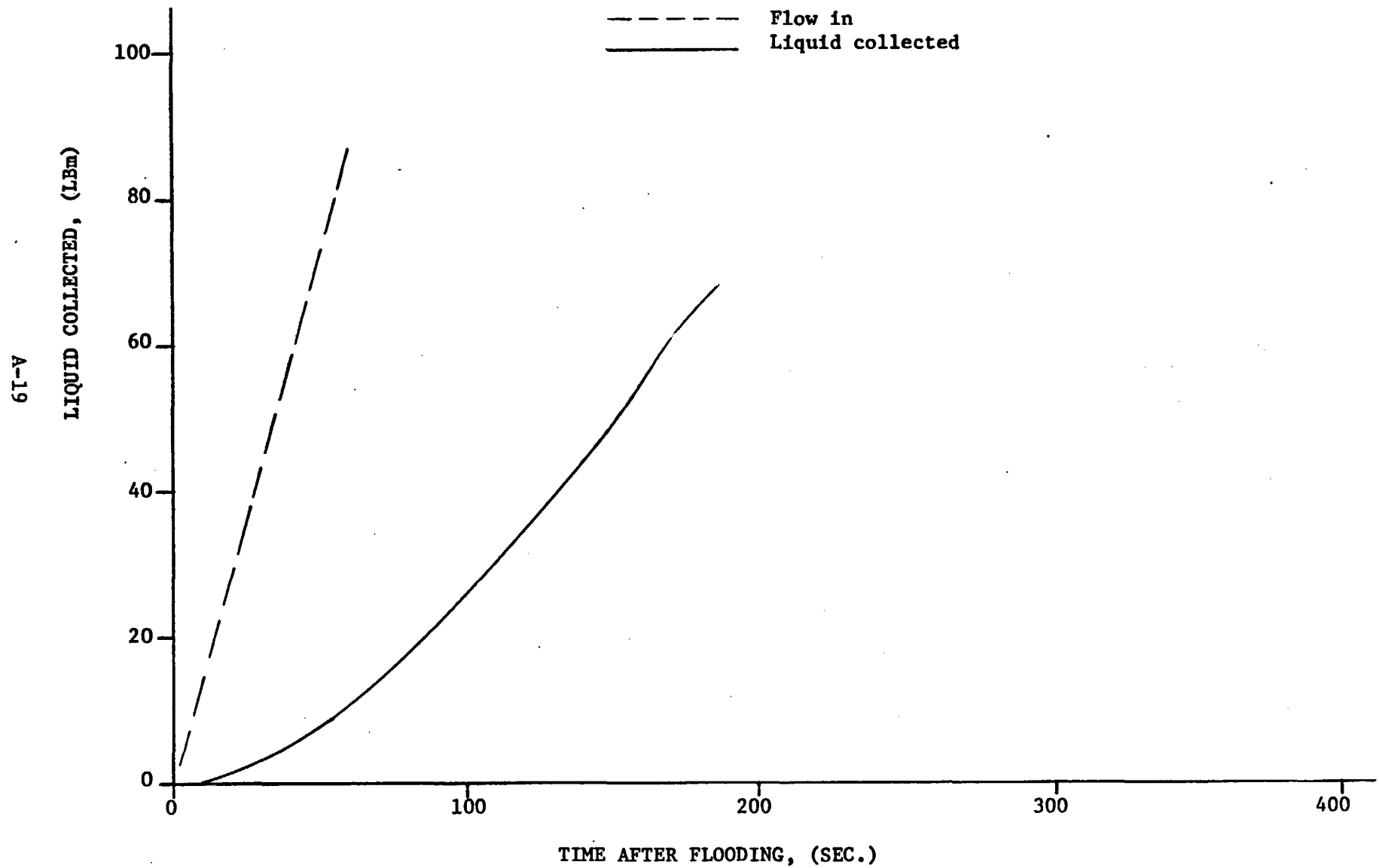
Run 9881
PRESSURE DROP VS. TIME.



Run 9881

ENTRAINED LIQUID COLLECTED

NOTE: Liquid Collected Not Necessarily Total Liquid Carryover



FLECHT RUN SUMMARY SHEET

RUN NO. 9983

DATE 12/17/71

A. RUN CONDITIONS

Bundle Size	10 x 10 - SS
Initial Clad Temperature	1586 °F
Flooding Rate	1 in/sec
Peak Power	1.24 kw/ft
Decay Power	Curve B Figure 2-3
Inlet Coolant Temperature	90 °F
Pressure	19 psia

B. HOUSING TEMPERATURES

Elevation (ft)	Initial Temperature (°F)	Temperature at Quench Time of Hot Rod Midplane (<u>424</u> Sec)
2	451	147
4	684	209
6	730	873
8	675	982
10	463	232

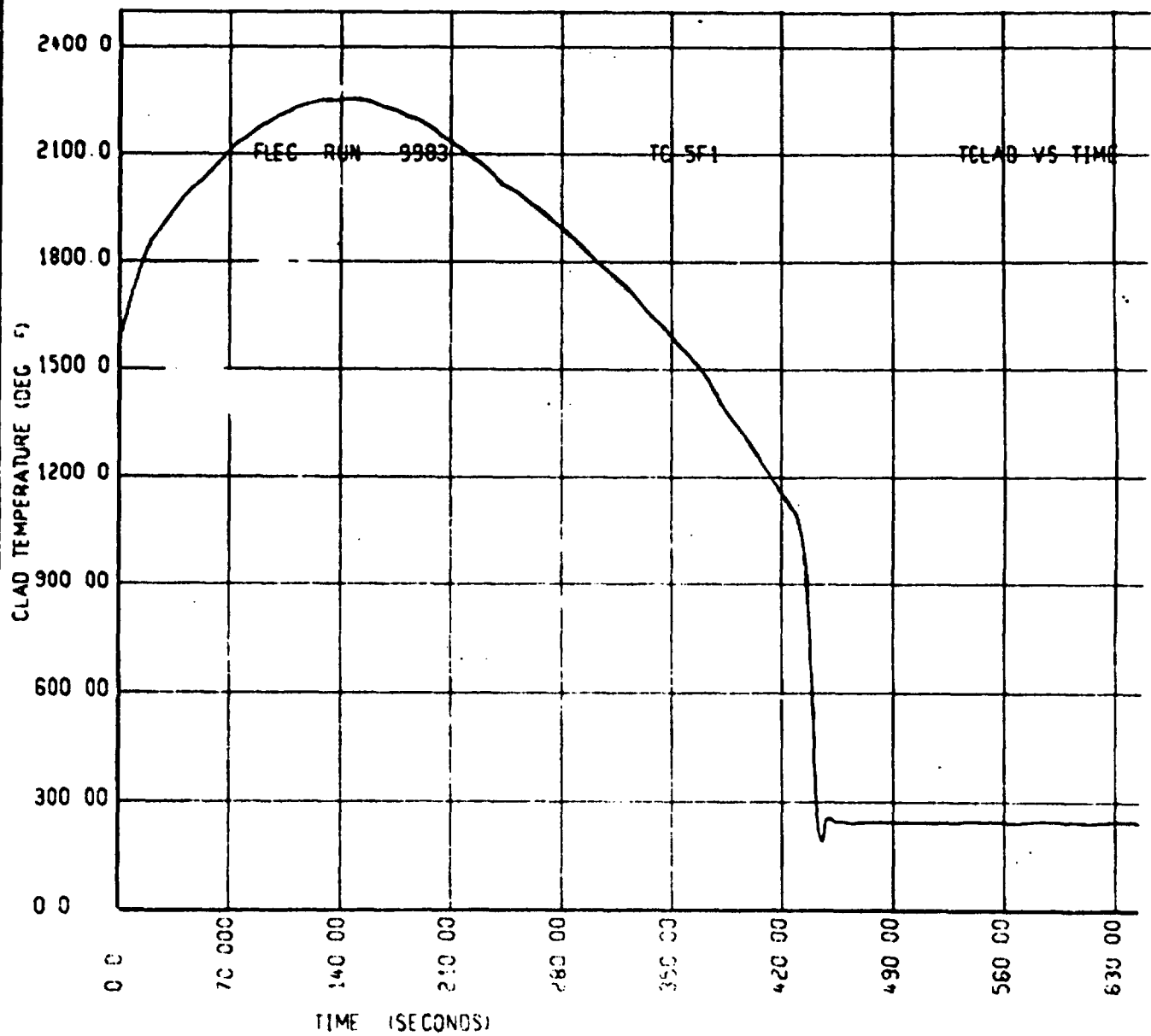
Initial T_{avg} Actual 575 °F

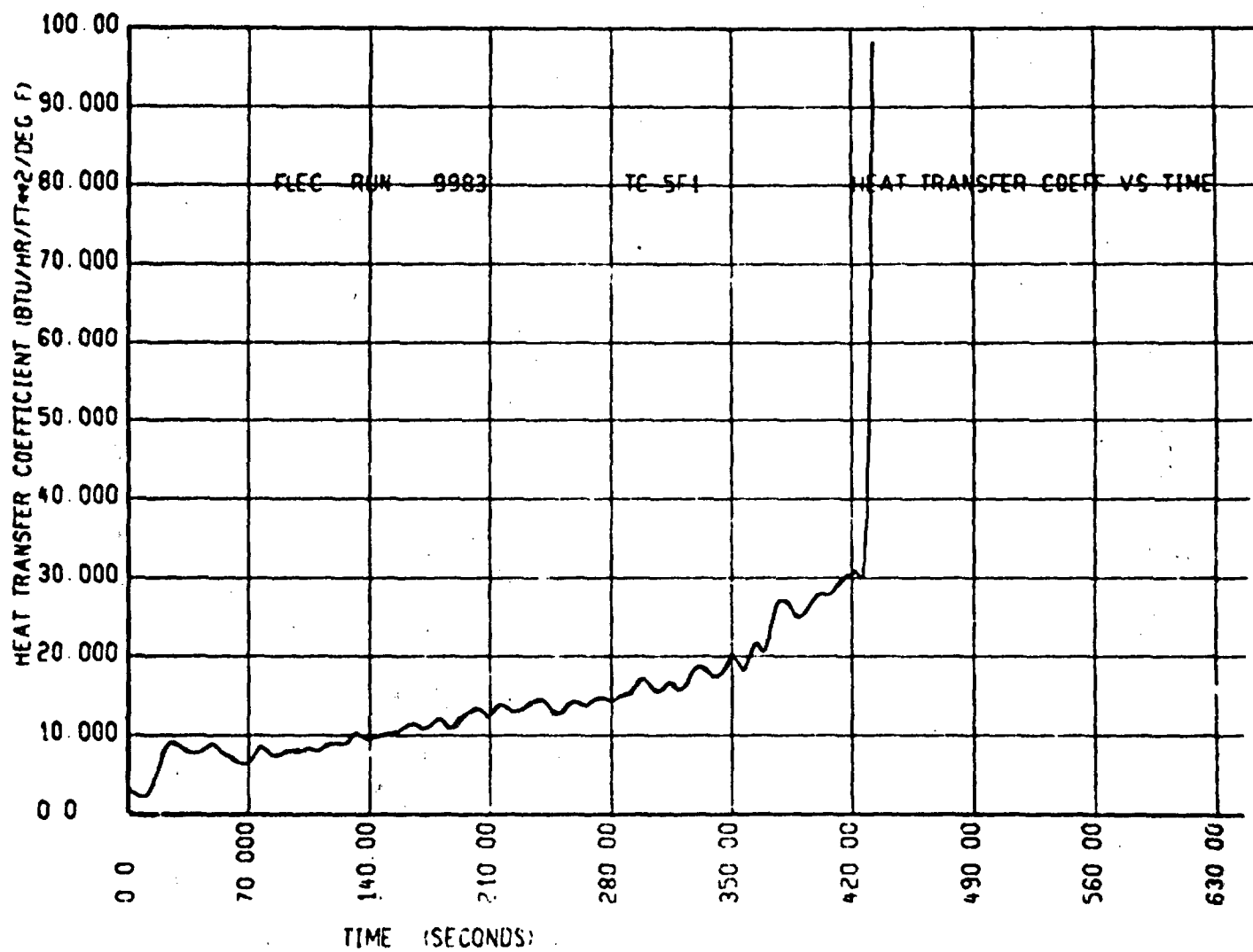
FLECHT RUN SUMMARY SHEET

RUN NO. 9983

C. HEATER THERMOCOUPLE DATA

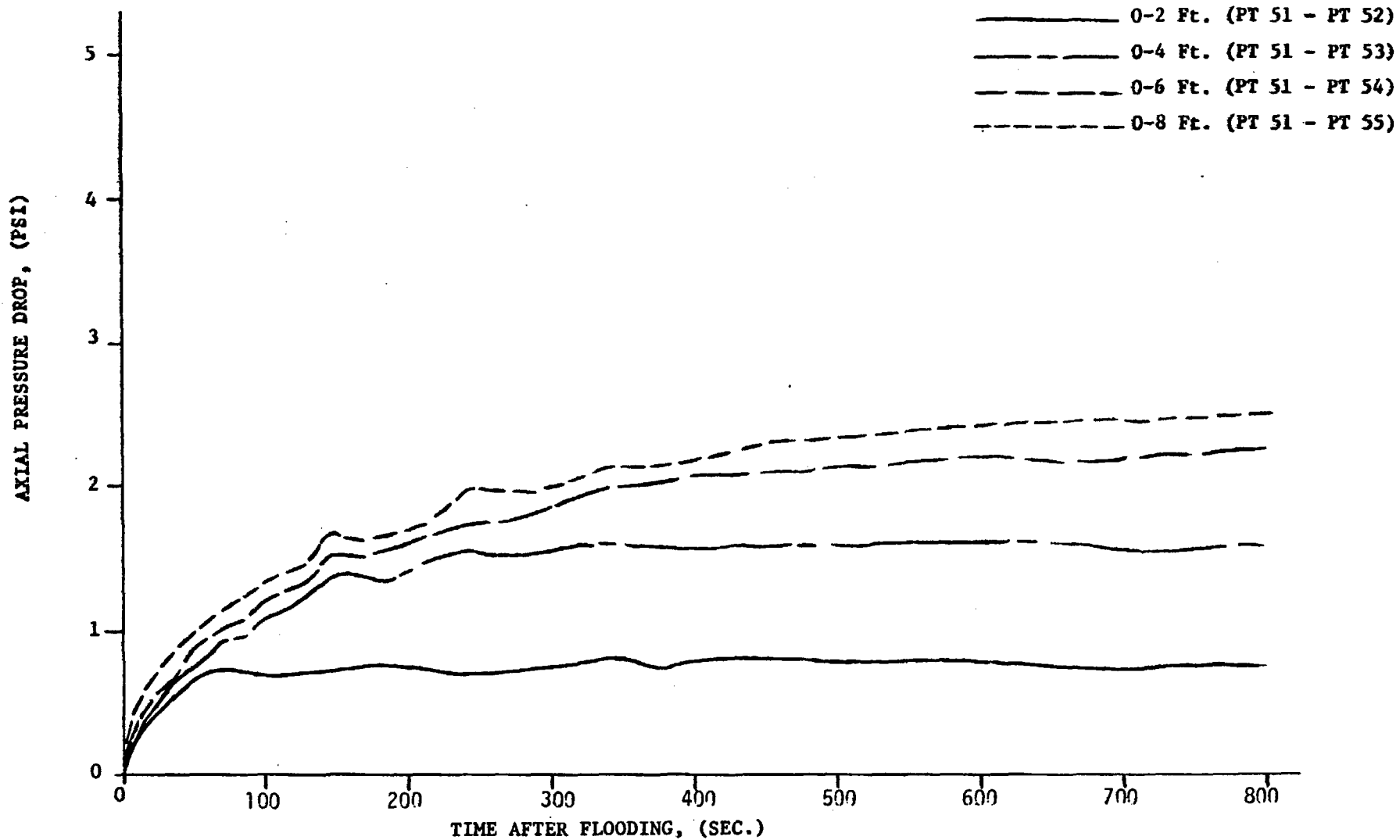
T/C No.	Elevation	Initial Temp. (°F)	Max. Temp. (°F)	Temp. Rise (°F)	Turnaround Time (Sec.)	Quench Temp. (°F)	Quench Time (sec)
5G1	6'	1601	2178	577	131	962	432
5G3	4'	1449	1733	284	48	617	231
5G5	10'	959	1567	608	191		
5G6	8'	Bad TC Signal Due To Pen Recorder Hookup					
5F1	6'	1586	2254	668	146	1049	424
5F6	8'	Bad TC Signal Due To Pen Recorder Hookup					
7G3	6'	1435	2128	643	144	850	442
6G3	6'	Bad TC Signal Due To Pen Recorder Hookup					
5E3	6'	1519	2192	673	137	983	424
4F2	6'	1540	2183	643	136	948	435
3F2	6'	1478	2119	641	128	926	425
1F2	6'	1516	1791	275	72	822	463
7D2	6'	1576	2217	641	134	1002	443
5E2	8'	1350	2119	769	191	849	742
5E4	4'	1341	1660	319	52	674	227
5E5	2'	908	988	80	15	655	72
5E1	10'	Bad TC Data					
6G5	2'	921	1005	84	15	759	68





Run 9983
PRESSURE DROP VS. TIME.

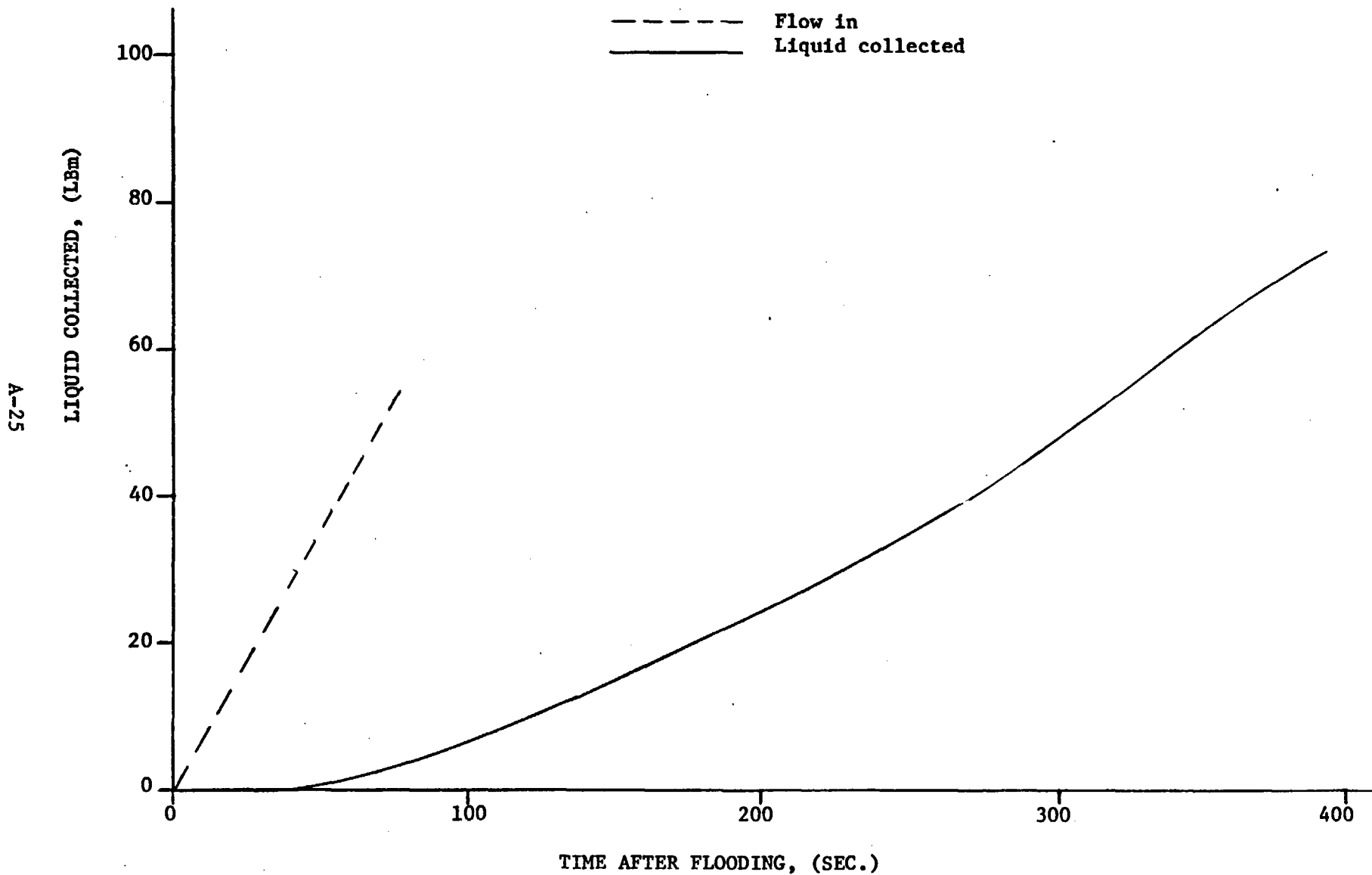
A-24



Run 9983

ENTRAINED LIQUID COLLECTED

NOTE: Liquid Collected Not Necessarily Total Liquid Carryover



FLECHT RUN SUMMARY SHEET

RUN NO. 8000

DATE 12/22/71

A. RUN CONDITIONS

Bundle Size	10 x 10 - SS
Initial Clad Temperature	1689 °F
Flooding Rate	1 in/sec
Peak Power	1.24 kw/ft
Decay Power	Curve B Figure 2-3
Inlet Coolant Temperature	134 °F
Pressure	58 psia

B. HOUSING TEMPERATURES

Elevation (ft)	Initial Temperature (°F)	Temperature at Quench Time of Hot Rod Midplane (262 Sec)
2	484	200
4	747	287
6	831	881
8	746	977
10	485	323

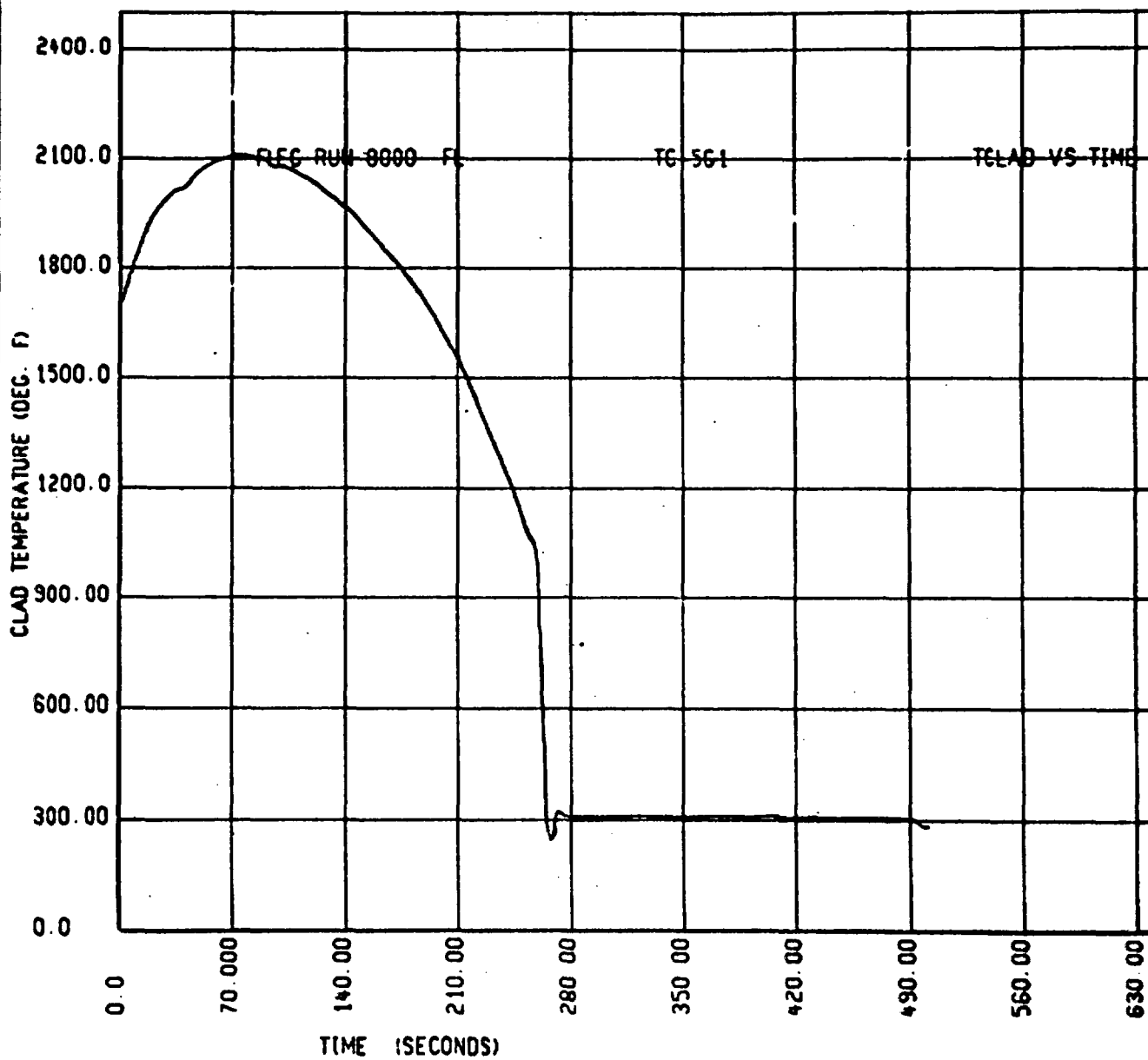
Initial T_{avg} Actual 630 °F

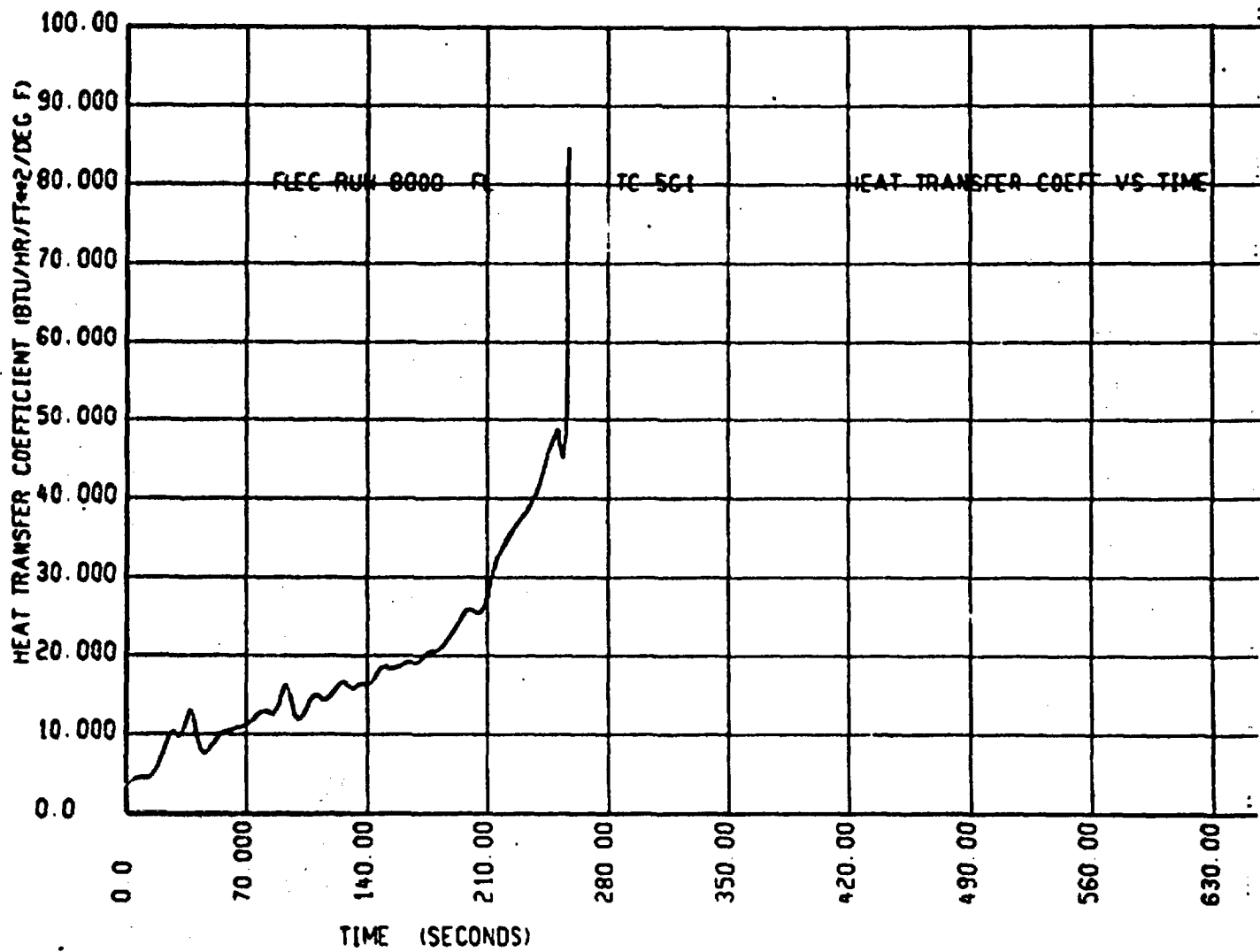
FLECHT RUN SUMMARY SHEET

RUN NO. 8000

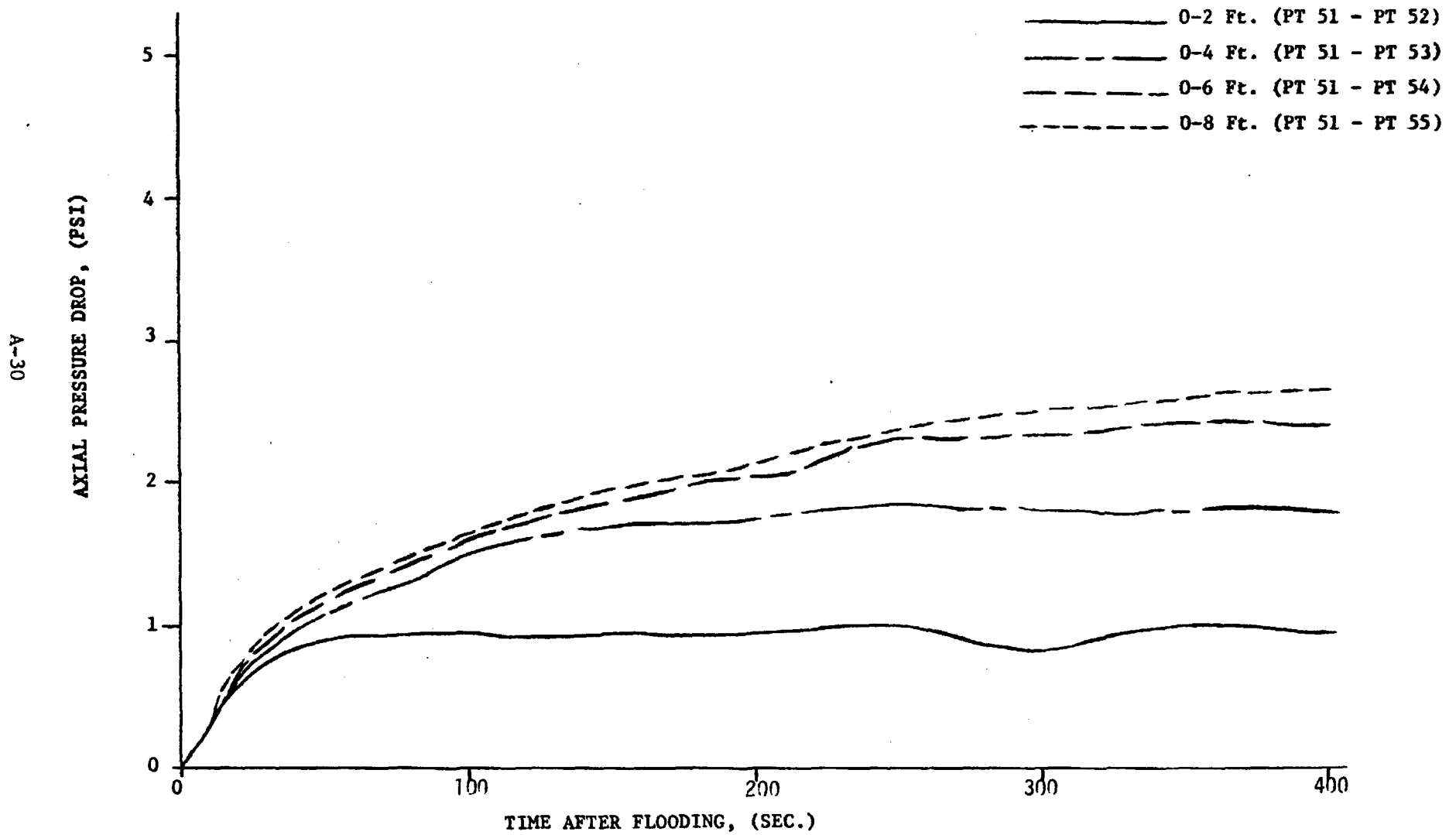
C. HEATER THERMOCOUPLE DATA

T/C No.	Elevation	Initial Temp. (°F)	Max. Temp. (°F)	Temp. Rise (°F)	Turnaround Time (Sec.)	Quench Temp. (°F)	Quench Time (sec)
5G1	6'	1689	2111	422	74	949	262
5G3	4'	1513	1703	190	28	816	135
5G5	10'	994	1786	792	162	584	491
5G6	8'	Bad TC Signal Due To Pen Recorder Hookup					
5F1	6'	1684	2111	427	76	847	263
5F6	8'	Bad TC Signal Due To Pen Recorder Hookup					
7G3	6'	1604	2016	412	64	986	258
6G3	6'	Bad TC Signal Due To Pen Recorder Hookup					
5E3	6'	1631	2076	447	74	998	251
4F2	6'	1644	2058	414	80	973	256
3F2	6'	1577	1987	410	70	912	252
1F2	6'	1545	1785	240	34	930	251
7D2	6'	1684	2098	414	58	1018	262
5E2	8'	1435	2209	774	140	850	426
5E4	4'	1424	1632	208	30	796	137
5E5	2'	951	1025	74	12	765	48
5E1	10'	971	1840	869	199	732	480
6G5	2'	964	1029	65	14	758	50





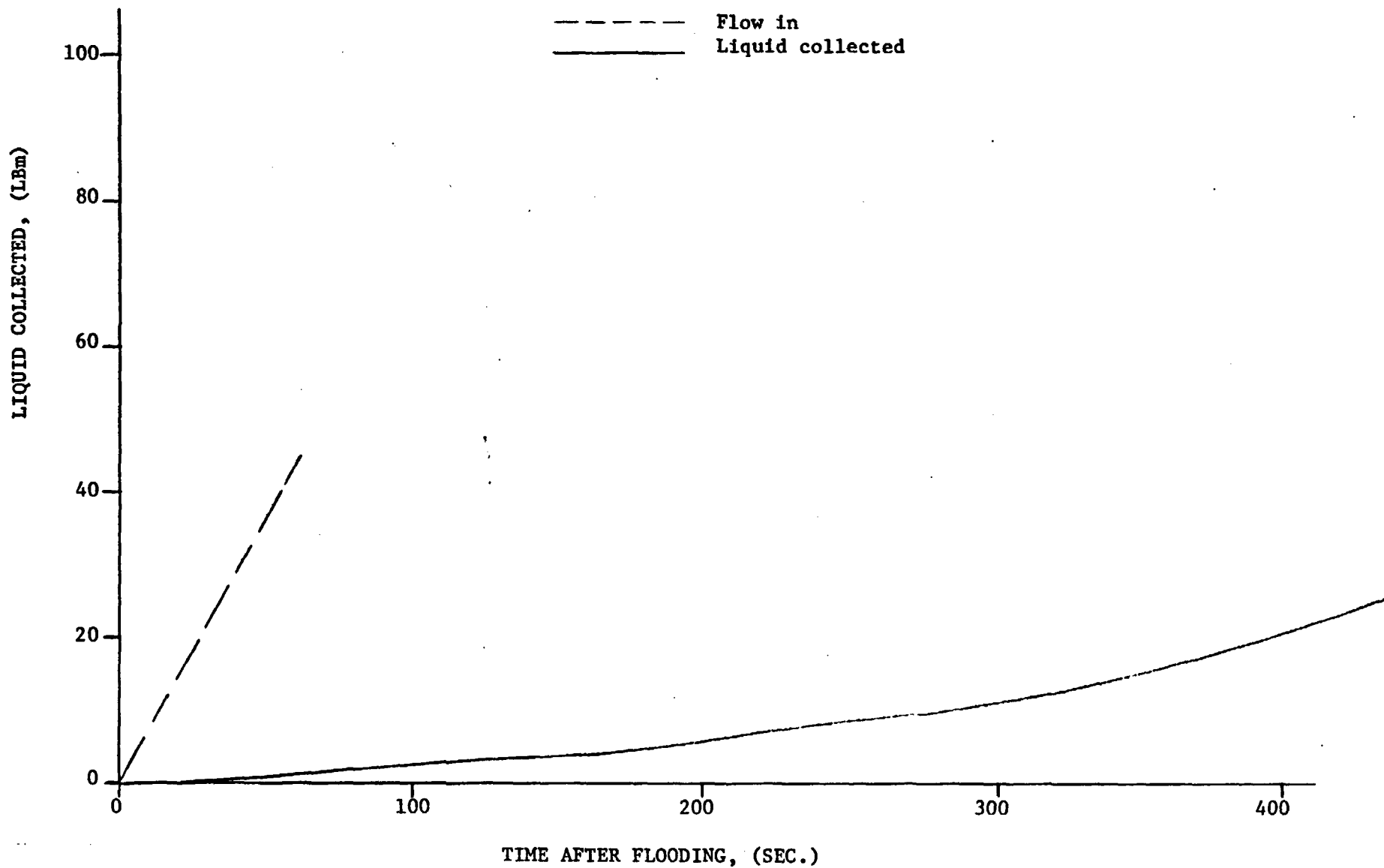
Run 8000
PRESSURE DROP VS. TIME.



Run 8000

ENTRAINED LIQUID COLLECTED

NOTE: Liquid Collected Not Necessarily Total Liquid Carryover



FLECHT RUN SUMMARY SHEET

RUN NO. 0085
DATE 12/20/71

A. RUN CONDITIONS

Bundle Size	10 x 10 - SS
Initial Clad Temperature	1586 °F
Flooding Rate	2 in/sec
Peak Power	1.24 kw/ft
Decay Power	Curve B Figure 2-3
Inlet Coolant Temperature	91 °F
Pressure	25 psia

B. HOUSING TEMPERATURES

Elevation (ft)	Initial Temperature (°F)	Temperature at Quench Time of Hot Rod Midplane (231 Sec)
2	433	142
4	647	186
6	703	427
8	647	367
10	447	237

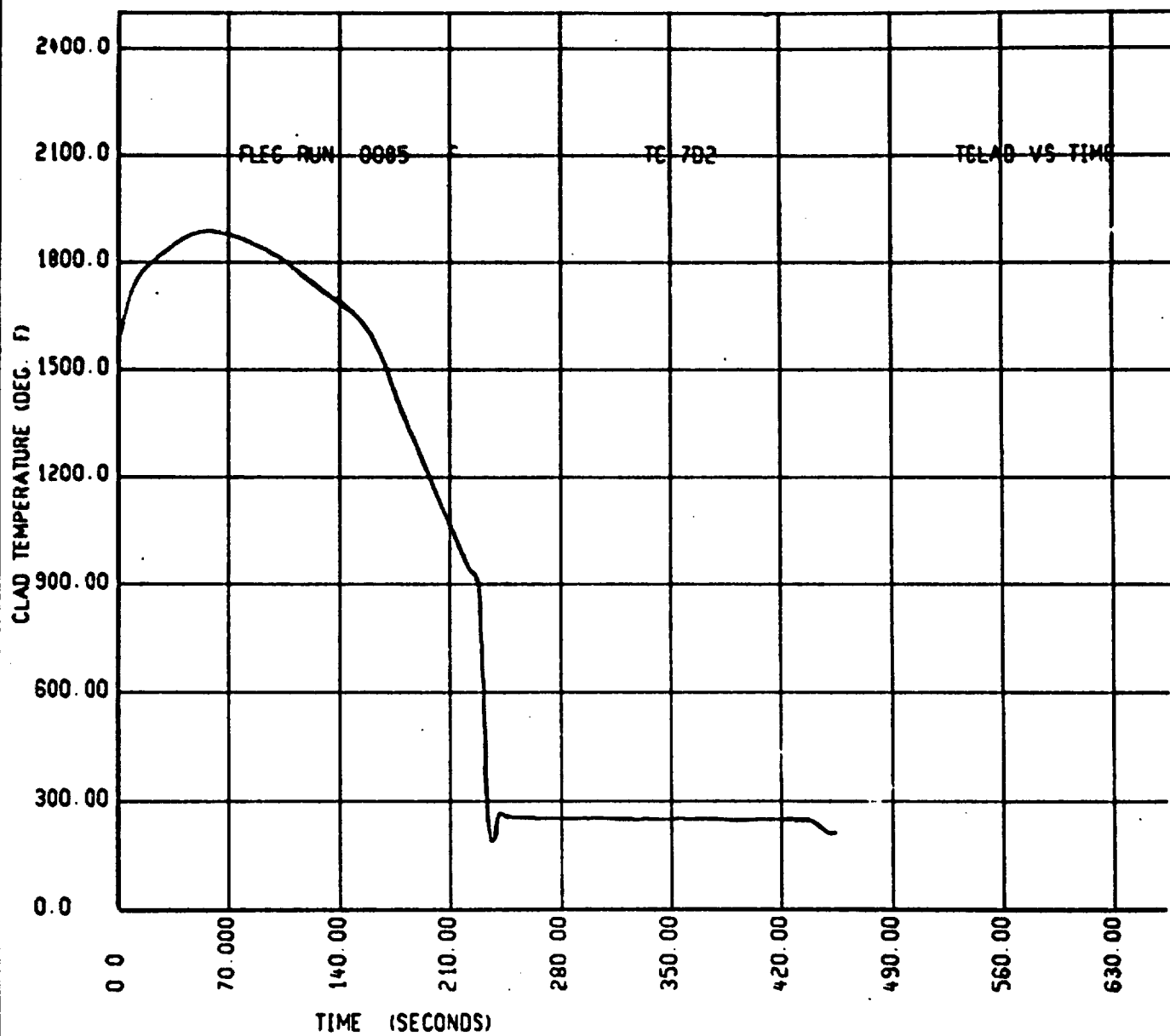
Initial T_{avg} Actual 549 °F

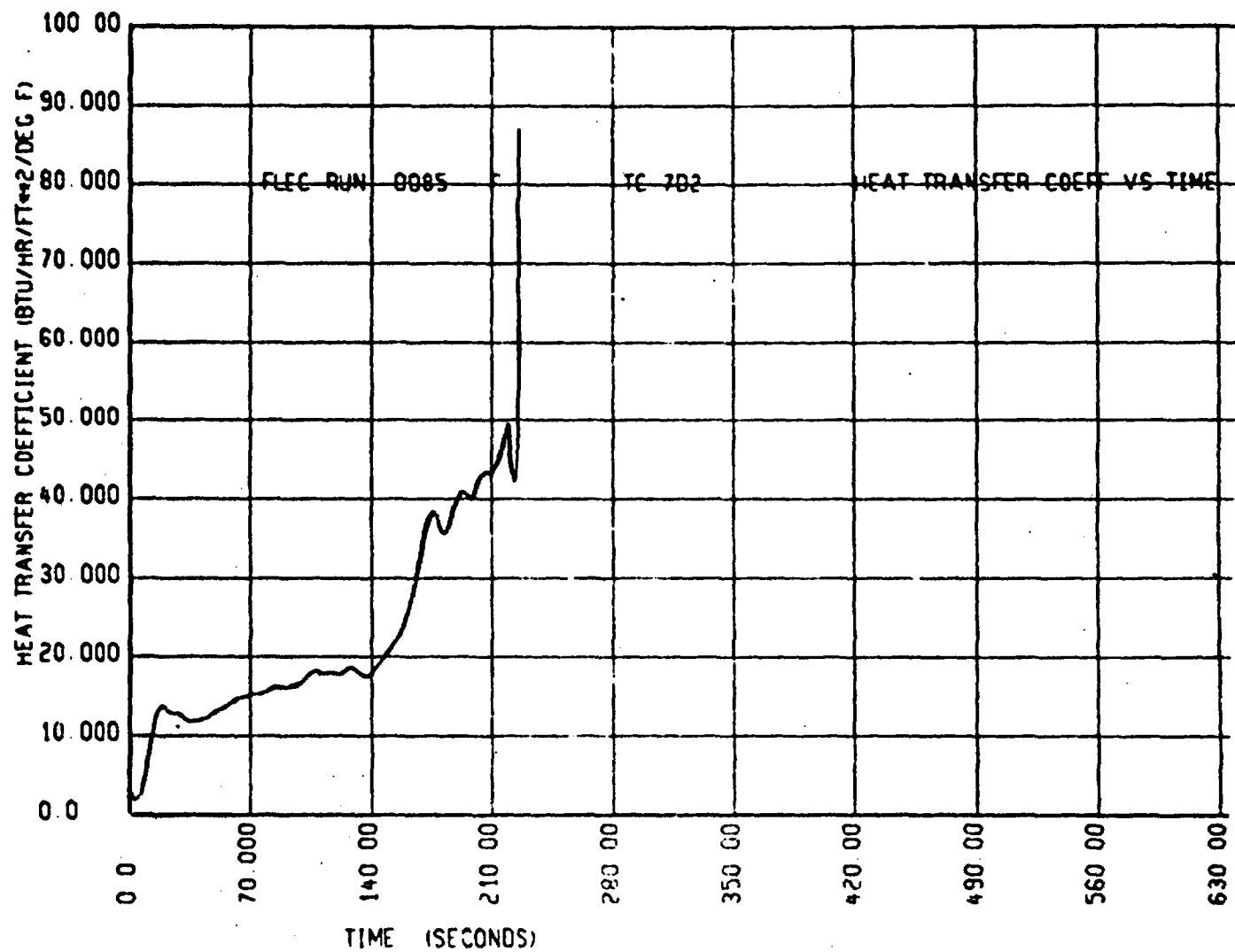
FLECHT RUN SUMMARY SHEET

RUN NO. 0085

C. HEATER THERMOCOUPLE DATA

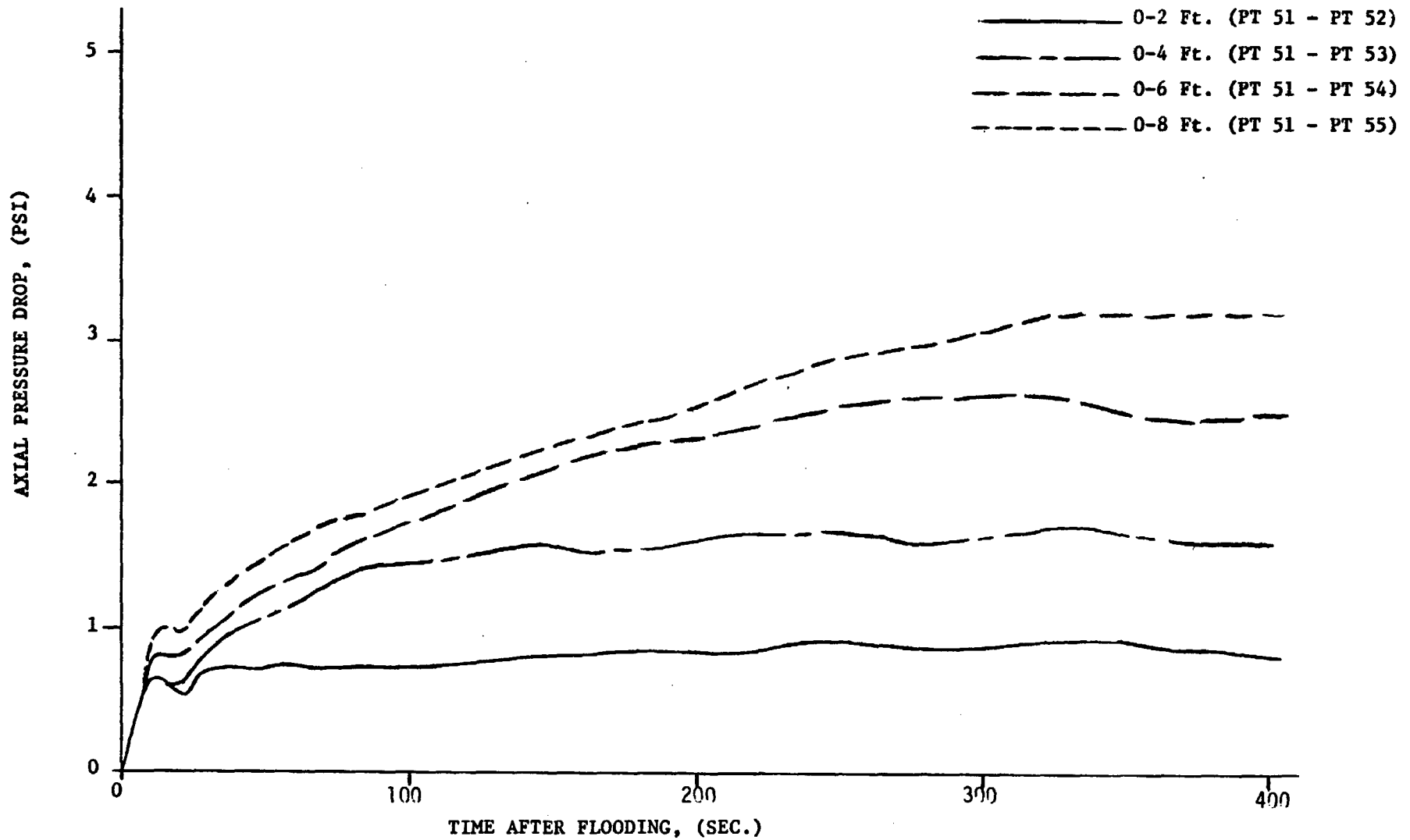
T/C No.	Elevation	Initial Temp. (°F)	Max. Temp. (°F)	Temp. Rise (°F)	Turnaround Time (Sec.)	Quench Temp. (°F)	Quench Time (sec)
5G1	6'	1592	1882	290	54	805	230
5G3	4'	1452	1610	158	25	844	110
5G5	10'	972	1162	190	68	600	416
5G6	8'	Bad TC Signal Due To Pen Recorder Holdup					
5F1	6'	1595	1888	293	66	885	226
5F6	8'	Bad TC Signal Due To Pen Recorder Holdup					
7G3	6'	1495	1800	305	66	776	226
6G36G3	6'	Bad TC Signal Due To Pen Recorder Holdup					
5E3	6'	1529	1855	326	59	830	219
4F2	6'	1546	1850	304	64	880	219
3F2	6'	1480	1799	319	63	810	220
1F2	6'	1499	1658	159	26	730	243
7D2	6'	1586	1888	302	57	858	231
5E2	8'	1358	1691	333	84	831	350
5E4	4'	1348	1527	179	26	867	105
5E5	2'	915	966	51	9	858	32
5E1	10'	924	1171	247	87	521	444
6G5	2'	928	973	45	9	839	34





Run 0085
PRESSURE DROP VS. TIME.

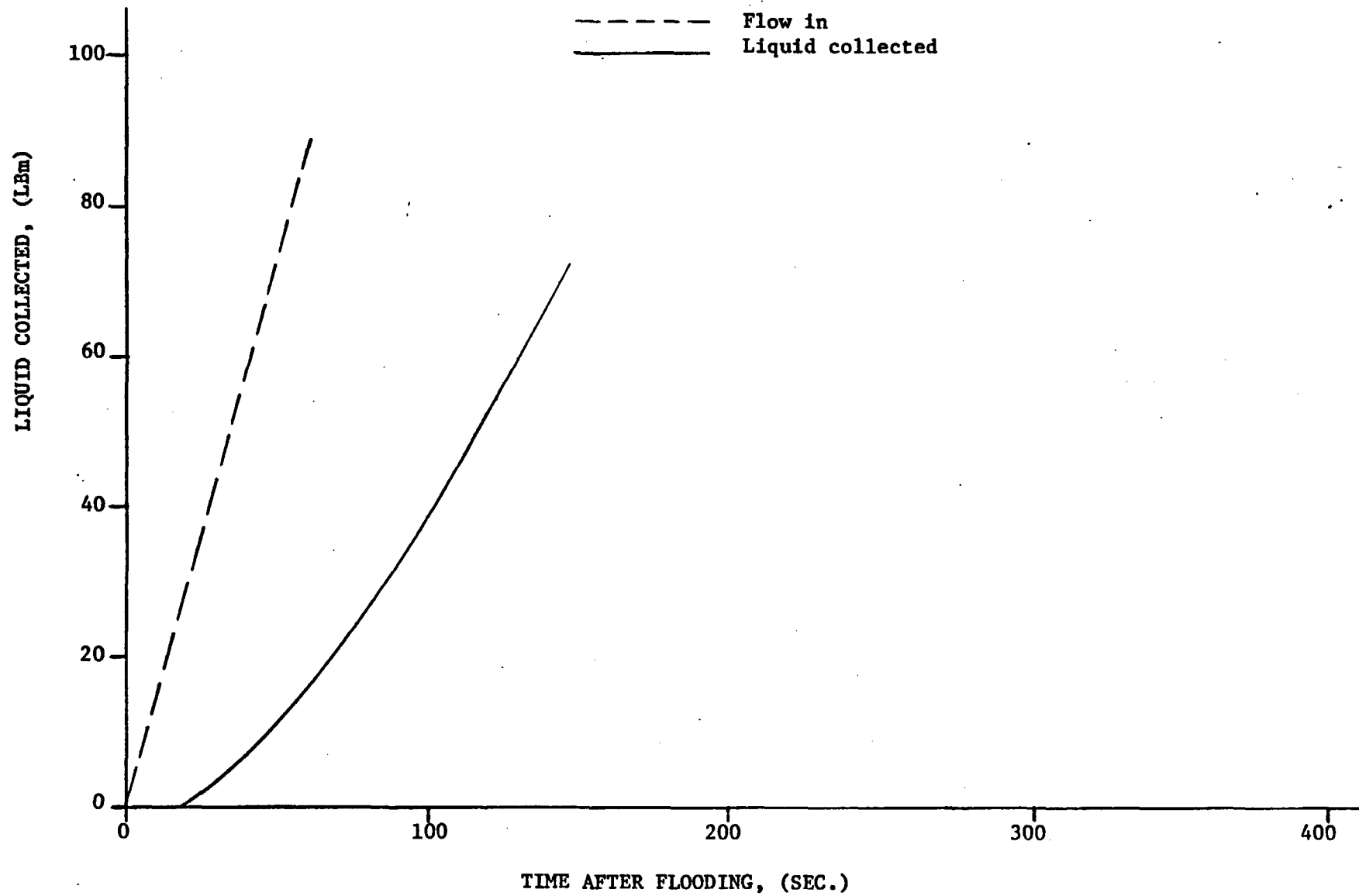
A-36



Run 0085

ENTRAINED LIQUID COLLECTED

NOTE: Liquid Collected Not Necessarily Total Liquid Carryover



A-37

FLECHT RUN SUMMARY SHEET

RUN NO. 0183

DATE 12/23/71

A. RUN CONDITIONS

Bundle Size	10 x 10 - SS
Initial Clad Temperature	1598 °F
Flooding Rate	1 in/sec
Peak Power	1.24 kw/ft
Decay Power	Curve B Figure 2-3
Inlet Coolant Temperature	84 °F
Pressure	21 psia

B. HOUSING TEMPERATURES

Elevation (ft)	Initial Temperature (°F)	Temperature at Quench Time of Hot Rod Midplane (420 Sec)
2	454	310
4	621	205
6	731	860
8	659	971
10	458	232

Initial T_{avg} Actual 556 °F

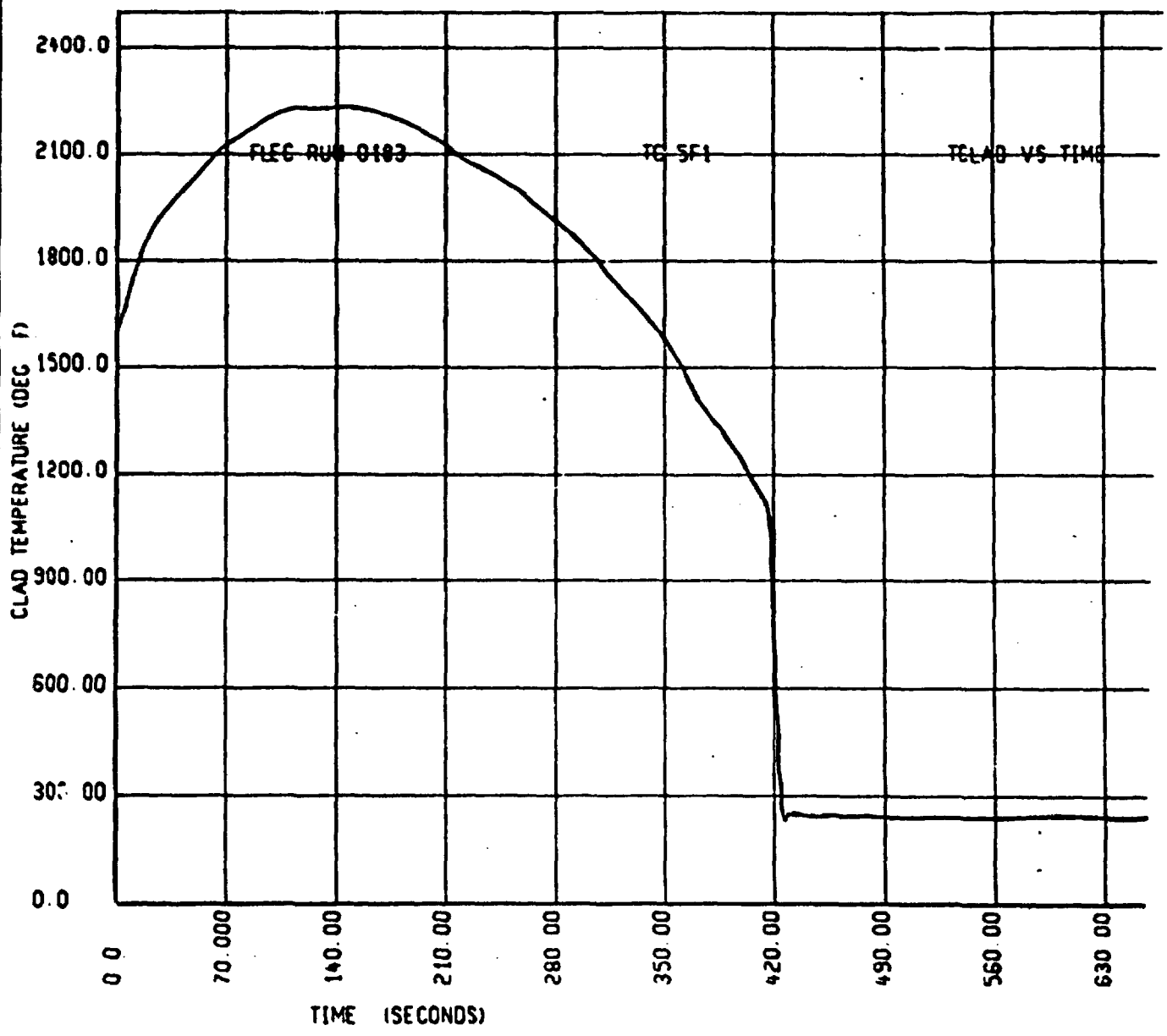
FLECHT RUN SUMMARY SHEET

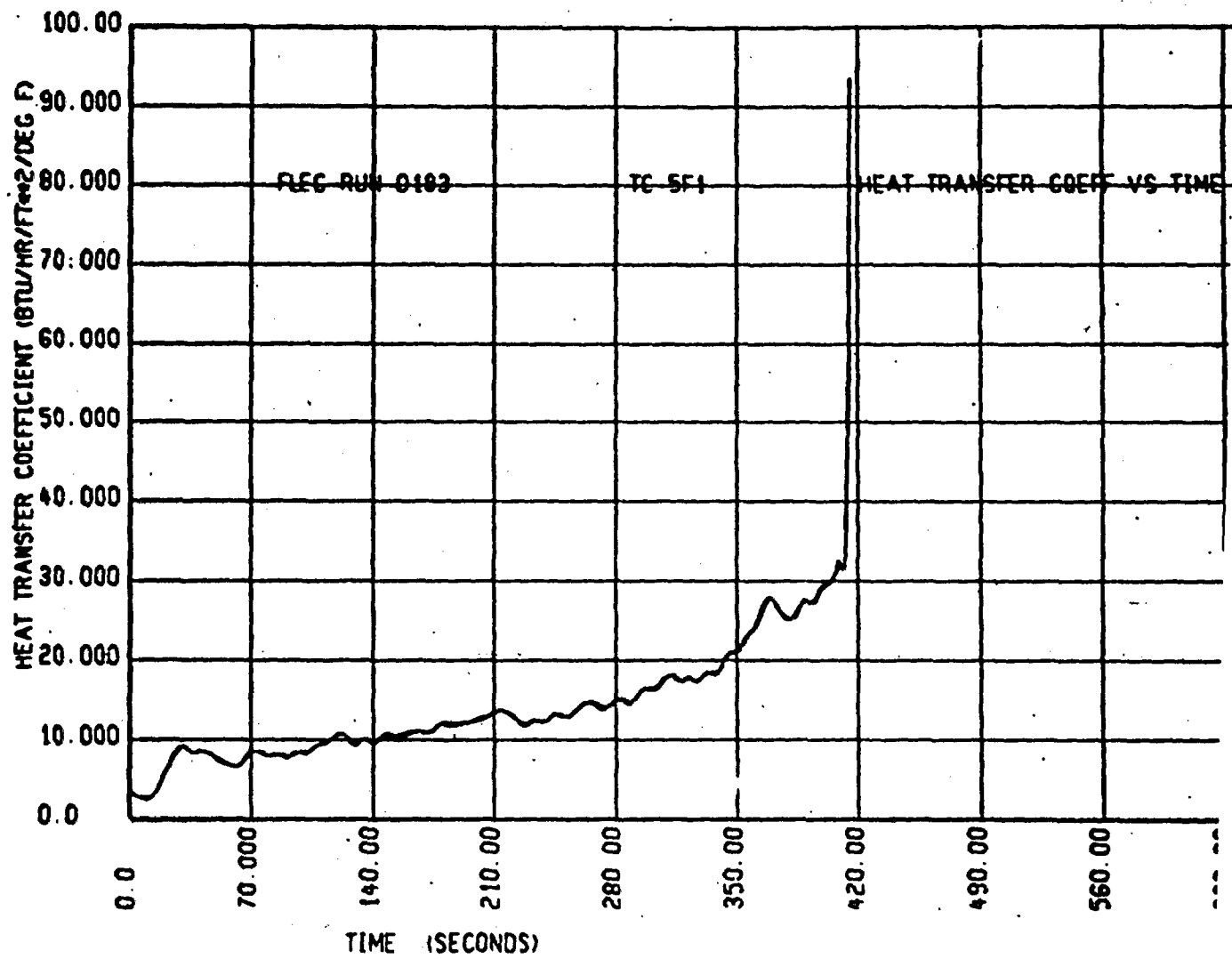
RUN NO. 0183

C. HEATER THERMOCOUPLE DATA

T/C No.	Elevation	Initial Temp. (°F)	Max. Temp. (°F)	Temp. Rise (°F)	Turnaround Time (Sec.)	Quench Temp. (°F)	Quench Time (sec)
5G1	6'	1600	2222	622	118	918	424
5G3	4'	1417	1695	278	45	737	215
5G5	10'	963	1569	606	231	743	797
5G6	8'	1396	2080	684	167	797	725
5F1	6'	1598	2234	636	142	1020	420
5F6	8'	1412	2137	725	179	788	747
7G3	6'	1511	2145	634	137	1018	415
6G3	6'	1586	2220	634	132	1009	421
5E3	6'	1532	2203	671	132	1001	415
4F2	6'	1555	2186	631	133	1016	413
3F2	6'	1487	2110	623	119	980	403
1F2	6'	1523	1804	281	48	699	458
7D2	6'	1598	2223	625	140	1076	424
5E2	8'	1344	2150	806	238	848	736
5E4	4'	1305	1623	318	64	648	216
5E5	2'	889	982	93	15	732	67
5E1	10'	913	1650	737	301	593	874
6G5	2'	904	992	88	16	685	68

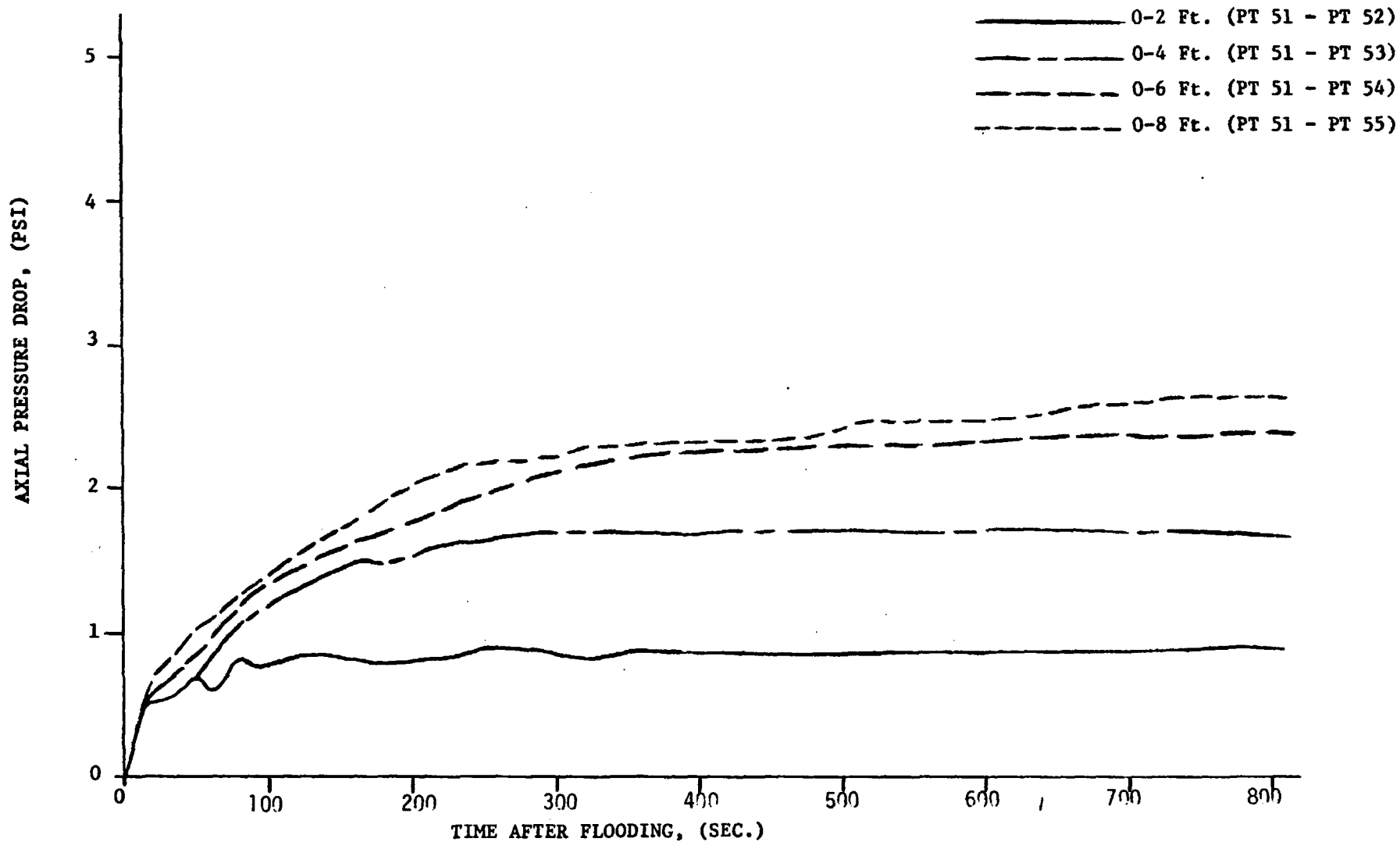
A-39





Run 0183
PRESSURE DROP VS. TIME.

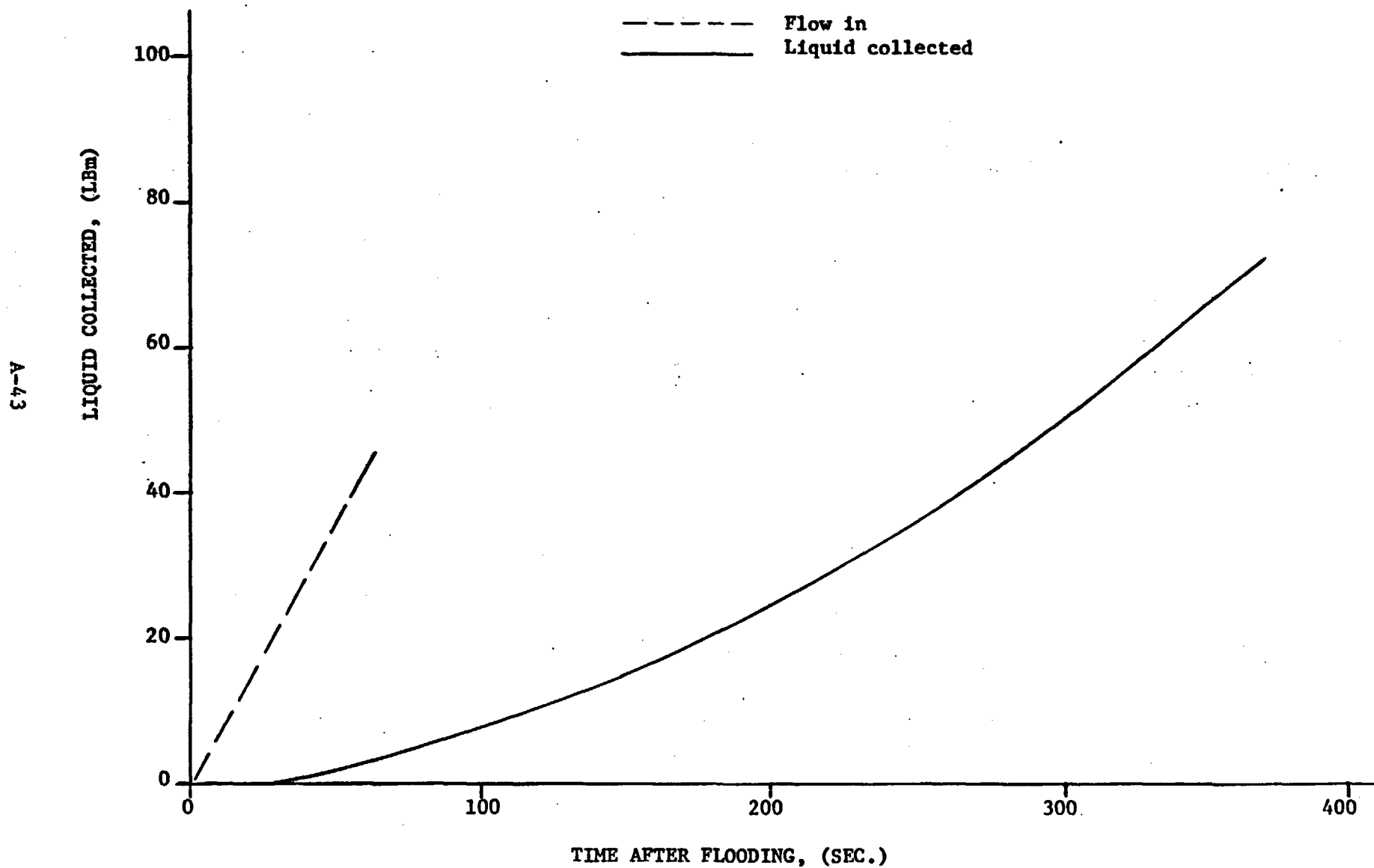
A-42



Run 0183

ENTRAINED LIQUID COLLECTED

NOTE: Liquid Collected Not Necessarily Total Liquid Carryover



FLECHT RUN SUMMARY SHEET

RUN NO. 0284

DATE 12/27/71

A. RUN CONDITIONS

Bundle Size	10 x 10 - SS
Initial Clad Temperature	1590 °F
Flooding Rate	1 in/sec
Peak Power	1.24 kw/ft
Decay Power	Curve B Figure 2-3
Inlet Coolant Temperature	183 °F
Pressure	21 psia

B. HOUSING TEMPERATURES

Elevation (ft)	Initial Temperature (°F)	Temperature at Quench Time of Hot Rod Midplane (614 Sec)
2	474	228
4	690	230
6	753	860
8	687	968
10	455	230

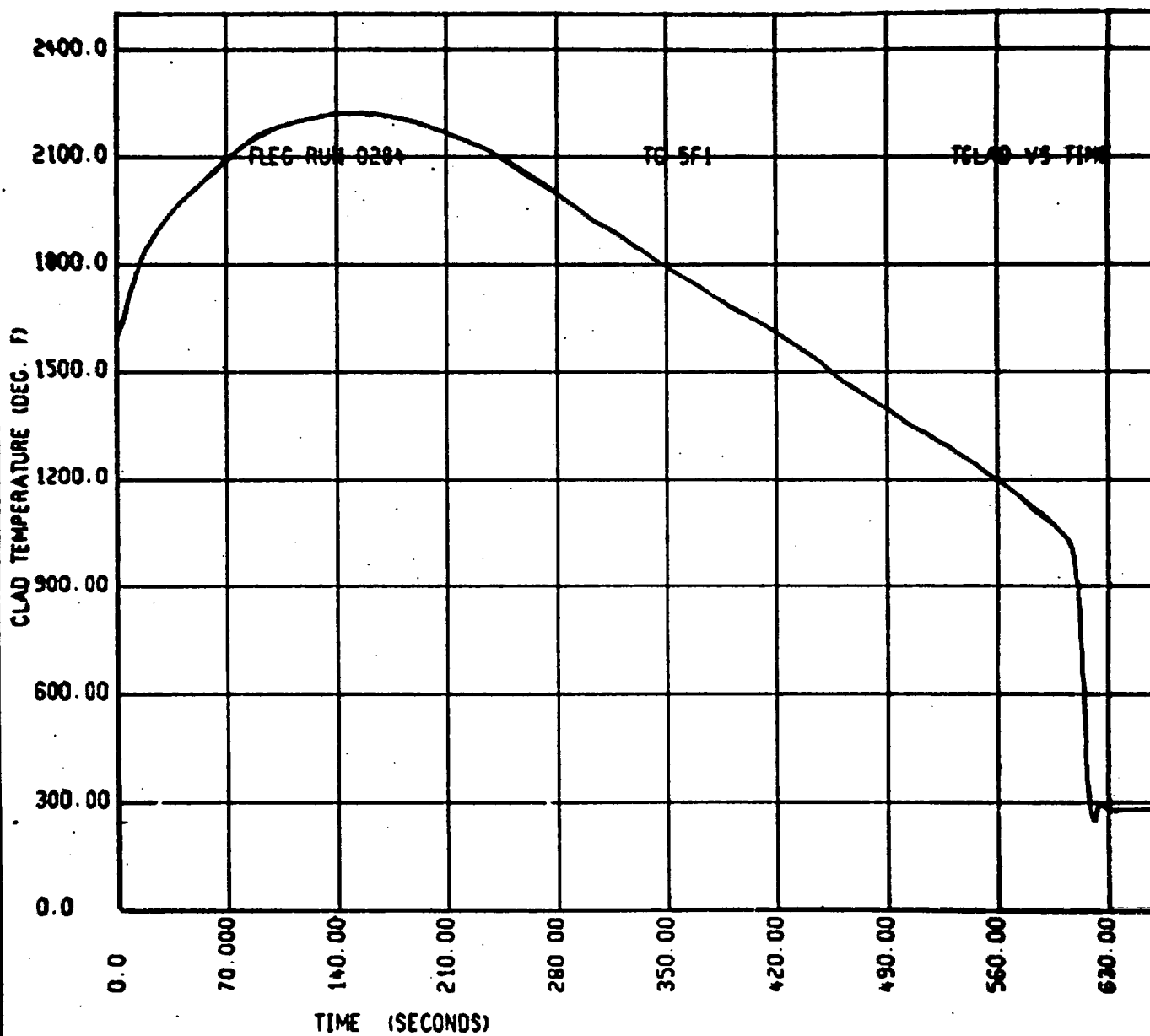
Initial T_{avg} Actual 592 °F

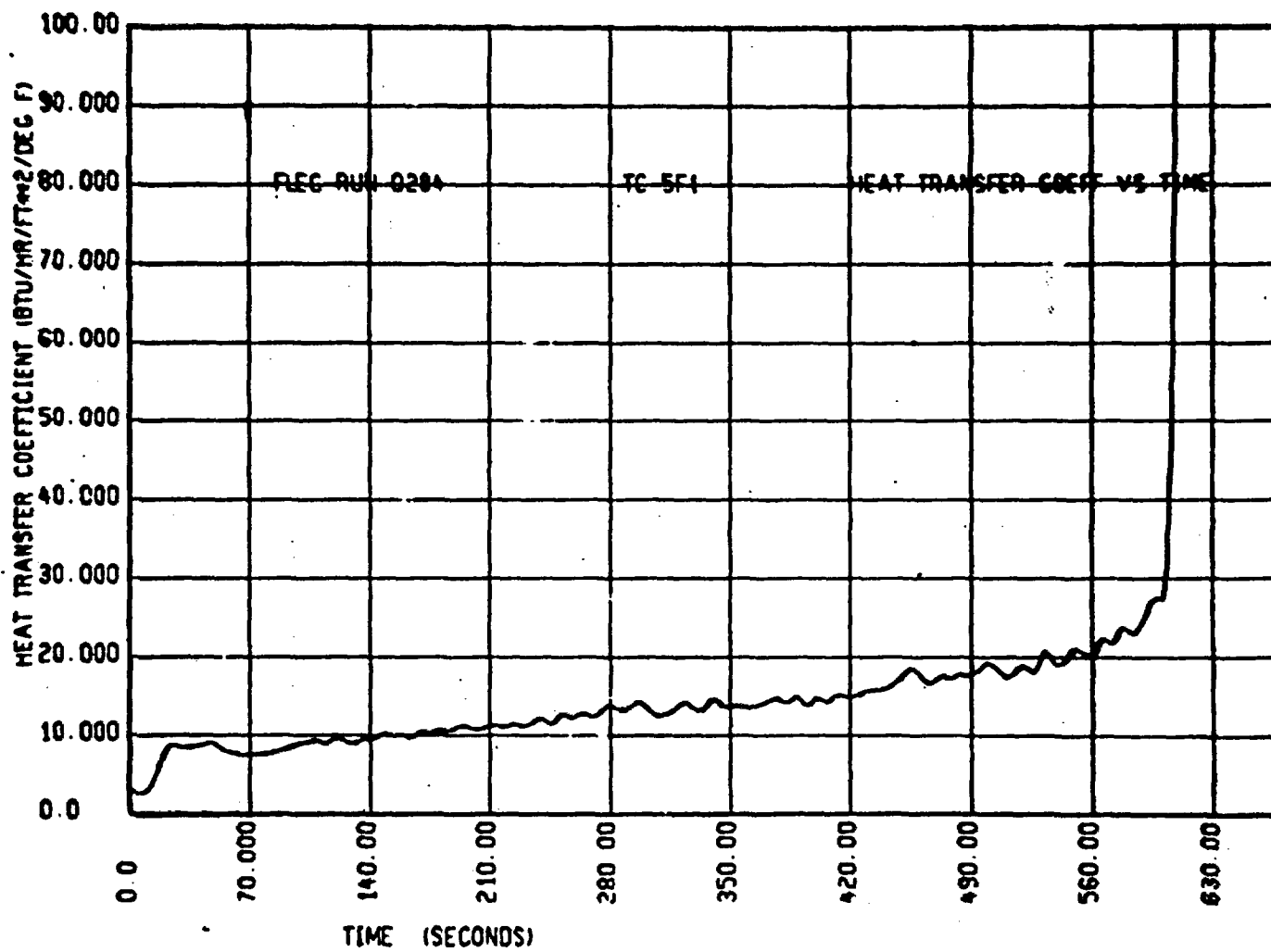
FLECHT RUN SUMMARY SHEET

RUN NO. 0284

C. HEATER THERMOCOUPLE DATA

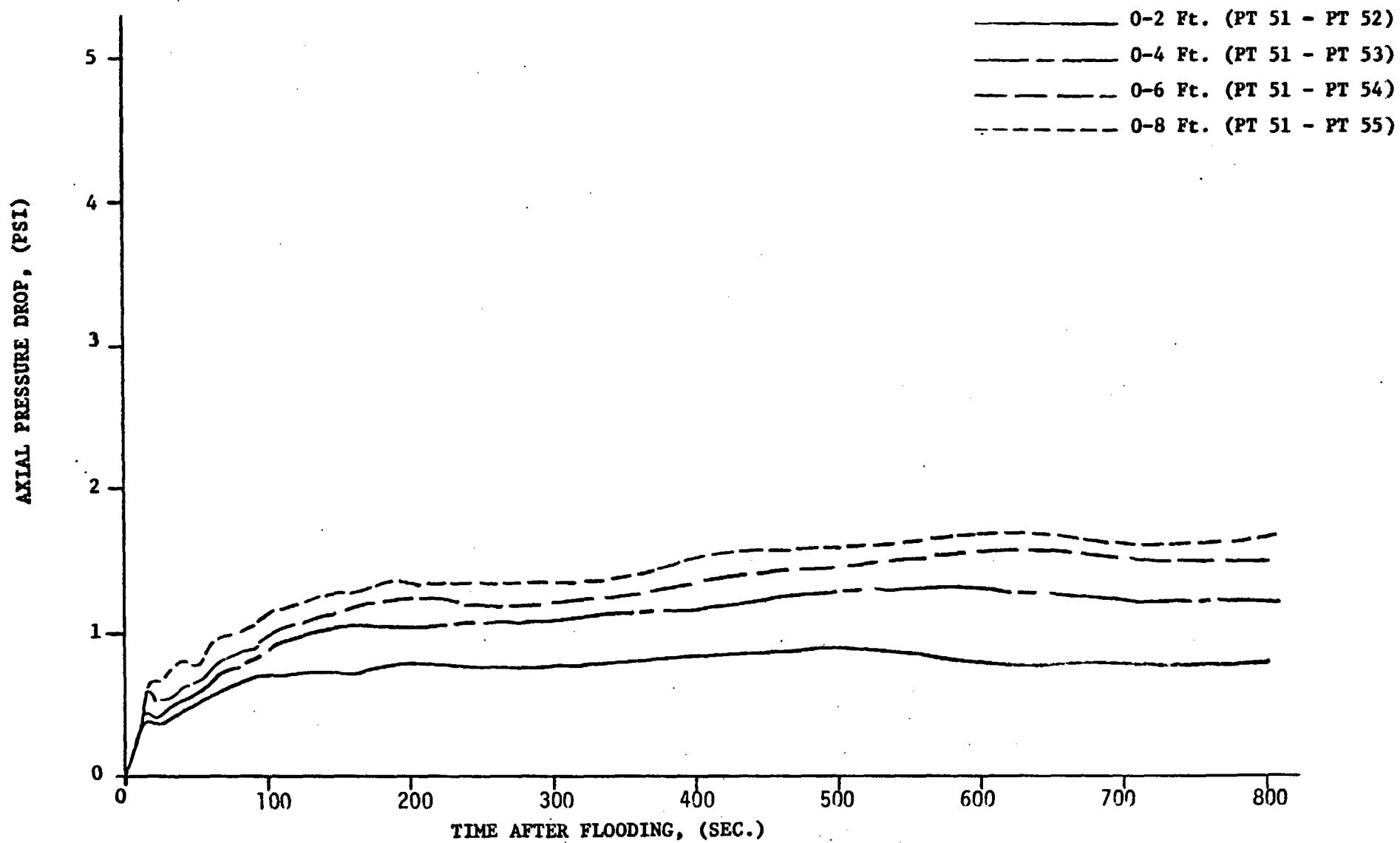
T/C No.	Elevation	Initial Temp. (°F)	Max. Temp. (°F)	Temp. Rise (°F)	Turnaround Time (Sec.)	Quench Temp. (°F)	Quench Time (sec)
5G1	6'	1593	2201	608	155	863	623
5G3	4'	1446	1716	270	45	855	232
5G5	10'	964	1517	553	193	602	1055
5G6	8'	1406	2032	626	178	786	907
5F1	6'	1590	2224	634	144	774	614
5G6	8'	1423	2089	666	191	886	934
7G3	6'	1488	2122	634	139	936	619
6G3	6'	1567	2194	627	154	903	631
5E3	6'	1525	2188	663	142	885	602
4F2	6'	1546	2157	611	149	902	612
3F2	6'	1481	2070	589	137	838	591
1F2	6'	1510	1774	264	59	840	646
7D2	6'	1572	2215	643	144	871	629
5E2	8'	1355	2098	743	200	784	935
5E4	4'	1344	1634	290	486	734	289
5E5	2'	924	999	75	14	708	86
5E1	10'	919	1562	643	219	623	1056
6G5	2'	939	1017	78	13	698	91





Run 0284
PRESSURE DROP VS. TIME.

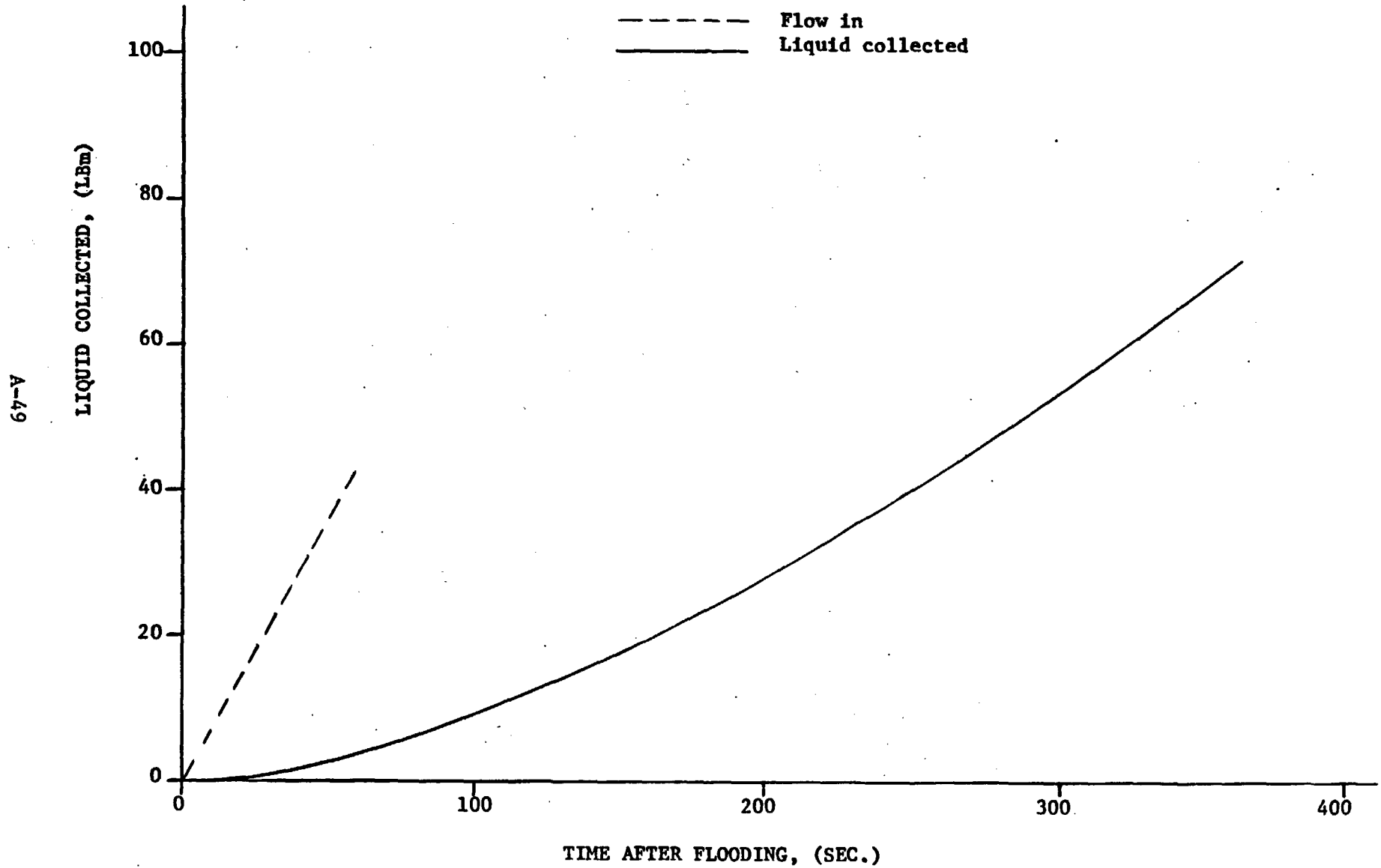
A-48



Run 0284

ENTRAINED LIQUID COLLECTED

NOTE: Liquid Collected Not Necessarily Total Liquid Carryover



FLECHT RUN SUMMARY SHEET

RUN NO. 0386

DATE 12/28/71

A. RUN CONDITIONS

Bundle Size	10 x 10 - SS
Initial Clad Temperature	1591 °F
Flooding Rate	1 in/sec
Peak Power	0.69 kw/ft
Decay Power	Curve B Figure 2-3
Inlet Coolant Temperature	189 °F
Pressure	20 psia

B. HOUSING TEMPERATURES

Elevation (ft)	Initial Temperature (°F)	Temperature at Quench Time of Hot Rod Midplane (<u>323</u> Sec)
2	404	224
4	495	228
6	585	270
8	540	666
10	387	229

Initial T_{avg} Actual 465 °F

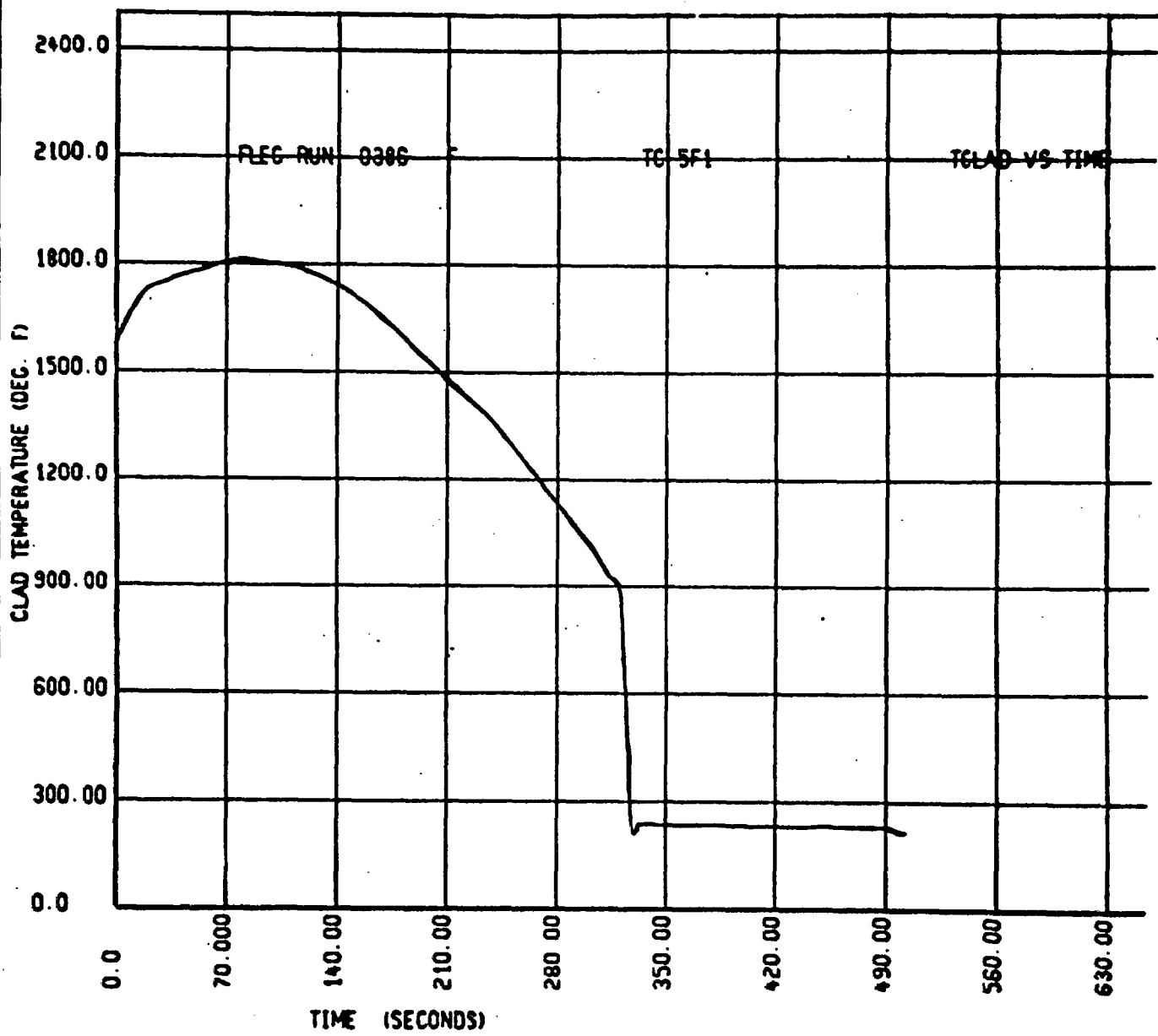
FLECHT RUN SUMMARY SHEET

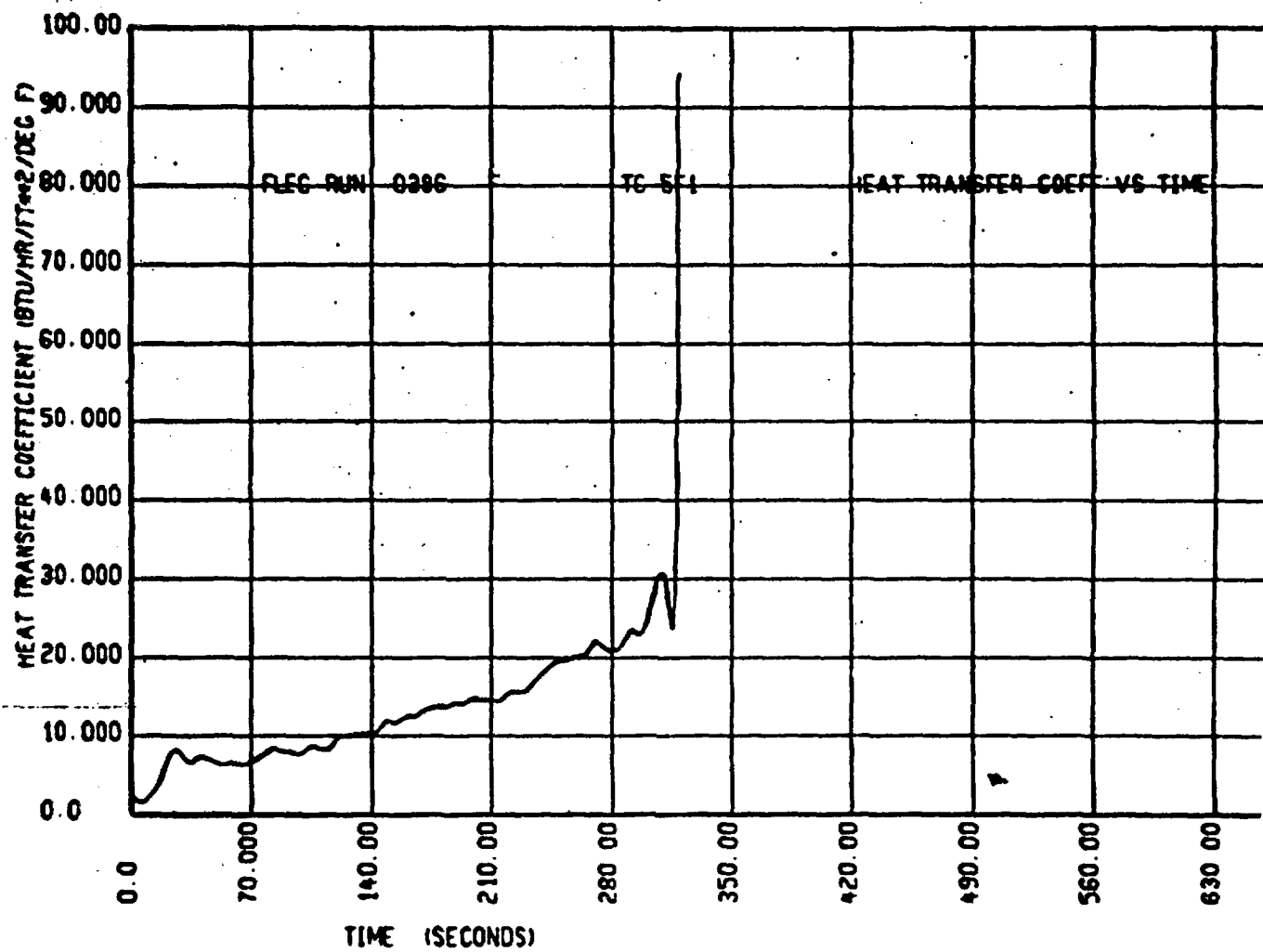
RUN NO. 0386

C. HEATER THERMOCOUPLE DATA

T/C No.	Elevation	Initial Temp. (°F)	Max. Temp. (°F)	Temp. Rise (°F)	Turnaround Time (Sec.)	Quench Temp. (°F)	Quench Time (sec)
5G1	6'	1582	1789	207	74	774	328
5G3	4'	1408	1507	101	99	628	191
5G5	10'	946	1185	239	118	810	414
5G6	8'	1392	1638	246	114	689	469
5F1	6'	1591	1810	219	77	850	323
5F6	8'	1407	1673	266	119	550	425
7G3	6'	1565	1782	217	75	796	325
6G3	6'	1501	1737	236	75	777	329
5E3	6'	1555	1788	233	75	757	322
4F2	6'	1549	1772	223	76	754	325
3F2	6'	1490	1714	224	77	810	312
1F2	6'	1464	1558	94	18	675	350
7D2	6'	1584	1807	223	78	801	334
5E2	8'	1356	1675	319	124	702	486
5E4	4'	1325	1446	121	35	586	197
5E5	2'	868	910	42	12	628	75
5E1	10'	899	1250	351	229		
6G5	2'	881	922	41	13	616	77

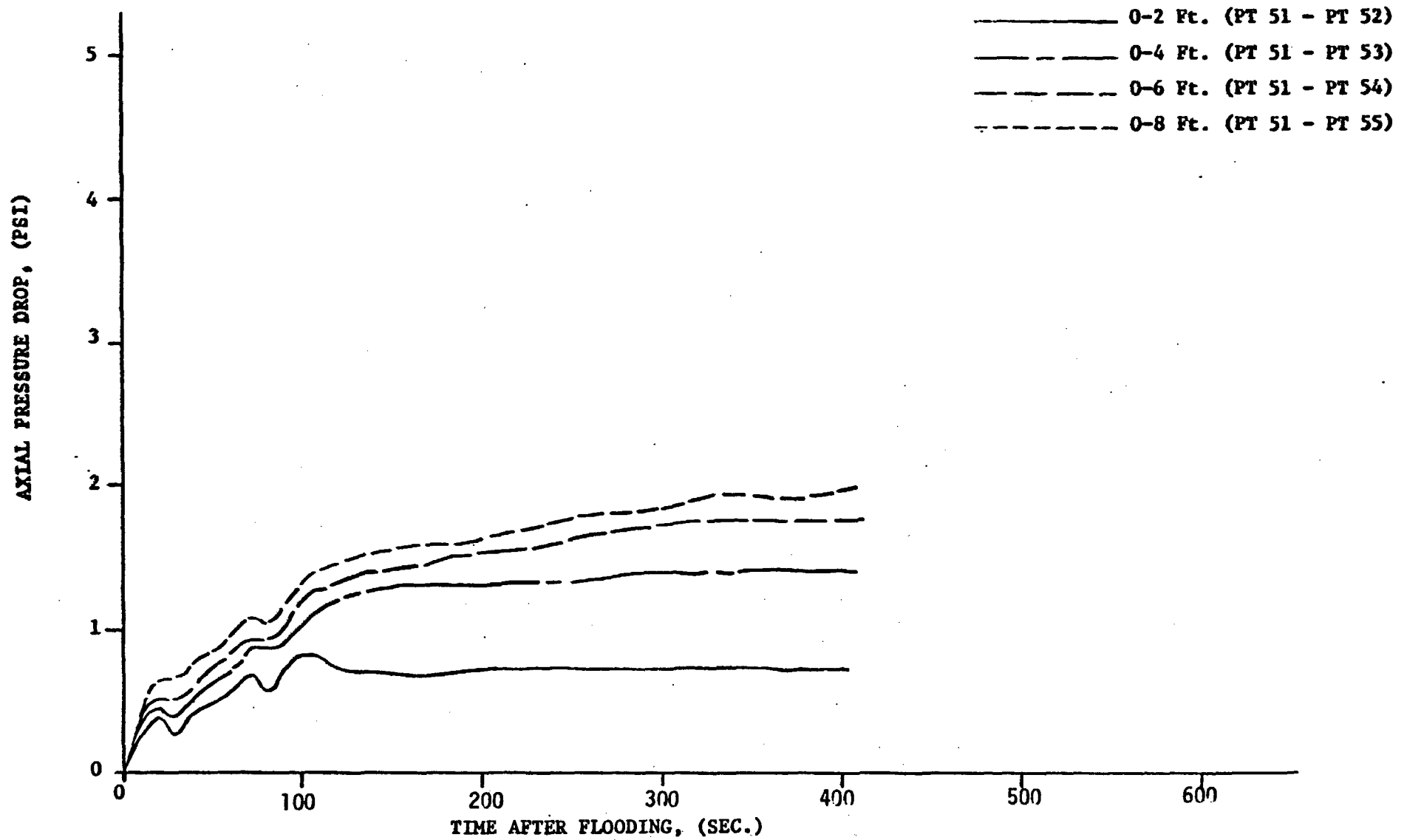
A-51





Run 0386
PRESSURE DROP VS. TIME.

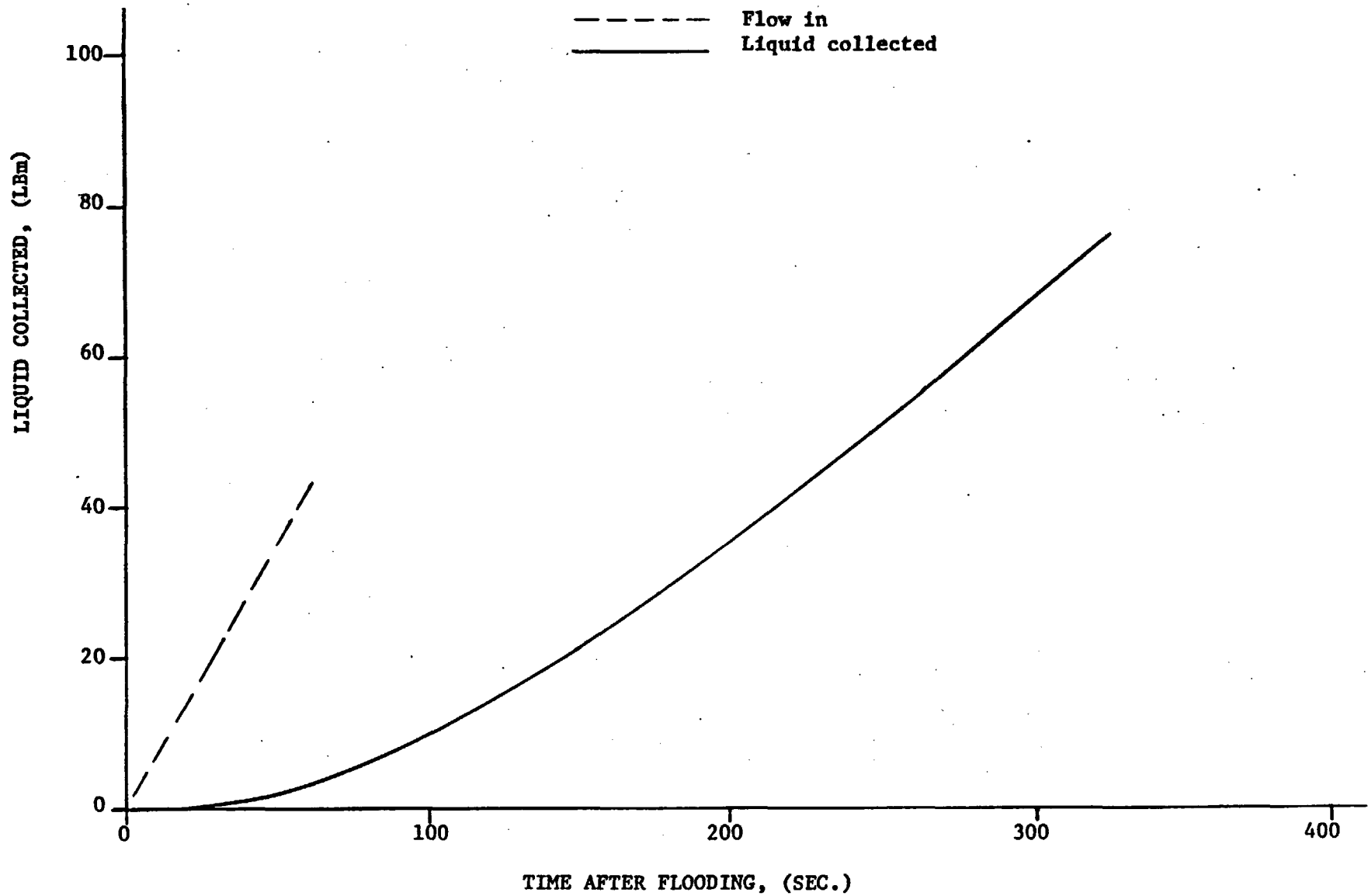
A-54



Run 0386

ENTRAINED LIQUID COLLECTED

NOTE: Liquid Collected Not Necessarily Total Liquid Carryover



A-55

FLECHT RUN SUMMARY SHEET

RUN NO. 0487

DATE 12/29/71

A. RUN CONDITIONS

Bundle Size	10 x 10 - SS
Initial Clad Temperature	1582 °F
Flooding Rate	0.8 in/sec
Peak Power	1.24 kw/ft
Decay Power	Curve B Figure 2-3
Inlet Coolant Temperature	187 °F
Pressure	18 psia

B. HOUSING TEMPERATURES

Elevation (ft)	Initial Temperature (°F)	Temperature at Quench Time of Hot Rod Midplane (819 Sec)
2	474	230
4	688	228
6	784	924
8	694	1114
10	496	228

Initial T_{avg} Actual 597 °F

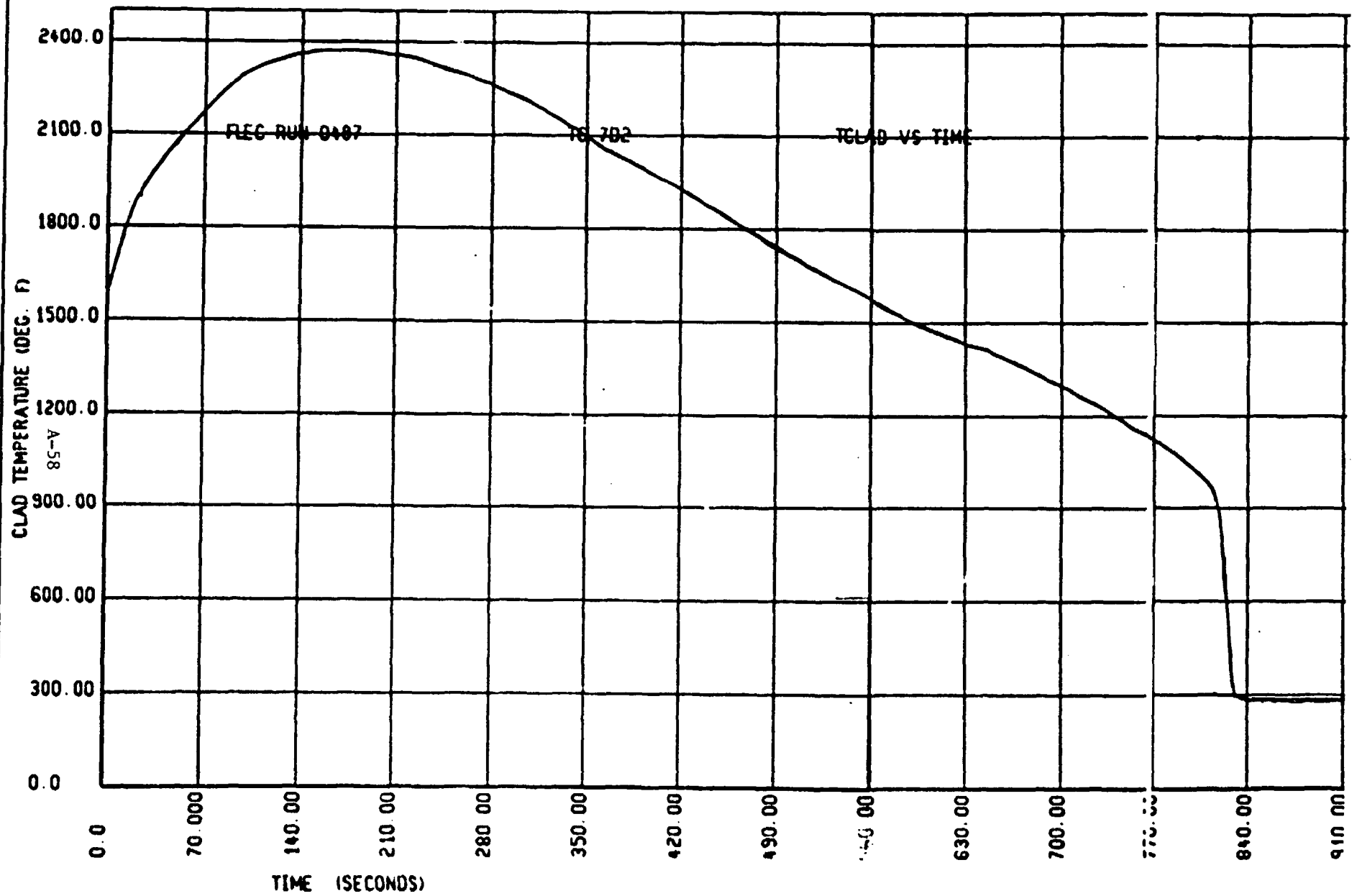
FLECHT RUN SUMMARY SHEET

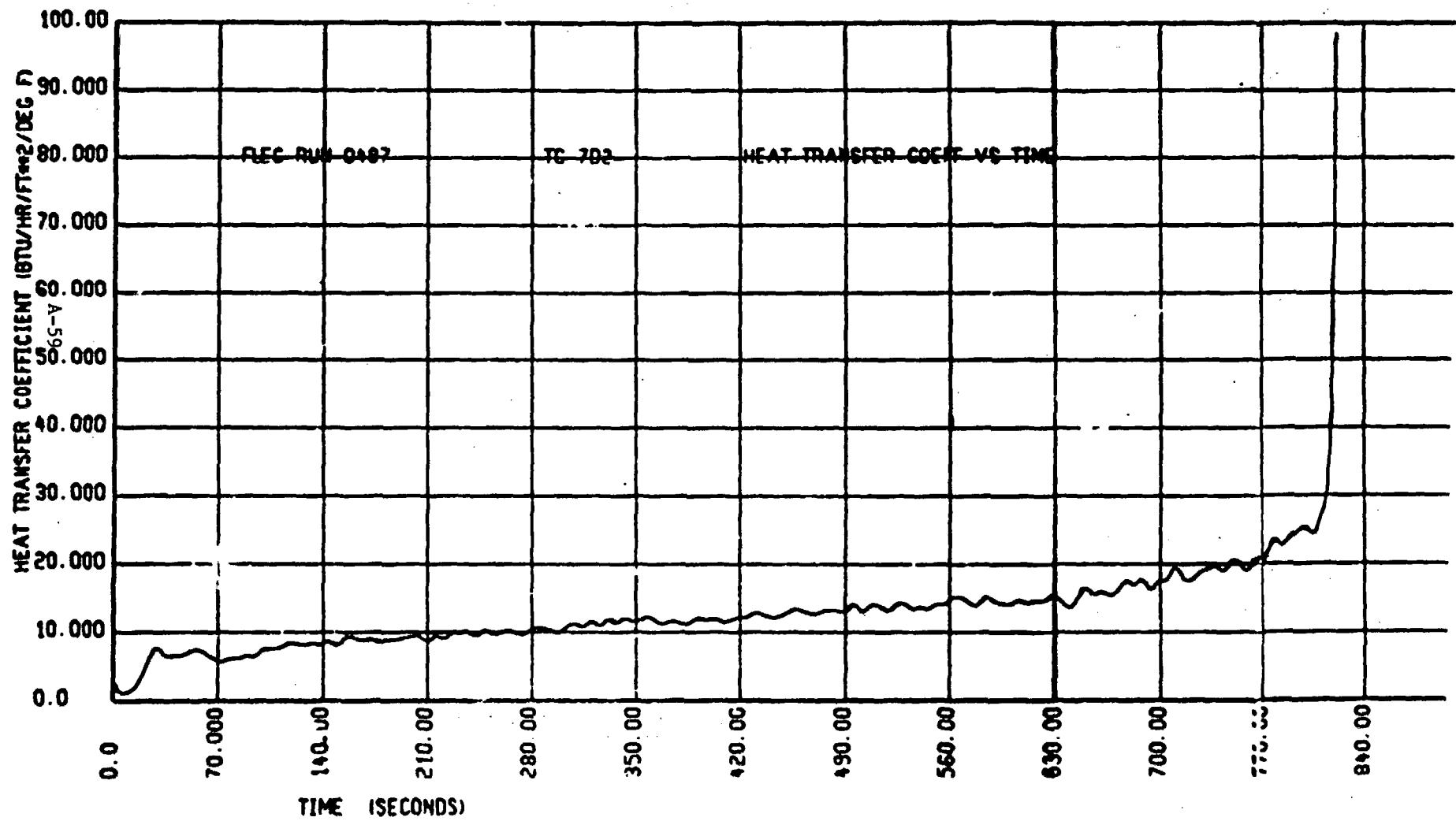
RUN NO. 0487

C. HEATER THERMOCOUPLE DATA

T/C No.	Elevation	Initial Temp. (°F)	Max. Temp. (°F)	Temp. Rise (°F)	Turnaround Time (Sec.)	Quench Temp. (°F)	Quench Time (sec)
5G1	6'	1595	2335	740	161	912	802
5G3	4'	1426	1782	356	64	820	352
5G5	10'	955	1702	747	258	626	1366
5G6	8'	1376	2197	821	216	746	1190
5F1	6'	1591	2371	780	177	893	767
5F6	8'	1401	2263	862	231	831	1196
7G3	6'	1513	2248	735	163	761	809
6G3	6'	1577	2311	734	159	885	815
5E3	6'	1554	2333	779	174	889	780
4F2	6'	1566	2314	748	178	903	791
3F2	6'	1515	2228	713	177	902	734
1F2	6'	1451	1818	367	107	850	824
7D2	6'	1582	2374	792	153	893	819
5E2	8'	1370	2282	912	253	721	1212
5E4	4'	1369	1729	360	63	783	352
5E5	2'	944	1034	90	15	715	104
5E1	10'	930	1755	825	279	621	1380
6G5	2'	943	1039	96	16	707	106

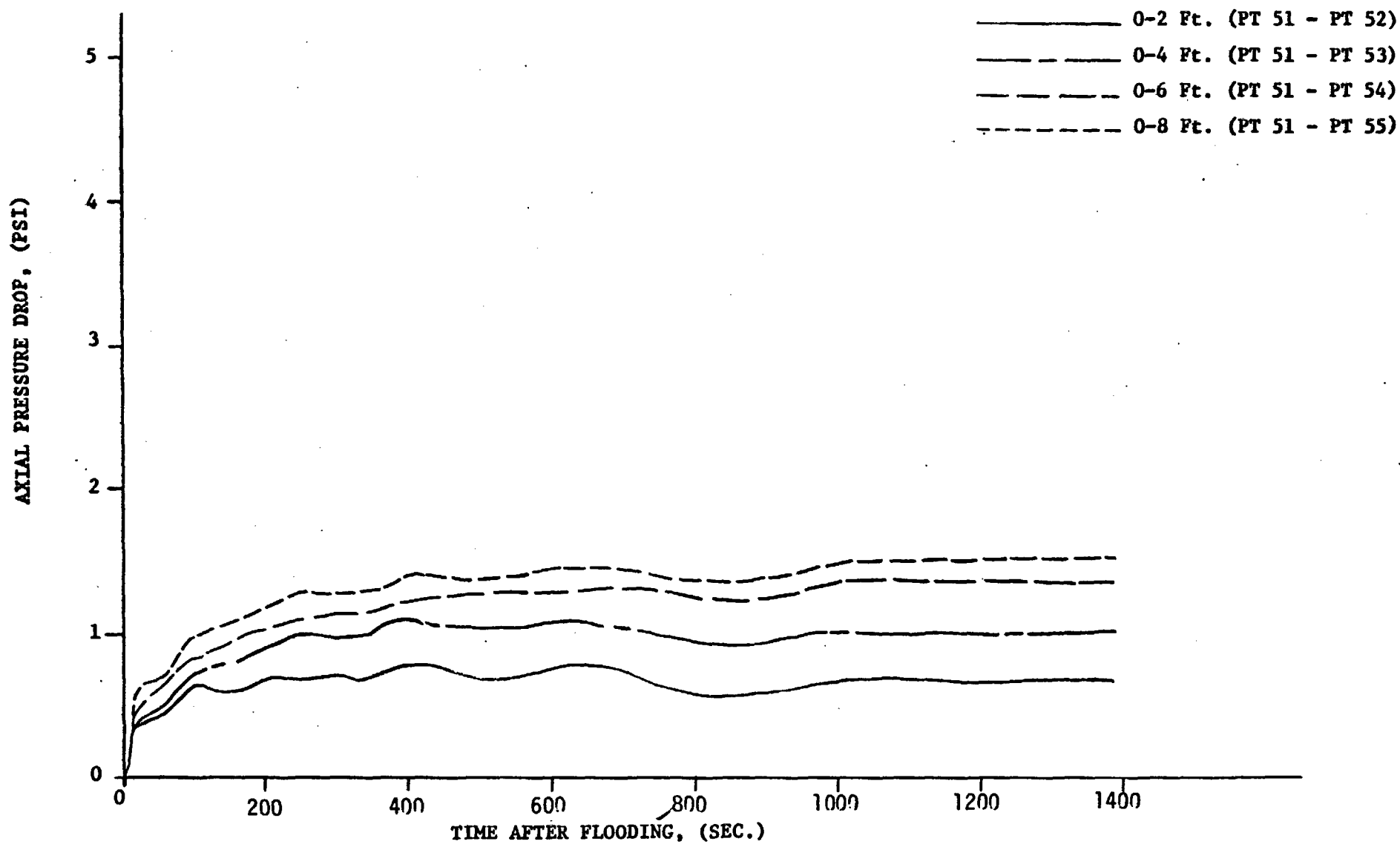
A-57





Run 0487
PRESSURE DROP VS. TIME.

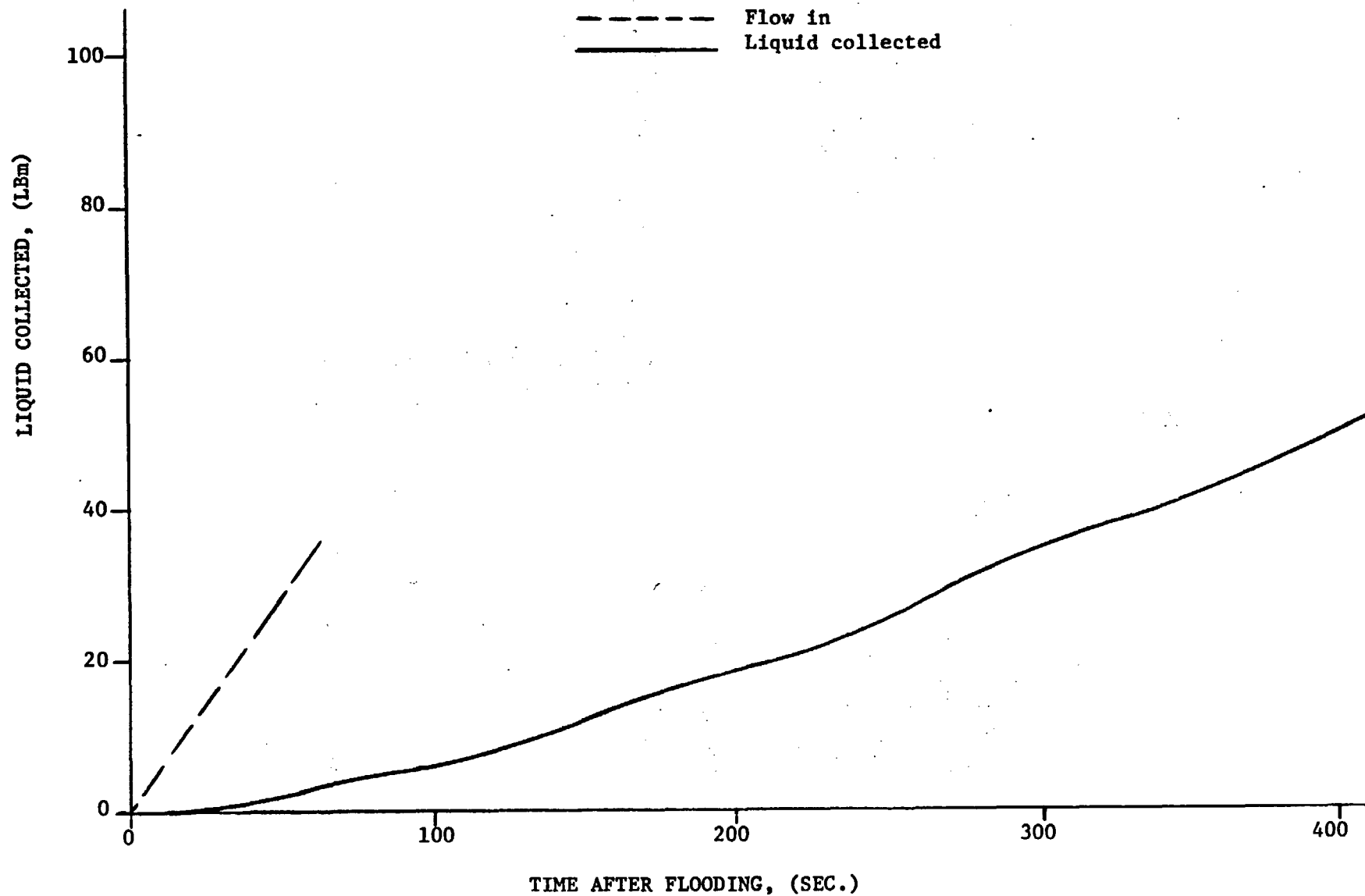
A-60



Run 0487

ENTRAINED LIQUID COLLECTED

NOTE: Liquid Collected Not Necessarily Total Liquid Carryover



A-61

FLECHT RUN SUMMARY SHEET

RUN NO. 0588

DATE 12/29/71

A. RUN CONDITIONS

Bundle Size	10 x 10 - SS
Initial Clad Temperature	1574 °F
Flooding Rate	0.6 in/sec
Peak Power	1.0 kw/ft
Decay Power	Curve D Figure 2-3
Inlet Coolant Temperature	188 °F
Pressure	15 psia

B. HOUSING TEMPERATURES

Elevation (ft)	Initial Temperature (°F)	Temperature at Quench Time of Hot Rod Midplane (_____Sec) *
2	443	
4	523	
6	680	
8	657	
10	472	

Initial T_{avg} Actual 509 °F

*Power off at 134 sec. after flood.

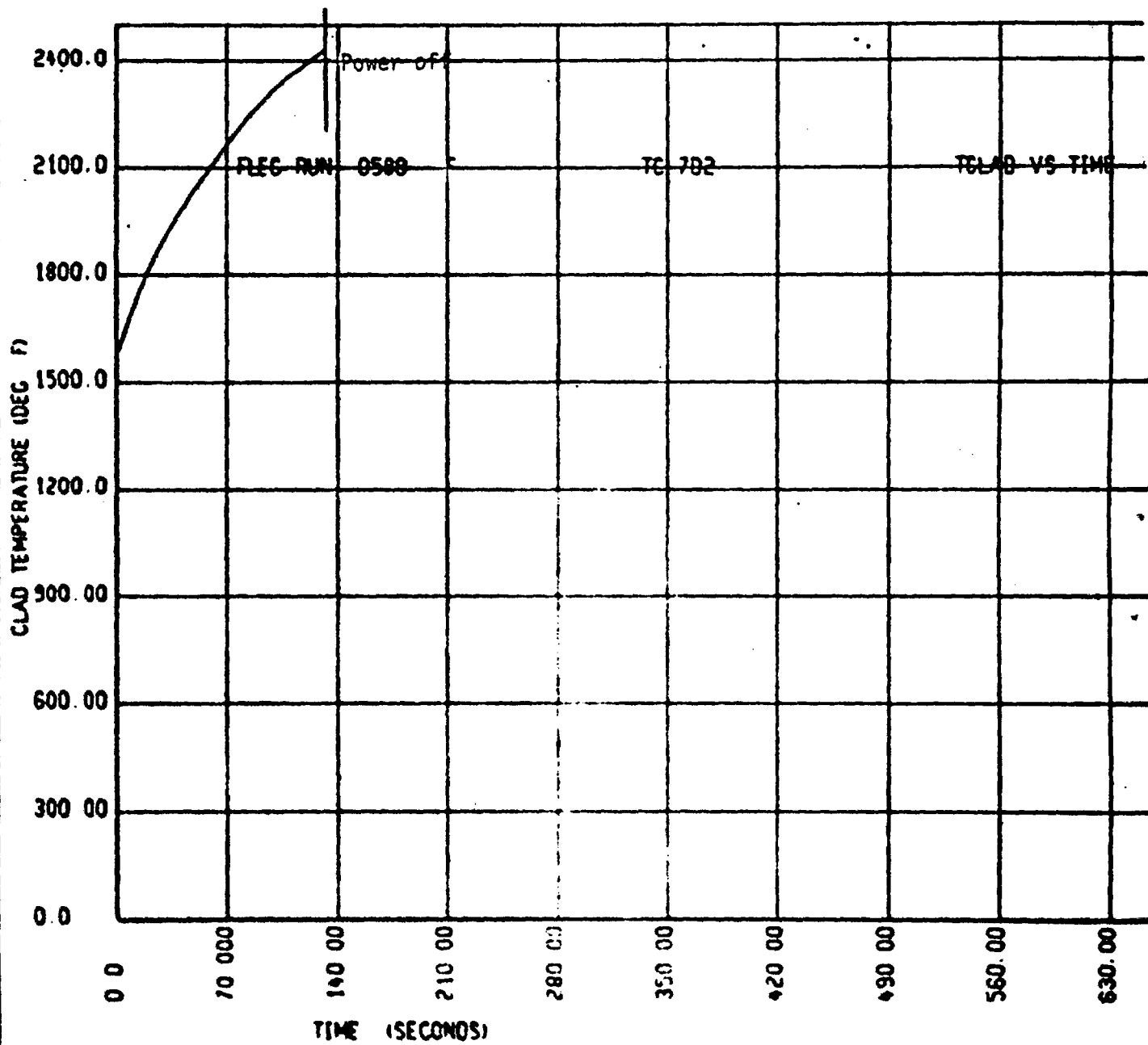
FLECHT RUN SUMMARY SHEET

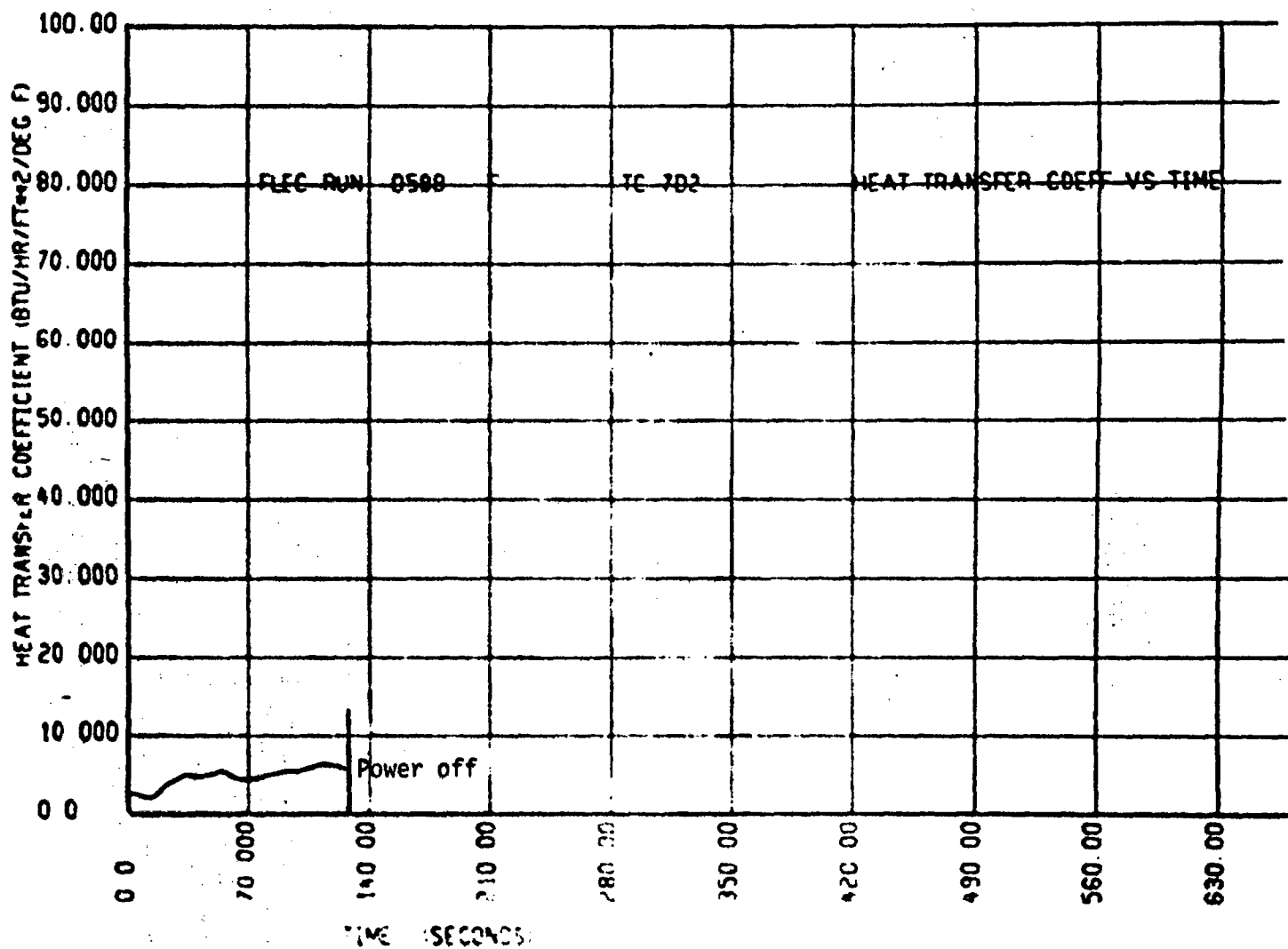
RUN NO. 0588

C. HEATER THERMOCOUPLE DATA

T/C No.	Elevation	Initial Temp. (°F)	Max. Temp. (°F)	Temp. Rise (°F)	Turnaround * Time (Sec.)	Quench Temp. (°F)	Quench Time (sec)
5G1	6'	1596	2378	782	134	--	--
5G3	4'	1412	1750	338	134	--	--
5G5	10'	1016	1600	584	134	--	---
5G6	8'	1425	2215	790	134	--	--
5F1	6'	1596	2404	808	134	--	--
5F6	8'	1445	2218	773	134	--	--
7G3	6'	1494	2282	788	134	--	--
6G3	6'	1565	2357	792	134	--	--
5E3	6'	1532	2382	850	134	--	--
4F2	6'	1547	2352	805	134	--	--
3F2	6'	1484	2256	772	134	--	--
1F2	6'	1485	1853	368	134	--	--
7D2	6'	1574	2431	857	134	--	--
5F2	8'	1380	2214	834	134	--	--
5E4	4'	1318	1685	367	134	--	--
5E5	2'	936	1014	78	19	680	126
5E1	10'	973	1638	665	134		
6G5	2'	945	1019	74	17	581	1335

*NOTE: 134 sec is power scram. Thus 134 indicates no turnaround.

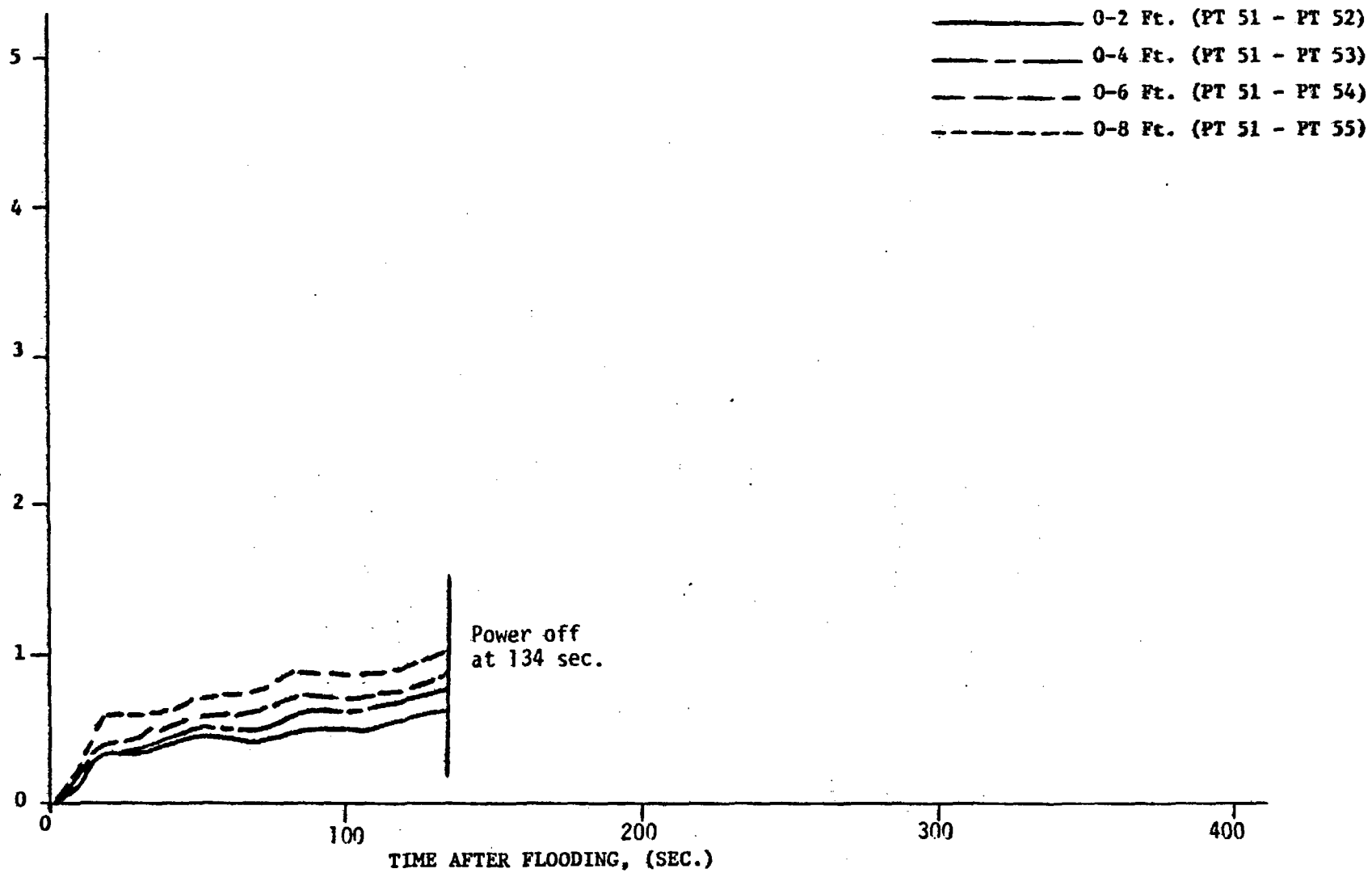




Run 0588
PRESSURE DROP VS. TIME.

99-V

AXIAL PRESSURE DROP, (PSI)

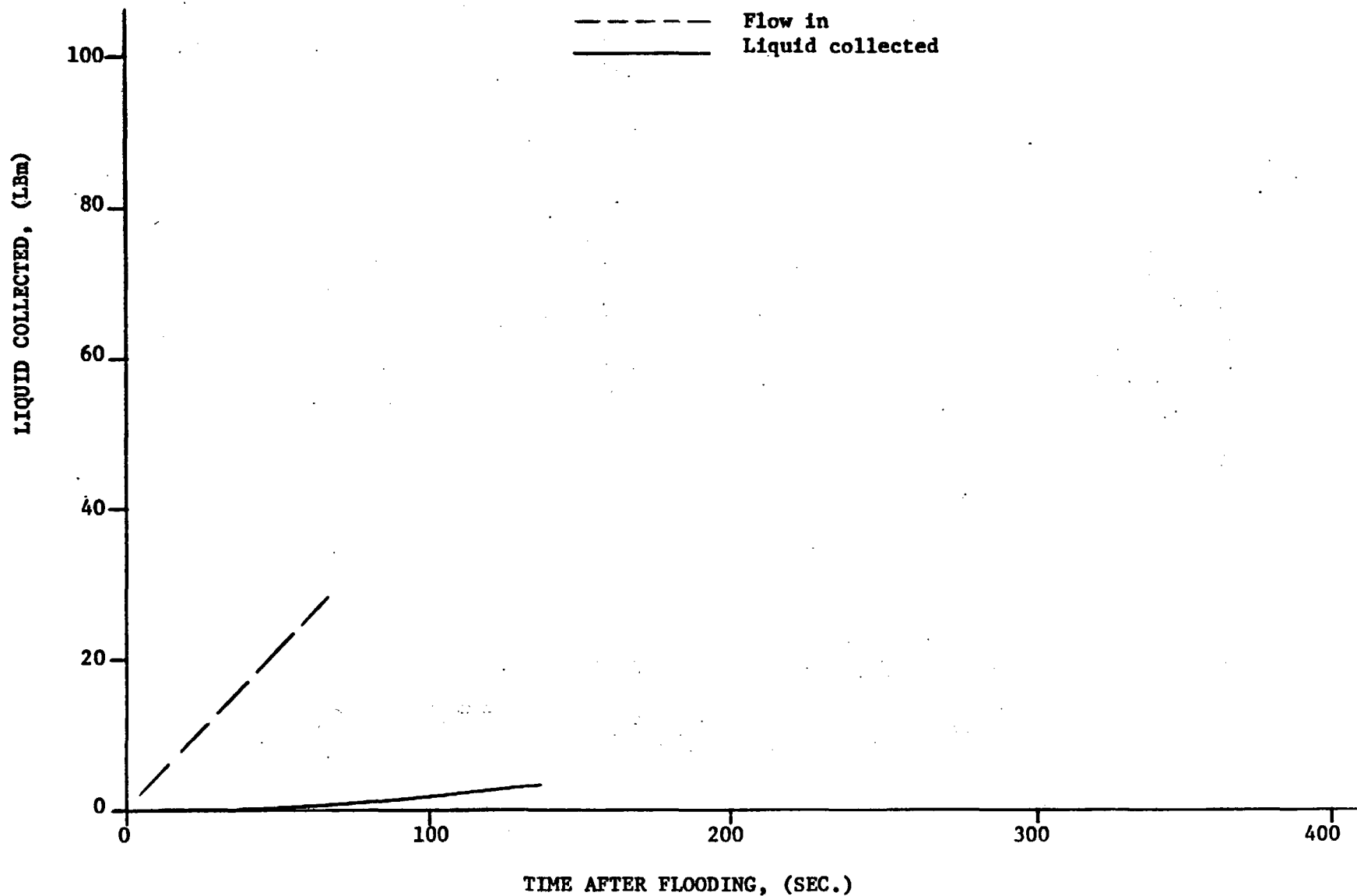


Run 0588

ENTRAINED LIQUID COLLECTED

NOTE: Liquid Collected Not Necessarily Total Liquid Carryover

A-67



FLECHT RUN SUMMARY SHEET

RUN NO. 0690

DATE 12/30/71

A. RUN CONDITIONS

Bundle Size	10 x 10 - SS
Initial Clad Temperature	1531 °F
Flooding Rate	0.6 in/sec
Peak Power	0.69 kw/ft
Decay Power	Curve D Figure 2-3
Inlet Coolant Temperature	190 °F
Pressure	15 psia

B. HOUSING TEMPERATURES

Elevation (ft)	Initial Temperature (°F)	Temperature at Quench Time of Hot Rod Midplane (713 Sec)
2	384	215
4	517	213
6	621	787
8	558	804
10	390	213

Initial T_{avg} Actual 468 °F

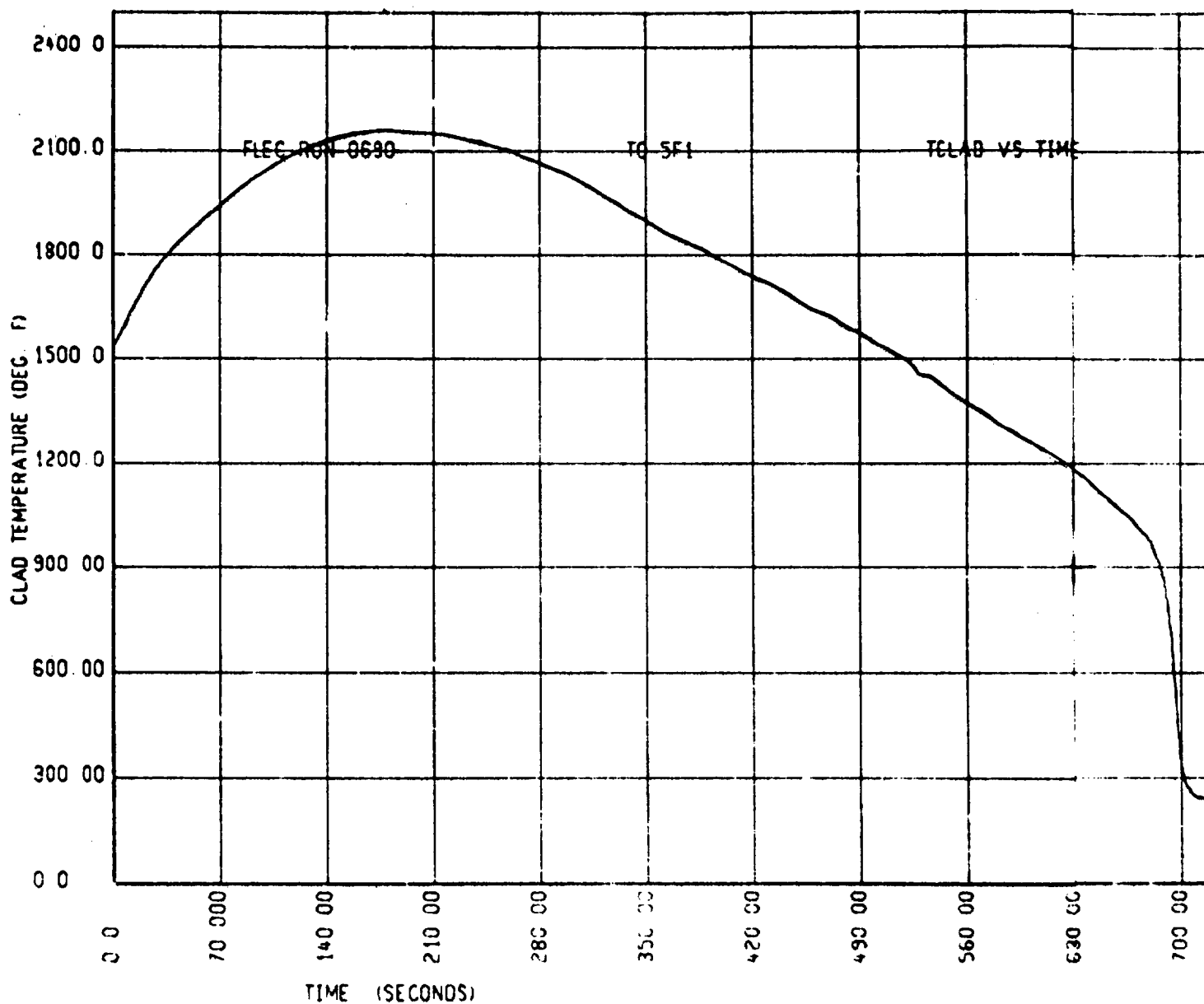
FLECHT RUN SUMMARY SHEET

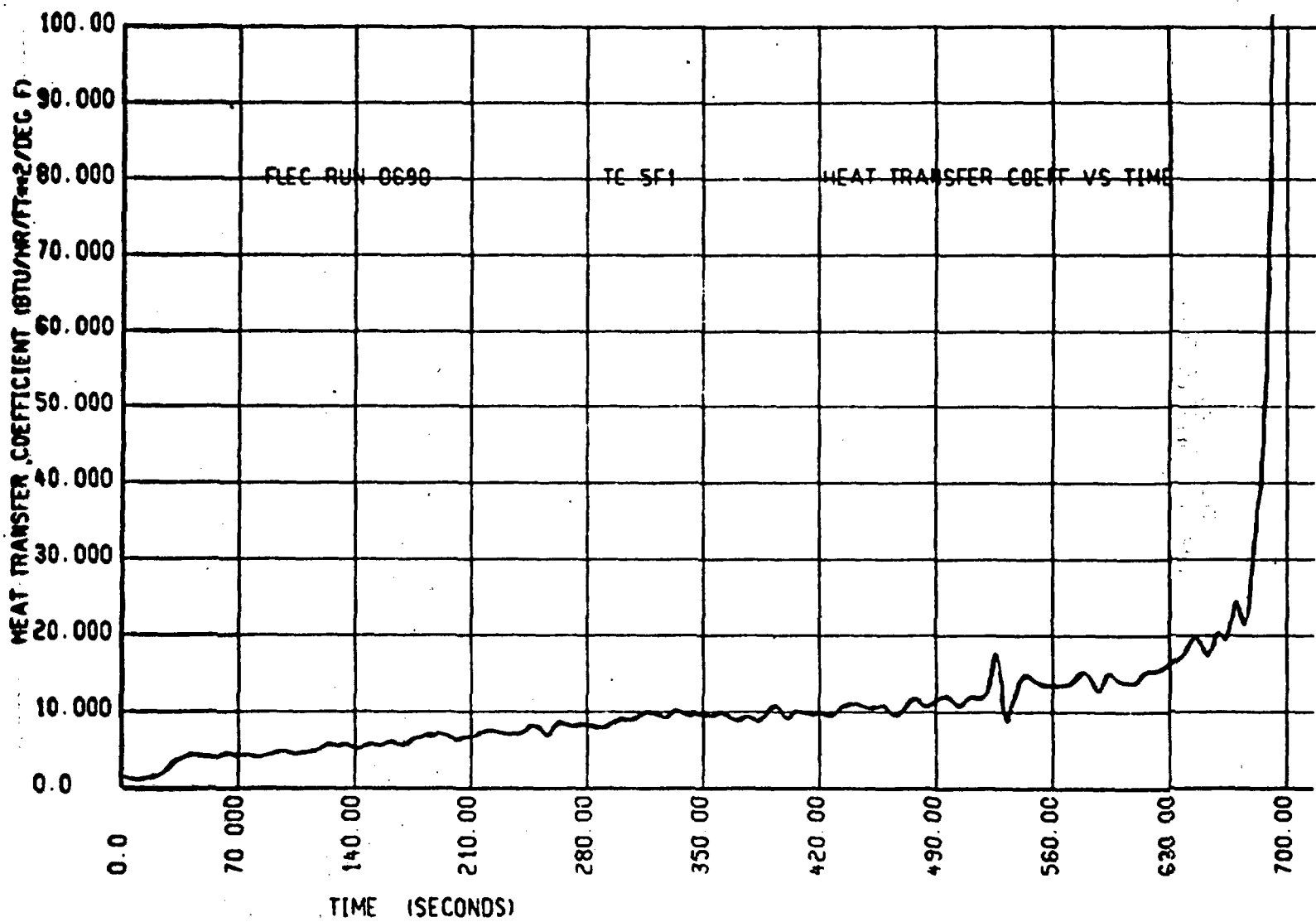
RUN NO. 0690

C. HEATER THERMOCOUPLE DATA

A-69

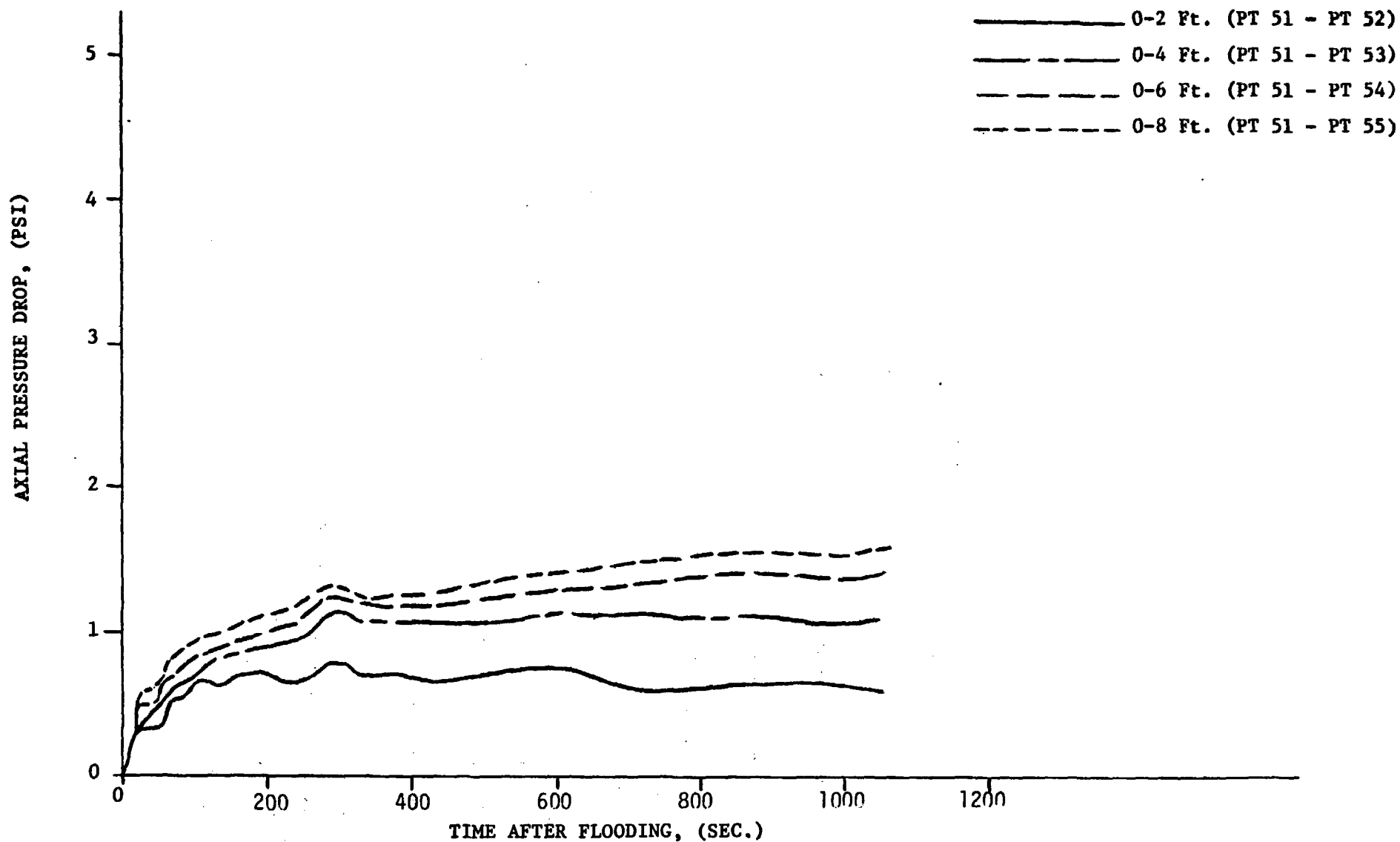
T/C No.	Elevation	Initial Temp. (°F)	Max. Temp. (°F)	Temp. Rise (°F)	Turnaround Time (Sec.)	Quench Temp. (°F)	Quench Time (sec)
5G1	6'	1573	2119	596	173	702	692
5G3	4'	1365	1616	251	91	771	351
5G5	10'	929	1500	571	220	--	--
5G6	8'	1340	1979	639	223	701	1030
5F1	6'	1531	2160	629	200	698	713
5F6	8'	1352	2049	697	232	740	1050
7G3	6'	1439	2046	607	194	689	721
6G3	6'	1493	2105	612	207	667	725
5E3	6'	1486	2147	661	182	778	681
4F2	6'	1493	2123	630	182	692	692
3F2	6'	1432	2024	592	192	613	696
1F2	6'	1412	1638	226	75	671	731
7D2	6'	1514	2144	630	171	816	709
5E2	8'	1302	2065	763	233	705	1058
5E4	4'	1281	1550	269	96	670	361
5E5	2'	869	953	83	46	638	128
5E1	10'	894	1622	728	433	--	--
6G5	2'	876	955	79	43	630	130





Run 0690
PRESSURE DROP VS. TIME.

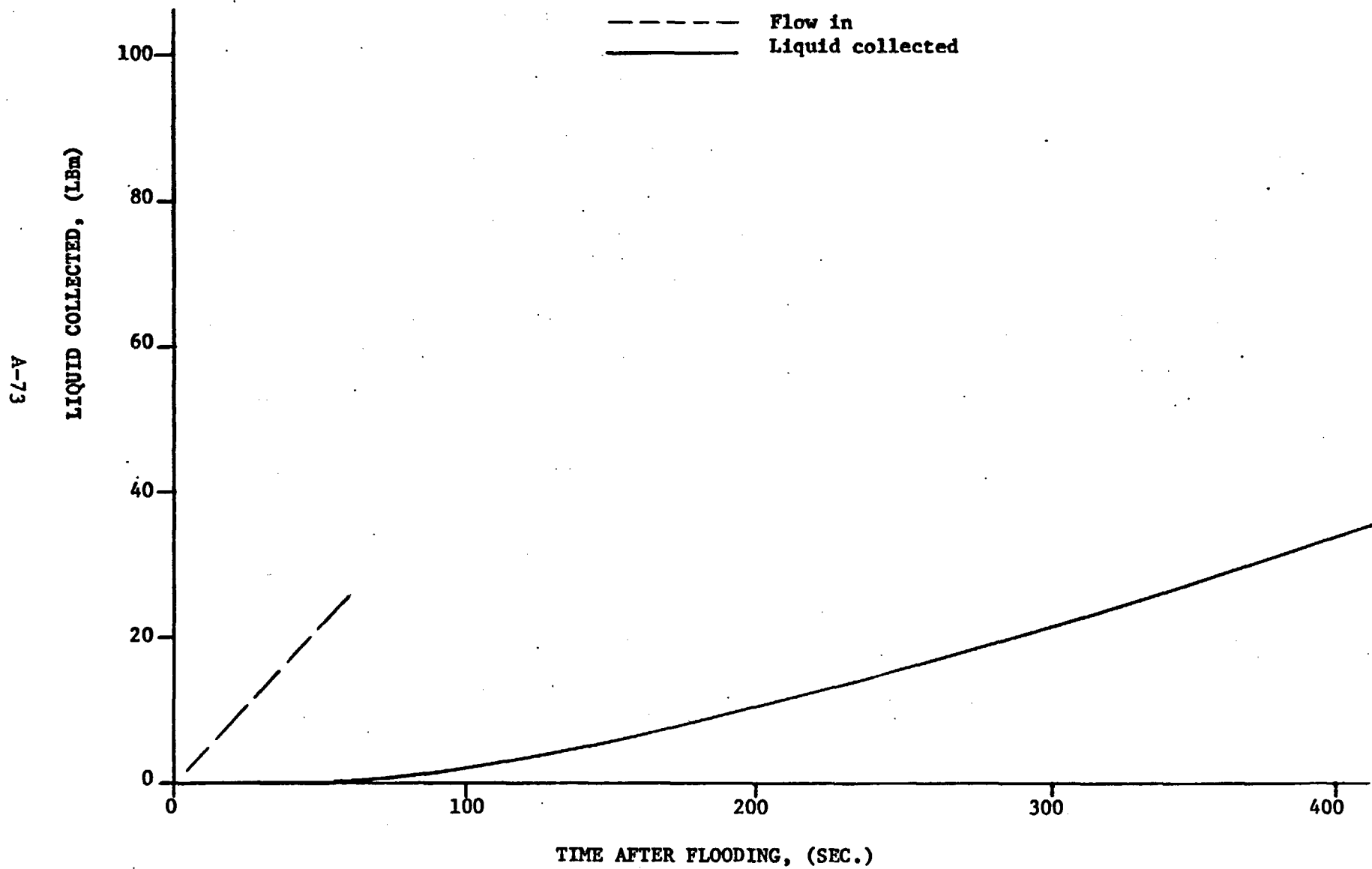
A-72



Run 0690

ENTRAINED LIQUID COLLECTED

NOTE: Liquid Collected Not Necessarily Total Liquid Carryover



FLECHT RUN SUMMARY SHEET

RUN NO. 0791

DATE 12/30/71

A. RUN CONDITIONS

Bundle Size	10 x 10 - SS
Initial Clad Temperature	1593 °F
Flooding Rate	0.4 in/sec
Peak Power	0.69 kw/ft
Decay Power	Curve D Figure 2-3
Inlet Coolant Temperature	188 °F
Pressure	15 psia

B. HOUSING TEMPERATURES

Elevation (ft)	Initial Temperature (°F)	Temperature at Quench Time of Hot Rod Midplane (<u>931</u> Sec)
2	410	214
4	533	213
6	654	887
8	655	1175
10	453	405

Initial T_{avg} Actual 492 °F

FLECHT RUN SUMMARY SHEET

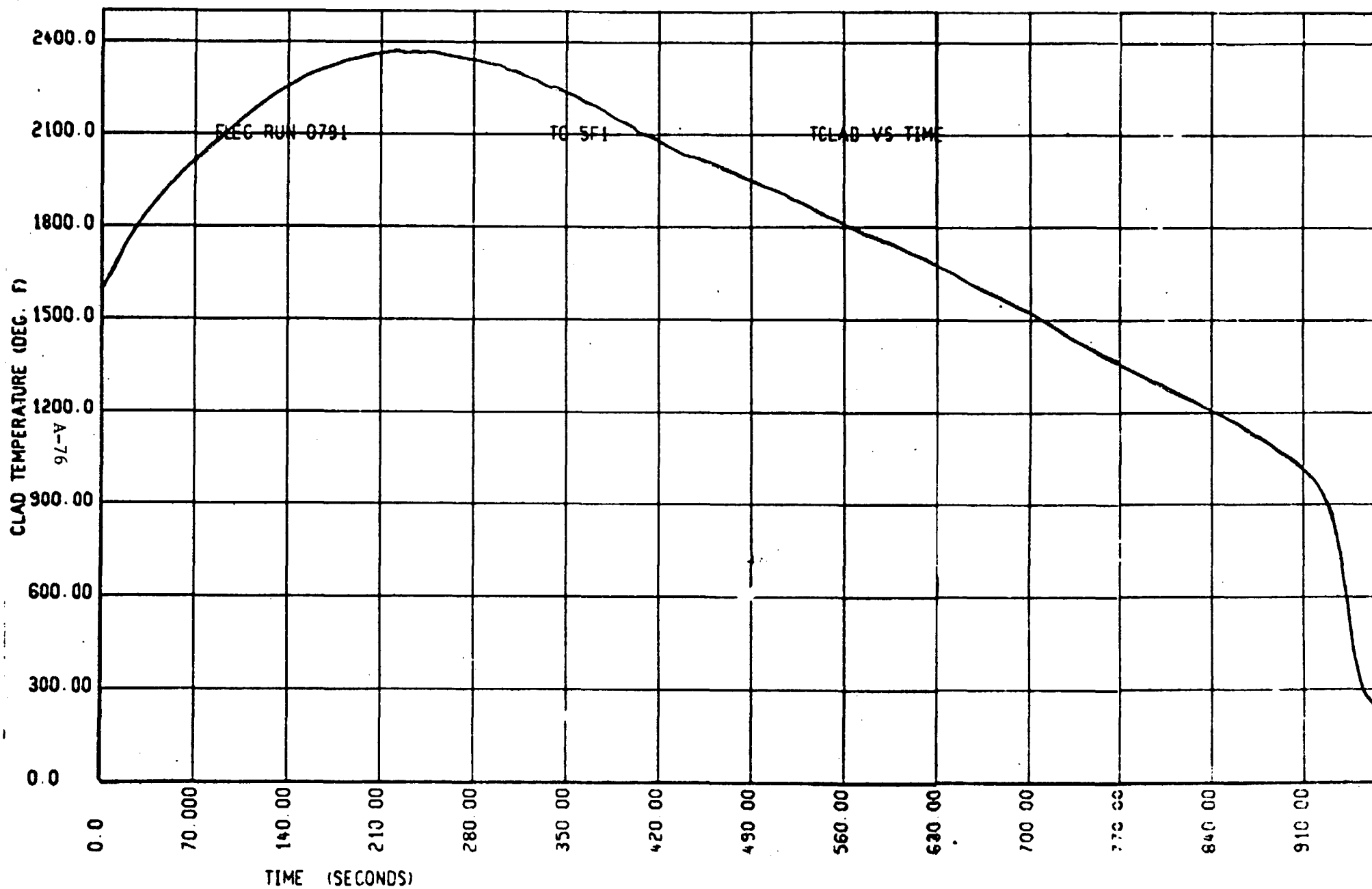
RUN NO. 0791

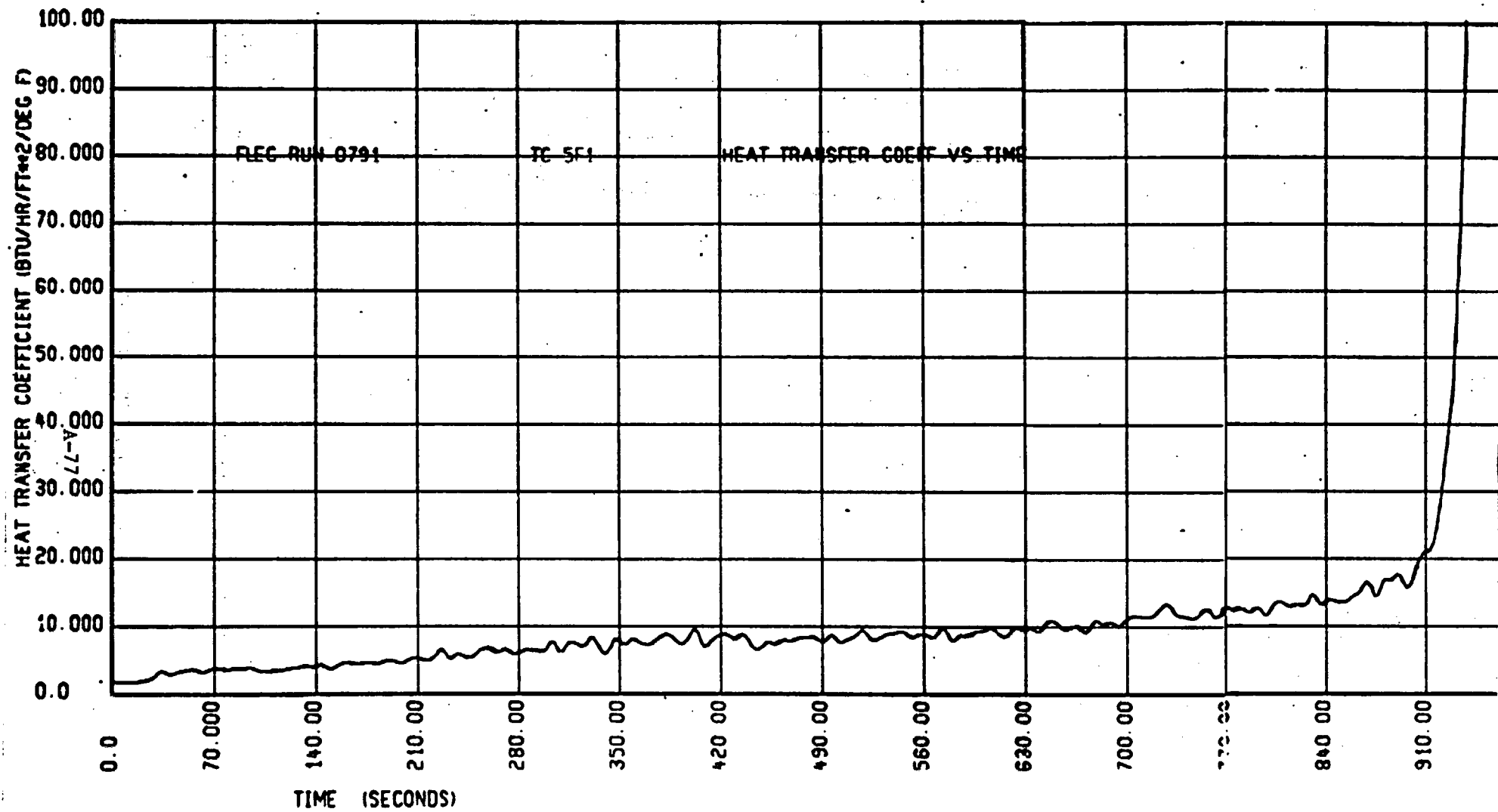
C. HEATER THERMOCOUPLE DATA

T/C No.	Elevation	Initial Temp. (°F)	Max. Temp. (°F)	Temp. Rise (°F)	Turnaround Time (Sec.)	Quench Temp. (°F)	Quench Time (sec)
5G1	6'	1583	2326	743	222	834	925
5G3	4'	1420	1720	282	86	785	388
5G5	10'	1002	1896	894	503	--	--
5G6	8'	1421	2225	804	282	--	--
5F1	6'	1593	2368	775	234	827	931
5F6	8'	1442	2315	873	283	--	--
7G3	6'	1489	2244	755	233	806	932
6G3	6'	1544	2316	772	230	798	943
5E3	6'	1547	2352	805	222	842	914
4F2	6'	1549	2319	770	234	736	919
3F2	6'	1486	2224	738	222	781	884
1F2	6'	1448	1722	274	167	733	973
7D2	6'	1570	2321	751	216	685	958
5E2	8'	1394	2347	953	297	--	--
5E4	4'	1339	1650	311	82	590	399
5E5	2'	929	1006	77	28	657	117
5E1	10'	974	1984	1010	519	--	--
6G5	2'	933	1007	74	27	539	125

A-75

Rod Failures: 7E

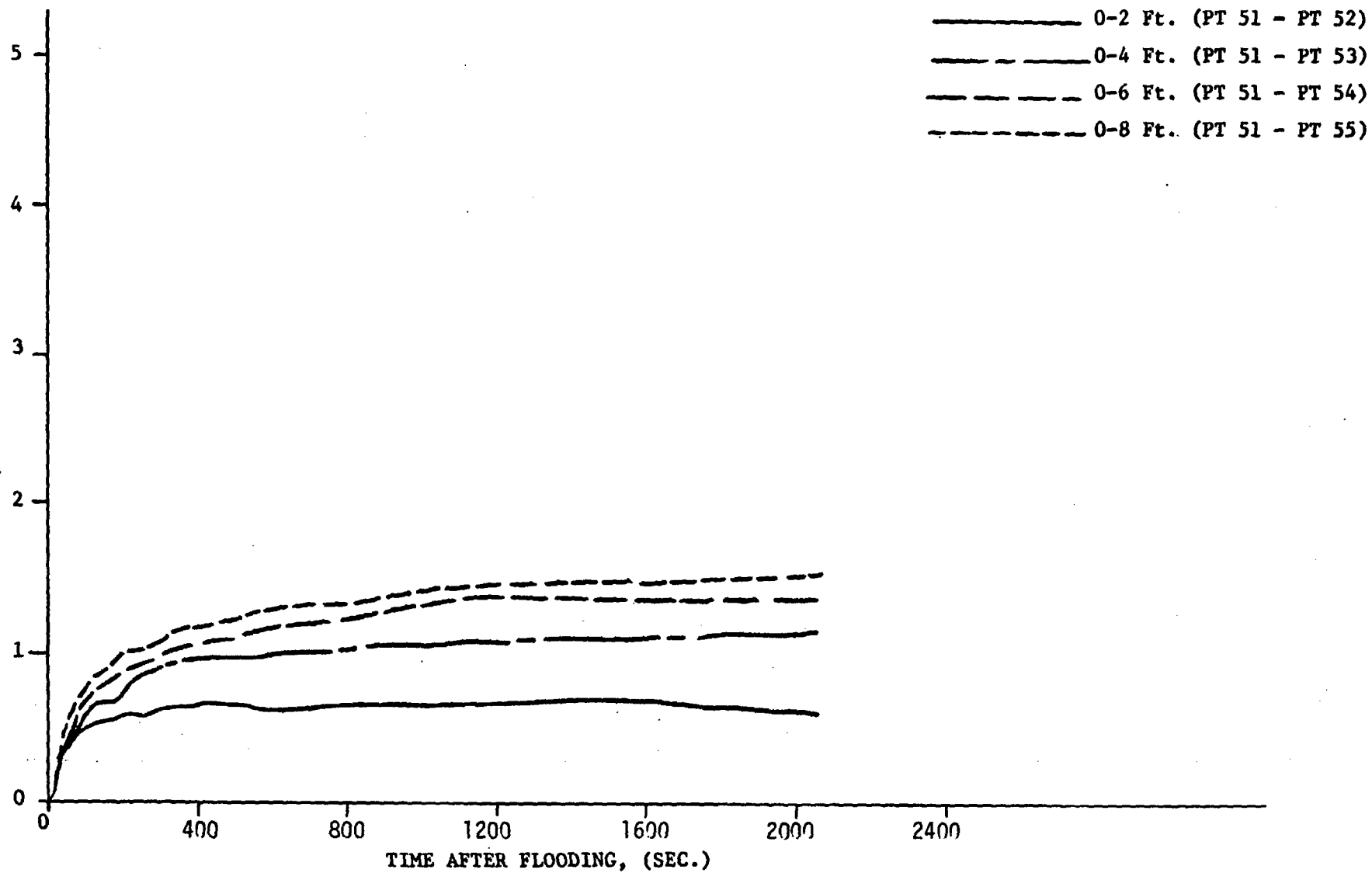




Run 0791
PRESSURE DROP VS. TIME.

A-78

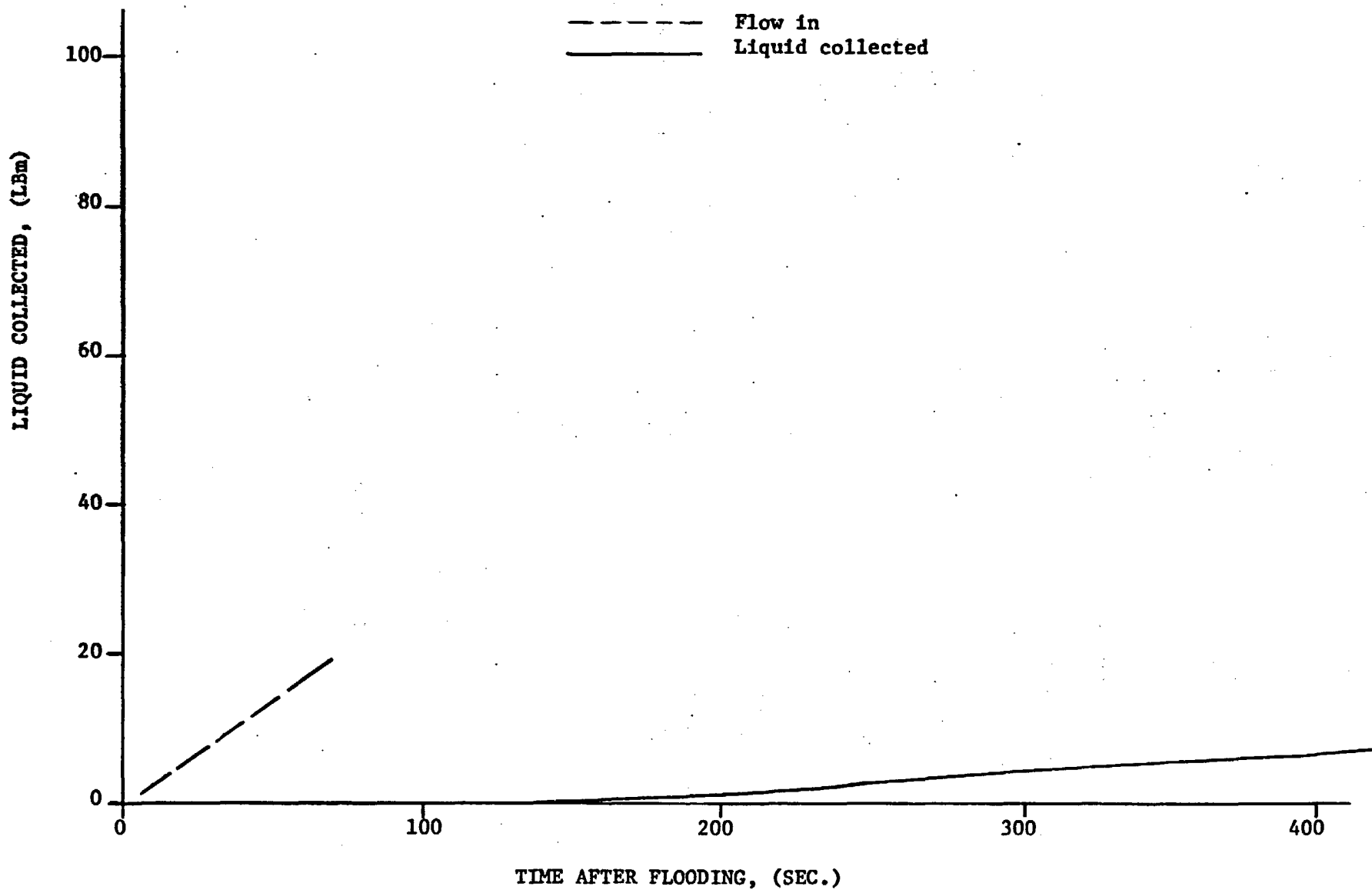
AXIAL PRESSURE DROP, (PSI)



Run 0791

ENTRAINED LIQUID COLLECTED

NOTE: Liquid Collected Not Necessarily Total Liquid Carryover



FLECHT RUN SUMMARY SHEET

RUN NO. 0889

DATE 12/30/71

A. RUN CONDITIONS

Bundle Size	10 x 10 - SS
Initial Clad Temperature	1592 °F
Flooding Rate	0.4 in/sec
Peak Power	1.00 kw/ft
Decay Power	Curve D Figure 2-3
Inlet Coolant Temperature	194 °F
Pressure	15 psia

B. HOUSING TEMPERATURES

Elevation (ft)	Initial Temperature (°F)	Temperature at Quench Time of Hot Rod Midplane (____ Sec)
2	430	*
4	550	
6	701	
8	680	
10	478	
Initial T _{avg} Actual		515 °F

*Power off at 91 sec. after flood.

FLECHT RUN SUMMARY SHEET

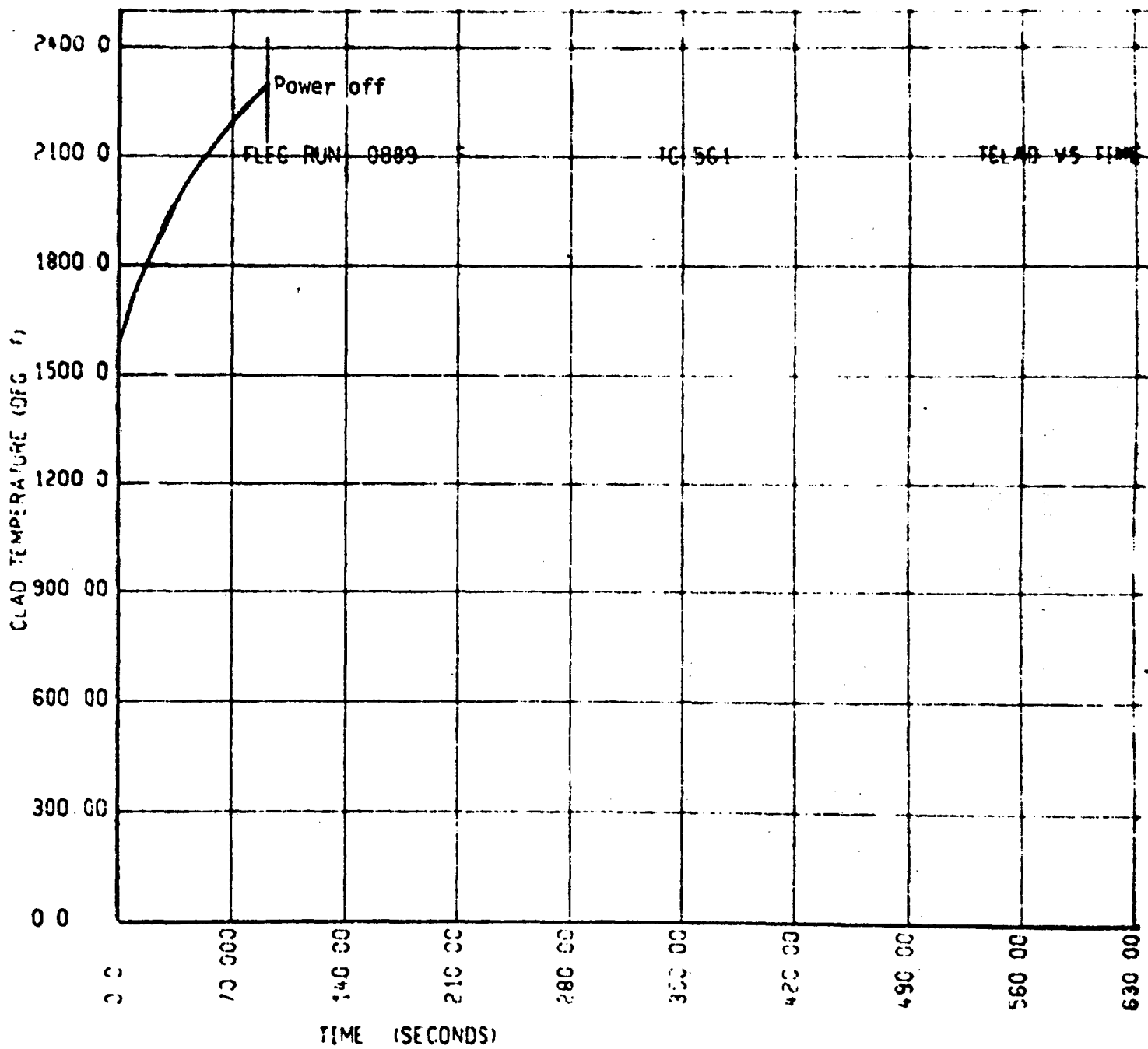
RUN NO. 0889

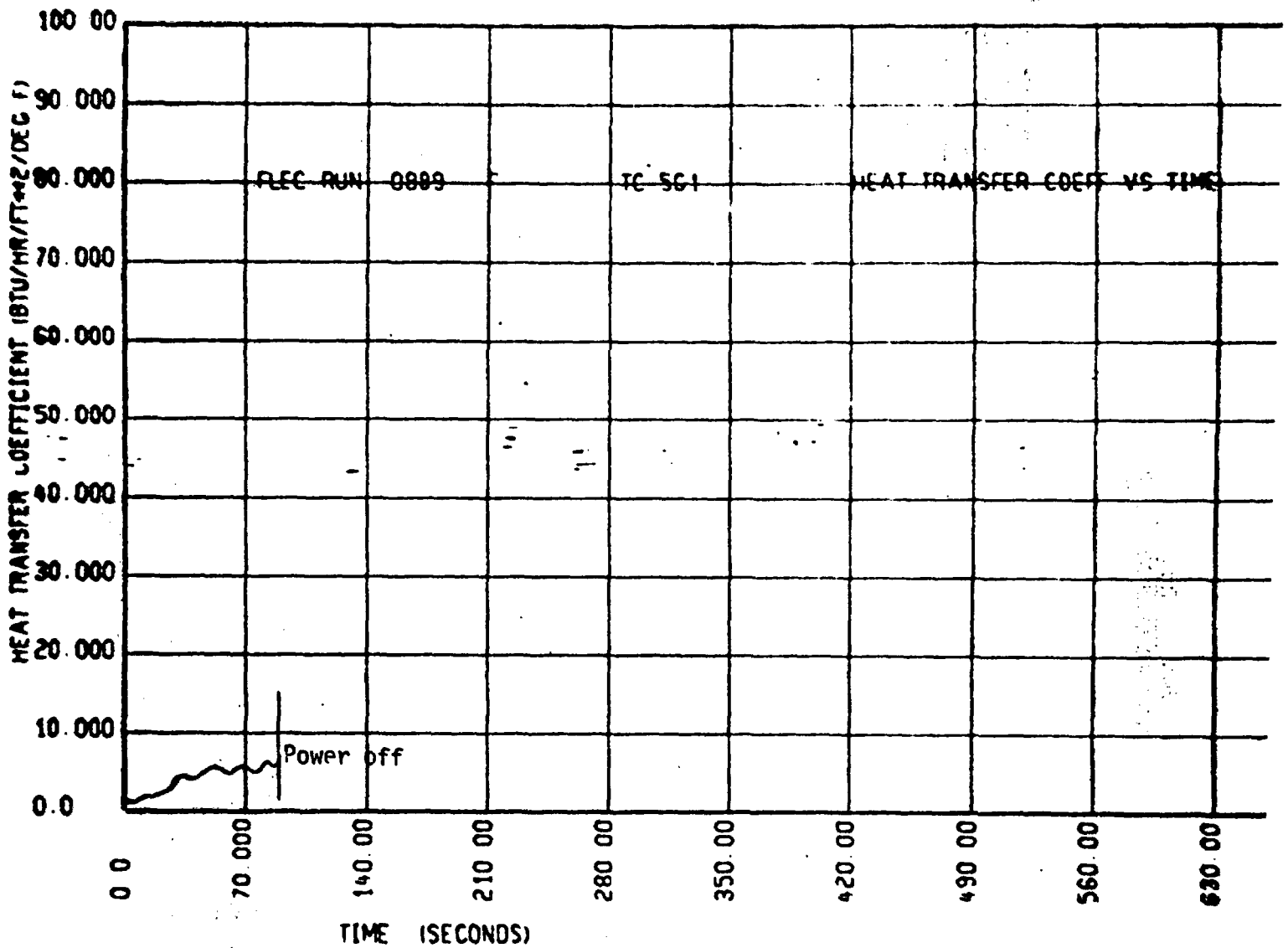
C. HEATER THERMOCOUPLE DATA

T/C No.	Elevation	Initial Temp. (°F)	Max. Temp. (°F)	Temp. Rise (°F)	Turnaround* Time (sec.)	Quench Temp. (°F)	Quench Time (sec.)
5G1	6'	1592	2296	704	91		
5G3	4'	1409	1911	502	91		
5G5	10'	1010	1492	482	91		
5G6	8'	1407	2063	656	91		
5F1	6'	1574	2271	697	91		
5F6	8'	1427	2060	633	91		
7G3	6'	1450	2150	700	91		
6G3	6'	1539	2280	741	91		
5E3	6'	1459	2142	683	91		
4F2	6'	1556	2284	727	91		
3F2	6'	1439	2219	780	91		
1F2	6'	1421	1900	479	91		
7D2	6'	1536	7D Rod failure during test				
5E2	8'	1323	1972	649	91		
5E4	4'	1290	1719	429	91		
5E5	2'						
5E1	10'	943	1433	495	91		
6G5	2'	965	1085	120	27		

*NOTE: 91 sec is power scram
Thus 91 indicates no
turnaround.

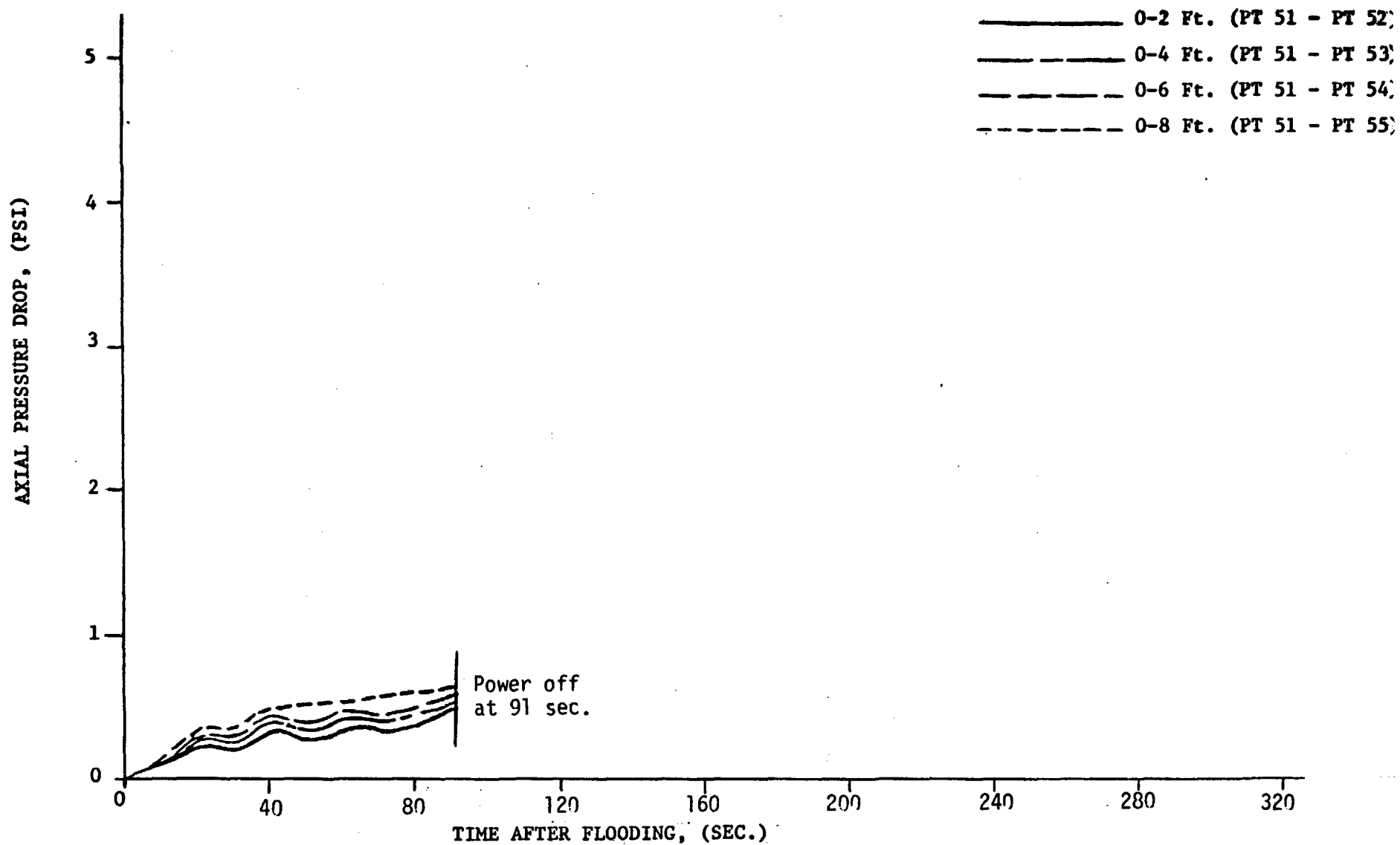
Rod Failures: 7D, 6E; 6D Near Failure.





Run 0889
PRESSURE DROP VS. TIME.

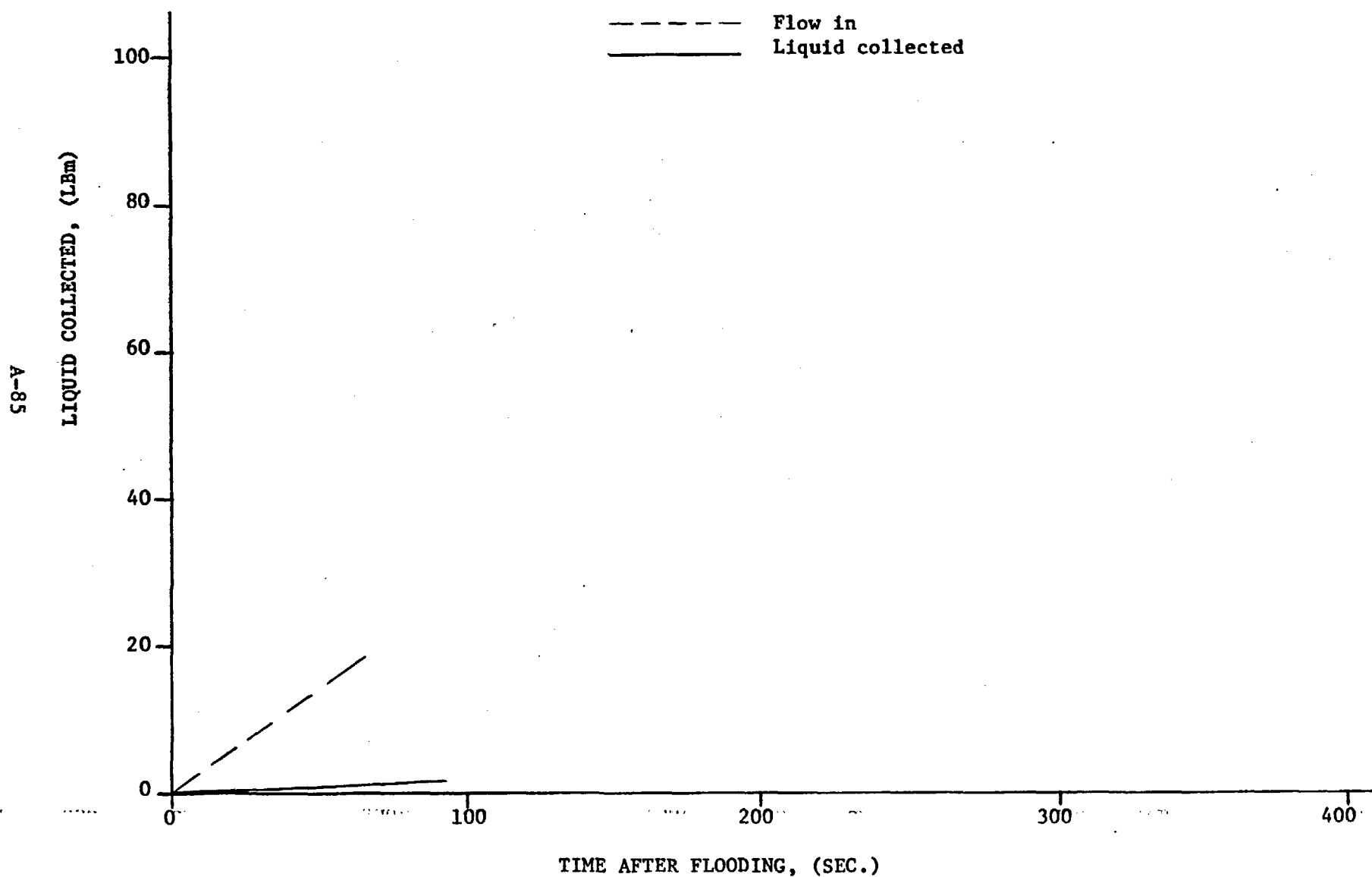
A-84



Run 0889

ENTRAINED LIQUID COLLECTED

NOTE: Liquid Collected Not Necessarily Total Liquid Carryover



FLECHT RUN SUMMARY SHEET

RUN NO. 0984

DATE 1/14/72

A. RUN CONDITIONS

Bundle Size	10 x 10 - SS
Initial Clad Temperature	1530 °F
Flooding Rate	1 in/sec
Peak Power	1.24 kw/ft
Decay Power	Curve B Figure 2-3
Inlet Coolant Temperature	195 °F
Pressure	21 psia

B. HOUSING TEMPERATURES

Elevation (ft)	Initial Temperature (°F)	Temperature at Quench Time of Hot Rod Midplane (<u>576</u> Sec)
2	459	233
4	670	229
6	736	848
8	682	952
10	468	232

Initial T_{avg} Actual 576 °F

FLECHT RUN SUMMARY SHEET

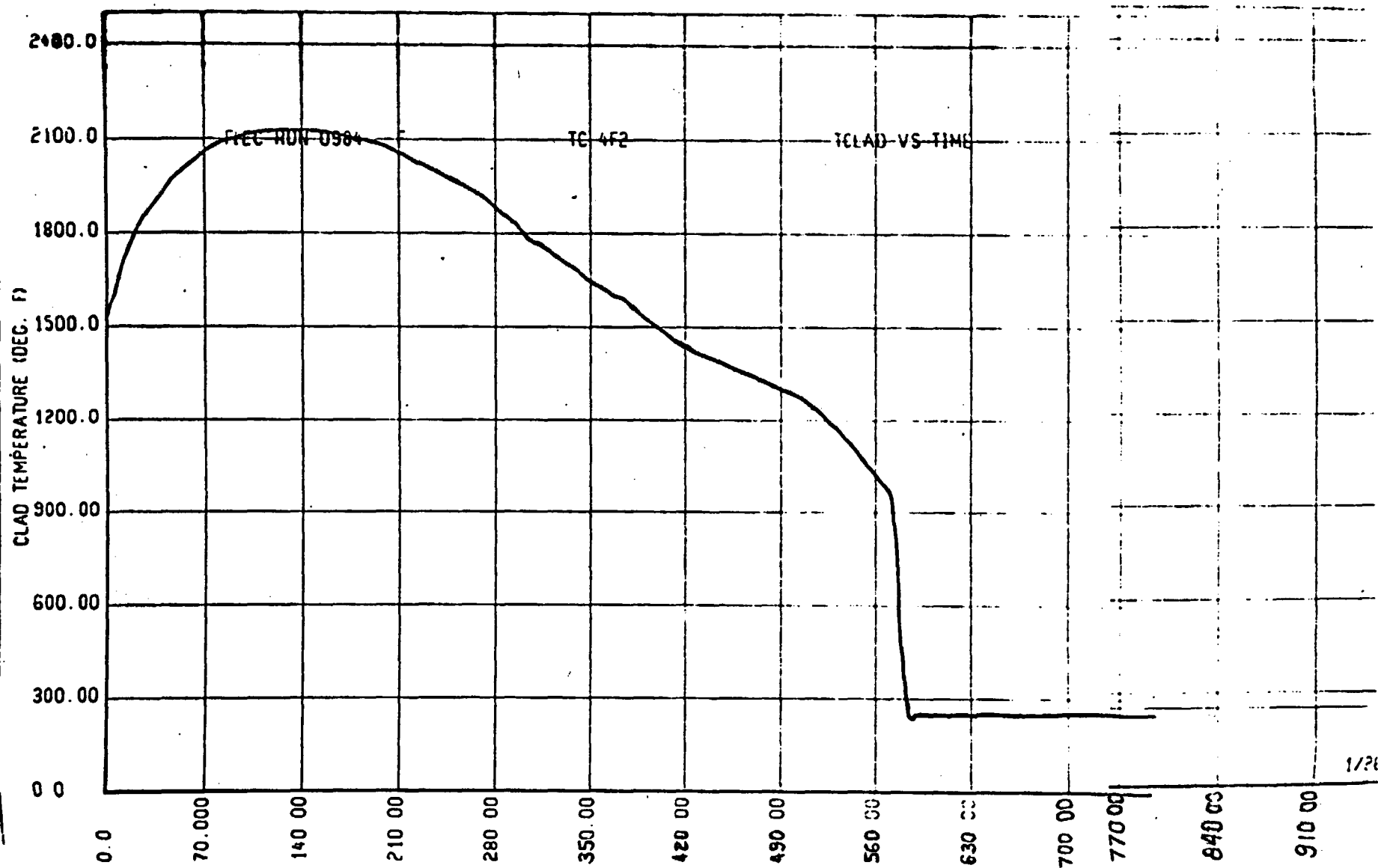
RUN NO. 0984

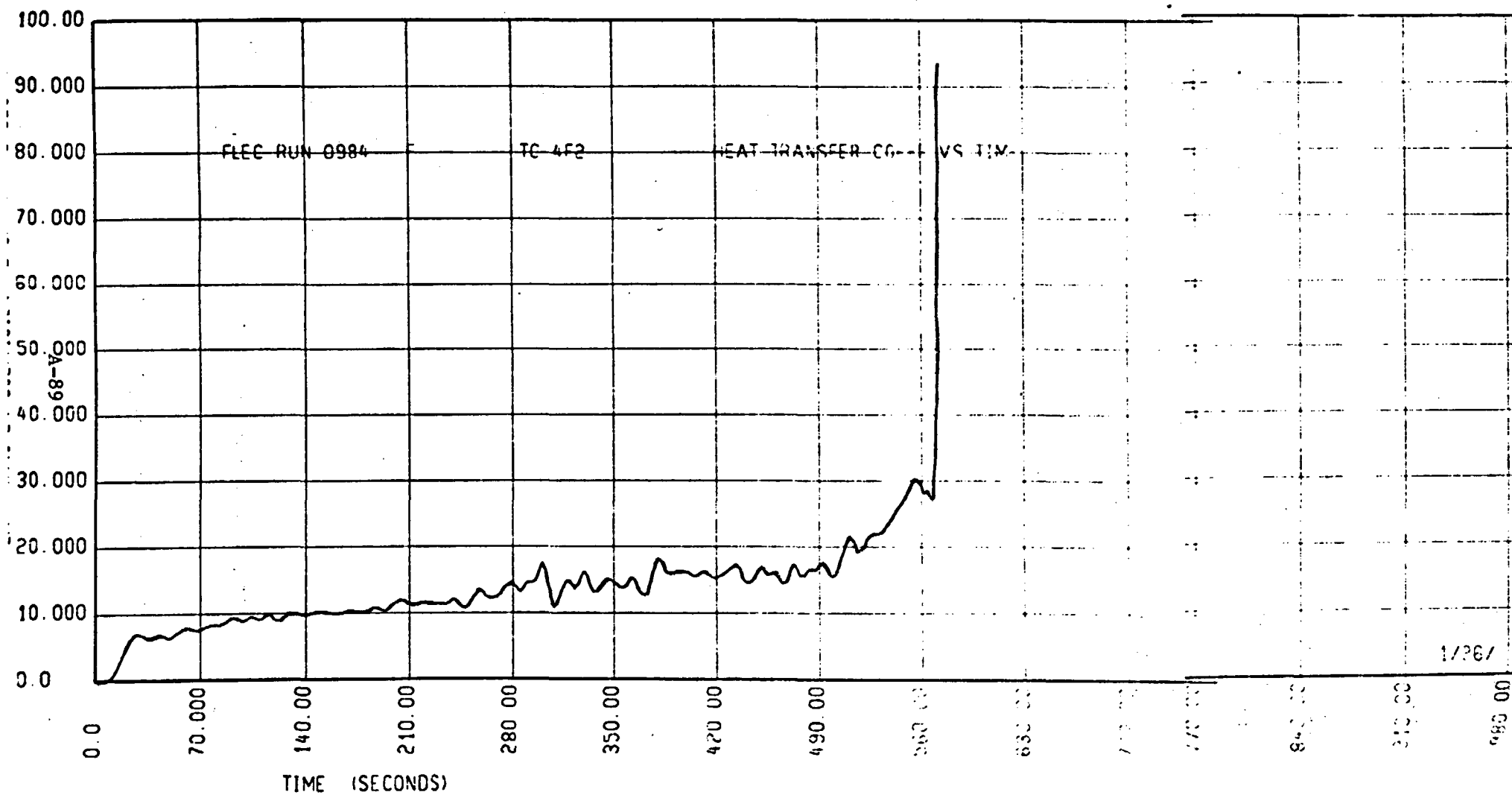
C. HEATER THERMOCOUPLE DATA

T/C No.	Elevation	Initial Temp. (°F)	Max. Temp. (°F)	Temp. Rise (°F)	Turnaround Time (Sec.)	Quench Temp. (°F)	Quench Time (sec)
5G1	6'	1599	2057	458	111	935	581
5G3	4'	1395	1657	262	45	840	282
5G5	10'	929	1415	486	161		
5G6	8'	1370	1946	576	171	823	821
5F1	6'	1567	2053	486	124	835	580
5F6	8'	Bad TC					
7G3	6'	1480	2028	548	120	882	584
6G3	6'	1562	2055	493	119	896	589
5F3	6'	1424	1805	381	104	784	565
4F2	6'	1530	2132	602	126	900	576
3F2	6'	1476	2113	637	126	838	554
1F2	6'	1504	1789	285	55	789	620
7D2	6'	Failed Rod					
5E2	8'	1288	1860	572	219	740	838
5E4	4'	1269	1490	221	45	724	291
5E5	2'	Bad TC					
5E1	10'	870	1496	626	309	638	959
6G5	2'	876	960	84	14	604	88

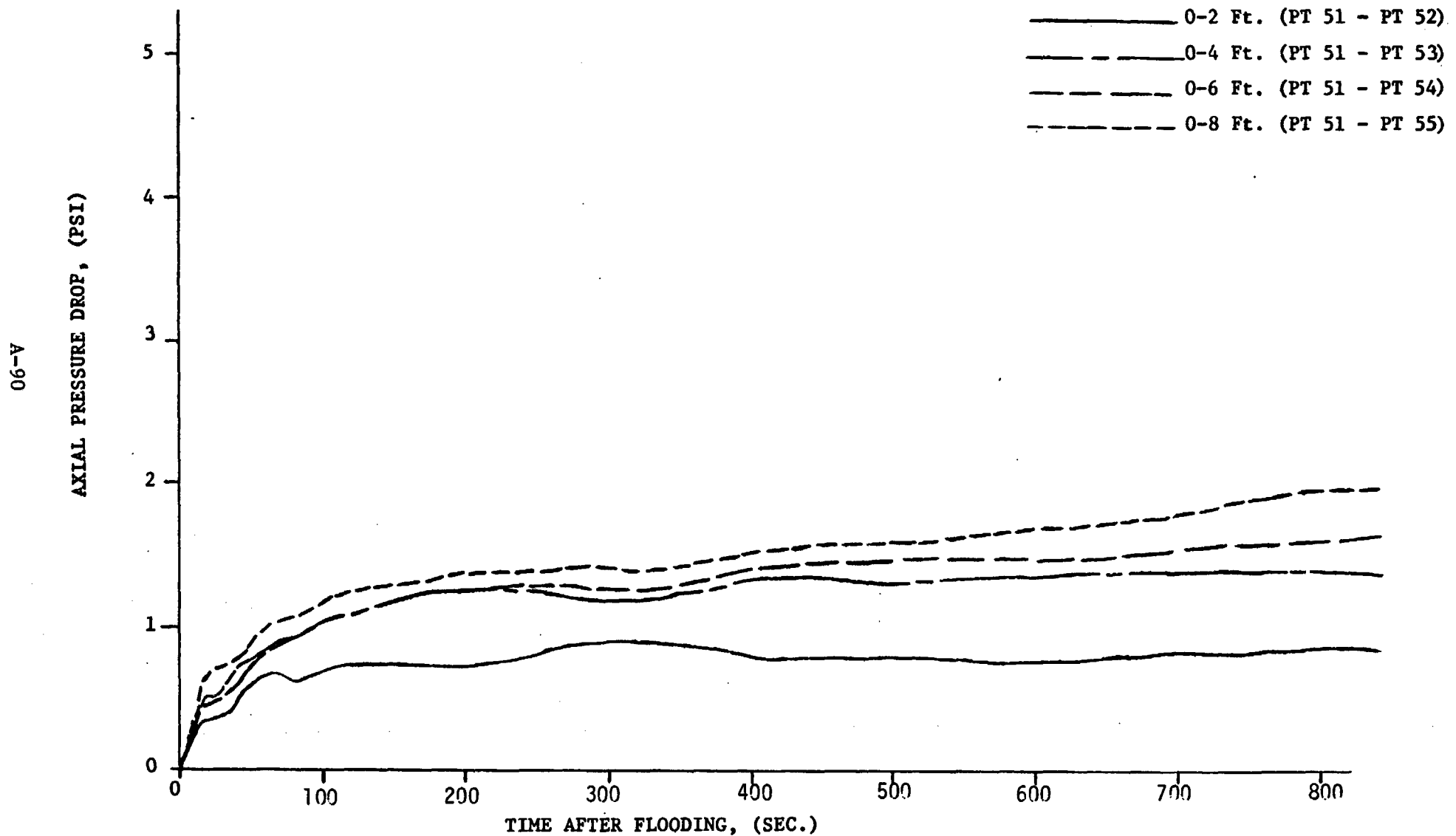
Bundle Includes 3 Failed Rods 7D, 7E, 6E and 6D Disconnected-Near Failure

A-88





Run 0984
PRESSURE DROP VS. TIME.



Run 0984

CARRYOVER DATA NOT VALID DUE
TO INSTRUMENTATION MALFUNCTION

FLECHT RUN SUMMARY SHEET

RUN NO. 1084

DATE 1/17/72

A. RUN CONDITIONS

Bundle Size	10 x 10 - SS
Initial Clad Temperature	1558 °F
Flooding Rate	1 in/sec
Peak Power	1.24 kw/ft
Decay Power	Curve B Figure 2-3
Inlet Coolant Temperature	193 °F
Pressure	21 psia

B. HOUSING TEMPERATURES

Elevation (ft)	Initial Temperature (°F)	Temperature at Quench Time of Hot Rod Midplane (<u>678</u> Sec)
2	653	233
4	868	229
6	1013	1009
8	937	1140
10	586	409

Initial T_{avg} Actual 785 °F

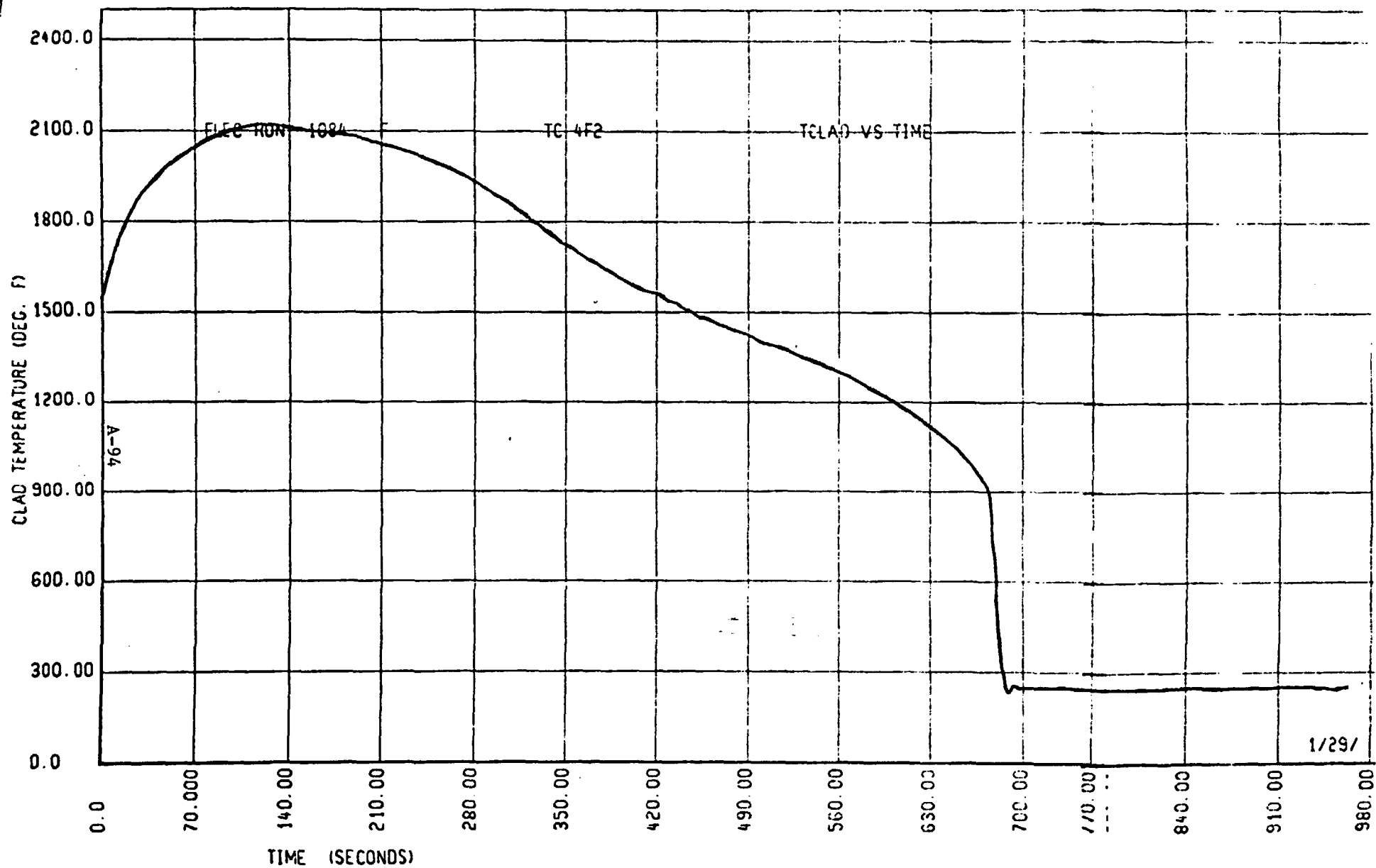
FLECHT RUN SUMMARY SHEET

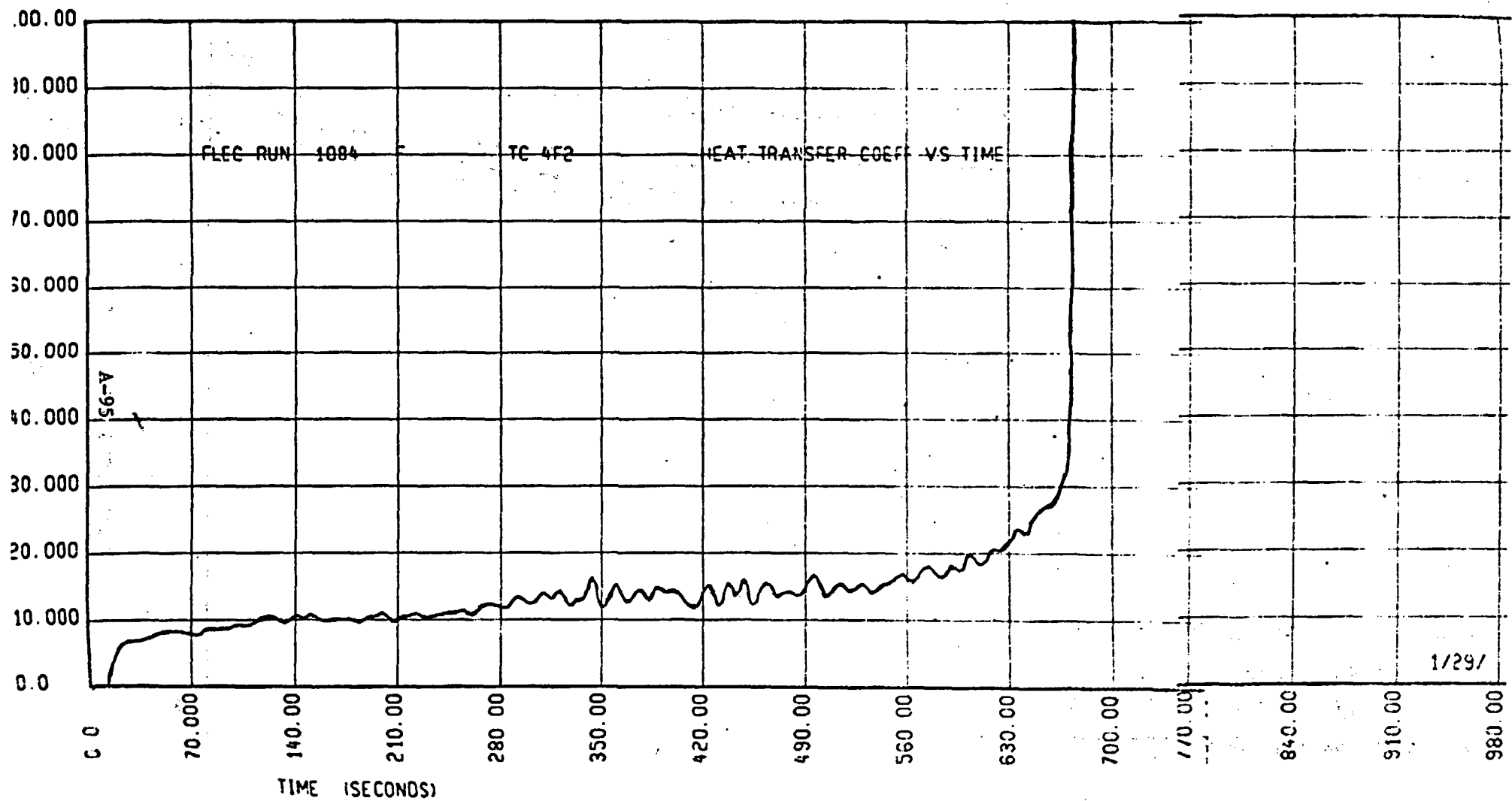
RUN NO. 1084

C. HEATER THERMOCOUPLE DATA

<u>T/C No.</u>	<u>Elevation</u>	<u>Initial Temp. (°F)</u>	<u>Max. Temp. (°F)</u>	<u>Temp. Rise (°F)</u>	<u>Turnaround Time (Sec.)</u>	<u>Quench Temp. (°F)</u>	<u>Quench Time (°F)</u>
5G1	6'	1609	2033	412	103	764	683
5G3	4'	1391	1675	284	53	793	321
5G5	10'	961	1407	446	155		
5G6	8'	Bad TC					
5F1	6'	1581	2026	445	113	839	685
5F6	8'	Bad TC					
7G3	6'	1506	2020	514	105	899	679
6G3	6'	1579	2047	468	107	783	691
5F3	6'	1480	1795	315	717	522	656
4F2	6'	1558	2120	562	119	864	670
3F2	6'	1498	2115	617	131	922	646
1F2	6'	1531	1850	319	99	893	694
7D2	6'	1076	1227	151	95	1115	108
5E2	8'	1352	1857	505	228		
5E4	4'	1295	1533	238	46	750	321
5E5	2'	Bad TC					
5E1	10'	920	1506	516	360		
6G5	2'	980	1857	77	14	690	97

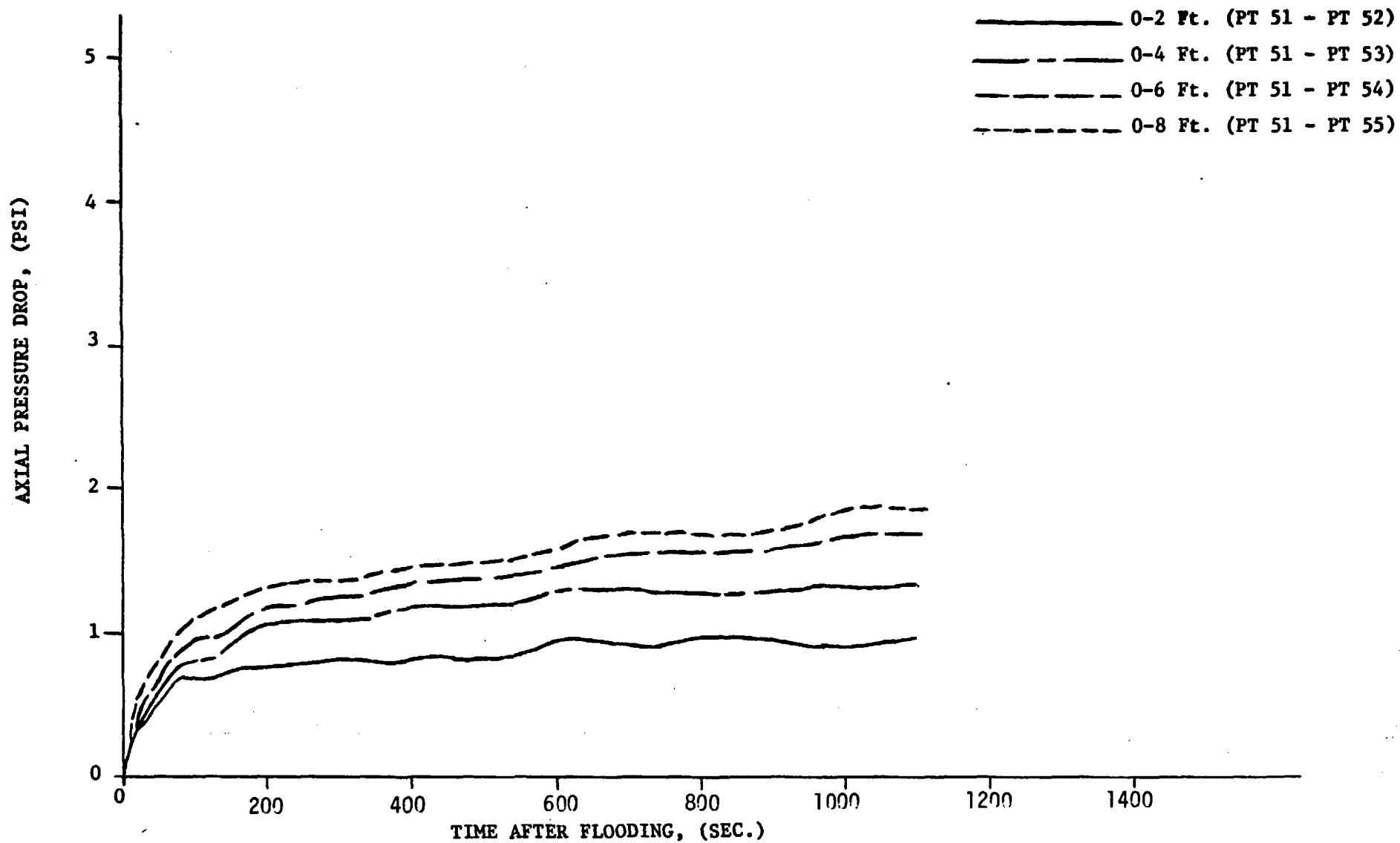
Bundle includes 3 failed rods 7D, 7E, 6E and 6D





Run 1084
PRESSURE DROP VS. TIME.

A-96



Run 1084

CARRYOVER DATA NOT VALID DUE TO
INSTRUMENTATION MALFUNCTION

APPENDIX B
METHOD OF CALCULATION
OF ROD AND HOUSING HEAT RELEASE
(SEC. 3.2.2.2)

I. Local Rate of Heat Release (Figure 3-15)

Rods: The local rate of rod heat release, q (Btu/hr/ft), is obtained from the DATAR code.

Housing: The local rate of housing heat release, q_h , is computed by

$$q_h = - C_{p,h} \rho_h A_h \frac{\Delta T_h}{\Delta t} \quad (1)$$

where the subscript "h" refers to the housing, C_p is the specific heat, ρ is the density, A is the cross section area, T is the housing temperature and t is the time. The housing temperature-time curves for runs 9077 and 9176 are shown in Figure B-1.

II. Rate of Heat Release Below 6 ft. Elevation (Figure 3-16)

Rods: The rate of rod heat release below 6 ft. elevation $\int_0^6 q dz$ can be evaluated by plotting the q vs Z curves and measuring the areas under the curves as illustrated in Figure B-2.

Housing: For the housing the heat release is mainly at quench. Therefore the rate of housing heat release below 6 ft. elevation including heat release below the quench front can be computed by

$$\int_0^6 q_h dz \approx C_{p,h} \rho_h A_h V_{q,h} (T_{init,h} - T_{sat}) + bh \Delta T_{sub} Z_{q,h} \exp \left(-\frac{hb}{C_{p,h} \rho_h A_h} t \right) \quad (2)$$

$$h = .023 (K_w/D_e) (\rho_w V_{in} D_e / \mu_w)^{0.8} (\mu_w C_{p,w} / K_w)^{0.4}$$

where

V_q = quench front velocity which is measured from the quench front elevation vs time curve, ft/hr (Figure B-3)

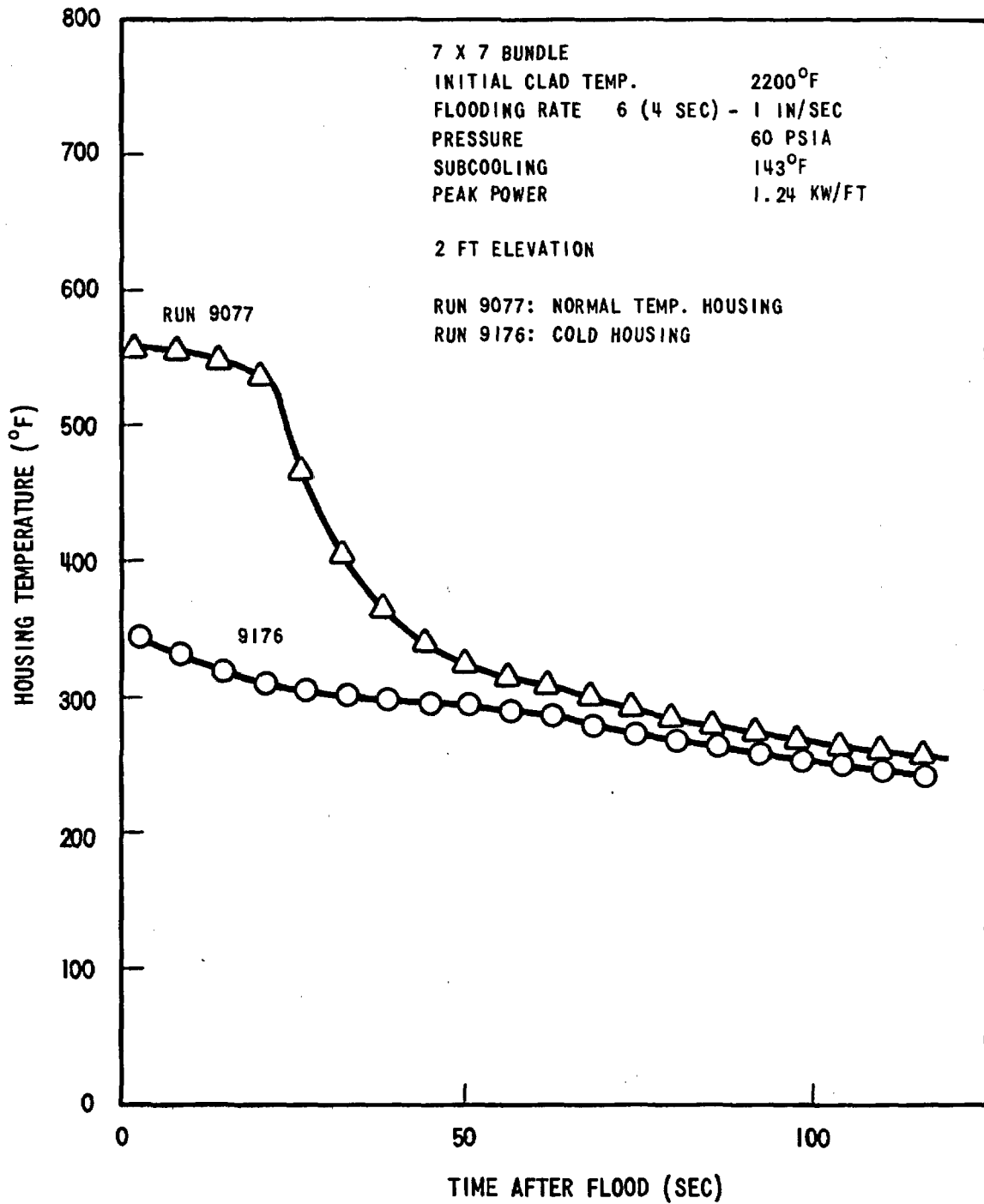


Figure B-1. Housing Temperature of FLECHT Run 9077 and 9176.

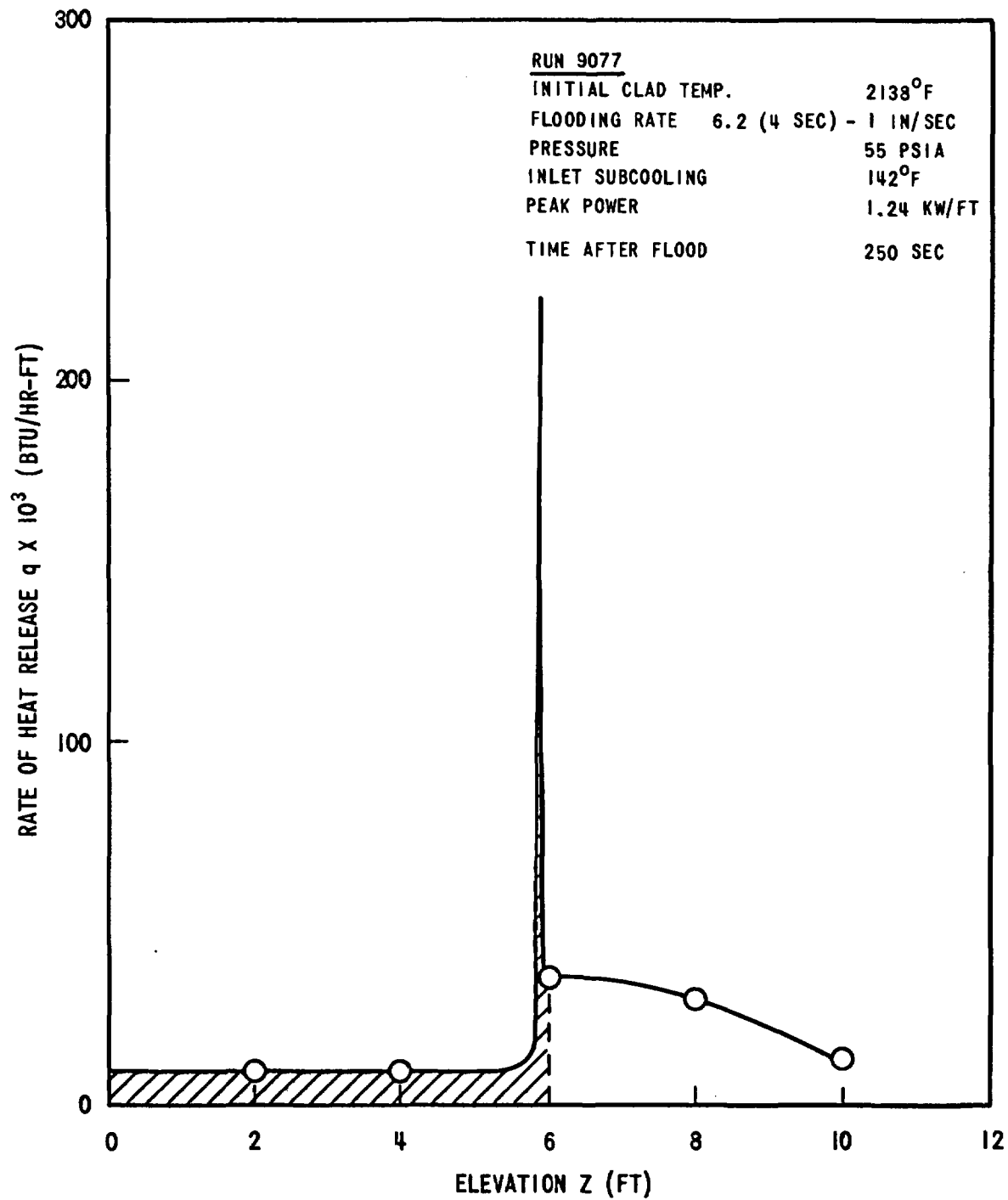


Figure B-2. Rate of Heat Release of an Equivalent Row of Rods vs Elevation.

B-5

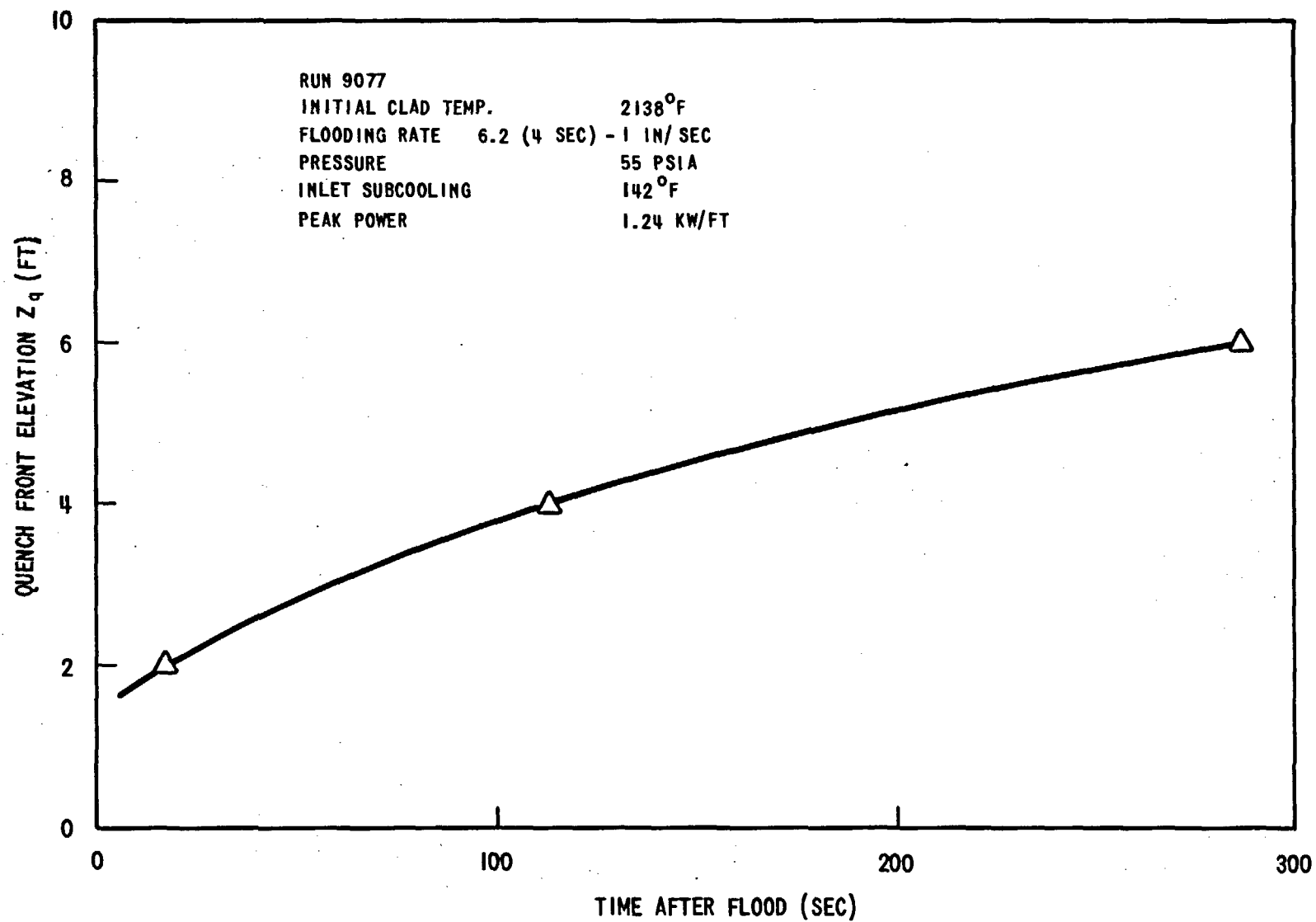


Figure B-3. Housing Quench Front Elevation versus Time

$T_{init,h}$	= initial housing temperature, °F
T_{sat}	= saturation temperature, °F
h	= heat transfer coefficient, Btu/hr-°F-ft ²
Z	= elevation, ft
b	= housing inside perimeter, ft
ΔT_{sat}	= $T_{sat} - T_{in,water}$ = inlet coolant subcooling, °F
Z_q	= quench front elevation, ft
K	= thermal conductivity, Btu/hr-°F-ft
μ	= viscosity, lb _m /ft-hr
D_e	= hydraulic diameter of the outer subchannel (0.52 inches), ft
V_{in}	= inlet coolant velocity, ft/hr
C_p	= specific heat, Btu/lb _m -°F
ρ	= Density, lb _m /ft ³
A	= cross section area, ft ²
q	= heat flux per length, Btu/hr-ft
t	= time, hr
subscript "h" - housing	
subscript "w" - water	

III. Total Heat Release from the Beginning of Flood to the Time t Below 6 ft Elevation (Figure 3-17)

Rods: The total rod heat release can be obtained by measuring the area under the curve of Figure 3-16 from $t = 0$ to $t = t$.

Housing: Method 1: The total housing heat release can also be obtained by measuring the area under the curves of Figure 3-16 from $t = 0$ to $t = t$. Figure 3-17 shows the results of this method.

Method 2: In order to check the validity of Equation (2), an alternative method is also presented here. The total housing heat release can also be computed from the stored heat released from the housing.

$$\text{Total heat release} = C_{p,h} \rho_h A_h \int_0^6 (T_{\text{init},h} - T_h) dZ \quad (3)$$

$$= C_{p,h} \rho_h A_h \left(\int_0^6 T_{\text{init},h} dZ - \int_0^6 T_h dZ \right)$$

where T_h is the housing temperature at the time t . By measuring the area under the $T_{\text{init},h}$ vs Z curve and the area under the T_h vs Z curve from $Z = 0$ to $Z = 6$ ft, (Figure B-4), one is able to compute the total heat release from Equation (3).

Comparison of the results of calculations by Method 1 and Method 2 are shown in Figure B-5. The agreement of the two methods is reasonably good. Thus the validity of Equation (2) is justified.

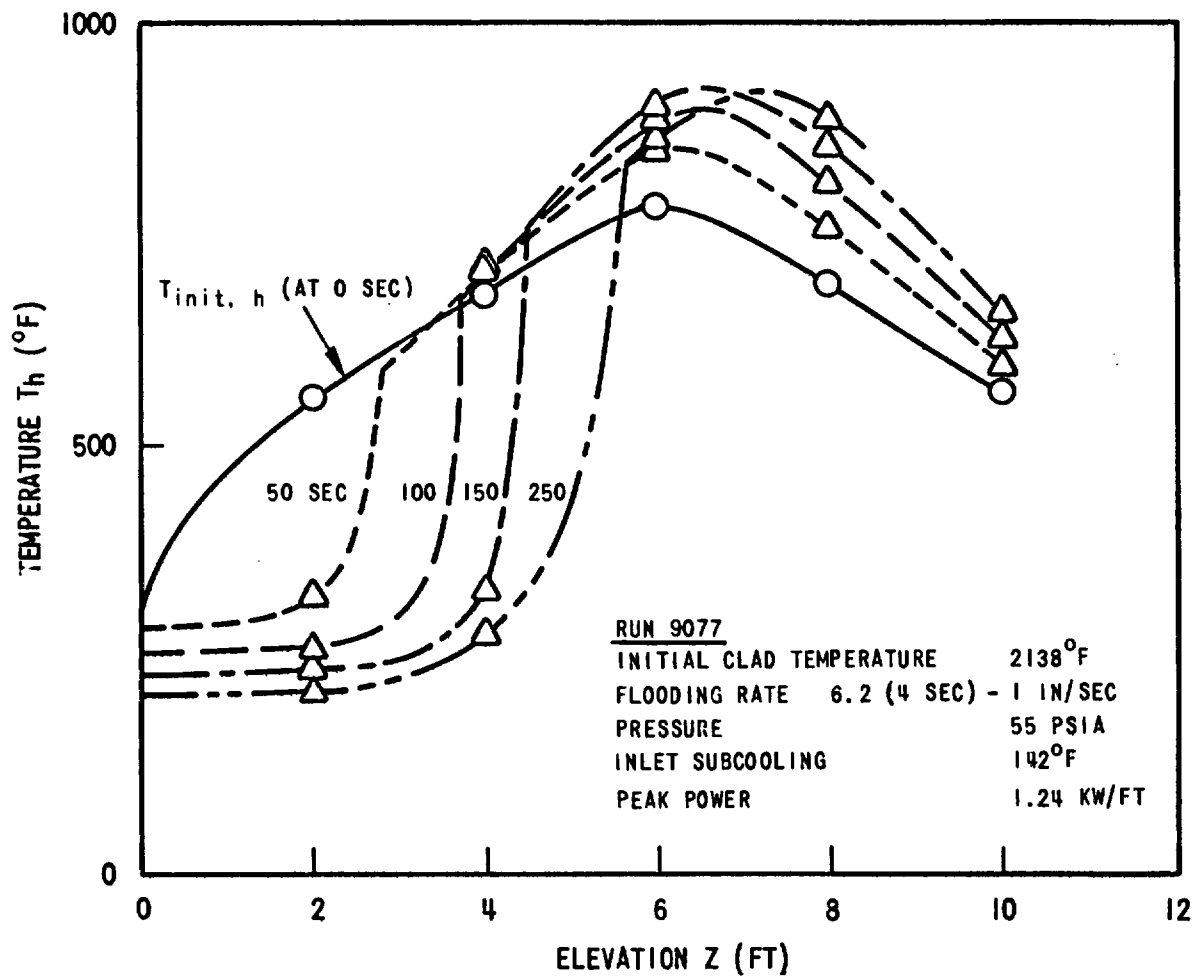


Figure B-4. Temperature of the Housing vs Elevation. The Abrupt Change in Temperature Indicates the Quench. The Quench Front Elevation is Determined by Figure B-3.

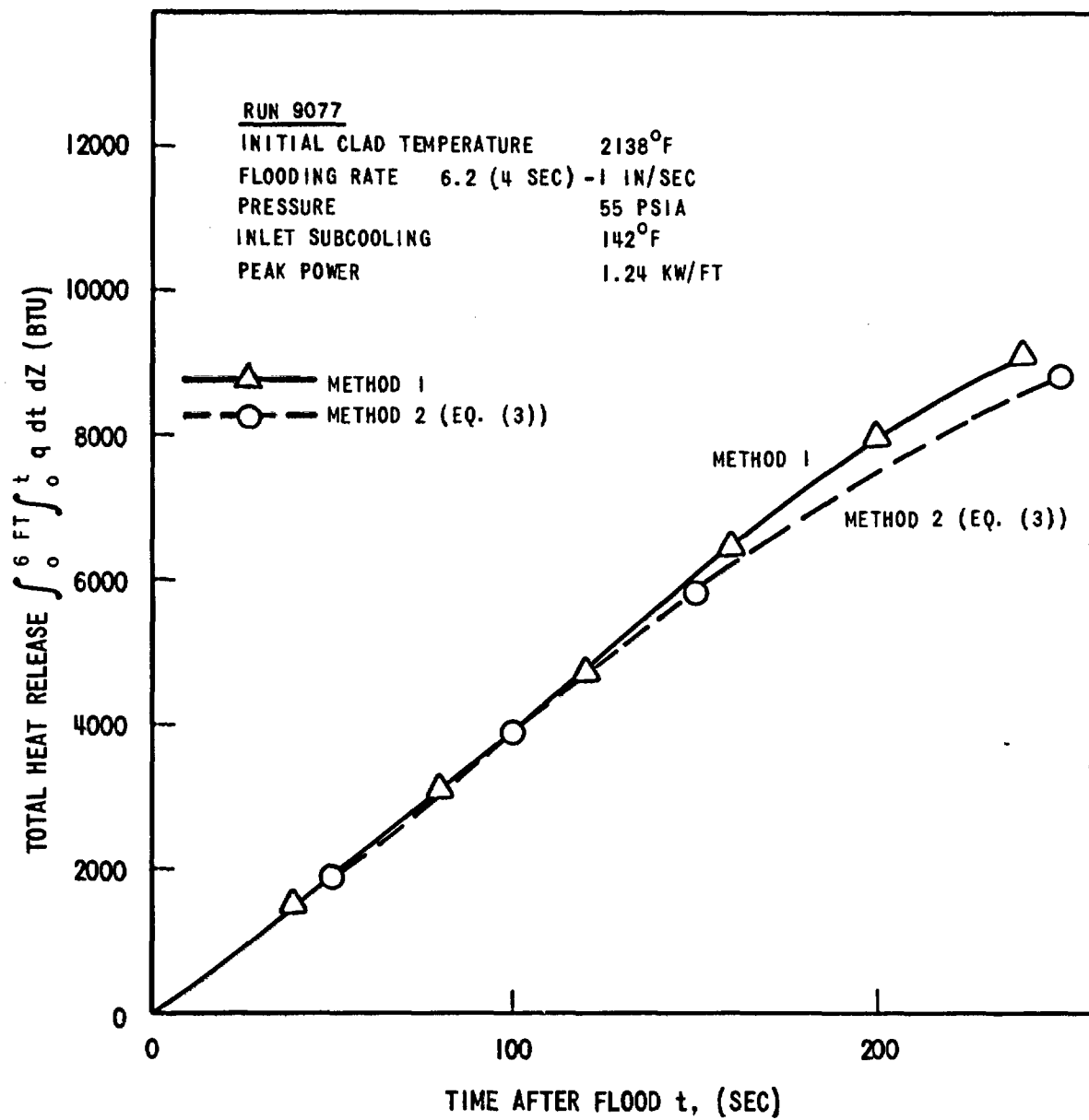


Figure B-5. Comparison of Housing Heat Releases Computed with Two Methods.

APPENDIX C
CLAD TEMPERATURE DISTRIBUTION
AT THE START OF FLOOD
UTILIZING EXTERNAL THERMOCOUPLE DATA

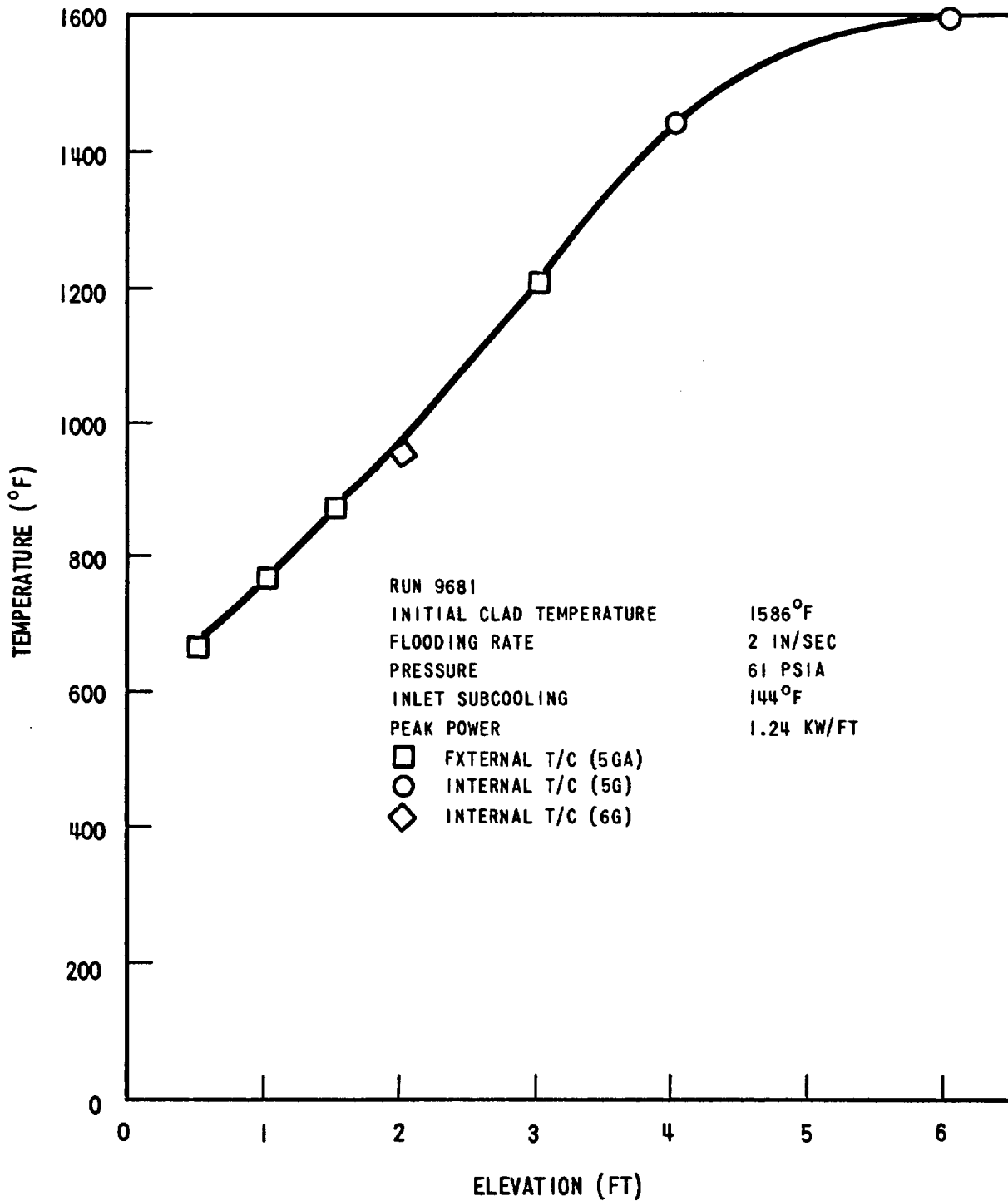


Figure C-1. Clad Temperature Distribution at the Start of Flood, Run 9681.

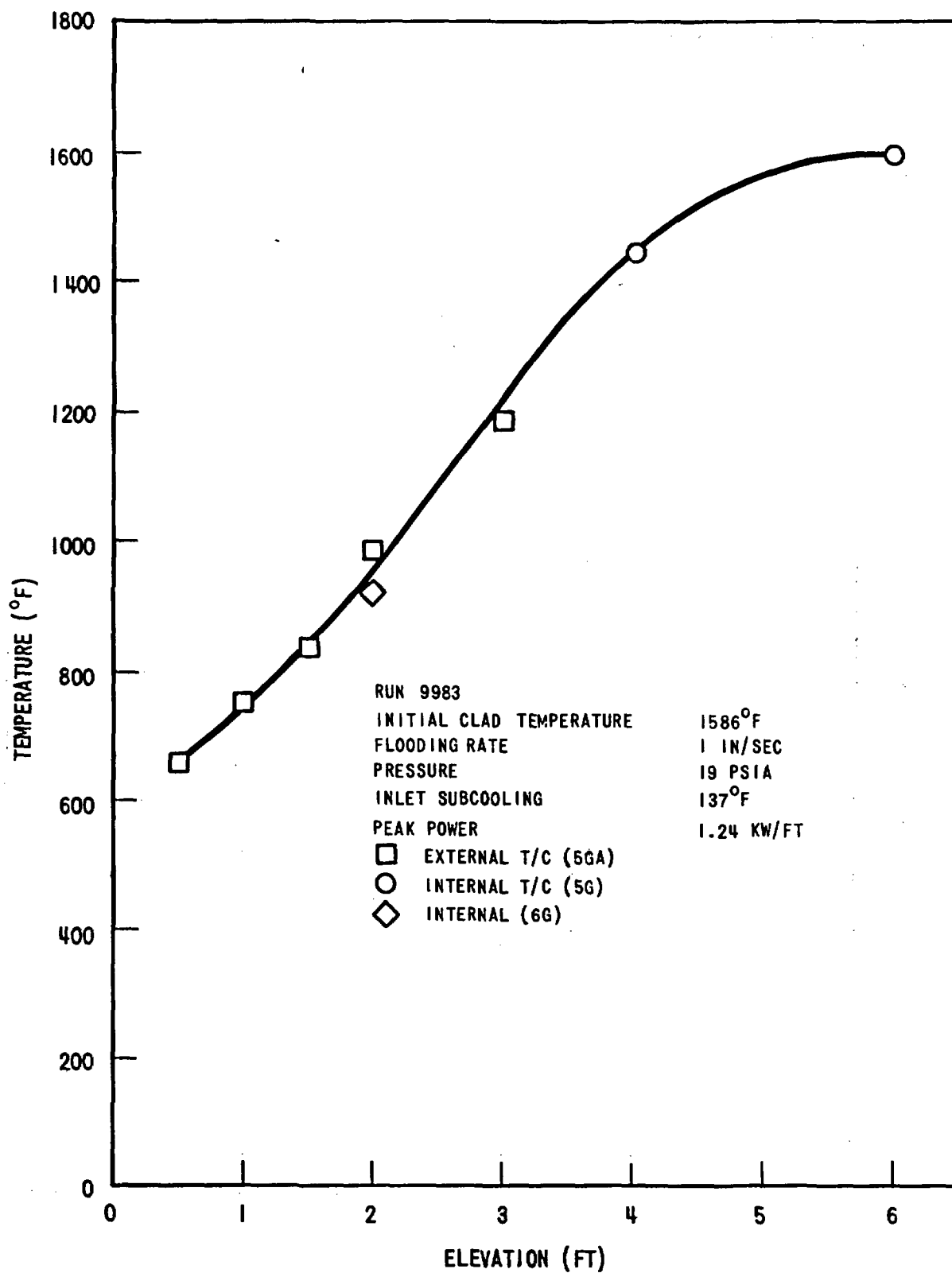


Figure C-4. Clad Temperature Distribution at the Start of Flood, Run 9983.

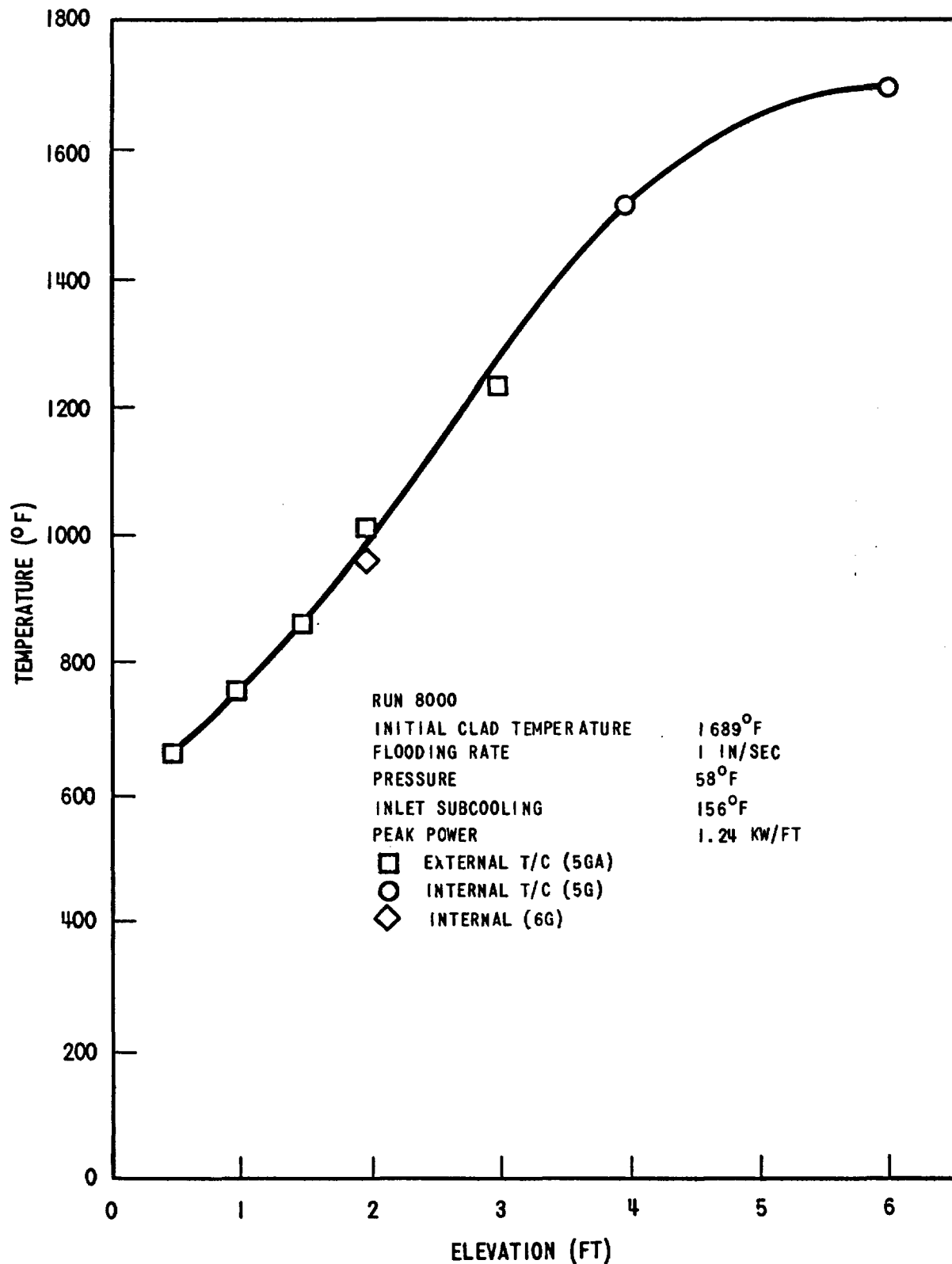


Figure C-5. Clad Temperature Distribution at the Start of Flood, Run 8000.

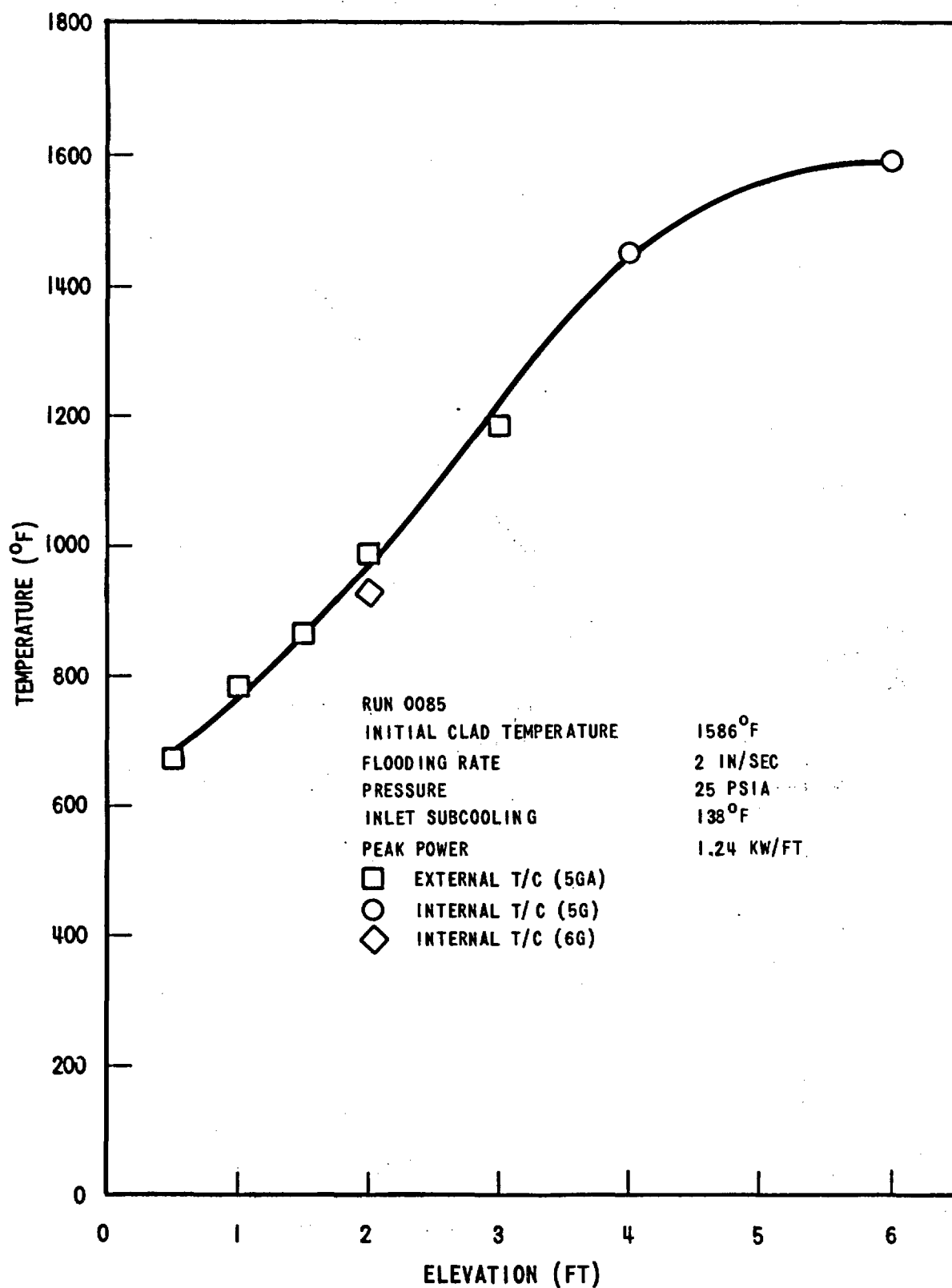


Figure C-6. Clad Temperature Distribution at the Start of Flood, Run 0085.

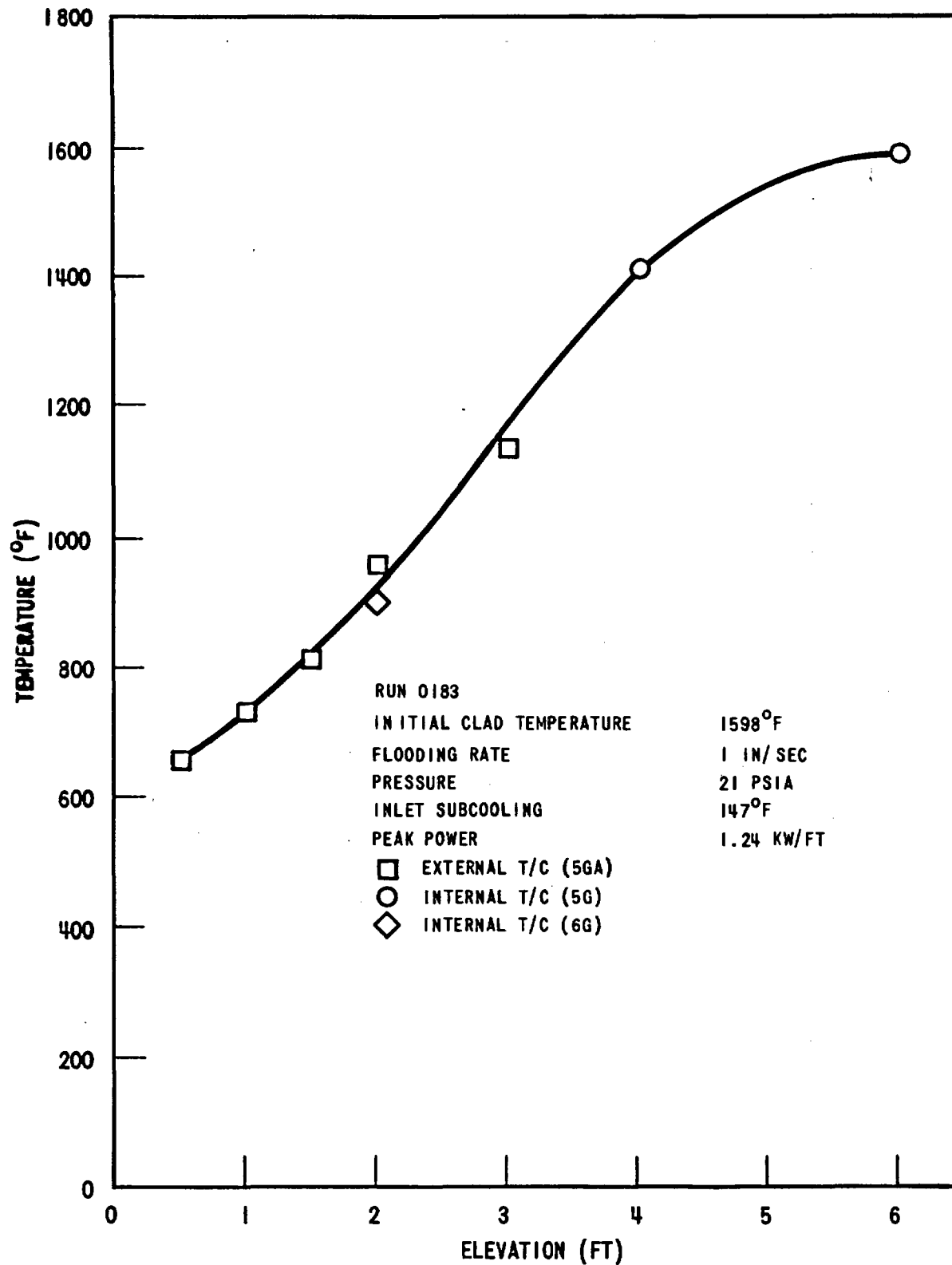


Figure C-7. Clad Temperature Distribution at the Start of Flood, Run 0183.

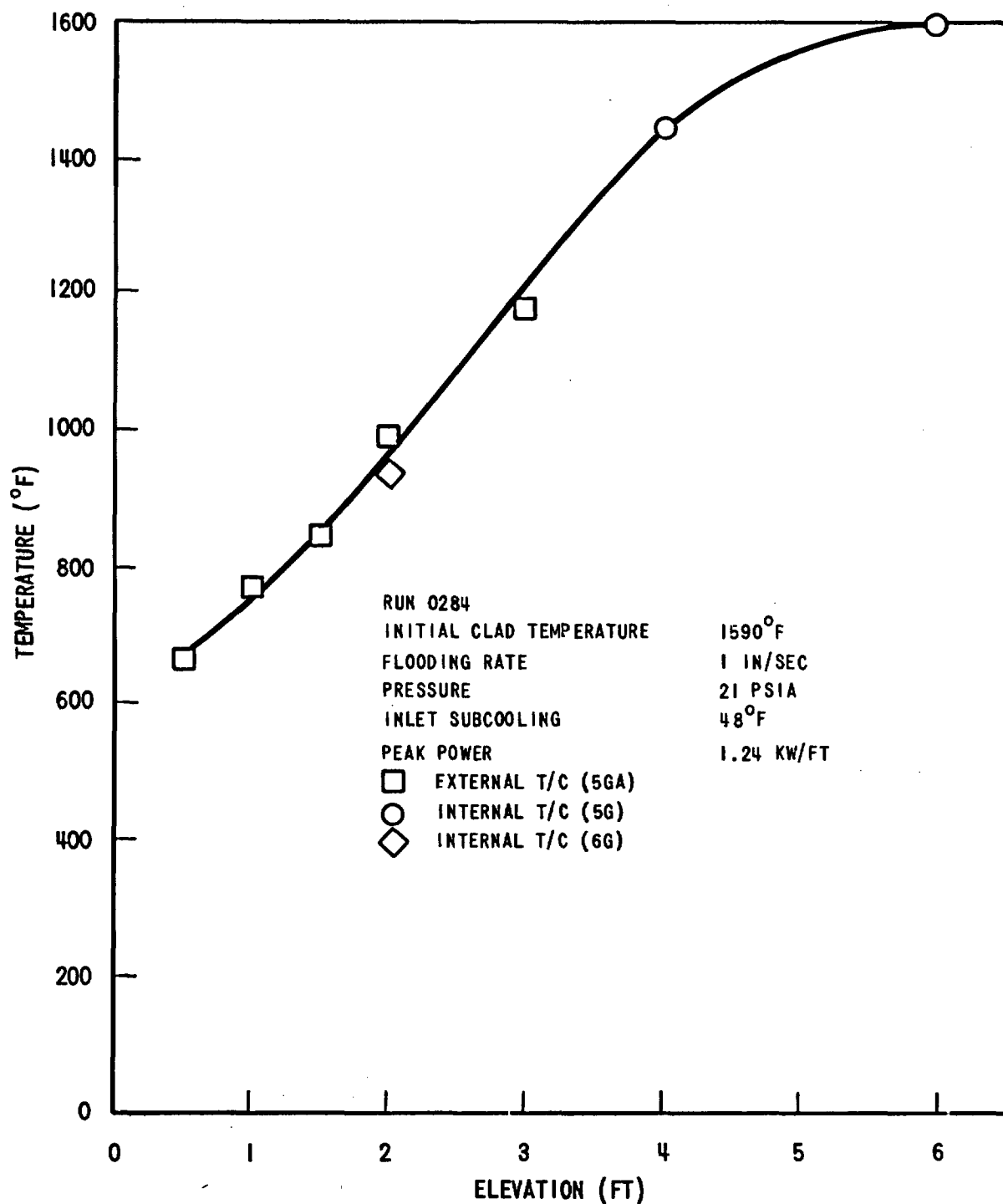


Figure C-8. Clad Temperature Distribution at the Start of Flood, Run 0284.

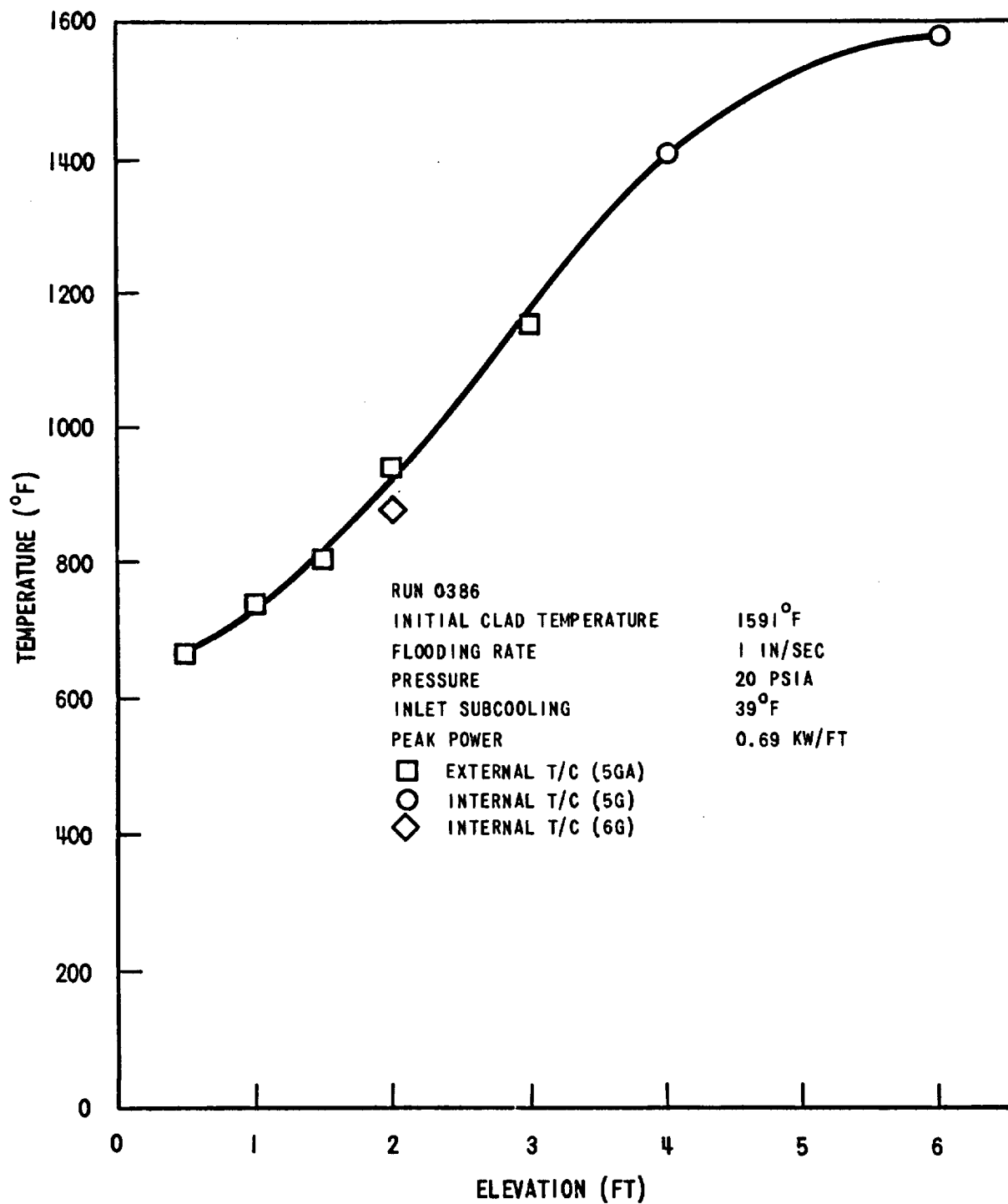


Figure C-9. Clad Temperature Distribution at the Start of Flood, Run 0386.

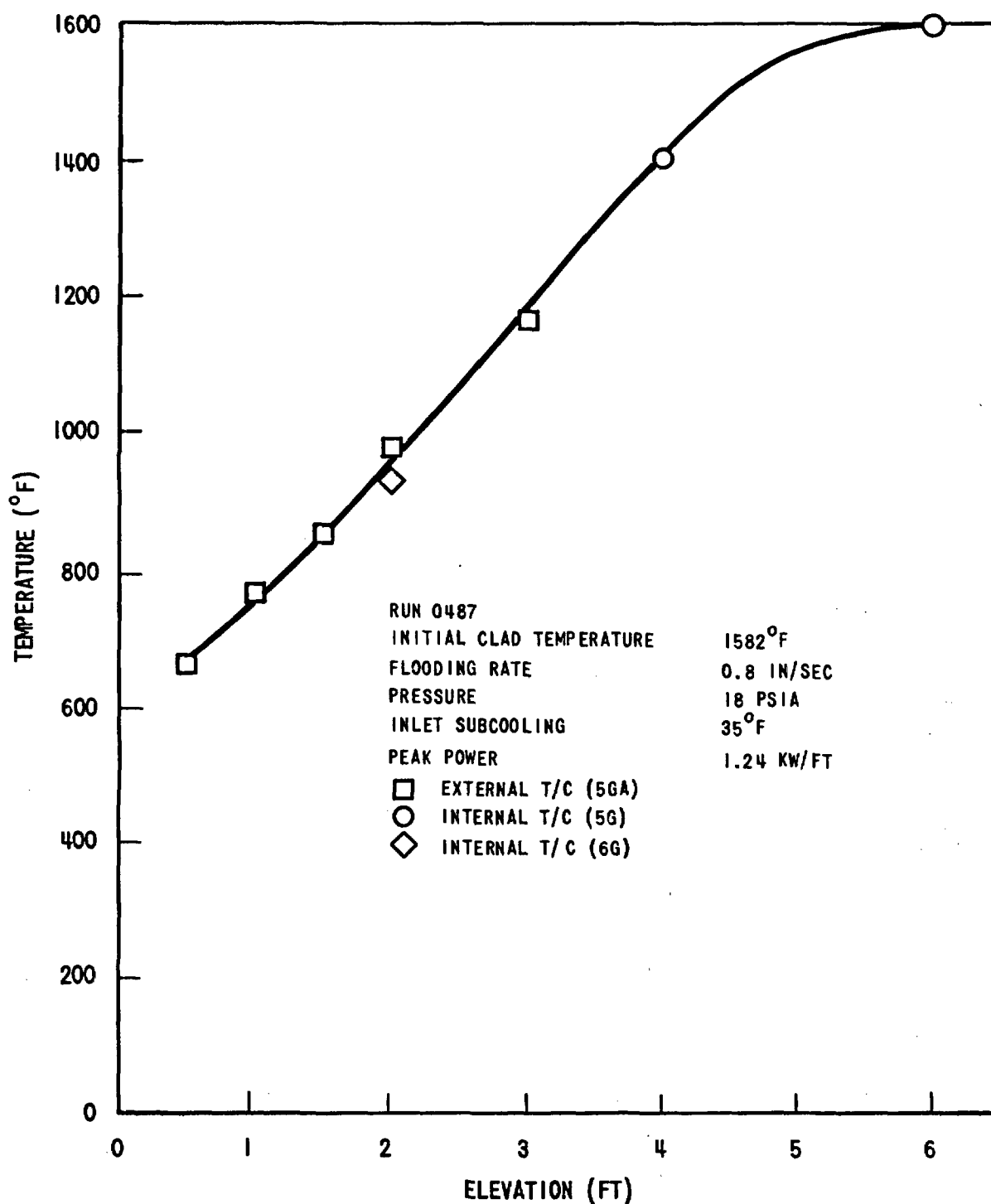


Figure C-10. Clad Temperature Distribution at the Start of Flood, Run 0487.

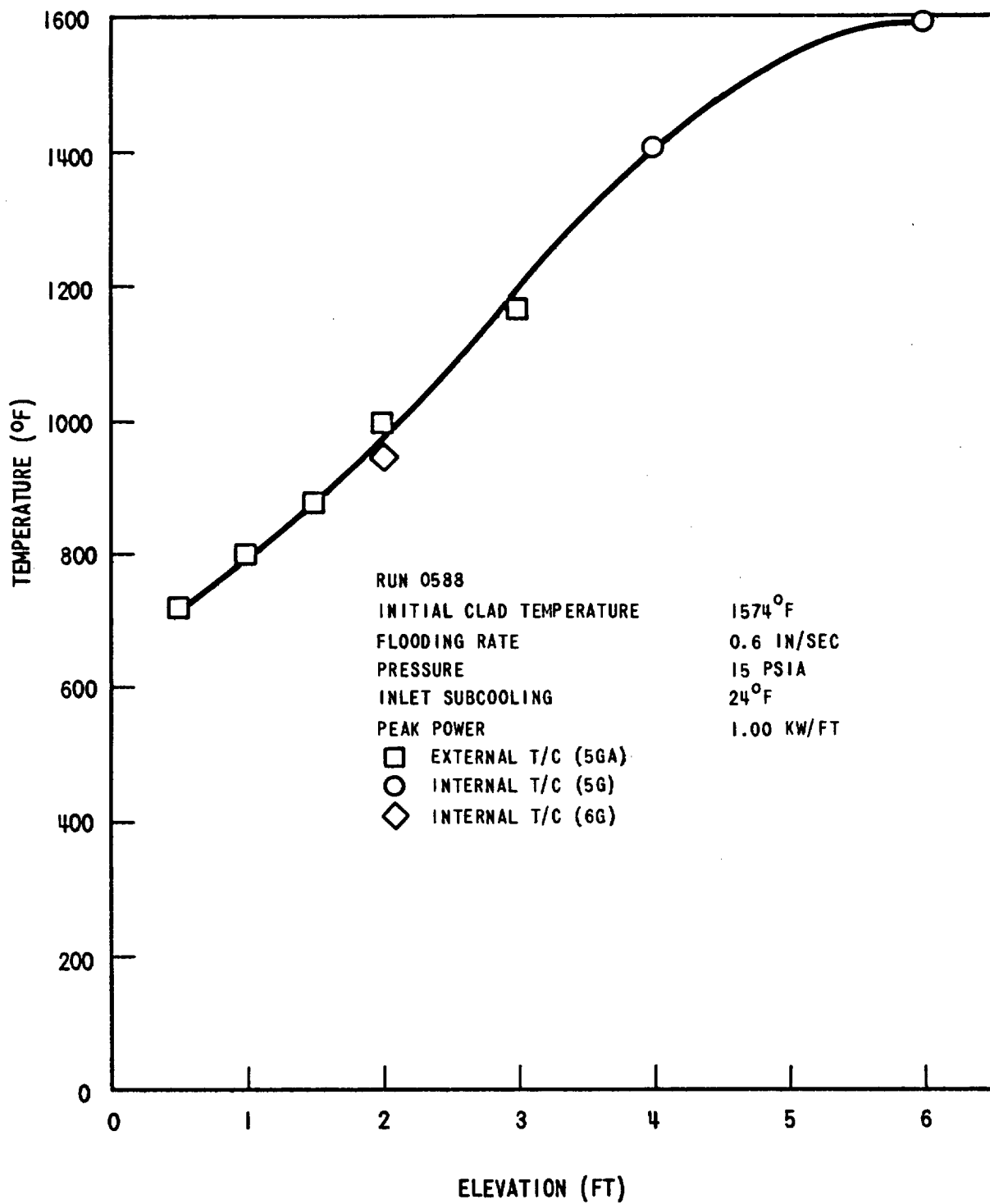


Figure C-11. Clad Temperature Distribution at the Start of Flood, Run 0588.

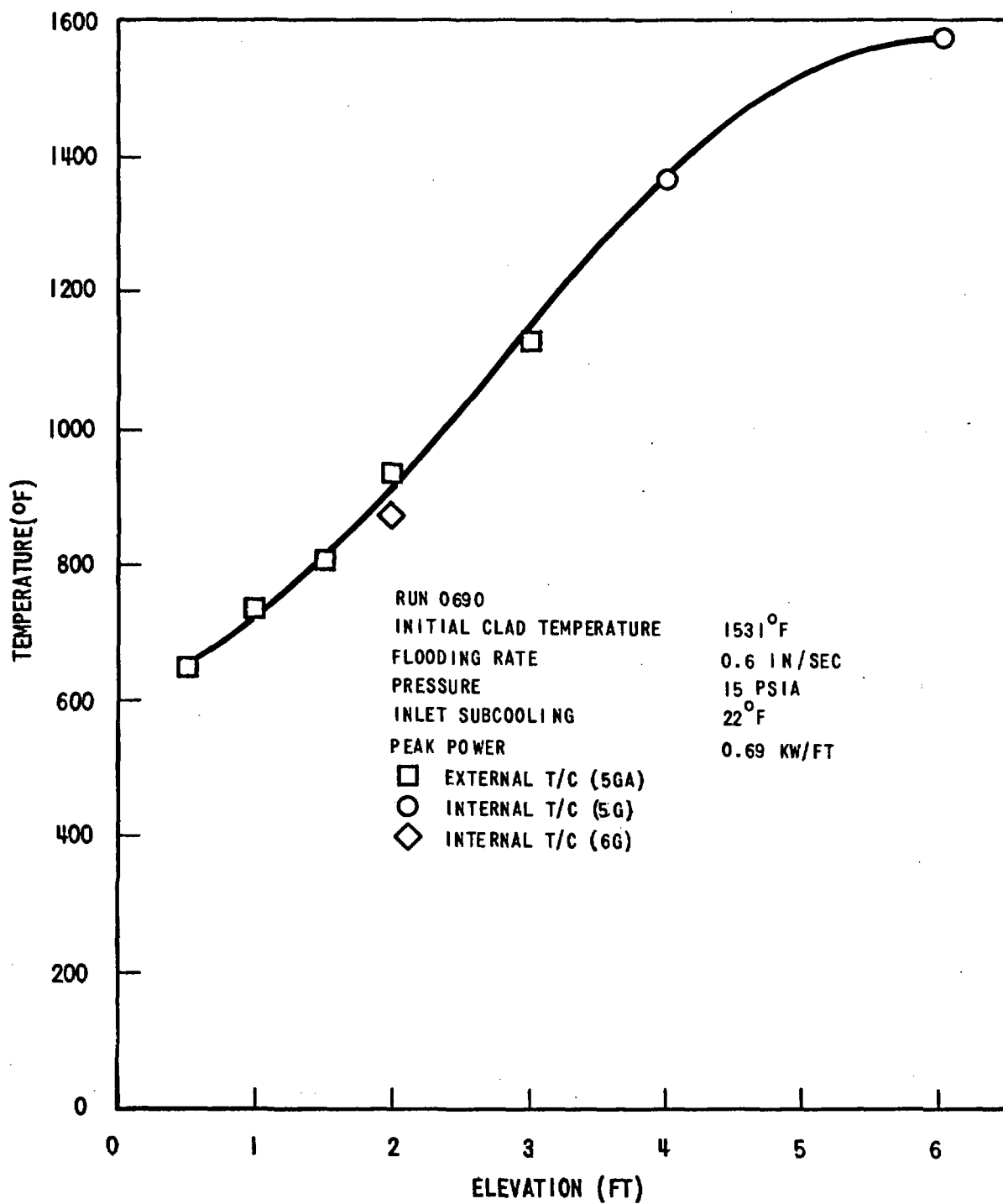


Figure C-12. Clad Temperature Distribution at the Start of Flood, Run 0690.

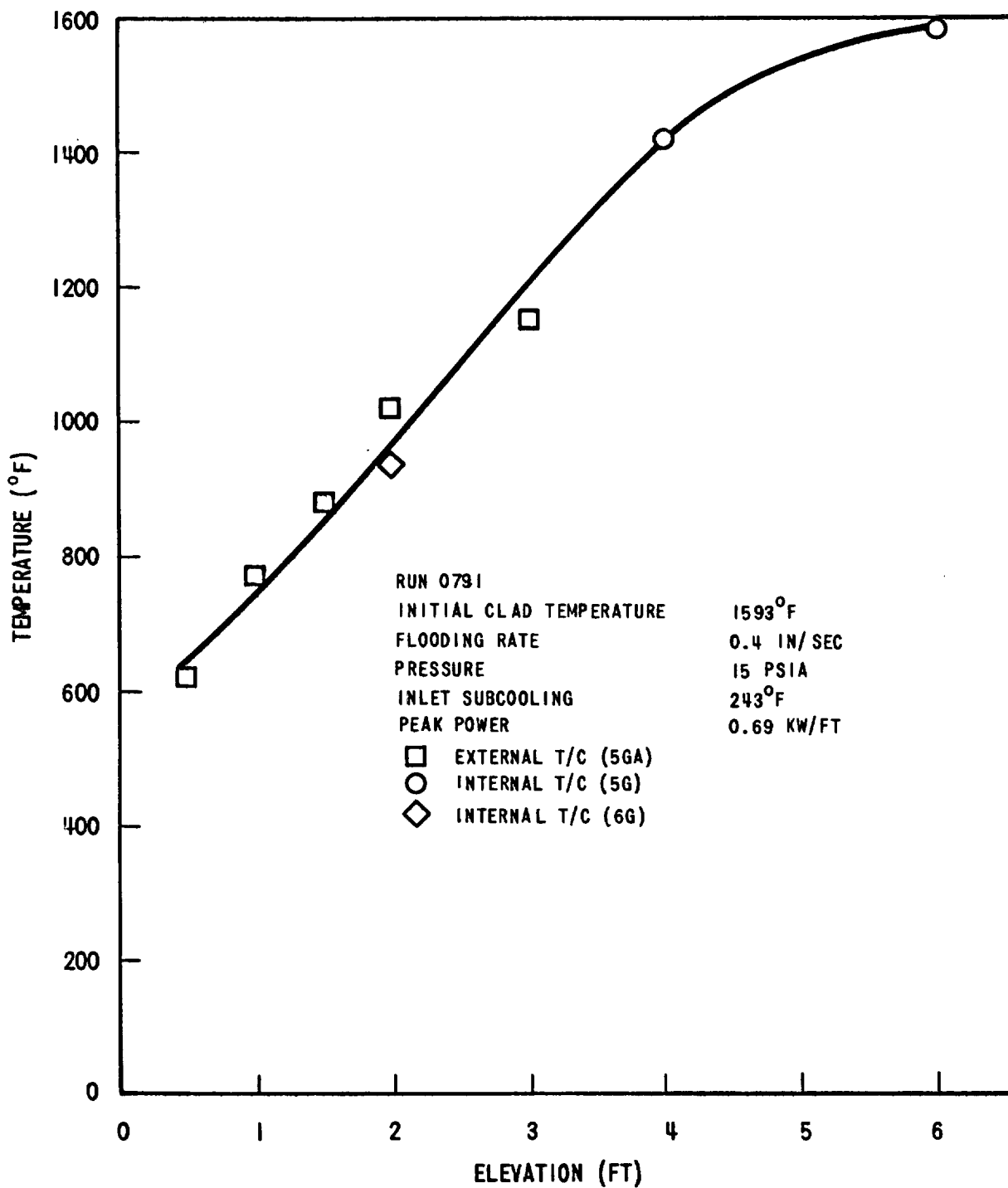


Figure C-13. Clad Temperature Distribution at the Start of Flood, Run 0791.

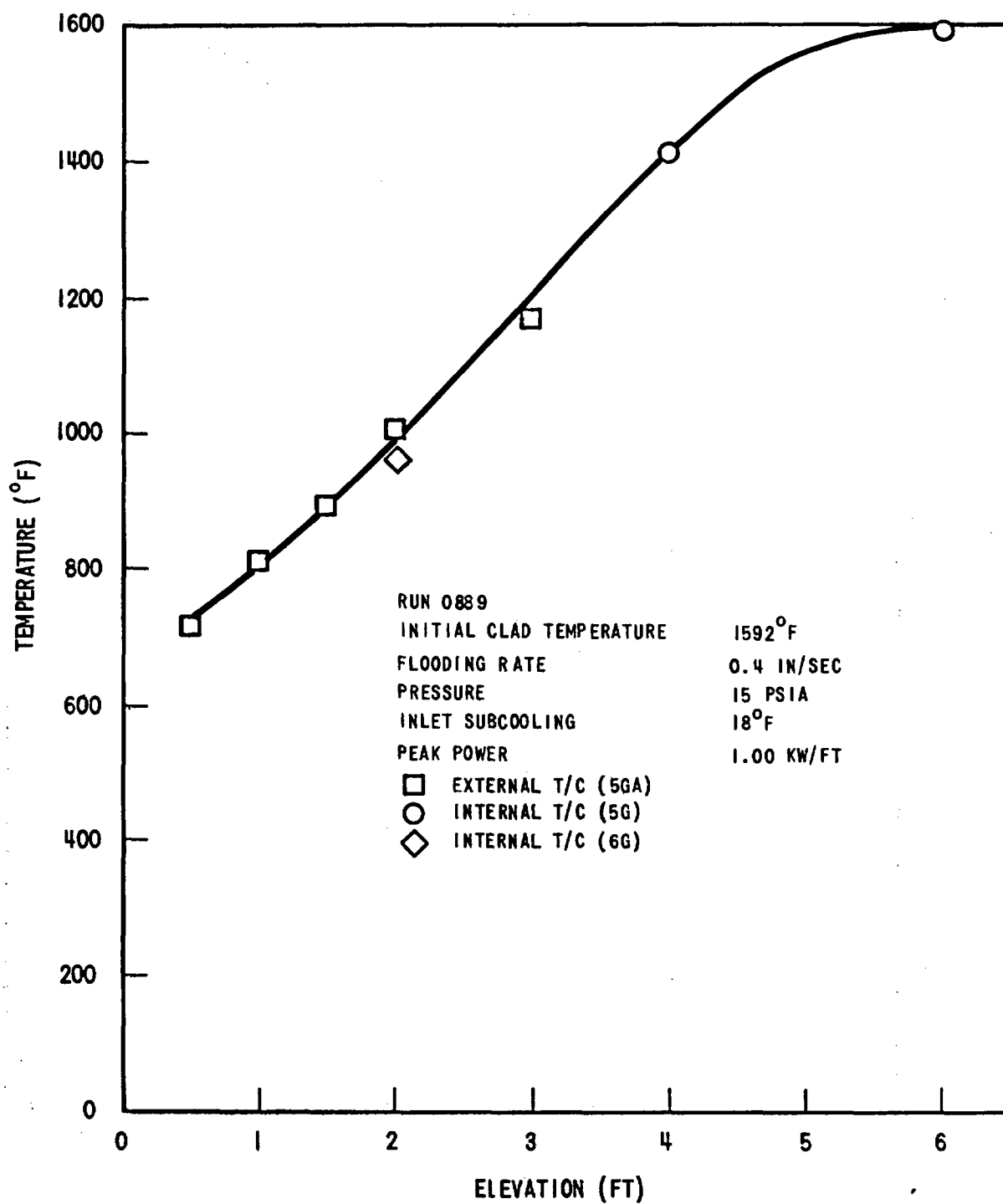


Figure C-14. Clad Temperature Distribution at the Start of Flood, Run 0889.

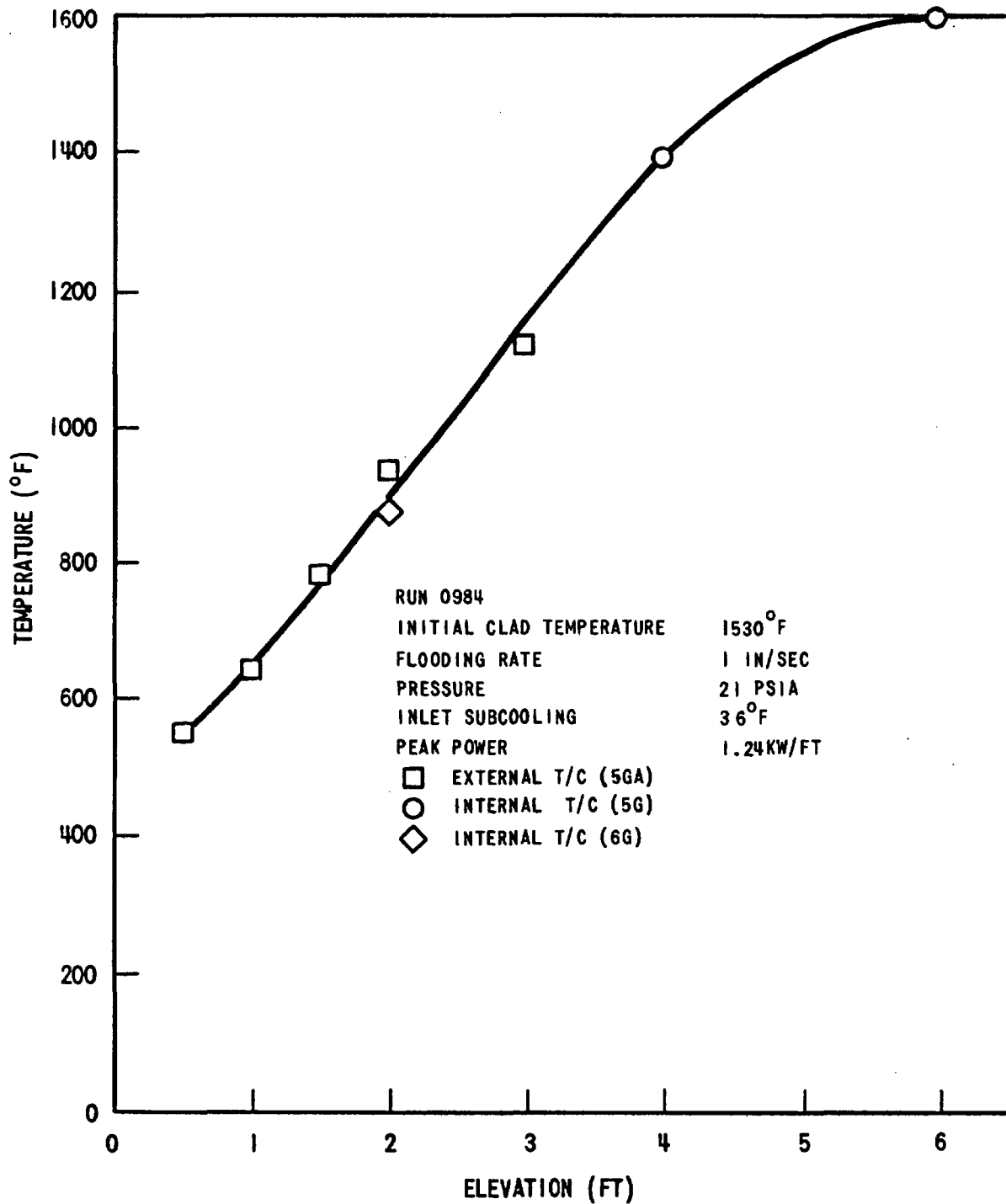


Figure C-15. Clad Temperature Distribution at the Start of Flood, Run 0984.

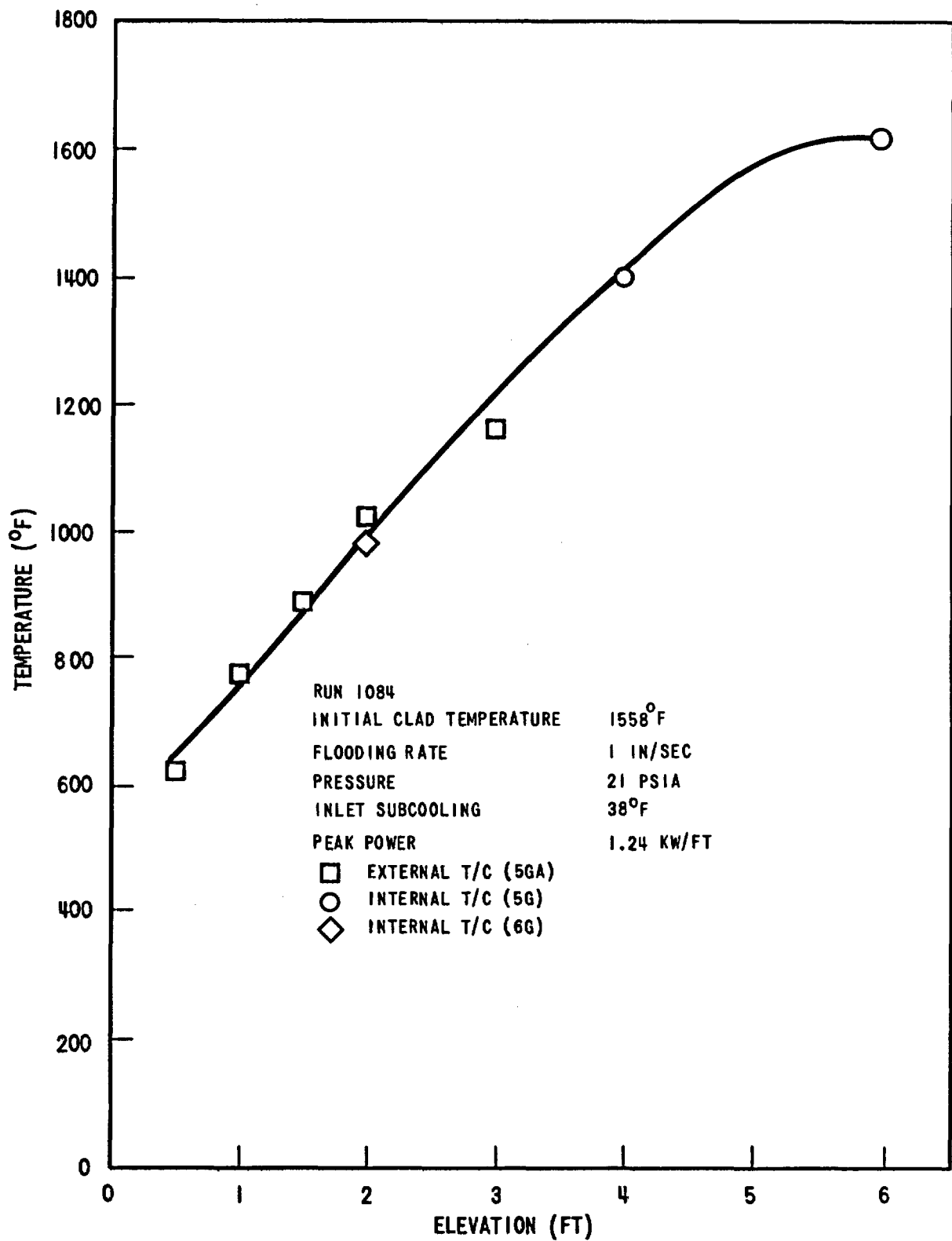


Figure C-16. Clad Temperature Distribution at the Start of Flood, Run 1084.

APPENDIX D

FORTRAN PROGRAM LISTINGS OF SIX FOOT
QUENCH TIME CORRELATION AND FLECHT
HEAT TRANSFER COEFFICIENT CORRELATION

FORTRAN PROGRAM LISTING OF 6 FT QUENCH TIME CORRELATION

TYPE TQ6FT.F4

```

00100      1 ACCEPT 100, DTSUB,VIN,P,TINIT,QMAX
00200      F1=EXP(-.0107*DTSUB)*(1.-EXP(-.667
00300      1*VIN))
00350      F4=1.+.5*EXP(-.000037*P*P*P)
00400      F2=F4+1.3*EXP(-.111*VIN*VIN)+17.3*EXP(-.000037
00500      1*P*P*P)*EXP(-.49*VIN*VIN)
00600      F3=3.28/VIN**1.1-2.8*EXP(-VIN)
00900      F5=1.+.0000588*TINIT
00910      F61=1.207*QMAX**1.5-.667
01000      TQ=98.39*(F1*F2*F61+F3*F4)*F5
01100      TYPE 200, TQ
01200      100  FORMAT (5F)
01300      200  FORMAT (F/)
01400      GO TO 1
01500      STOP
01600      END

```

FORTRAN PROGRAM LISTING OF HEAT TRANSFER COEFFICIENT CORRELATION

.TYPE HCALF.F4

```

00100      1      ACCEPT 100, DTSUB,VIN,P,TINIT,QMAX,TQ6FT
00200      ACCEPT 150, Z,B,H1,T1,DT,IMAX
00250      C      T1=INITIAL TIME, FIRST POINT TO BE PRINTED.
00260      C      IMAX=NO. OF POINTS TO BE PRINTED.
00280      TYPE 200
00300      100    FORMAT (6F)
00400      150    FORMAT (5F,1)
00500      200    FORMAT (5X,4HTIME,7X,1HH)
00600      H12A=22.-.00303*Z**4.1
00700      H12B=1.-EXP(-.0333*P)-.034*P*EXP(-.0011*P*P)
00800      H12C=1.-EXP(-.2*VIN)
00900      H12D=8.*(1.-EXP(-VIN/.5))*(1.-EXP(-B/25.))
01000      H12=4.+(35.7+H12A*H12B)*H12C+H12D
01010      XA=1.+4.37*EXP(-.0166*DTSUB)
01020      XB=1.-EXP(-(0.0075+.0000272*(VIN-8.)*(VIN-8.))
01100      1)*(TINIT-650.))
01200      XAB=17.6*XA*XB
01300      TTQ2=.62*((1.-EXP(-.192*Z))-.115*Z*EXP(-.0368*Z
01400      1*Z))
01500      TTQ3=1.55*((1.-EXP(-.205*Z))-.154*Z*EXP(-.0421
01600      1*Z*Z))
01700      X2=XAB*TTQ2
01800      H2=H12*((1.-EXP(-X2))-.9*X2*EXP(-X2*X2))
02000      B1A=682.-650.*(1.-EXP(4.-Z))
02200      B1B=1.-EXP(-.95*(1.-.0488*Z)*VIN)
02300      B1C=1.-EXP(-.0238*DTSUB)
02500      B1D=.696+.304*EXP(-B/25.)
02600      B1=B1A*B1B*B1C*B1D
02700      B2A=1.-EXP(-2.*(Z-3.5))
02800      B2B=1.33*(1.-EXP(-.0227*P))-1.
02900      B2C=2.9*(1.-EXP(-VIN/2.5))*(1.-EXP(-B/25.))
03000      B2=.4*Z*B2A*B2B-B2C
03100      B3=2.55*(Z-3.7)*(Z-3.7)*EXP(3.7-Z)
03150      B4=87.5*VIN*EXP(-VIN*VIN)*EXP(-.036*DTSUB)
03200      Y3=TTQ3-TTQ2
03300      H3=H2+B1*(Y3*Y3+B2*(Y3*Y3-B3*Y3*Y3*Y3))
03350      H3=H3+B1*B4*Y3*Y3*EXP(-6.38*Y3)
03400      C=420.*(1.-EXP(-.00625*B1))
03900      T=T1-DT
04000      DO 40 I=1,IMAX
04100      T=T+DT
04200      TTQ=T/TQ6FT
04300      IF (TTQ .GT. TTQ2) GO TO 10
04400      X=XAB*TTQ
04500      U=9.*TTQ*TTQ/TTQ2/TTQ2
04700      HB=(1.-EXP(-X))-.9*X*EXP(-X*X)
04800      HC=1.-2.21*EXP(-.4*VIN)*U*EXP(-U)*EXP(-
04900      1(.588*Z-3.824)**2)
04950      HA=H1*(1.-HB*HC)*(1.-EXP(-10.*(X2-X)/X2))
05000      H=HA+H12*HB*HC

```

FORTTRAN PROGRAM LISTING OF HEAT TRANSFER COEFFICIENT CORRELATION (cont)

```

05100      GO TO 30
05200      10      IF (TTQ .GT. TTQ3)GO TO 20
05300          Y=TTQ-TTQ2
05400          H=H2+B1*(Y*Y+B2*(Y*Y-B3*Y*Y*Y))
05450          H=H+B1*B4*Y*Y*EXP(-6.38*Y)
05500      GO TO 30
05600      20      H=H3+C*(TTQ-TTQ3)
05700      30      TYPE 500,T,H
05800      500     FORMAT (2F10.4)
05900      40      CONTINUE
06000          TYPE 600
06100      600     FORMAT (1H )
06200      GO TO 1
06300      STOP
06400      END

```

APPENDIX E
RADIATIVE HEAT TRANSFER ANALYSIS
OF A HEATER ROD

To compute radiation from a heater rod to all other rods and thimbles in a bundle for emissivity other than one is very complicated. Therefore a simplified model was devised for the calculation of gray body radiative heat transfer from the heater rods.

I. Physical Model

The configuration of a heater rod surrounded by adjacent rods and two thimbles is shown in Figure E1. For the present analysis this configuration is replaced by the model shown in Figure E2. In this model, the surrounding rods and thimbles are replaced by a circular enclosure which consists of three portions; two of which represent thimbles and the other which is equivalent to the other rods in the bundle including those not shown in Figure E1. The diameter D of the enclosure is computed by equating the cross section area inside the dotted line in E1 (excluding rods and thimbles) to the cross section area inside the enclosure, i.e.

$$\frac{\pi D^2}{4} = \text{(Cross section area inside the dotted line of Figure E1 excluding rods and thimbles but including the hot rod.)}$$

The direct exchange view factor from the hot rod to each thimble and from one thimble to another thimble (i.e., F_{42} , F_{43} , and F_{23} , respectively) in the configuration of Figure E-1 can be computed by the crossed-string method (c.f., H. C. Hottel and A. F. Sarofim "Radiative Transfer", McGraw-Hill Book Company, P31, 1967). The view factor from the hot rod to the other rods, F_{41} , can then be computed by

$$F_{41} = 1 - F_{42} - F_{43}$$

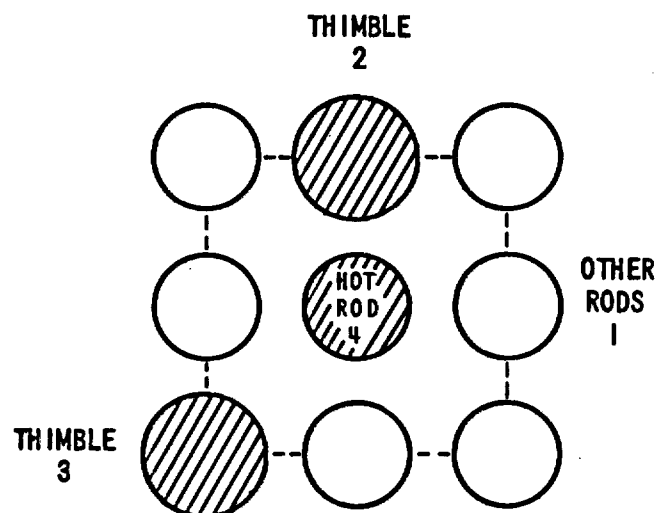


Figure E1. Configuration of Heater Rods and Thimbles Surrounding a Hot Rod

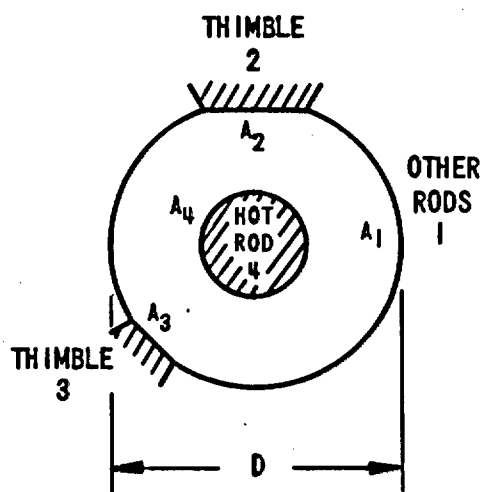


Figure E2. Equivalent Model of Configuration (E1)

The equivalent surface areas A_1 , A_2 and A_3 of the surrounding rods, thimble 2 and 3, respectively, of Figure E2 are computed as follows

$$A_1 = F_{41} \pi D \quad A_2 = F_{42} \pi D \quad A_3 = F_{43} \pi D$$

where πD is the total surface area of the enclosure. The other view factors are computed by

$$\sum_i A_i F_{ji} = A_j$$

and $A_i F_{ij} = A_j F_{ji}$

Table 1 summarizes the results of computation.

TABLE 1
Surface Areas and View Factors of Figure E2

$F_{41} = .7453$	$A_1 = 2.433$ inches	$A_4 F_{41} = A_1 F_{14} = .988$ inches
$F_{42} = .1671$	$A_2 = 0.5456$ inches	$A_4 F_{42} = A_2 F_{24} = .222$ inches
$F_{43} = .0876$	$A_3 = 0.2861$ inches	$A_4 F_{43} = A_3 F_{34} = .116$ inches
$F_{23} = .012$	$A_4 = 1.326$ inches	$A_2 F_{23} = A_3 F_{32} = .0205$ inches
		$A_1 F_{13} = A_3 F_{31} = .1499$ inches
		$A_1 F_{12} = A_2 F_{21} = .3034$ inches
		$A_1 F_{11} = .992$ inches
		$A_2 F_{22} = A_3 F_{33} = A_4 F_{44} = 0$

It is interesting to note that the equivalent surface area A_2 of thimble 2 turns out to be approximately equal to the diameter of the thimble, which is 0.545 inches.

II. Analysis

The equations for radiative interchange among the four surfaces of Figure E2 are

$$\begin{bmatrix} \overline{11} - A_1/\rho & \overline{12} & \overline{13} & \overline{14} \\ \overline{12} & -A_2/\rho & \overline{23} & \overline{24} \\ \overline{13} & \overline{23} & -A_3/\rho & \overline{34} \\ \overline{14} & \overline{24} & \overline{34} & -A_4/\rho \end{bmatrix} \begin{bmatrix} W_1 \\ W_2 \\ W_3 \\ W_4 \end{bmatrix} = -\frac{\epsilon}{\rho} \begin{bmatrix} A_1 E_1 \\ A_2 E_2 \\ A_3 E_3 \\ A_4 E_4 \end{bmatrix} \quad (1)$$

where

$$\overline{ij} = A_i F_{ij}$$

$$W_i = \text{leaving - flux density (radiosity)}$$

$$E_i = \text{emissive power of black body}$$

$$\epsilon = \text{emissivity}$$

$$\rho = \text{reflectance}$$

Equation (1) can be reduced to

$$\begin{bmatrix} (\overline{12}^2 + \overline{11}A_2/\rho - A_1A_2/\rho^2) & (\overline{12}\overline{13} - \overline{11}\overline{23} + \overline{23}A_1/\rho) & (\overline{12}\overline{14} - \overline{11}\overline{24} + \overline{24}A_1/\rho) \\ (-\overline{13}A_2/\rho - \overline{12}\overline{23}) & (\overline{12}\overline{23} + \overline{12}A_3/\rho) & (\overline{13}\overline{24} - \overline{12}\overline{34}) \\ (\overline{14}\overline{23} - \overline{13}\overline{24}) & (-\overline{14}A_3/\rho - \overline{13}\overline{34}) & (\overline{14}\overline{34} + \overline{13}A_4/\rho) \end{bmatrix} \begin{bmatrix} W_2 \\ W_3 \\ W_4 \end{bmatrix} = -.171 \frac{\epsilon}{\rho} \begin{bmatrix} \overline{12}A_1(T_1/100)^4 - \overline{11}A_2(T_2/100)^4 + A_1A_2(T_2/100)^4/\rho \\ \overline{13}A_2(T_2/100)^4 - \overline{12}A_3(T_3/100)^4 \\ \overline{14}A_3(T_3/100)^4 - \overline{13}A_4(T_4/100)^4 \end{bmatrix}$$

by eliminating W_1 , where T's are in °R, or in brevity

$$\begin{bmatrix} B_{11} & B_{12} & B_{13} \\ B_{21} & B_{22} & B_{23} \\ B_{31} & B_{32} & B_{33} \end{bmatrix} \begin{bmatrix} W_2 \\ W_3 \\ W_4 \end{bmatrix} = -.171 \frac{\epsilon}{\rho} \begin{bmatrix} G_1 \\ G_2 \\ G_3 \end{bmatrix}$$

The solution for W_4 is

$$W_4 = -.171 \frac{\epsilon}{\Delta \rho} [B_{11}(B_{22}G_3 - B_{32}G_2) - B_{21}(B_{21}G_3 - B_{32}G_1) + B_{31}(B_{12}G_2 - B_{22}G_1)],$$

where

$$\Delta = B_{11}(B_{22}B_{33} - B_{23}B_{32}) - B_{21}(B_{12}B_{33} - B_{13}B_{32}) + B_{31}(B_{12}B_{23} - B_{13}B_{22}).$$

The net heat flux from the hot rod is

$$\begin{aligned} q_{4, \text{net}} &= (\text{leaving flux density}) - (\text{incident flux density}) \\ &= W_4 - (W_4 - \epsilon E_4)/\rho \\ &= \frac{\epsilon}{\rho} (E_4 - W_4) \end{aligned}$$

Therefore the equivalent radiative heat transfer coefficient is

$$h = \frac{\epsilon}{\rho} \frac{E_4 - W_4}{T_4 - T_{\text{sat}}} = \frac{\epsilon}{\rho} \frac{.171(T_4/100)^4 - W_4}{T_4 - T_{\text{sat}}}$$